

Spatial navigation impairment is proportional to right hippocampal volume

Zuzana Nedelska^{a,b}, Ross Andel^{b,c}, Jan Laczó^{a,b}, Kamil Vlcek^{b,d}, Daniel Horinek^{b,e}, Jiri Lisy^f, Katerina Sheardova^b, Jan Bureš^{d,1}, and Jakub Hort^{a,b,1}

^aMemory Disorders Clinic, Department of Neurology, Charles University in Prague, 2nd Faculty of Medicine and Motol University Hospital, 150 06 Prague 5, Czech Republic; ^bInternational Clinical Research Center, St. Anne's University Hospital Brno, 656 91 Brno, Czech Republic; ^cSchool of Aging Studies, College of Behavioral and Community Sciences, University of South Florida, Tampa, FL 33620; ^dDepartment of Neurophysiology of Memory, Institute of Physiology, Czech Academy of Sciences, 14220 Prague 4, Czech Republic; ^eDepartment of Neurosurgery, Philipps-Universität, 35033 Marburg, Germany; and ^fDepartment of Radiology, Charles University in Prague, 2nd Faculty of Medicine and Motol University Hospital, 150 06 Prague 5, Czech Republic

Contributed by Jan Bureš, December 31, 2011 (sent for review October 9, 2011)

Cognitive deficits in older adults attributable to Alzheimer's disease (AD) pathology are featured early on by hippocampal impairment. Among these individuals, deterioration in spatial navigation, manifested by poor hippocampus-dependent allocentric navigation, may occur well before the clinical onset of dementia. Our aim was to determine whether allocentric spatial navigation impairment would be proportional to right hippocampal volume loss irrespective of general brain atrophy. We also contrasted the respective spatial navigation scores of the real-space human Morris water maze with its corresponding 2D computer version. We included 42 cognitively impaired patients with either amnesic mild cognitive impairment ($n = 23$) or mild and moderate AD ($n = 19$), and 14 cognitively intact older controls. All participants underwent 1.5T MRI brain scanning with subsequent automatic measurement of the total brain and hippocampal (right and left) volumes. Allocentric spatial navigation was tested in the real-space version of the human Morris water maze and in its corresponding computer version. Participants used two navigational cues to locate an invisible goal independent of the start position. We found that smaller right hippocampal volume was associated with poorer navigation performance in both the real-space ($\beta = -0.62$, $P < 0.001$) and virtual ($\beta = -0.43$, $P = 0.026$) versions, controlling for demographic variables, total brain and left hippocampal volumes. In subsequent analyses, the results were significant in cognitively impaired ($P \leq 0.05$) but not in cognitively healthy ($P > 0.59$) subjects. The respective real-space and virtual scores strongly correlated with each other. Our findings indicate that the right hippocampus plays a critical role in allocentric navigation, particularly when cognitive impairment is present.

Persons with Alzheimer's disease (AD) (1, 2) and with amnesic mild cognitive impairment (MCI) (3), who are known to be at higher risk for developing AD, experience difficulties with spatial navigation. Based on animal research, two basic navigation types were distinguished (4). Egocentric navigation is route or body centered and is dependent mainly on parietal cortices and caudate nucleus (4–8). The more flexible and complex allocentric type is world centered and it is dependent mainly on the hippocampus (5, 9). In humans, medial temporal lobe function is highly lateralized with the right hippocampus predominantly associated with spatial navigation and topographical memory (10). Recent research has underscored the importance of the hippocampus for spatial navigation in cognitively impaired subjects (11, 12). For example, a case study of a patient with early AD (13) reported a distinct navigation deficit indicative of hippocampal atrophy. However, structural background of the allocentric navigation impairment has not yet been entirely elucidated, particularly in the real-space environment.

The navigation disability in AD and MCI patients has been found to involve selective impairment of spatial cognition associated with atrophy of the right-lateralized navigational network (11). However, this study did not differentiate between allocentric and egocentric types of navigation. A recent study using virtual reality environment reported impaired egocentric and allocentric

spatial navigation and reduced right/left hippocampal volumes in amnesic MCI (aMCI) patients compared with cognitively healthy controls (12). However, a significant association was not found between the allocentric navigation performance and hippocampal volume, and navigation in real space was not assessed.

In our previous study, we found allocentric spatial navigation impairment in subjects with aMCI and AD in both the real-space and computerized versions of the test (3). However, these results were not supported with structural data. In the present study, we extend these previous findings by evaluating whether impairment in allocentric spatial navigation may be proportional to atrophy in the right hippocampus, an area crucial for performance of such tasks. Accordingly, we hypothesized that allocentric navigation performance would be dependent on the right hippocampal volume.

Specifically, we hypothesized that

- i) Allocentric navigation performance would be associated with right hippocampal volume independent of total brain volume, suggesting that the result is not a function of total brain atrophy but is specific to the right hippocampus.
- ii) The association between the right hippocampal volume and allocentric navigation would be more pronounced in cognitively impaired older adults.
- iii) The 2D computerized test results would be consistent with results from a real-space setting.

Virtual reality environments do not fully reflect navigation in the real space, whereas a real-space setting has a better ability to mimic real-life situations. In our study, allocentric navigation was investigated in a real-space human analog of the Morris water maze (hMWM) (3, 14) and its corresponding 2D computerized version (3, 14). The subject had to find a hidden goal inside a circular arena using orientation cues on the arena circumference. The results of both versions of the hMWM test were regressed on volumes of both the right and left hippocampi, controlling for total brain volume and differences in age, sex, and education, to evaluate proportion of brain atrophy in relation to navigational errors.

Results

In correlational analyses with the entire sample (Table 1), age correlated negatively with hippocampal volume but not with total brain volume, and positively with the magnitude of errors in the real-space version of the hMWM but not in the virtual version. Women had lower total brain volume, but not lower hippocampal volume (potentially due to the lower likelihood to detect significant differences in such a relatively small structure)

Author contributions: J.B. and J.H. designed research; Z.N., J. Laczó, K.V., J. Lisy, K.S., and J.H. performed research; Z.N., R.A., and D.H. analyzed data; and Z.N., R.A., J. Laczó, and D.H. wrote the paper.

The authors declare no conflict of interest.

¹To whom correspondence may be addressed. E-mail: jakub.hort@lfmotol.cuni.cz or bureš@biomed.cas.cz.

Table 1. Correlational matrix (n = 56)

| Variable | 1 | 2 | 3 | 4 | 5 | 6 | 7 | 8 |
|-----------------------------|--------|----------|----------|---------------------|-------------|-------------|------------|------------|
| 1) Age | – | | | | | | | |
| 2) Female sex | –0.09 | – | | | | | | |
| 3) Years of education | –0.08 | –0.27* | – | | | | | |
| 4) Total brain volume | –0.02 | –0.50*** | 0.26 | – | | | | |
| 5) Right hippocampal volume | –0.31* | –0.23 | 0.34* | 0.54*** | – | | | |
| 6) Left hippocampal volume | –0.31* | –0.01 | 0.34* | 0.46*** | 0.81*** | – | | |
| 7) hMWM real version | 0.41** | –0.03 | –0.42** | –0.46*** | –0.71*** | –0.63*** | – | |
| 8) hMWM virtual version | 0.26 | 0.05 | –0.48*** | –0.40** | –0.64*** | –0.61*** | 0.83*** | – |
| Mean | 72.0 | – | 13.7 | 1,483,036 | 3,182 | 3,251 | 82.4 | 82.1 |
| SD | 8.2 | – | 3.5 | 125,957 | 659 | 693 | 46.3 | 37.7 |
| Range | 53–87 | – | 9–22 | 1,257,139–1,815,347 | 1,814–4,622 | 1,759–4,742 | 15.3–154.6 | 15.5–168.6 |

* $P < 0.05$, ** $P < 0.01$, *** $P < 0.001$.

than men. Years of education correlated positively with hippocampal volume and negatively with the extent of errors on the spatial navigation tests. Positive correlations between brain and hippocampal volumes were strong as expected, as were negative correlations between brain/hippocampal volumes and the magnitude of errors on the spatial navigation tests. Finally, there was a strong correlation between navigation performance in the real-space and in the 2D computerized version, which is illustrated in Fig. 1. Figs. 2 and 3 illustrate the observed correlations between right hippocampal volume and performance on the real-space and 2D computerized versions of the navigation test, respectively.

In multivariate regression analyses (Table 2) adjusted for age, sex, and years of education, the initial model (model 1), which included the covariates plus total brain volume score, yielded a significant association between smaller total brain volume and poorer performance (i.e., greater average distance error) on both the real-space and computerized version of the spatial navigation test. When the measure of the right hippocampal volume was added to variables from model 1 (model 2), there was a significant association between smaller right hippocampal volume and

poorer performance on both versions of the spatial navigation test, whereas the association between total brain volume and spatial navigation was reduced to nonsignificant. The addition of right hippocampal volume into the regression model also led to a significant improvement in model fit, as indicated by the significant change in the R^2 value. Finally, the addition of left hippocampal volume to the variables from model 2 in the final model (model 3), presumed to reflect verbal ability (and the potential bias by the level of understanding instructions), did not affect the results and did not contribute to model fit. Next, we assessed potential mediation of the link between total brain volume and spatial navigation by the right hippocampal volume using the Sobel test (15). The test was significant for the real-space ($z = -3.62$, $P < 0.001$) and 2D computerized ($z = -3.35$, $P < 0.001$) spatial navigation test.

We also estimated regression models for those with and without cognitive impairment separately (Table 3). Because model 2 was superior with respect to model fit in analyses with the entire sample, only results from this model were reported. The pattern of results was retained for those with but not those without cognitive impairment. The Sobel test assessing mediation of the associations between total brain volume and spatial navigation in cognitively impaired participants by right hippocampal volume was significant

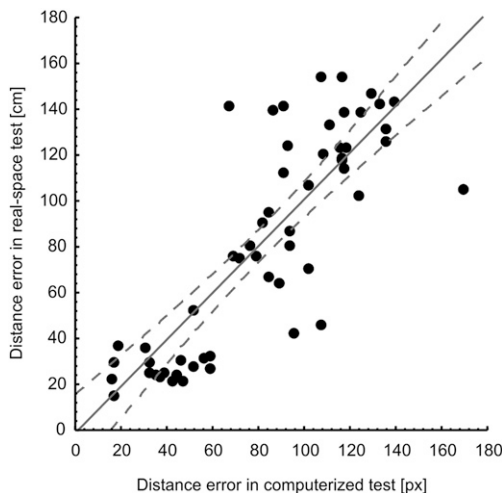


Fig. 1. Correlation between allocentric spatial navigation accuracy obtained from the real-space and 2D computerized versions of the hMWM in the entire sample ($r = 0.83$, $P < 0.001$).

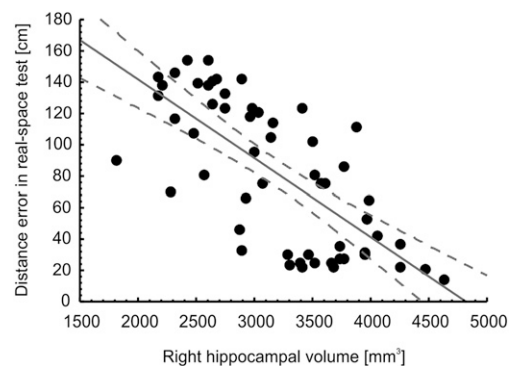


Fig. 2. Correlation between right hippocampal volume in mm^3 and allocentric spatial navigation accuracy evaluated as an average of distance error in centimeters between the participant's choice and the correct result across eight trials of each participant in the real-space version of the hMWM in the entire sample.

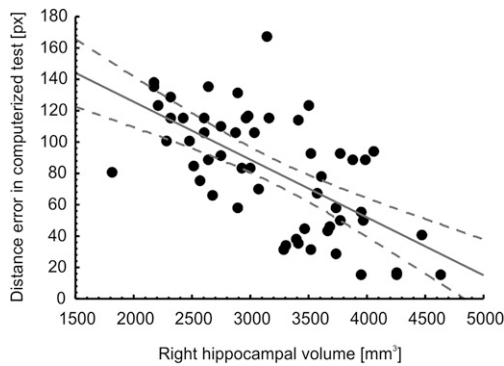


Fig. 3. Correlation between right hippocampal volume in mm^3 and allocentric spatial navigation accuracy evaluated as an average of distance error in pixels between the participant's choice and the correct result across eight trials of each participant in the 2D computerized version of the hMWM in the entire sample.

in the real space ($z = -2.42$, $P = 0.015$), but only approached significance in the virtual space ($z = -1.75$, $P = 0.080$).

Discussion

We found that allocentric navigation impairment in a real-space setting and in its corresponding 2D computerized versions was proportional to the right hippocampal volume. These results appeared to reflect a link between the extent of right hippocampal atrophy and spatial navigation performance, particularly in those with cognitive impairment represented by aMCI or AD. We concluded that smaller right hippocampal volume irrespective of a total brain atrophy, as well as age, sex, education, and left hippocampal atrophy, is responsible for decline in allocentric navigation performance. Our results are consistent with previous studies indicating that the hippocampus is a key structure for allocentric navigation in animals (9, 16, 17) and humans (9, 18, 19).

DeIpoli et al. (11) reported an association between overall navigation impairment (without distinguishing between egocentric and allocentric types of navigation) and atrophy of the right hippocampus in cognitively impaired subjects (aMCI and AD). We build on these findings by presenting allocentric navigation in relation to hippocampal volume in older cognitively impaired and cognitively healthy subjects examined within one study, and using both real-space and 2D computerized settings. One advantage of our study is that our test is a direct analogy of MWM, which is widely used to study animal spatial navigation (16, 17).

A recent study (12) reported impairment of allocentric navigation in the virtual reality park and smaller right and left hippocampal volumes in aMCI patients than in controls. However, hippocampal volumes did not correlate with allocentric navigation accuracy neither in the main analysis (with all subjects together) nor in the subanalyses (with aMCI and control subjects separately). Conversely, we found an association between right hippocampal volume and allocentric navigation that was demonstrated in the real-space and its corresponding 2D computerized version.

We found the associations between right hippocampal atrophy and spatial navigation performance to be independent of total brain atrophy. In fact, we found that right hippocampal atrophy served as a mediator of the initially observed association between total brain atrophy and navigation performance, providing further evidence for the importance of right hippocampal volume for navigation performance. Our hMWM test was shown to reflect hippocampal impairment. Given that the hippocampus is impaired early on during the course of AD and aMCI, our test might be used as an early marker of aMCI and AD, despite the relatively large heterogeneity within aMCI patients with respect to clinical progression (20). Future research that includes follow-up data should explore the utility of the test to predict the conversion from aMCI to AD and the onset of aMCI.

We also tested whether left hippocampal volume may partially explain the association between right hippocampal volume and navigation performance. We found essentially no effect of left hippocampus, indicating that the results were not confounded by abilities associated with this brain structure.

We found a parallel pattern of results in the real-space and computerized versions, confirming our previous findings (3). Although the two versions may not be fully interchangeable, including some reliance of computer skills of the subject, this finding still points to the utility of the relatively simple-to-administer computer-based test to assess potential spatial navigation deficits to identify early signs of incipient AD, as was suggested previously (3).

We should mention that we were unable to evaluate the association between allocentric navigation and brain structures other than the hippocampus. Neuroimaging studies using patients with MCI (21) indicate significant differences in volumes of multiple brain regions, including, for example, entorhinal cortical thickness and volume and parahippocampal gyrus volume. There are human functional MRI studies suggesting that allocentric navigation may be dependent on parahippocampal activity during exploration of a virtual-reality maze (22). Thus, we might expect that hippocampus-adjacent structures such as parahippocampal gyrus (predominantly on the right) may also relate to allocentric

Table 2. Associations between spatial navigation performance and right hippocampal volume

| | Model 1 | | Model 2 | | Model 3 | |
|-----------------------------|---------|----------------|---------|----------------|---------|----------------|
| | β | <i>P</i> value | β | <i>P</i> value | β | <i>P</i> value |
| Navigation in real space | | | | | | |
| Total brain volume | -0.54 | <0.001 | -0.30 | 0.008 | -0.33 | 0.004 |
| Right hippocampal volume | | | -0.48 | <0.001 | -0.62 | <0.001 |
| Left hippocampal volume | | | | | 0.19 | 0.225 |
| Adjusted R^2 | 0.51*** | | 0.65*** | | 0.65 | |
| Navigation in virtual space | | | | | | |
| Total brain volume | -0.40 | <0.001 | -0.16 | 0.225 | -0.15 | 0.280 |
| Right hippocampal volume | | | -0.48 | <0.001 | -0.43 | 0.026 |
| Left hippocampal volume | | | | | -0.07 | 0.715 |
| Adjusted R^2 | 0.35*** | | 0.48*** | | 0.48 | |

β , standardized regression coefficient; age, sex, and years of education are controlled. Model 1: covariates plus total brain volume; model 2: variables in model 1 plus right hippocampal volume; model 3: variables in model 2 plus left hippocampal volume. *** $P < 0.001$. *P* values reported with adjusted R^2 indicate whether the addition of each variable led to a significant improvement in model fit compared with the previous model, adjusting for the change in the number of variables in the model.

Table 3. Associations between spatial navigation performance and right hippocampal volume estimated separately by cognitive impairment

| | With CI, <i>n</i> = 42 | | Without CI, <i>n</i> = 14 | |
|-----------------------------|------------------------|----------------|---------------------------|----------------|
| | β | <i>P</i> value | β | <i>P</i> value |
| Navigation in real space | | | | |
| Total brain volume | -0.28 | 0.063 | 0.27 | 0.430 |
| Right hippocampal volume | -0.45 | 0.004 | 0.03 | 0.933 |
| <i>R</i> ² | 0.39*** | | 0.08 | |
| Navigation in virtual space | | | | |
| Total brain volume | -0.23 | 0.168 | -0.11 | 0.760 |
| Right hippocampal volume | -0.33 | 0.054 | -0.22 | 0.521 |
| <i>R</i> ² | 0.21** | | 0.08 | |

β , standardized regression coefficient. ****P* < 0.001, ***P* < 0.01. *P* values indicate whether the variance in spatial navigation explained by the independent variables is significant.

navigation. However, structural correlates of allocentric navigation in MCI and AD subjects are still underexplored. Future studies should focus on more complex structural correlates of allocentric navigation, especially in cognitively impaired individuals.

In conclusion, our results indicate that the right hippocampus plays a critical role in allocentric navigation in older adults in the real space and virtual space, especially in those with cognitive impairment. Together, the results can serve as a basis for future research to ascertain the ability of spatial navigation testing to identify patients in the preclinical stage of AD, where hippocampal deficits are among the primary symptoms. In addition, the findings indicate that our computer version of the human analog of the Morris water maze can reasonably imitate navigation in the real world and serve as a useful, inexpensive, and reliable screening tool for early detection of hippocampal dysfunction in older adults.

Methods

Subjects. We recruited all participants at the Memory Clinic, Department of Neurology, Motol University Hospital and 2nd Faculty of Medicine, Charles University in Prague. Cognitively intact controls were caregivers and/or family members of the patients or volunteers from among students of the University of the Third Age, associated with 2nd Faculty of Medicine, Charles University in Prague. All participants signed an informed consent on the study approved by the university hospital ethical committee. Only right-handed persons were included. Participants underwent standard neurological and laboratory evaluation, followed by a semistructured interview and extended neuropsychological testing. The test battery included Clinical Dementia Rating, Activities of Daily Living, Hachinski Ischemic Scale, Geriatric Depression Scale (GDS), Mini Mental State Examination (MMSE). The neuropsychological test battery was comprised of the Clock Drawing Test, Auditory Verbal Learning Test (AVLT), Free and Cued Selective Reminding Test with Immediate Recall (FCSRT-IR), digit span forward and reversed, Initial Letter Fluency, Trail-Making Tests (TMT) A and B, and Rey-Osterrieth complex figure. Participants with depression (GDS > 7) were excluded.

Participants were classified using established clinical criteria and the results of neuropsychological tests (Table 4). The group with cognitive impairment (*n* = 42) included 16 patients with mild probable AD and three with moderate probable AD, and 23 patients with aMCI (see Table 5 for demographic information for study participants). Subjects with AD met the Diagnostic and Statistical Manual of Mental Disorders IV-TR criteria for dementia (23) and the National Institute of Neurological and Communicative Disorders and Stroke and Alzheimer Disease and Related Disorders Association criteria for probable AD (24). Patients with aMCI met the clinical criteria for MCI established by Petersen and colleagues (20, 25). The threshold for memory impairment was derived from the same literature as scoring >1.5 SD below the mean of age- and education-adjusted norms on any memory test. We

Table 4. Neuropsychological results

| | Cognitively intact, mean (SD) | Cognitively impaired, mean (SD)* |
|------------------------------------|-------------------------------|----------------------------------|
| AVLT1-6 | 62.0 (11.0) | 32.5 (13.1) |
| AVLT1-5 | 52.7 (10.9) | 28.8 (10.5) |
| AVLT after 30 min | 11.6 (3.02) | 2.4 (3.1) |
| TMT A | 17.6 (4.2) | 30.7 (17.3) |
| TMT B | 69.3 (26.9) | 253.1 (158.9) |
| FAS total | 43.2 (6.2) | 31.1 (12.4) |
| Digit span forward numbers | 6.7 (1.3) | 5.3 (1.1) |
| Digit span reversed numbers | 5.1 (1.0) | 3.9 (1.1) |
| FCSRT-IR total score (free + cued) | 15.9 (0.3) | 12.3 (4.1) |
| FCSRT-IR free recall score | 10.9 (2.1) | 4.6 (3.3) |
| Benton A errors | 3.2 (2.1) | 13.1 (4.6) |
| Benton C errors | 0.6 (1.4) | 2.5 (1.9) |

*In independent *t* tests, the groups differed significantly in all neuropsychological test scores (*P* < 0.001).

also included 14 older controls who did not meet the criteria for cognitive impairment.

Spatial Navigation Testing: The Hidden Goal Task. The Hidden Goal Task (HGT) is a human analog of the MWM (14), where the allocentric vs. egocentric types of navigation are tested separately. Allocentric navigation is independent of individual's position on the start; it is the prominent distal cues in the subject's environment that are used to navigate toward the goal. However, egocentric navigation is dependent on individual's body position on the start. The start-goal distance and the start-goal direction are used to find the goal. Following our hypothesis, in this study we evaluated allocentric subtask. The main task of the participant was to find the hidden goal, using allocentric strategy. We used two versions of the HGT. In brief, it was the real-space version, represented by circular velvet arena, 2.9 m in diameter, and virtual 2D computerized test. First, the 2D computerized version was administered. A map-like view of the arena was projected on a 17-inch computer touch-screen. The arena was depicted as a large white circle with the start position and two distinct, red and green, orientation cues on its circumference. The red circle inside the arena represented the goal. In the beginning of the 2D computerized test, the correct goal position and mutual relationship with the orientation cues was presented to the participant. This feedback was provided before the first trial of the task and after each trial of eight (to facilitate learning), but not during the real-space version testing. The participant was requested to move a touch-screen pen from the start to the supposed goal and draw the entire route. Similarly, in the real-space version, the goal position on the floor was pointed out with a handheld pointer stick. The entire procedure is described in detail elsewhere (3).

The mutual relationship of the hidden goal and the orientation cues was stable across all trials. The navigation performance was measured as the average distance error between goal position determined by participant and the correct goal position that was programmed for each trial of eight. There was no time limit.

Table 5. Demographic information for the participants in this study

| | Cognitively intact, mean (SD) | Cognitively impaired, mean (SD) | <i>P</i> value |
|--------------------|-------------------------------|---------------------------------|----------------|
| <i>N</i> | 14 | 42 | – |
| Age (y) | 68.1 (7.1) | 73.3 (8.2) | 0.038 |
| Years of education | 15.4 (3.9) | 13.1 (3.5) | 0.033 |
| % female | 85.2 | 59.5 | 0.078 |
| MMSE | 29.4 (0.7) | 24.8 (3.6) | <0.001 |

P values are based on independent *t* tests for differences in means and a χ^2 test for a difference in frequencies.

MRI Acquisition. All participants were examined in a 1.5 T MRI scanner (Gyrosan; Philips Medical Systems). A 3D T1-weighted fast field echo sequence was obtained with the following scanning variables: coronal acquisition, 1.0-mm slice thickness; total scanning time, 14 min; TR = 25 ms; TE = 5 ms; flip angle = 30°; field of view, 256 mm; and matrix 256 × 256. Initial visual assessment was performed by an experienced neuroradiologist to discard any other relevant brain pathology and to ensure appropriate study quality.

MRI Volumetry. Automatic cortical parcellation and labeling of total brain, right and left hippocampal volumes was performed by free experimental software FreeSurfer package (26) (v4.4.0; <http://surfer.nmr.mgh.harvard.edu>), implemented into a Mac OS X (Apple) workstation. The original raw Digital Imaging and Communications in Medicine data were converted to FreeSurfer's appropriate .mgz format. FreeSurfer provides a fully automatic cortical parcellation and segmentation of subcortical structures. The program calculates brain subvolumes by assigning a neuroanatomical label to each voxel based on probabilistic information estimated automatically from a manually labeled training set. In brief, FreeSurfer's processing includes motion correction; removal of nonbrain tissue using a hybrid watershed/surface deformation procedure; multiple intensity and spatial normalization; Talairach transformation; and segmentation of the subcortical white matter and deep gray matter structures (27, 28). The overall process and analysis pipeline has been described elsewhere (<http://surfer.nmr.mgh.harvard.edu>). FreeSurfer was evaluated as a reasonable substitute for manual tracing (29) and is commonly used in the studies (21). The analysis outputs were checked by knowledgeable operator. Finally, the total brain, right and left hippocampal volumes were calculated in cubic centimeters and millimeters, respectively.

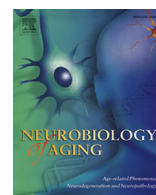
Data Analysis. For analysis, the average distance error across eight trials between the participant's choice and the correct goal position was evaluated. The average distance error was measured in centimeters in the real-space and in pixels in the 2D computerized versions. Initially, we calculated Pearson correlation coefficients to explore bivariate relationships within the data. We also inspected score distribution for all continuous variables, and found both skewness and kurtosis within acceptable range (± 0.5). In the

main analyses, we used multivariate linear regression models to estimate associations between spatial navigation performance and the right hippocampal volume. Participants with and without cognitive impairment differed significantly with respect to age [$t(54) = 2.12, P < 0.05$] and education [$t(54) = 2.19, P < 0.05$], and the result for sex differences approached significance [$\chi^2(1) = 3.21, P = 0.073$]. These variables have also been found to relate to spatial navigation ability in previous studies (30–33) and therefore were controlled in the analyses. Total brain (model 1), right (model 2), and left (model 3) hippocampal volume measures were added sequentially. We report standardized regression coefficients, which allow a direct comparison of the magnitude of the associations by standardizing the variance of each variable to the same metric. Model fit was assessed by the R^2 value adjusted for the number of variables in the model. In subsequent analyses, we also estimated the same associations separately in cognitively impaired and cognitively intact participants.

We performed the Sobel test (15) to assess whether the apparent mediation of the association between total brain volume and spatial navigation performance by right hippocampal volume would reach statistical significance. The Sobel test was estimated in a mediation analysis proposed by Preacher and Hayes (34), which extends the work of Baron and Kenny (35); the advantages include estimation of all three hypothesized pathways (predictor to outcome; predictor to mediator, and mediator to outcome) simultaneously and incorporating a bootstrapping technique, which reduces sample size demands (36). The result is expressed as a Z test, where the absolute value > 1.96 corresponds to statistical significance at $P < 0.05$. SAS software version 9 was used in all analyses, with statistical significance set at a two-tailed 0.05 level.

ACKNOWLEDGMENTS. Support for this work was provided by Grant Agency of the Czech Republic Grants 309/09/1053 and 309/09/0286; European Regional Development Fund Project St. Anne's University Hospital, Brno, International Clinical Research Center CZ.1.05/1.1.00/02.0123; Ministry of Education, Youth and Sports of the Czech Republic Grants 1M0517 and LC554; Research Project AV0250110509; and Internal Grant Agency of the Ministry of Health Grant IGA NS 10331.

- McShane R, et al. (1998) Getting lost in dementia: A longitudinal study of a behavioral symptom. *Int Psychogeriatr* 10:253–260.
- Pai MC, Jacobs WJ, Int J (2004) Topographical disorientation in community-residing patients with Alzheimer's disease. *Int J Geriatr Psychiatry* 19:250–255.
- Hort J, et al. (2007) Spatial navigation deficit in amnesic mild cognitive impairment. *Proc Natl Acad Sci USA* 104:4042–4047.
- O'Keefe J, Nadel L (1978) *The Hippocampus as a Cognitive Map* (Oxford Univ Press, New York).
- Maguire EA, et al. (1998) Knowing where and getting there: A human navigation network. *Science* 280:921–924.
- Packard MG, Knowlton BJ (2002) Learning and memory functions of the basal ganglia. *Annu Rev Neurosci* 25:563–593.
- White NM, McDonald RJ (2002) Multiple parallel memory systems in the brain of the rat. *Neurobiol Learn Mem* 77:125–184.
- Weniger G, Ruhleder M, Wolf S, Lange C, Irle E (2009) Egocentric memory impaired and allocentric memory intact as assessed by virtual reality in subjects with unilateral parietal cortex lesions. *Neuropsychologia* 47:59–69.
- O'Keefe J, Dostrovsky J (1971) The hippocampus as a spatial map. Preliminary evidence from unit activity in the freely-moving rat. *Brain Res* 34:171–175.
- Spiers HJ, et al. (2001) Unilateral temporal lobectomy patients show lateralized topographical and episodic memory deficits in a virtual town. *Brain* 124:2476–2489.
- delpoly AR, Rankin KP, Mucke L, Miller BL, Gorno-Tempini ML (2007) Spatial cognition and the human navigation network in AD and MCI. *Neurology* 69:986–997.
- Weniger G, Ruhleder M, Lange C, Wolf S, Irle E (2011) Egocentric and allocentric memory as assessed by virtual reality in individuals with amnesic mild cognitive impairment. *Neuropsychologia* 49:518–527.
- Burgess N, Trinkler I, King J, Kennedy A, Cipolotti L (2006) Impaired allocentric spatial memory underlying topographical disorientation. *Rev Neurosci* 17:239–251.
- Kalová E, Vlcek K, Jarolimová E, Bures J (2005) Allothetic orientation and sequential ordering of places is impaired in early stages of Alzheimer's disease: Corresponding results in real space tests and computer tests. *Behav Brain Res* 159:175–186.
- Sobel ME (1982) *Sociological Methodology*, ed Leinhardt S (Am Soc Assoc, Washington, DC), pp 290–312.
- Morris RG, Garrud P, Rawlins JN, O'Keefe J (1982) Place navigation impaired in rats with hippocampal lesions. *Nature* 297:681–683.
- Morris RG (1981) Spatial localization does not require the presence of local cues. *Learn Motiv* 12:239–261.
- Burgess N, Jeffery KJ, O'Keefe J (1999) *The Hippocampal and Parietal Foundations of Spatial Cognition* (Oxford Univ Press, Oxford).
- Astur RS, Taylor LB, Mamelak AN, Philpott L, Sutherland RJ (2002) Humans with hippocampus damage display severe spatial memory impairments in a virtual Morris water task. *Behav Brain Res* 132:77–84.
- Petersen RC (2004) Mild cognitive impairment. *Continuum (N Y)* 10:9–28.
- Desikan RS, et al.; Alzheimer's Disease Neuroimaging Initiative (2009) Automated MRI measures identify individuals with mild cognitive impairment and Alzheimer's disease. *Brain* 132:2048–2057.
- Aguirre GK, Detre JA, Alspop DC, D'Esposito M (1996) The parahippocampus subserves topographical learning in man. *Cereb Cortex* 6:823–829.
- American Psychiatric Association (2000) *Diagnostic and Statistical Manual of Mental Disorders* (Am Psych Assoc, Washington, DC), 4th Ed, text rev.
- McKhann G, et al. (1984) Clinical diagnosis of Alzheimer's disease: Report of the NINCDS-ADRDA work group under the auspices of Department of Health and Human Services Task Force on Alzheimer's disease. *Neurology* 34:939–944.
- Petersen RC, et al. (1999) Mild cognitive impairment: Clinical characterization and outcome. *Arch Neurol* 56:303–308.
- Fischl B, et al. (2002) Whole brain segmentation: Automated labeling of neuroanatomical structures in the human brain. *Neuron* 33:341–355.
- Ségonne F, et al. (2004) A hybrid approach to the skull stripping problem in MRI. *Neuroimage* 22:1060–1075.
- Fischl B, et al. (2004) Automatically parcellating the human cerebral cortex. *Cereb Cortex* 14:11–22.
- Morey RA, et al. (2009) A comparison of automated segmentation and manual tracing for quantifying hippocampal and amygdala volumes. *Neuroimage* 45:855–866.
- Iaria G, Palermo L, Committeri G, Barton JJ (2009) Age differences in the formation and use of cognitive maps. *Behav Brain Res* 196:187–191.
- Moffat SD, Resnick SM (2002) Effects of age on virtual environment place navigation and allocentric cognitive mapping. *Behav Neurosci* 116:851–859.
- Astur RS, Tropp J, Sava S, Constable RT, Markus EJ (2004) Sex differences and correlations in a virtual Morris water task, a virtual radial arm maze, and mental rotation. *Behav Brain Res* 151:103–115.
- Rahman Q, Koerting J (2008) Sexual orientation-related differences in allocentric spatial memory tasks. *Hippocampus* 18:55–63.
- Preacher KJ, Hayes AF (2004) SPSS and SAS procedures for estimating indirect effects in simple mediation models. *Behav Res Methods Instrum Comput* 36:717–731.
- Baron RM, Kenny DA (1986) The moderator-mediator variable distinction in social psychological research: Conceptual, strategic, and statistical considerations. *J Pers Soc Psychol* 51:1173–1182.
- MacKinnon DP, Lockwood CM, Hoffman JM, West SG, Sheets V (2002) A comparison of methods to test the significance of the mediated effect. *Psychol Methods* 7:83–10.



Brief communication

Exploring the contribution of spatial navigation to cognitive functioning in older adults



Jan Laczó^{a,b,*}, Ross Andel^{b,c}, Zuzana Nedelska^{a,b}, Martin Vyhnalek^{a,b}, Kamil Vlcek^d, Sebastian Crutch^e, John Harrison^{f,g}, Jakub Hort^{a,b}

^a Department of Neurology, Memory Clinic, 2nd Faculty of Medicine, Charles University and Motol University Hospital, Prague, Czech Republic

^b International Clinical Research Center, St. Anne's University Hospital Brno, Brno, Czech Republic

^c School of Aging Studies, University of South Florida, Tampa, FL, USA

^d Department of Neurophysiology of Memory, Institute of Physiology Academy of Sciences of the Czech Republic v.v.i., Prague, Czech Republic

^e Dementia Research Centre, UCL Institute of Neurology, University College London, London, UK

^f Metis Cognition Ltd., Kilmington, UK

^g Faculty of Medicine, Imperial College, London, UK

ARTICLE INFO

Article history:

Received 8 August 2016

Received in revised form 9 November 2016

Accepted 5 December 2016

Available online 14 December 2016

Keywords:

Alzheimer's disease

Mild cognitive impairment

Morris Water Maze

Spatial navigation

Hippocampus

Neuropsychology

ABSTRACT

Spatial navigation (SN) impairment is present early in Alzheimer's disease (AD). We tested whether SN performance, self-centered (egocentric) and world-centered (allocentric), was distinguishable from performance on established cognitive functions—verbal and nonverbal memory, executive and visuospatial function, attention/working memory, and language function. 108 older adults (53 cognitively normal [CN] and 55 with amnesic mild cognitive impairment [aMCI]) underwent neuropsychological examination and real-space navigation testing. Subset ($n = 63$) had automated hippocampal volumetry. In a factor analysis, allocentric and egocentric navigation tasks loaded highly onto the same factor with low loadings on other factors comprising other cognitive functions. In linear regression, performance on other cognitive functions was not, or was only marginally, associated with spatial navigation performance in CN or aMCI groups. After adjustment for age, gender, and education, right hippocampal volume explained 26% of the variance in allocentric navigation in aMCI group. In conclusion, spatial navigation, a known cognitive marker of early AD, may be distinguished from other cognitive functions. Therefore, its assessment along with other major cognitive functions may be highly beneficial in terms of obtaining a comprehensive neuropsychological profile.

© 2016 Elsevier Inc. All rights reserved.

1. Introduction

Alzheimer's disease (AD) is one of the most common and devastating diseases of older age. Among cognitive deficits related to underlying AD pathology, episodic memory dysfunction is considered to be the main early marker of the disease (Mistridis et al., 2015). Recently, an increased attention has been paid to spatial navigation (SN) (Lithfous et al., 2013) as another promising cognitive marker of early AD (Benke et al., 2014). Despite research on the utility of SN in identifying early AD (for review see Vlcek and Laczó, 2014), only little attention has been paid to how SN fits among the established cognitive functions (deLpolyi et al., 2007). The question remains as to whether SN is a component of the

established cognitive domains or a distinct function? Two types of SN are recognized—self-centered (egocentric), dependent on an individual's position, and world-centered (allocentric), which is independent of an individual's position and relies on distal cues for navigation (Maguire et al., 1998). Allocentric navigation, in particular, appears to be impaired in amnesic mild cognitive impairment (aMCI) (Weniger et al., 2011) and preclinical AD (Allison et al., 2016).

Our primary aim was to examine the association between egocentric and allocentric types of SN in relation to established cognitive functions, and to assess the relative contribution of hippocampal volume to the performance on SN and memory functions. We used a sample of 55 cognitively normal (CN) participants and 53 with aMCI to specifically examine whether (1) scores from egocentric and allocentric SN tasks and scores from neuropsychological tests on 6 established cognitive functions (verbal and nonverbal memory, executive and visuospatial function, attention/working memory, and language function) would load on separate factors in a factor analysis, indicating that separate underlying

* Corresponding author at: Department of Neurology, 2nd Faculty of Medicine, Charles University and Motol University Hospital, V Uvalu 84, Praha 5 - Motol, 150 06 Prague, Czech Republic. Tel.: +420 224 436 816; fax: +420 224 436 875.

E-mail address: JanLaczó@seznam.cz (J. Laczó).

processes may govern SN performance versus other cognitive functions; (2) 6 established cognitive functions would be associated with egocentric and allocentric navigation; and (3) volume of the right hippocampus, a key structure for allocentric navigation (Maguire et al., 1998), which tends to be impaired early in AD (Braak and Braak, 1991), would be associated with allocentric navigation more strongly than with memory performance.

2. Materials and methods

2.1. Participants

A total of 108 older adults aged 60 years or more were recruited from the Czech Brain Aging Study, a longitudinal study on risk factors for AD. The detailed recruitment strategies were described previously (Laczó et al., 2015). Participants underwent neuropsychological and SN testing within 2 months of brain MRI. Participants with depression (>5 points on the 15-item Geriatric Depression Scale), history of other major neurological or psychiatric disorders, Hachinski Ischemic Scale score >4, and those meeting the criteria for dementia were not included. The participants with aMCI ($n = 55$) met revised Petersen's criteria for aMCI (Petersen, 2004) including memory complaints reported by the patient or caregiver, evidence of memory dysfunction on neuropsychological testing, generally intact activities of daily living and absence of dementia. Memory impairment was established when they scored more than 1.5 standard deviations below the mean of age- and education-adjusted norms on any memory test (Laczó et al., 2015). The group included patients with isolated memory impairment (single-domain aMCI) and patients with memory impairment and additional deficits in at least one other cognitive domain (multiple domain aMCI). The CN participants ($n = 53$) reported no cognitive problems and scored less than 1.5 standard deviations below the mean of age- and education-adjusted norms on any cognitive test. Above and beyond the exclusion criteria, they had normal brain MRI and did not take any psychiatric medication. All participants signed written informed consent approved by the institutional ethics committee.

2.2. Neuropsychological battery

The following tests were included in the neuropsychological battery: (1) the Auditory Verbal Learning Test (AVLT)—trials 1–6 and 30-minute Delayed Recall trial and a 16-item picture version of the Enhanced Cued Recall Test (ECR)—total recall score as the measures of verbal memory; (2) the Rey-Osterrieth Complex Figure Test (ROCF)—the Delayed Recall condition (ROCF-D) as the measure of nonverbal memory; (3) the ROCF—the Copy condition as the measure of visuospatial function; (4) the Trail Making Test (TMT) B, and Controlled Oral Word Association Test as the measures of executive function; (5) the Backward Digit Span and TMT A as the measures of attention and working memory; and (6) the Boston Naming Test (30-item version) as the measure of language function. The Mini-Mental State Examination was used to measure global cognitive function. Neuropsychological characteristics are described in [Supplementary Table 1](#).

2.3. Spatial navigation testing

We used the real-space version of a Hidden Goal Task. The Hidden Goal Task is designed as a human analog of the Morris Water Maze (hMWM) test that allows for to separately evaluate allocentric versus egocentric types of navigation (Hort et al., 2007). The Hidden Goal Task was performed in a real-space setting—the Blue Velvet Arena ([Supplementary Fig. 1A](#)) (Kalova et al., 2005).

The task for individual participants was to locate the invisible goal on the arena floor using the start position (egocentric) or 2 distal orientation cues on the wall (allocentric), respectively ([Supplementary Fig. 1B](#)). This was preceded by the initial phase that involved locating the goal using both the start position and the 2 distal orientation cues on the arena wall to initially provide maximum available information on the goal position. The egocentric task involved using only the start position to locate the goal with no distal orientation cues displayed. The allocentric task involved using only 2 distal orientation cues at the arena wall for navigation to the goal from the start position unrelated to the goal position. Both egocentric and allocentric tasks had 8 trials and the correct position of the goal was shown after each trial to provide the feedback. The relative positions (distances and directions) of the goal to the start or orientation cues in the egocentric and allocentric tasks remained constant across all trials. After each trial, the goal position along with the start position and the positions of the cues in the egocentric and allocentric tasks were rotated in a pseudo-random sequence and the participant was instructed to go to the new start position at each consecutive trial. The goal positions and the number of trials were identical across all participants. SN performance derived as distance error in centimeters from the correct hidden goal position was automatically recorded by in-house developed software. The tasks had no time limit.

2.4. MRI acquisition and analysis

Brains were scanned at 1.5T MR scanner (Gyrosan, Philips Medical Systems, Best, The Netherlands). A T1 weighted, 3-dimensional pulse sequence Fast Field Echo with 170 contiguous coronal partitions and following parameters was used: TE/TR = 5/25 ms, flip angle 30°, FOV = 256 mm, matrix 256 × 256, 1.0 mm slice thickness, no gap, voxel size 1 × 1 × 1.25 mm and in-plane resolution 1 mm. In the CN ($n = 27$) and aMCI ($n = 36$) groups, we used fully automated FreeSurfer algorithm, v 4.4.0 (<http://surfer.nmr.mgh.harvard.edu>) (Fischl et al., 2004) to compute left and right hippocampal volumes. Volumes were adjusted for the differences in head size (Jack et al., 1989).

2.5. Data and statistical analyses

To assess SN performance, we calculated the average distance error across all 8 attempts for allocentric and egocentric navigation tasks, respectively. The score for each individual cognitive function was expressed as a unit-weighted composite z-score from the relevant neuropsychological tests. The values from TMT A and B expressed in seconds to completion of these tests were reversed before the z-scores were generated. All data were found to be adequate for parametric analysis. Initially, we examined descriptive statistics and correlations (Pearson) among study variables. To delineate SN and other specific cognitive functions, we performed an exploratory factor analysis separately for CN and aMCI groups. Principal components factor extraction with Varimax rotation was used to derive common underlying factors. Rotated factors with eigenvalues >1 were extracted. Association between particular cognitive function and allocentric or egocentric navigation was evaluated for CN and for aMCI groups using multivariate linear regression controlling for age, gender, and education. Change in model fit, reported as change in r-squared (ΔR^2), was assessed by adding individual cognitive function score to a covariate-adjusted model. Identical approach was used to explore the association between hippocampal volumes and memory tests (AVLT, ECR, and ROCF-D), allocentric or egocentric navigation. Significance was set at two-tailed 0.05. All analyses were conducted with IBM SPSS 20.0 software.

Table 1
Factor analyses of spatial navigation tasks and neuropsychological tests

| Variables | Cognitively normal older adults ^a | | | | | Amnesic mild cognitive impairment ^b | | | | |
|------------------------|--|-------------|-------------|-------------|-------------|--|-------------|-------------|--------------|--------------|
| | Factor 1 | Factor 2 | Factor 3 | Factor 4 | Factor 5 | Factor 1 | Factor 2 | Factor 3 | Factor 4 | Factor 5 |
| Egocentric task | −0.19 | −0.27 | 0.44 | 0.65 | 0.28 | −0.18 | 0.01 | 0.93 | −0.05 | 0.11 |
| Allocentric task | 0.03 | −0.01 | 0.03 | 0.90 | −0.06 | 0.37 | 0.02 | 0.78 | 0.31 | 0.04 |
| AVLT sum of trials 1–6 | −0.01 | 0.97 | 0.14 | −0.04 | 0.01 | 0.90 | 0.21 | −0.20 | −0.12 | −0.14 |
| AVLT 30 | 0.10 | 0.81 | 0.29 | −0.06 | 0.08 | 0.77 | −0.12 | −0.15 | 0.07 | 0.44 |
| ECR Total recall score | −0.12 | 0.07 | −0.04 | 0.04 | 0.89 | 0.59 | −0.28 | −0.36 | 0.43 | 0.26 |
| ROCF-D | 0.19 | 0.18 | 0.71 | 0.16 | −0.14 | 0.86 | −0.21 | 0.03 | 0.37 | −0.01 |
| ROCF copy condition | −0.05 | 0.20 | 0.72 | 0.13 | 0.10 | 0.02 | −0.06 | −0.13 | 0.14 | −0.90 |
| Trail making test B | 0.72 | 0.07 | 0.14 | −0.13 | 0.05 | 0.21 | 0.13 | 0.05 | 0.88 | −0.04 |
| COWAT | 0.62 | 0.01 | 0.15 | −0.21 | −0.13 | 0.23 | 0.74 | 0.10 | 0.33 | −0.21 |
| Backward digit span | 0.92 | 0.05 | −0.11 | 0.11 | −0.06 | −0.01 | 0.95 | 0.03 | −0.8 | 0.09 |
| Trail making Test A | 0.57 | 0.02 | 0.32 | 0.04 | 0.43 | −0.13 | −0.09 | −0.48 | 0.65 | −0.01 |
| Boston naming test | −0.54 | −0.44 | −0.09 | 0.44 | 0.15 | 0.07 | 0.03 | 0.49 | −0.72 | 0.36 |
| Eigenvalue | 3.30 | 2.86 | 2.18 | 1.58 | 1.15 | 3.63 | 3.06 | 2.44 | 2.31 | 1.42 |

Key: AVLT, Auditory Verbal Learning Test; AVLT 30, AVLT 30-min Delayed Recall; COWAT, Controlled Oral Word Association Test; ECR, Enhanced Cued Recall Test; ROCF, Rey-Osterrieth complex figure test; ROCF-D, ROCF Delayed Recall condition.

^a Note. N = 53. These 5 factors explained 73.7% of total variance in the model. Factor 1 = working memory, attention, executive, and language; Factor 2 = verbal memory without cueing; Factor 3 = visuospatial and nonverbal memory; Factor 4 = spatial navigation; Factor 5 = verbal memory with cueing. The tests within the same factor are highlighted in bold.

^b Note. N = 55. These 5 factors explained 85.7% of total variance in the model. Factor 1 = memory; Factor 2 = attention and executive; Factor 3 = spatial navigation; Factor 4 = executive, working memory and language; Factor 5 = visuospatial. The tests within the same factor are highlighted in bold.

3. Results

3.1. Descriptive analysis

Descriptive statistics and the results of correlation analyses of demographic variables, neuropsychological, SN scores, and volumes of right and left hippocampi are displayed in [Supplementary Tables 1–3](#).

3.2. Factor analysis

Results of the factor analysis in the CN and aMCI groups showing the highest loading for each item are summarized in [Table 1](#). Both analyses yielded 5 factors with eigenvalues >1. Allocentric and egocentric navigation loaded highly onto the same single factor (“SN”) and showed low loadings on other factors in both CN and aMCI groups. Conversely, each of the neuropsychological tests showed low loading on (or low relation with) the SN factor in both CN and aMCI groups. Although other factors were represented by different variables across the CN and aMCI groups, the SN factor remained the same.

3.3. Association between individual cognitive functions and SN

In the CN group ([Supplementary Table 4](#)), the established cognitive functions were not associated with allocentric or egocentric navigation. In the aMCI group ([Supplementary Table 5](#)), executive function was associated with allocentric navigation and explained 11% of its variance above and beyond the covariates. There was a trend for association between visuospatial function and allocentric navigation. Verbal memory was associated with egocentric navigation and explained 9% of its variance.

3.4. Association between hippocampal volumes, SN, and memory tests

In the CN group ([Supplementary Table 6](#)), hippocampal volumes were not associated with either performance on SN or memory tests. In the aMCI group ([Supplementary Table 7](#)), both right and left hippocampal volumes were associated with allocentric navigation and explained 26% and 12%, respectively, of its variance after adjustment for the covariates. Left hippocampal volume was

associated with performance on AVLT and ECR and explained 9%–14% of their variance. In addition, right hippocampal volume was associated with performance on ECR and explained 13% of its variance. The associations between hippocampal volumes, egocentric navigation, and ROCF-R were not significant.

4. Discussion

We examined the notion that SN may be distinguished from other cognitive functions by using a data reduction technique (factor analysis) to identify discrete factors and by linear regression to test associations (1) between established cognitive functions and SN and (2) between SN, memory performance, and hippocampal volume, the known biomarker of AD. Using a real-space hMWM to assess SN, we found that allocentric and egocentric navigation scores loaded on its own factor that was separate from 6 established cognitive functions (verbal and nonverbal memory, executive, and visuospatial function, attention/working memory, and language function) in an exploratory factor analysis. Therefore, it appears that SN shares only limited variance with other cognitive abilities. Further, SN performance was not associated with performance on any established cognitive function among the CN older adults. Only executive function was associated with allocentric navigation and verbal memory was associated with egocentric navigation among those with aMCI. Still, these associations accounted only for a small proportion of the variance in SN (11% and 9%, respectively). Finally, left and right hippocampal volumes were not found to be associated with SN or any other cognitive function among CN older adults. However, among participants with aMCI, both left and right hippocampal volumes were associated with allocentric navigation, and explained 12% and 26%, respectively, of the variance in allocentric navigation after adjustment for age, gender, and education.

Although hippocampal volumes were also related to memory tests, especially the tests of episodic memory, volumes did not explain more than 14% of the variance in memory performance, which is in line with previous findings ([Sarazin et al., 2010](#)). Therefore, hippocampal volumes explained substantially smaller proportion of the variance in memory than in allocentric navigation. Together, these findings support the notion that SN may be distinguished from other cognitive functions and that its testing provides additional relevant information about the cognitive profile beyond the established neuropsychological tests. Our findings build

on previous research suggesting that SN is impaired early in the course of AD (Benke et al., 2014) and that right hippocampal atrophy indicates the severity of SN impairment (Nedelska et al., 2012). Given the central role of the hippocampus in AD pathology (Braak and Braak, 1991), these results further underscore the utility and additional value of SN testing in the assessment of people at risk for AD. Among participants with aMCI, our findings for the associations between right and left hippocampal volumes and allocentric, but not for egocentric, navigation performance also fit into the current knowledge about spatial navigation which indicates that allocentric navigation relies more on the hippocampus (Nedelska et al., 2012), whereas egocentric navigation relies more on the medial parietal regions (Weniger et al., 2011).

This study is not without limitations. First, our results are based on SN testing in real-space hMWM, which may be somewhat difficult to implement broadly. However, it is likely that the presented results would be replicated with an easier-to-use computerized hMWM that provided almost identical results in the previous studies (Laczó et al., 2014) and strongly correlated with the real-space setting (Laczó et al., 2012). Second, brain MRI volumetry was not performed in all subjects and was restricted to the hippocampus. This may limit power to detect significant associations between cognitive performance and brain morphometric characteristics and reduces generalizability of our findings. Third, spatial navigation and spatial memory, which was unavailable in this study, may form the same construct. While we focused on a standard battery of well-established neuropsychological tests that measures established cognitive functions, the overlap with spatial memory should be studied in future research. However, the finding that spatial navigation and memory together form a distinct construct may only underscore the need for a more widespread assessment of these abilities. Finally, it would be of interest to elucidate the underlying cognitive factors assessed by different neuropsychological tests in CN and impaired older adults. This should also be the focus of future studies.

In conclusion, our results suggest that SN may be distinguished from other cognitive functions and its assessment is beneficial when characterizing cognitive performance in older adults, particularly in those at risk for AD. These results can serve as a basis for future research to further improve our understanding of SN, its relation to other cognitive functions, and its utility in detecting early signs and monitoring the course of AD.

Disclosure statement

Dr Harrison has consulted for AbbVie, AstraZeneca, Avraham, Boehringer Ingelheim, Bracket (Clinical), CRF Health, EnVivo Pharma, ePharmaSolutions, Eisai, Eli Lilly, Heptares, Janssen AI, Kyowa Hakko Kirin, Lundbeck, MedAvante, Merck, MyCognition, Novartis, Nutricia, Orion Pharma, Pharmanet/i3, Pfizer, Prana Biotech, ProStrakan, Reviva, Shire, Servier, TCG and TransTech Pharma & Velacor. Dr Hort consulted for Pfizer, Merck, Axon, Sotio, Elan, Novartis, Ipsen, Janssen and Zentiva. Dr Laczó, Dr Anđel, Dr Nedelska, Dr Vyhnašek, Dr Vlček, and Dr Crutch report no disclosures.

Acknowledgements

This study was supported by the project no. LQ1605 (MEYS CR, NPU II); European Regional Development Fund—Project FNUSA-ICRC (No. CZ.1.05/1.1.00/02.0123) and by project ICRC-ERA-HumanBridge

(No. 316345); Ministry of Health, Czech Republic—conceptual development of research organization, University Hospital Motol, Prague, Czech Republic Grant No. 00064203; Institutional Support of Laboratory Research Grant No. 2/2012 (699002); Institutional Support of Excellence Grant; research projects AV0Z50110509 and RVO:67985823.

Appendix A. Supplementary data

Supplementary data associated with this article can be found, in the online version, at <http://dx.doi.org/10.1016/j.neurobiolaging.2016.12.003>.

References

- Allison, S.L., Fagan, A.M., Morris, J.C., Head, D., 2016. Spatial navigation in preclinical Alzheimer's disease. *J. Alzheimers Dis.* 52, 77–90.
- Benke, T., Karner, E., Petermichl, S., Prantner, V., Kemmler, G., 2014. Neuropsychological deficits associated with route learning in Alzheimer disease, MCI, and normal aging. *Alzheimer Dis. Assoc. Disord.* 28, 162–167.
- Braak, H., Braak, E., 1991. Neuropathological staging of Alzheimer-related changes. *Acta Neuropathol.* 82, 239–259.
- delpolyi, A.R., Rankin, K.P., Mucke, L., Miller, B.L., Gorno-Tempini, M.L., 2007. Spatial cognition and the human navigation network in AD and MCI. *Neurology* 69, 986–997.
- Fischl, B., van der, K.A., Destrieux, C., Halgren, E., Segonne, F., Salat, D.H., Busa, E., Seidman, L.J., Goldstein, J., Kennedy, D., Caviness, V., Makris, N., Rosen, B., Dale, A.M., 2004. Automatically parcellating the human cerebral cortex. *Cereb. Cortex* 14, 11–22.
- Hort, J., Laczó, J., Vyhnašek, M., Bojar, M., Bures, J., Vlček, K., 2007. Spatial navigation deficit in amnesic mild cognitive impairment. *Proc. Natl. Acad. Sci. U. S. A.* 104, 4042–4047.
- Jack Jr., C.R., Twomey, C.K., Zinsmeister, A.R., Sharbrough, F.W., Petersen, R.C., Cascino, G.D., 1989. Anterior temporal lobes and hippocampal formations: normative volumetric measurements from MR images in young adults. *Radiology* 172, 549–554.
- Kalova, E., Vlček, K., Jarolimova, E., Bures, J., 2005. Allothetic orientation and sequential ordering of places is impaired in early stages of Alzheimer's disease: corresponding results in real space tests and computer tests. *Behav. Brain Res.* 159, 175–186.
- Laczó, J., Anđel, R., Vyhnašek, M., Matoska, V., Kaplan, V., Nedelska, Z., Lerch, O., Gazova, I., Moffat, S.D., Hort, J., 2015. The effect of TOMM40 on spatial navigation in amnesic mild cognitive impairment. *Neurobiol. Aging* 36, 2024–2033.
- Laczó, J., Anđel, R., Vyhnašek, M., Vlček, K., Magerova, H., Varjassyova, A., Nedelska, Z., Gazova, I., Bojar, M., Sheardova, K., Hort, J., 2012. From Morris Water Maze to computer tests in the prediction of Alzheimer's disease. *Neurodegener. Dis.* 10, 153–157.
- Laczó, J., Anđel, R., Vyhnašek, M., Vlček, K., Nedelska, Z., Matoska, V., Gazova, I., Mokrisova, I., Sheardova, K., Hort, J., 2014. APOE and spatial navigation in amnesic MCI: results from a computer-based test. *Neuropsychology* 28, 676–684.
- Lithfous, S., Dufour, A., Despres, O., 2013. Spatial navigation in normal aging and the prodromal stage of Alzheimer's disease: insights from imaging and behavioral studies. *Ageing Res. Rev.* 12, 201–213.
- Maguire, E.A., Burgess, N., Donnett, J.G., Frackowiak, R.S., Frith, C.D., O'Keefe, J., 1998. Knowing where and getting there: a human navigation network. *Science* 280, 921–924.
- Mistridis, P., Krumm, S., Monsch, A.U., Berres, M., Taylor, K.I., 2015. The 12 Years preceding mild cognitive impairment due to Alzheimer's disease: the temporal emergence of cognitive decline. *J. Alzheimers Dis.* 48, 1095–1107.
- Nedelska, Z., Anđel, R., Laczó, J., Vlček, K., Horinek, D., Lisy, J., Sheardova, K., Bures, J., Hort, J., 2012. Spatial navigation impairment is proportional to right hippocampal volume. *Proc. Natl. Acad. Sci. U. S. A.* 109, 2590–2594.
- Petersen, R.C., 2004. Mild cognitive impairment as a diagnostic entity. *J. Intern. Med.* 256, 183–194.
- Sarazin, M., Chauvire, V., Gerardin, E., Colliot, O., Kinkingnehun, S., de Souza, L.C., Hugonot-Diener, L., Garnero, L., Lehericy, S., Chupin, M., Dubois, B., 2010. The amnesic syndrome of hippocampal type in Alzheimer's disease: an MRI study. *J. Alzheimers Dis.* 22, 285–294.
- Vlček, K., Laczó, J., 2014. Neural correlates of spatial navigation changes in mild cognitive impairment and Alzheimer's disease. *Front. Behav. Neurosci.* 8, 89.
- Weniger, G., Ruhleder, M., Lange, C., Wolf, S., Irle, E., 2011. Egocentric and allocentric memory as assessed by virtual reality in individuals with amnesic mild cognitive impairment. *Neuropsychologia* 49, 518–527.

RESEARCH

Open Access



Emotional prosody recognition is impaired in Alzheimer's disease

Jana Amlerova^{1*}, Jan Lacz^{2,3}, Zuzana Nedelska^{2,3}, Martina Lacz^{2,3}, Martin Vyh^{2,3}, Bing Zhang⁴, Kateřina Sheardova³, Francesco Angelucci^{2,3} , Ross Anel^{2,5} and Jakub Hort^{2,3}

Abstract

Background: The ability to understand emotions is often disturbed in patients with cognitive impairments. Right temporal lobe structures play a crucial role in emotional processing, especially the amygdala, temporal pole (TP), superior temporal sulcus (STS), and anterior cingulate (AC). Those regions are affected in early stages of Alzheimer's disease (AD). The aim of our study was to evaluate emotional prosody recognition (EPR) in participants with amnesic mild cognitive impairment (aMCI) due to AD, AD dementia patients, and cognitively healthy controls and to measure volumes or thickness of the brain structures involved in this process. In addition, we correlated EPR score to cognitive impairment as measured by MMSE. The receiver operating characteristic (ROC) analysis was used to assess the ability of EPR tests to differentiate the control group from the aMCI and dementia groups.

Methods: Eighty-nine participants from the Czech Brain Aging Study: 43 aMCI due to AD, 36 AD dementia, and 23 controls, underwent Prosody Emotional Recognition Test. This experimental test included the playback of 25 sentences with neutral meaning each recorded with different emotional prosody (happiness, sadness, fear, disgust, anger). Volume of the amygdala and thickness of the TP, STS, and rostral and caudal parts of AC (RAC and CAC) were measured using FreeSurfer algorithm software. ANCOVA was used to evaluate EPR score differences. ROC analysis was used to assess the ability of EPR test to differentiate the control group from the aMCI and dementia groups. The Pearson's correlation coefficients were calculated to explore relationships between EPR scores, structural brain measures, and MMSE.

Results: EPR was lower in the dementia and aMCI groups compared with controls. EPR total score had high sensitivity in distinguishing between not only controls and patients, but also controls and aMCI, controls and dementia, and aMCI and dementia. EPR decreased with disease severity as it correlated with MMSE. There was a significant positive correlation of EPR and thickness of the right TP, STS, and bilateral RAC.

Conclusions: EPR is impaired in AD dementia and aMCI due to AD. These data suggest that the broad range of AD symptoms may include specific deficits in the emotional sphere which further complicate the patient's quality of life.

Keywords: Emotion recognition, Prosody, Alzheimer's disease, Mild cognitive impairment, Temporal pole, Superior temporal sulcus

Introduction

Emotion recognition (ER) plays a crucial role in interpersonal communication [1]. Emotional signals can be conveyed through different modalities including facial expressions, gestures, and voice or prosody (meaning melody, rhythm, rate, tone and loudness of speech) [1]. A deficit of ER can cause a series of problems ranging

*Correspondence: jana.amler@gmail.com

¹ Department of Neurology, Second Faculty of Medicine, Motol Epilepsy Center, Charles University, Motol University Hospital, Prague, Czech Republic

Full list of author information is available at the end of the article



from disturbed interpersonal relationships to decreased quality of life [2].

ER includes a complex of behavior related to perception, motor mimicry, interoception, expression, and social judgment [3]. ER can be affected in a broad spectrum of neurological and psychiatric disorders [4], particularly in disorders where the brain structures responsible for those functions are typically impaired [5]. ER impairments have been demonstrated in frontotemporal dementia [6], Alzheimer's disease (AD) and its prodromal phase of mild cognitive impairment (MCI) [7], Huntington's disease [8], Parkinson's disease [9], epilepsy [10], and traumatic brain injury [11].

According to the literature there is evidence that ER is connected with right temporal lobe structures [temporal pole (TP), superior temporal sulcus (STS), amygdala and anterior cingulate (AC)] [12–17]. Those structures are affected early during the course of AD [18, 19]; therefore, those patients may be at risk of ER deficit.

Assessments of ER have most often focused on facial ER using photographs of faces with different emotional expressions requiring participants to choose the proper emotion from a list. These studies usually test recognition of a core set of “basic emotions” [20], typically consisting of a group of negative emotions (e.g., anger, disgust, fear, sadness) and a single positive emotion (happiness).

In AD dementia and MCI, a deficit in facial recognition of emotions has been demonstrated but the data are often conflicting, with evidence of both impaired [21, 22] and preserved [23, 24] recognition. When considering specific emotions, the findings have been also inconsistent. While some studies report deficits in recognizing disgust, anger, sadness, fear, and happiness [25, 26], others report intact recognition for select emotions, such as disgust [27], anger [25, 28], and happiness [23, 24, 28].

Emotional prosody recognition (EPR) is a novel modality for experimental ER examination. EPR is frequently underutilized compared to other conventional ER tests, most likely due to its difficult testing protocol. Studies on EPR in AD have focused on sound properties of language, which can be demonstrated for example in the recognition of interrogative, notification, relative, and imperative sentences [29, 30].

In our study, we evaluated EPR using voice recordings in participants with amnesic MCI (aMCI) and dementia due to AD and compared these recordings with EPR in cognitively normal controls. Furthermore, we investigated the association between the EPR performance and either volume or thickness of selected brain regions, which are tightly connected with ER [13, 31].

We hypothesized that EPR

- 1) Is lower in aMCI and AD group and could be used as a clinical marker for early stages of dementia due to AD
- 2) Correlates with the volume/thickness of the right TP, amygdala, and STS and AC

To our knowledge, this is the first study evaluating EPR using real voice recordings in a large cohort of patients with aMCI and AD.

Methods

Participants

One hundred and two participants from the database of the Czech Brain Aging Study, a longitudinal, memory clinic-based study on aging and cognitive impairment [32], were investigated [33]. Of these, 43 participants were aMCI with high (30%) and intermediate (70%) biomarker probability of underlying AD pathology, 36 were diagnosed with dementia due to AD with high (25%) and intermediate (75%) biomarker probability of AD etiology, and 23 were cognitively normal participants. Biomarkers used included cerebrospinal fluid levels of amyloid beta, total tau, and phosphorylated tau proteins. In participants with aMCI, memory impairment was established when the participant scored more than 1.5 standard deviations below the mean of age and education-adjusted norms on any memory test, and activities of daily living were preserved to meet the Petersen et al. 2004 criteria [32, 34]. The aMCI group included both aMCI single-domain and aMCI multiple-domain phenotypes. All participants involved in this study signed written informed consent approved by the Motol University Hospital ethics committee.

Exclusion criteria

Participants were excluded from the study if they reported a history of major neurological or psychiatric disorders, hearing difficulties, depression (≥ 6 points on the 15-item Geriatric Depression Scale) [35], or had significant vascular impairment on brain MRI (Fazekas scale more than 2) [36].

Emotional Prosody Recognition Test

The Emotional Prosody Recognition Test was designed according to the methodology of Ariatti et al. published in 2008 [37]. The experimental battery was prepared in collaboration with four professional actors who produced 200 recordings in total using two Czech sentences with neutral meaning (“The table has four legs” or “Dogs that bark do not bite”). These sentences were spoken by two male and two female performers, native speakers, who were instructed to produce a specific emotional tone of

voice (3-s duration) representing five emotions: sadness, fear, happiness, disgust, and anger.

From this large dataset the most appropriate emotions were chosen by 88 healthy volunteers recruited from the clinical staff of Motol University Hospital (mean age 31.6, M to F 1:1) to build the experimental battery. Volunteers invited to validate this test were relatively young because originally this test was prepared for examination of patients with epilepsy who are younger than patients with AD.

The final experimental test included 25 short recordings (spoken by one male and one female performer) each with a 3-s duration. Although the sentences held neutral semantic meaning, these recordings were presented with emotionally charged voices representing happiness, sadness, fear, disgust, and anger; thus, each emotion was represented 5 times. Recordings were presented to subjects on a computer using headphones. The 25 recordings were presented in the same order to each participant. Participants had to select the appropriate emotion from the list of emotions after each of the 25 recordings. There was no time limit to reduce stress during testing. When the participants hesitated, the examiner repeated the instruction to choose one answer from the list and waited until the participant made a choice. The test was scored as correct or incorrect after each recording and the maximum score was 25 points.

MRI acquisition and analysis

Participants' brain MR scans were performed on a 1.5T system (Siemens, Erlangen, Germany). A T1 weighted, 3-dimensional high resolution magnetization-prepared rapid acquisition with gradient echo (MPRAGE) was acquired with TR/TE/TI = 2000/3.08/1100 ms, flip angle 15, 192 continuous partitions, slice thickness 1.0 mm, and in-plane resolution 1 mm [38]. Participants' scans were visually inspected to determine sufficient technical quality and to exclude participants with radiologic findings that could interfere with cognitive functioning (i.e., cortical infarctions, tumors, subdural hematomas, hydrocephalus or more extensive white matter hyperintensities equal to Fazekas scale above 2). To measure right- and left-sided amygdala volume and thickness of the temporal pole, superior temporal sulcus, and rostral and caudal parts of the AC (RAC and CAC), we used an automated algorithm from FreeSurfer, version 5.3. (<http://surfer.nmr.mgh.harvard.edu>), described in detail elsewhere [39, 40].

Amygdala volumes were normalized for the differences in head size by regressing the estimated total intracranial volume (eTIV) among participants, as previously described [41, 42]. Temporal pole, superior temporal sulcus, and RAC and CAC thickness were not eTIV adjusted.

Statistical analysis

A one-way analysis of variance (ANOVA) with post hoc Sidak's test was used to evaluate differences between the groups in continuous demographic variables. The χ^2 test was used to evaluate differences in gender proportions. An analysis of covariance (ANCOVA) with post hoc Sidak's test was used to evaluate differences between the groups in emotional prosody scores. The analysis was controlled for age (mean-centered) and years of education (mean-centered). The receiver operating characteristic (ROC) analysis was used to assess the ability of the Emotional Prosody Recognition Test to differentiate the control group from the aMCI and dementia groups. Sizes of the areas under the ROC curves (AUCs) and optimal sensitivity and specificity based on the Youden's index were calculated. The Pearson's correlation coefficients were calculated to explore the bivariate relationships between emotional prosody scores, structural brain measures, and Mini-Mental State Examination (MMSE) scores (a measure of disease severity). Holm-Bonferroni correction for multiple comparisons was used. Next, significant associations were tested using the hierarchical linear regression models adjusted for demographic characteristics, age (mean-centered), and years of education (mean-centered). A two-tailed p value < 0.05 was considered statistically significant. Analyses were performed using R statistical language environment [43] and IBM SPSS 25.0 software.

Results

Demographic characteristics

Group demographic and clinical characteristics are reported in Table 1. There was no difference in sex distribution among the groups. There was a significant group effect for age indicating that the control group was younger than the aMCI and dementia groups (both $p < 0.001$). There were no differences between the aMCI and dementia groups ($p = 1.000$).

The dementia group had significantly fewer years of education compared to the control group ($p < 0.001$) and the aMCI group ($p = 0.012$). The difference in education between the control group and the aMCI group was not significant ($p = 0.362$). MMSE score was significantly lower in the aMCI and dementia groups compared to the control group (both $p < 0.001$). The dementia group had lower MMSE scores than the aMCI group ($p < 0.001$).

Evaluation of emotional prosody recognition

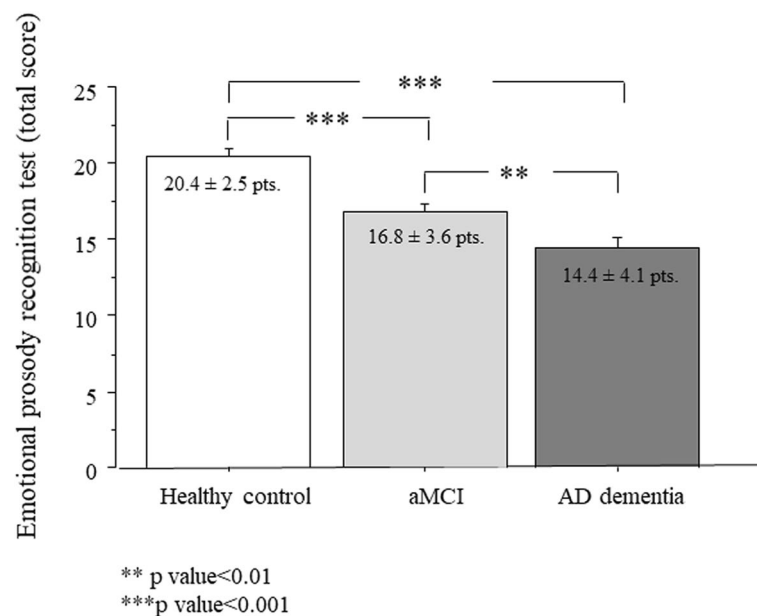
The total score for EPR is shown in Fig. 1. There was a significant group effect in total EPR score ($p = 0.002$). The post hoc analysis controlling for age and education confirmed that EPR scores were lower in the dementia

Table 1 Demographic and clinical features of aMCI and AD patients and healthy controls. Data are expressed as mean \pm standard deviation

| Demographic and clinical features | MCI patients (n = 43) | AD patients (n = 36) | Normal participants (n = 23) | p-value (group difference) |
|-----------------------------------|-----------------------|----------------------|------------------------------|----------------------------|
| Age | 74.47 \pm 6.09 | 74.47 \pm 6.54 | 67.04 \pm 6.67 | 0.00 * |
| Gender | 26F/17M | 25F/11M | 17F/6M | 0.836 |
| Years of education | 15.49 \pm 2.83 | 13.47 \pm 3.56 | 16.65 \pm 2.37 | 0.00* |
| MMSE | 26.60 \pm 2.57 | 22.75 \pm 2.55 | 29.52 \pm 0.73 | 0.00 * |

MMSE Mini Mental State Examination, M male, F female

*Statistically significant

**Fig. 1** Prosody emotion recognition total score in aMCI and AD patients and healthy controls. Data are the mean \pm SEM. Asterisk (*) indicates significant difference between the groups. ** $p < 0.001$; *** $p < 0.0001$

group compared to the control group ($p = 0.002$). The dementia group also had lower total EPR score compared to the aMCI group ($p = 0.033$) (Fig. 1).

In the ROC analyses, the total score for EPR differentiated the control group from the patients' groups (pooled aMCI and dementia groups) with AUC values of 0.85 ($p < 0.001$), sensitivity of 87.0% and specificity of 72.2%, the control group from the aMCI group with AUC values of 0.80 ($p < 0.001$), sensitivity of 73.9% and specificity of 74.4%, the control group from the dementia group with AUC values of 0.91 ($p < 0.001$), sensitivity of 87.0% and specificity of 83.3%, and the aMCI group from the dementia group with AUC values of 0.67 ($p = 0.009$), sensitivity of 62.8% and specificity of 61.1%.

Associations of emotional prosody recognition with MMSE and structural brain measures

EPR total score significantly correlated with disease severity according to MMSE score in the entire sample ($r = 0.471$, $p < 0.001$). The association remained significant in the regression analysis adjusted for age and education, where lower EPR total scores were associated with lower MMSE scores ($\beta = 0.35$, $p < .001$, 95% CI [0.07, 0.27]).

EPR total score significantly correlated with left and right TP thickness (both $r \geq 0.35$, $p < .001$), left and right STS thickness (both $r \geq 0.52$, $p < .001$), and left and right RAC thickness (both $r \geq 0.35$, $p < .001$). The correlation between ERP total score and left and right amygdala

volumes (both $r \geq 0.23$, $p \leq .026$) did not survive the correction for multiple comparisons.

The associations with right-sided structural brain measures of TP and STS and bilateral structural brain measures of RAC remained significant in the regression analysis adjusted for age and education, where lower EPR total scores were associated with smaller right TP ($\beta = 0.33$, $p = .002$, 95% CI [0.41, 1.71]), right STS ($\beta = 0.37$, $p < .001$, 95% CI [1.32, 4.29]) and right ($\beta = 0.31$, $p < .001$, 95% CI [1.85, 5.70]) and left ($\beta = 0.29$, $p = .001$, 95% CI [1.39, 5.09]) RAC thickness. The associations between EPR total scores and left-sided structural brain measures of TP and STS were not significant in the regression analysis (all $\beta \leq 0.14$, $p \geq .199$, 95% CI [-0.39, 0.94] and [-0.58, 2.76]).

Discussion

This study investigated whether EPR is impaired in participants with aMCI due to AD and AD dementia as compared to cognitively normal participants. Secondly, we evaluated the correlations of EPR scores with volume of the amygdala and thickness of TP, STS, RAC, and CAC and cognitive deficit as measured by MMSE score. The ROC analysis was used to assess the ability of the EPR test to differentiate the control group from the aMCI and dementia groups. The results showed that EPR total scores were reduced in a group of aMCI and dementia as compared to cognitively normal controls. Also, EPR score was lower for the dementia group compared to aMCI. These results remain significant when age and education differences were controlled. ROC analysis showed that there was a high sensitivity to distinguish not only between controls and patients (dementia plus aMCI) but also between the controls and aMCI, controls and dementia, and aMCI and dementia groups.

In addition, the association between EPR and global cognitive functioning as measured by MMSE was also significant, with lower MMSE scores associated with a lower ability to recognize emotions from prosody (controlled for age and education differences). Several studies suggest that the disease severity may account for differences in ER between AD individuals and controls [44]. Therefore, it is important to consider the disease stage when analyzing ER in AD individuals.

Our findings indicate that EPR is impaired within the AD continuum ranging from dementia to prodromal stages of aMCI in a similar way to facial ER [45], and this aligns well with previous studies suggesting general ER impairment in AD [21, 22, 25].

In another study, it was shown that only facial ER is impaired in subjects affected by dementia of AD type, while EPR is unaffected [25]. This discrepancy with our data could be due to the low number of subjects

included ($n = 7$). In addition, all subjects were diagnosed as MCI, thus excluding AD patients from their analysis. In another study [46] performed in a larger group of AD individuals with lower MMSE scores (19.9 ± 2.7), these participants showed a worse performance than controls in all ER tasks and particularly when identifying emotional prosody.

Thus, one possibility is that different results for emotional prosody in AD studies are due to recruitment of participants in different stage of the disease. This hypothesis is supported by our findings showing the positive correlation between MMSE and EPR total score. Current literature suggests that facial ER is impaired earlier than EPR during the course of the disease. Another explanation could be the possible heterogeneity of the sample used in those studies due to different methodology and AD diagnostic criteria used. Our study used biomarkers and extensive neuropsychology to define the AD and its prodromal stages, while a lot of studies depend only on MMSE staging.

The correlation with disease severity also suggests that assessment of EPR can be used as an additional tool to characterize the disease stage. There are studies using additional aspects of prosody or even complex music stimuli, and it has been recently proposed that speech sound analysis can be used to screen older adults for MCI or AD [47]. In another study, it was shown that subjects with dementia and aMCI also experience difficulty in recognizing the emotions conveyed by music [48]. The use of prosody score could be an important additional tool to stage AD combined with other classic methods like MRI, which is insufficient as a stand-alone tool [49].

In our study, correlation analyses showed positive correlations of EPR total score with thickness of TP, STS, and RAC. Controlled for between group differences, only right TP, STS thickness, and right and left RAC remain significant.

These brain structures, especially in right sided hemisphere, are involved in emotional processing in general. There are many studies supporting the role of the right hemisphere in emotional regulation [50]. For example, it has been shown that children with temporal lobe epilepsy, particularly those affected in the right lobe, have reduced EPR scores [51]. Similar data have also been found in adults [52]. It has long been thought that the superior temporal sulcus is connected with facial recognition; however, recent studies now show its importance also in perception of emotional prosody [53, 54]. By using real-time functional magnetic resonance imaging (rt-fMRI) techniques, it has been confirmed that the ACC is a central hub for cognitive and emotional networks [55] and its modulation has been suggested to elicit mood changes [56]. Moreover, analysis of the cerebral activity

maps obtained by fMRI during EPR tests showed that these brain areas share a neural substrate for mentalizing and processing verbal and prosodic emotional cues [57]. These results are in line with current understanding of the right hemisphere to be involved in emotional processing in general [50, 52].

The correlations with volumetric data of distinct brain regions provide additional support for the use of EPR scores as a diagnostic tool. Specifically, we observed a positive correlation with right TP and STS thickness and bilateral RAC thickness, which are regions primarily involved in ER [58–60] and also affected early during the course of AD [16, 18, 19].

After the correction for multiple comparisons, the amygdala volume was not correlated to EPR score. Reduction in hippocampal and amygdala volume on structural MRI is considered to be an early marker of AD [61]. Although the amygdala is associated with emotional processing and generating emotional responses to presented faces [62], studies are not consistently in agreement on whether amygdala atrophy is present in AD versus controls [63, 64]. Furthermore, amygdala function in regulating and sustaining emotional processing is probably independent from the actual amygdala volume.

Limitations

One possible limitation of our study is the significant difference in age and education between controls and individuals with aMCI and dementia. By adjusting our analyses for age and education we tried to address this issue. Additionally, we focused only on specific brain regions in volumetry analysis. A notable strength of our data set is the homogeneity of the study groups, provided by strict CBAS criteria including AD biomarkers. In order to quantify the predictive power of EPR for the identification of individuals at risk of AD, larger group studies would need to be performed and machine learning approaches utilized. Other limitations could include the sample size and lack of controls for other covariates, which may have impacted the EPR and volume associations (e.g., depression).

Conclusions

In conclusion, this study demonstrates that aMCI due to AD and AD dementia individuals have lower EPR scores as compared to cognitively healthy participants. Given that EPR scores correlate with MMSE scores and regional temporal brain atrophy, these data suggest that EPR may be an additional tool to stage AD and/or improve early diagnosis of AD and to guide clinical and social management of individuals with cognitive impairment.

Acknowledgements

None

Authors' contributions

Conceptualization: F.A., J.H., and J.A.; writing—original draft preparation: F.A., J.A., and J.H.; data acquisition: J.A., J.L., Z.N., M.L., M.V., B.Z., and K.S.; statistical analysis: J.A. and R.A. Writing—review and editing: F.A., J.A., J.L., Z.N., M.V., B.Z., K.S., R.A., and J.H.; funding acquisition: J.A., M.V., K.S., and J.H.; all authors read and approved the final manuscript.

Funding

Institutional Support of Excellence 2. LF UK grant no. 6990332.

Availability of data and materials

The datasets used and/or analyzed during the current study are available from the corresponding author on reasonable request.

Declarations

Ethics approval and consent to participate

All participants involved in this study signed written informed consent approved by the Motol University Hospital ethics committee.

Consent for publication

Not applicable

Competing interests

The authors declare that they have no competing interests.

Author details

¹Department of Neurology, Second Faculty of Medicine, Motol Epilepsy Center, Charles University, Motol University Hospital, Prague, Czech Republic. ²Memory Clinic, Department of Neurology, Second Faculty of Medicine, Charles University, Motol University Hospital, Prague, Czech Republic. ³International Clinical Research Center, St. Anne's University Hospital Brno, Brno, Czech Republic. ⁴Department of Radiology, Drum Tower Hospital of Nanjing University Medical School, Nanjing, China. ⁵School of Aging Studies, University of South Florida, Tampa, FL, USA.

Received: 10 May 2021 Accepted: 10 March 2022

Published online: 05 April 2022

References

1. Ferretti V, Papaleo F. Understanding others: emotion recognition abilities in humans and other animals. *Genes, Brain Behav.* 2018:e12544 Available from: <https://onlinelibrary.wiley.com/doi/abs/10.1111/gbb.12544>.
2. Hasson-Ohayon I, Mashiach-Eizenberg M, Arnon-Ribenfeld N, Kravetz S, Roe D. Neuro-cognition and social cognition elements of social functioning and social quality of life. *Psychiatry Res.* 2017;258:538–43 Available from: <https://linkinghub.elsevier.com/retrieve/pii/S0165178117300318>.
3. Adolphs R. Neural systems for recognizing emotion. *Curr Opin Neurobiol* [Internet]. 2002;12:169–77 Available from: <https://linkinghub.elsevier.com/retrieve/pii/S095943880200301X>.
4. Marcó-García S, Ferrer-Quintero M, Usall J, Ochoa S, Del Cacho N, Huerta-Ramos E. Facial emotion recognition in neurological disorders: a narrative review. *Rev Neurol.* 2019;69(5):207–219. <https://doi.org/10.33588/rn.6905.2019047>.
5. Fortier J, Besnard J, Allain P. Theory of mind, empathy and emotion perception in cortical and subcortical neurodegenerative diseases. *Rev Neurol (Paris)* [Internet]. 2018;174:237–46 Available from: <https://linkinghub.elsevier.com/retrieve/pii/S0035378717304551>.
6. Hutchings R, Palermo R, Piguot O, Kumfor F. Disrupted face processing in frontotemporal dementia: a review of the clinical and neuroanatomical evidence. *Neuropsychol Rev* [Internet]. 2017;27:18–30 Available from: <http://link.springer.com/10.1007/s11065-016-9340-2>.
7. Elferink MW-O, Van Tilborg I, Kessels RPC. Perception of emotions in mild cognitive impairment and Alzheimer's dementia: does intensity matter? *Transl Neurosci* [Internet]. 2015;6:139–49 Available from: <https://www.degruyter.com/document/doi/10.1515/tnsci-2015-0013/html>.
8. Henley SMD, Novak MJU, Frost C, King J, Tabrizi SJ, Warren JD. Emotion recognition in Huntington's disease: a systematic review. *Neurosci*

- Biobehav Rev [Internet]. 2012;36:237–53 Available from: <https://linkinghub.elsevier.com/retrieve/pii/S0149763411001126>.
9. Wasser CI, Evans F, Kempnich C, Glikmann-Johnston Y, Andrews SC, Thyagarajan D, et al. Emotion recognition in Parkinson's disease: static and dynamic factors. *Neuropsychologia* [Internet]. 2018;32:230–4 Available from: <http://doi.apa.org/getdoi.cfm?doi=10.1037/neu0000400>.
 10. Bora E, Meletti S. Social cognition in temporal lobe epilepsy: a systematic review and meta-analysis. *Epilepsy Behav* [Internet]. Elsevier BV. 2016;60:50–7. Available from <https://doi.org/10.1016/j.yebeh.2016.04.024>
 11. Byom L, Duff M, Mutlu B, Turkstra L. Facial emotion recognition of older adults with traumatic brain injury. *Brain Inj* [Internet]. 2019;33:322–32 Available from: <https://www.tandfonline.com/doi/full/10.1080/02699052.2018.1553066>.
 12. Spunt RP, Adolphs R. The neuroscience of understanding the emotions of others. *Neurosci Lett* [Internet]. Elsevier BV. 2019;693:44–8. Available from <https://doi.org/10.1016/j.neulet.2017.06.018>.
 13. Olson IR, Plotzker A, Ezzyat Y. The Enigmatic temporal pole: a review of findings on social and emotional processing. *Brain* [Internet]. 2007;130:1718–31 Available from: <https://academic.oup.com/brain/article-lookup/doi/10.1093/brain/awm052>.
 14. Gallagher M, Chiba AA. The amygdala and emotion. *Curr Opin Neurobiol* [Internet]. Elsevier BV. 1996;6:221–7. Available from [https://doi.org/10.1016/S0959-4388\(96\)80076-6](https://doi.org/10.1016/S0959-4388(96)80076-6).
 15. Deen B, Saxe R, Kanwisher N. Processing communicative facial and vocal cues in the superior temporal sulcus. *Neuroimage* [Internet]. 2020;221:117191. Available from <https://doi.org/10.1016/j.neuroimage.2020.117191>.
 16. Bush G, Luu P, Posner MI. Cognitive and emotional influences in anterior cingulate cortex. *Trends Cogn Sci* [Internet]. 2000;4:215–22. Available from [https://doi.org/10.1016/S1364-6613\(00\)01483-2](https://doi.org/10.1016/S1364-6613(00)01483-2).
 17. Iidaka T. Role of the fusiform gyrus and superior temporal sulcus in face perception and recognition: an empirical review. *Jpn Psychol Res* [Internet]. Wiley. 2013;56:33–45. Available from <https://doi.org/10.1111/jpr.12018>.
 18. Berron D, van Westen D, Ossenkoppele R, Strandberg O, Hansson O. Medial temporal lobe connectivity and its associations with cognition in early Alzheimer's disease. *Brain* [Internet]. 2020;143:1233–48 Available from: <https://academic.oup.com/brain/article/143/4/1233/5816707>.
 19. ten Kate M, Barkhof F, Boccardi M, Visser PJ, Jack CR, Lovblad K-OO, et al. Clinical validity of medial temporal atrophy as a biomarker for Alzheimer's disease in the context of a structured 5-phase development framework. *Neurobiol Aging* [Internet]. 2017;52:167–182.e1 Available from: <https://linkinghub.elsevier.com/retrieve/pii/S0197458016301452>.
 20. Herzog ED, Muglia LJ. You are when you eat. *Nat Neurosci* [Internet]. 2006;9:300–2 Available from: <http://www.ncbi.nlm.nih.gov/pubmed/16498421>.
 21. Albert MS, Cohen C, Koff E. Perception of affect in patients with dementia of the Alzheimer type. *Arch Neurol* [Internet]. 1991;48:791–5 Available from: <http://archneur.jamanetwork.com/article.aspx?articleid=591021>.
 22. Shimokawa A, Yatomi N, Anamizu S, Torii S, Isono H, Sugai Y. Recognition of facial expressions and emotional situations in patients with dementia of the Alzheimer and vascular types. *Dement Geriatr Cogn Disord* [Internet]. 2003;15:163–8 Available from: <https://www.karger.com/Article/FullText/68479>.
 23. Burnham H, Hogervorst E. Recognition of facial expressions of emotion by patients with dementia of the Alzheimer type. *Dement Geriatr Cogn Disord* [Internet]. 2004;18:75–9 Available from: <https://www.karger.com/Article/FullText/77813>.
 24. Lavenu I, Pasquier F, Lebert F, Petit H, Van Der Linden M. Perception of emotion in frontotemporal dementia and Alzheimer disease. *Alzheimer Dis Assoc Disord* [Internet]. 1999;13:96–101 Available from: <http://journals.lww.com/00002093-199904000-00007>.
 25. Drapeau J, Gosselin N, Gagnon L, Peretz I, Lorrain D. Emotional recognition from face, voice, and music in dementia of the Alzheimer type. *Ann N Y Acad Sci* [Internet]. 2009;1169:342–5. Available from <https://doi.org/10.1111/j.1749-6632.2009.04768.x>.
 26. Hargrave R, Maddock RJ, Stone V. Impaired recognition of facial expressions of emotion in Alzheimer's disease. *J Neuropsychiatry Clin Neurosci* [Internet]. 2002;14:64–71 Available from: <http://psychiatryonline.com/doi/abs/10.1176/jnp.14.1.64>.
 27. Henry JD, Ruffman T, McDonald S, O'Leary MAP, Phillips LH, Brodaty H, et al. Recognition of disgust is selectively preserved in Alzheimer's disease. *Neuropsychologia* [Internet]. 2008;46:1363–70 Available from: <https://linkinghub.elsevier.com/retrieve/pii/S0028393207004459>.
 28. Weiss EM, Kohler CG, Vonbank J, Stadelmann E, Kemmler G, Hinterhuber H, et al. Impairment in emotion recognition abilities in patients with mild cognitive impairment, early and moderate Alzheimer disease compared with healthy comparison subjects. *Am J Geriatr Psychiatry* [Internet]. 2008;16:974–80 Available from: <https://linkinghub.elsevier.com/retrieve/pii/S1064748112603996>.
 29. Horley K, Reid A, Burnham D. Emotional prosody perception and production in dementia of the Alzheimer's type. *J Speech, Lang Hear Res* [Internet]. 2010;53:1132–46 Available from: <http://pubs.asha.org/doi/10.1044/1092-4388%282010/09-0030%29>.
 30. Bucks RS, Radford SA. Emotion processing in Alzheimer's disease. *Aging Ment Heal* [Internet]. 2004;8:222–32 Available from: <https://www.tandfonline.com/doi/full/10.1080/13607860410001669750>.
 31. Watson R, Latinus M, Noguchi T, Garrod O, Crabbe F, Belin P. Crossmodal adaptation in right posterior superior temporal sulcus during face-voice emotional integration. *J Neurosci* [Internet]. 2014;34:6813–21 Available from: <http://www.jneurosci.org/cgi/doi/10.1523/JNEUROSCI.4478-13.2014>.
 32. Sheardova K, Vyhnaek M, Nedelska Z, Laczó J, Andel R, Marciniak R, et al. Czech Brain Aging Study (CBAS): prospective multicentre cohort study on risk and protective factors for dementia in the Czech Republic. *BMJ Open* [Internet]. 2019;9:e030379 Available from: <https://bmjopen.bmj.com/lookup/doi/10.1136/bmjopen-2019-030379>.
 33. Laczó J, Andel R, Vyhnaek M, Matoska V, Kaplan V, Nedelska Z, et al. The effect of TOMM40 on spatial navigation in amnesic mild cognitive impairment. *Neurobiol Aging* [Internet]. 2015;36:2024–33 Available from: <https://linkinghub.elsevier.com/retrieve/pii/S0197458015001657>.
 34. Petersen RC. Mild cognitive impairment as a diagnostic entity. *J Intern Med* [Internet]. 2004;256:183–94 Available from: <http://www.ncbi.nlm.nih.gov/pubmed/15324362>.
 35. Yesavage JA. Geriatric Depression Scale. *Psychopharmacol Bull*. 1988;24:709–11.
 36. Fazekas F, Chawluk J, Alavi A, Hurtig H, Zimmerman R. MR signal abnormalities at 1.5 T in Alzheimer's dementia and normal aging. *Am J Roentgenol* [Internet]. 1987;149:351–6 Available from: <http://www.ajronline.org/doi/10.2214/ajr.149.2.351>.
 37. Ariatti A, Benuzzi F, Nichelli P. Recognition of emotions from visual and prosodic cues in Parkinson's disease. *Neurol Sci* [Internet]. 2008;29:219–27 Available from: <http://link.springer.com/10.1007/s10072-008-0971-9>.
 38. Kerbler GM, Nedelska Z, Fripp J, Laczó J, Vyhnaek M, Lisý J, et al. Basal forebrain atrophy contributes to allocentric navigation impairment in Alzheimer's disease patients. *Front Aging Neurosci* [Internet]. 2015;7 Available from: <http://journal.frontiersin.org/article/10.3389/fnagi.2015.00185>.
 39. Fischl B, Salat DH, Busa E, Albert M, Dieterich M, Haselgrove C, et al. Whole brain segmentation: automated labeling of neuroanatomical structures in the human brain. *Neuron*. 2002;33:341–55.
 40. Fischl B, van der Kouwe A, Destrieux C, Halgren E, Ségonne F, Salat DH, et al. Automatically parcellating the human cerebral cortex. *Cereb Cortex* [Internet]. Oxford University Press. 2004;14:11–22 Available from: <https://academic.oup.com/cercor/article-lookup/doi/10.1093/cercor/bhg087>.
 41. Bhatia S, Bookheimer SY, Gaillard WD, Theodore WH. Measurement of whole temporal lobe and hippocampus for MR volumetry: normative data. *Neurology* [Internet]. 1993;43:2006 Available from: <http://www.neurology.org/cgi/doi/10.1212/WNL.43.10.2006>.
 42. Cechova K, Andel R, Angelucci F, Chmatalova Z, Markova H, Laczó J, et al. Impact of APOE and BDNF Val66Met gene polymorphisms on cognitive functions in patients with amnesic mild cognitive impairment. *Lim YY, editor. J Alzheimer's Dis*. 2020;73:247–57 Available from: <https://www.medra.org/servelet/aliasResolver?alias=iospress&doi=10.3233/JAD-190464>.
 43. Team R. RStudio: integrated development environment for R. Boston: RStudio, Inc.; 2016.
 44. Spoletini I, Marra C, Di Iulio F, Gianni W, Sancésario G, Giubilei F, et al. Facial emotion recognition deficit in amnesic mild cognitive impairment and Alzheimer disease. *Am J Geriatr Psychiatry* [Internet]. 2008;16:389–98

- Available from: <https://linkinghub.elsevier.com/retrieve/pii/S10647481260606X>.
45. Varjassyová A, Hořínek D, Andel R, Amlerova J, Laczó J, Sheardová K, et al. Recognition of facial emotional expression in amnesic mild cognitive impairment. *J Alzheimer's Dis* [Internet]. 2013;33:273–80 Available from: <https://www.medra.org/servelet/aliasResolver?alias=iospress&doi=10.3233/JAD-2012-120148>.
 46. Templier L, Chetouani M, Plaza M, Belot Z, Bocquet P, Chaby L. Altered identification with relative preservation of emotional prosody production in patients with Alzheimer's disease. *Geriatr Psychol Neuropsychiatr Vieil* [Internet]. 2015;13:106–15 Available from: <http://www.john-libbey-eurot-ext.fr/medline.md?doi=10.1684/pnw.2015.0524>.
 47. Kato S, Homma A, Sakuma T. Easy screening for mild Alzheimer's disease and mild cognitive impairment from elderly speech. *Curr Alzheimer Res* [Internet]. 2017;15:104–10 Available from: <https://www.eurkaselect.com/157382/article>.
 48. Zhou S-SS, Gao X, Hu Y-JJ, Zhu Y-MM, Tian Y-HH, Wang K. Selective impairment of musical emotion recognition in patients with amnesic mild cognitive impairment and mild to moderate Alzheimer disease. *Chin Med J (Engl)* [Internet]. 2019;132:2308–14 Available from: <https://journals.lww.com/10.1097/CM9.0000000000000460>.
 49. Lombardi G, Crescioli G, Cavedo E, Lucenteforte E, Casazza G, Bellatorre AG, et al. Structural magnetic resonance imaging for the early diagnosis of dementia due to Alzheimer's disease in people with mild cognitive impairment. *Cochrane Database Syst Rev* [Internet]. 2020;3:CD009628 Available from: <http://doi.wiley.com/10.1002/14651858.CD009628.pub2>.
 50. Killgore WDS, Yurgelun-Todd DA. The right-hemisphere and valence hypotheses: could they both be right (and sometimes left)? *Soc Cogn Affect Neurosci* [Internet]. 2007;2:240–50. Available from: <https://doi.org/10.1093/scan/nsm020>.
 51. Cohen M, Prather A, Town P, Hynd G. Neurodevelopmental differences in emotional prosody in normal children and children with left and right temporal lobe epilepsy. *Brain Lang* [Internet]. Elsevier BV. 1990;38:122–34. Available from: [https://doi.org/10.1016/0093-934x\(90\)90105-p](https://doi.org/10.1016/0093-934x(90)90105-p).
 52. Monti G, Meletti S, Petersen RC. Emotion recognition in temporal lobe epilepsy: a systematic review. *Neurosci Biobehav Rev* [Internet]. 2015;55:280–93 Available from: <https://linkinghub.elsevier.com/retrieve/pii/S0149763415001359>.
 53. Pichon S, Kell CA. Affective and sensorimotor components of emotional prosody generation. *J Neurosci* [Internet]. 2013;33:1640–50. Available from: <https://doi.org/10.1523/jneurosci.3530-12.2013>.
 54. Ethofer T, Bartscher J, Wiethoff S, Bisch J, Schlipf S, Wildgruber D, et al. Functional responses and structural connections of cortical areas for processing faces and voices in the superior temporal sulcus. *Neuroimage* [Internet]. Elsevier BV. 2013;76:45–56. Available from <https://doi.org/10.1016/j.neuroimage.2013.02.064>.
 55. Gröne M, Dyck M, Koush Y, Bergert S, Mathiak KA, Alawi EM, et al. Upregulation of the rostral anterior cingulate cortex can alter the perception of emotions: fMRI-based neurofeedback at 3 and 7 T. *Brain Topogr* [Internet]. Springer Scie Business Media LLC. 2014;28:197–207. Available from <https://doi.org/10.1007/s10548-014-0384-4>.
 56. Kanske P, Kotz SA. Emotion speeds up conflict resolution: a new role for the ventral anterior cingulate cortex? *Cereb Cortex* [Internet]. 2010;21:911–9. Available from <https://doi.org/10.1093/cercor/bhq157>.
 57. Hervé P-Y, Razafimandimby A, Jobard G, Tzourio-Mazoyer N. A shared neural substrate for mentalizing and the affective component of sentence comprehension. *PLoS One* [Internet]. 2013;8:e54400. Available from <https://doi.org/10.1371/journal.pone.0054400>.
 58. Alaerts K, Woolley DG, Steyaert J, Di Martino A, Swinnen SP, Wenderoth N. Underconnectivity of the superior temporal sulcus predicts emotion recognition deficits in autism. *Soc Cogn Affect Neurosci* [Internet]. 2013;9:1589–600 Available from: <http://www.ncbi.nlm.nih.gov/pubmed/24078018>.
 59. Sliwinska MW, Pitcher D. TMS demonstrates that both right and left superior temporal sulci are important for facial expression recognition. *Neuroimage* [Internet]. 2018;183:394–400 Available from: <https://linkinghub.elsevier.com/retrieve/pii/S1053811918307237>.
 60. Corradi-Dell'Acqua C, Hofstetter C, Vuilleumier P. Cognitive and affective theory of mind share the same local patterns of activity in posterior temporal but not medial prefrontal cortex. *Soc Cogn Affect Neurosci* [Internet]. 2014;9:1175–84 Available from: <https://academic.oup.com/scan/article/9/8/1175/2375360>.
 61. Lupton MK, Strike L, Hansell NK, Wen W, Mather KA, Armstrong NJ, et al. The effect of increased genetic risk for Alzheimer's disease on hippocampal and amygdala volume. *Neurobiol Aging* [Internet]. 2016;40:68–77 Available from: <https://linkinghub.elsevier.com/retrieve/pii/S0197458015006399>.
 62. Rapcsak SZ. Face recognition. *Curr Neurol Neurosci Rep* [Internet]. 2019;19:–41. Available from <https://doi.org/10.1007/s11910-019-0960-9>.
 63. Guzmán-Vélez E, Warren DE, Feinstein JS, Bruss J, Tranel D. Dissociable contributions of amygdala and hippocampus to emotion and memory in patients with Alzheimer's disease. *Hippocampus* [Internet]. 2016;26:727–38. Available from <https://doi.org/10.1002/hipo.22554>.
 64. Hořínek D, Varjassyová A, Hort J. Magnetic resonance analysis of amygdalar volume in Alzheimer's disease. *Curr Opin Psychiatry* [Internet]. 2007;20:273–7. Ovid Technologies (Wolters Kluwer Health); . Available from. <https://doi.org/10.1097/yco.0b013e3280ebb613>.

Publisher's Note

Springer Nature remains neutral with regard to jurisdictional claims in published maps and institutional affiliations.

Ready to submit your research? Choose BMC and benefit from:

- fast, convenient online submission
- thorough peer review by experienced researchers in your field
- rapid publication on acceptance
- support for research data, including large and complex data types
- gold Open Access which fosters wider collaboration and increased citations
- maximum visibility for your research: over 100M website views per year

At BMC, research is always in progress.

Learn more biomedcentral.com/submissions



¹H-MRS metabolites and rate of β -amyloid accumulation on serial PET in clinically normal adults

OPEN

Zuzana Nedelska, MD
Scott A. Przybelski
Timothy G. Lesnick, MS
Christopher G. Schwarz,
PhD
Val J. Lowe, MD
Mary M. Machulda, PhD
Walter K. Kremers, PhD
Michelle M. Mielke, PhD
Rosebud O. Roberts, MB,
BCh, MS
Bradley F. Boeve, MD
David S. Knopman, MD
Ronald C. Petersen, MD,
PhD
Clifford R. Jack, Jr., MD
Kejal Kantarci, MD, MS

Correspondence to
Dr. Kantarci:
kantarci.kejal@mayo.edu

ABSTRACT

Objective: To assess whether noninvasive proton magnetic resonance spectroscopy (¹H-MRS) tissue metabolite measurements at baseline can predict an increase in the rate of β -amyloid (A β) accumulation on serial PET in clinically normal (CN) older adults.

Methods: Consecutive participants aged 60 years and older ($n = 594$) from the Mayo Clinic Study of Aging who were CN at baseline and who underwent ¹H-MRS from the posterior cingulate voxel and longitudinal ¹¹C-Pittsburgh compound B (PiB)-PET were included. The rate of A β accumulation by serial cortical PiB standardized uptake value ratios was estimated as a function of baseline ¹H-MRS metabolite ratios and time using mixed-effect models adjusted for age, sex, and APOE $\epsilon 4$. Effect of APOE $\epsilon 4$ on the relationship between baseline MRS and an increased rate of A β accumulation was also assessed.

Results: Among all participants, a higher myo-inositol (mI)/creatinine ($p = 0.011$) and a lower *N*-acetylaspartate/ml ($p = 0.006$) at baseline were associated with an increased A β accumulation over time after adjusting for age, sex, and APOE $\epsilon 4$. APOE $\epsilon 4$ did not modify the association of baseline ¹H-MRS metabolite ratios and rate of A β accumulation. However, APOE $\epsilon 4$ carriers accumulated A β faster than noncarriers regardless of the baseline A β load ($p = 0.001$).

Conclusion: Among CN older adults, early metabolic alterations on ¹H-MRS and APOE $\epsilon 4$ status are independently associated with an increased rate of A β accumulation. Our findings could have important implications for early diagnosis and identification of individuals for secondary prevention trials, because an increased rate of A β accumulation in CN older adults may confer a higher risk for cognitive decline and mild cognitive impairment. *Neurology*® 2017;89:1391-1399

GLOSSARY

A β = β -amyloid; **AD** = Alzheimer disease; **Cho** = choline; **CN** = clinically normal; **Cr** = creatine; **MCI** = mild cognitive impairment; **mI** = myo-inositol; **MPRAGE** = magnetization-prepared rapid acquisition gradient echo; **MRS** = magnetic resonance spectroscopy; **NAA** = *N*-acetylaspartate; **PC** = posterior cingulate; **PiB** = Pittsburgh compound B; **SUVR** = standardized uptake value ratio; **WM** = white matter.

Twenty to forty percent of clinically normal (CN) older adults have significant β -amyloid (A β) load on cross-sectional PET.¹⁻³ An increased rate of A β accumulation may put them at a higher risk for cognitive decline⁴ and mild cognitive impairment (MCI).⁵ Cost-effective and noninvasive biomarkers that can predict a further increase in A β accumulation over time are necessary for better identification of at-risk individuals who may benefit from preventive and disease-modifying strategies.

In CN older adults, elevated myo-inositol (mI), a marker of glial activation, has been associated with a higher A β load on PET,^{6,7} lower CSF A β_{1-42} ,⁷ and a higher A β density in an autopsy-confirmed cohort.⁸ Moreover, an elevated mI has been found in APOE $\epsilon 4$ carriers with no evidence of A β deposition on PET.⁷ Although the mechanistic relationship between APOE $\epsilon 4$ and elevated mI is unclear, it has been suggested that APOE $\epsilon 4$ enhances glial activation and

Supplemental data
at Neurology.org

From the Departments of Radiology (Z.N., C.G.S., V.J.L., C.R.J., K.K.), Health Sciences Research (S.A.P., T.G.L., W.K.K., M.M.M., R.O.R.), Psychiatry and Psychology (M.M.M.), and Neurology (M.M.M., R.O.R., B.F.B., D.S.K., R.C.P.), Mayo Clinic, Rochester, MN; and Department of Neurology (Z.N.), Charles University, Second Faculty of Medicine and Motol University Hospital, Prague, Czech Republic.

Go to Neurology.org for full disclosures. Funding information and disclosures deemed relevant by the authors, if any, are provided at the end of the article. The Article Processing Charge was funded by the Department of Radiology, Mayo Clinic Rochester, MN.

This is an open access article distributed under the terms of the Creative Commons Attribution-NonCommercial-NoDerivatives License 4.0 (CC BY-NC-ND), which permits downloading and sharing the work provided it is properly cited. The work cannot be changed in any way or used commercially without permission from the journal.

modulates the relationship between A β and glial activation.^{9–11} However, the *APOE* $\epsilon 4$ effect on magnetic resonance spectroscopy (MRS) metabolite levels among CN elderly has been equivocal.^{7,9,12} Further, all of the studies examining MRS, A β -related pathology, and *APOE* $\epsilon 4$ were cross-sectional.

Our objective was to investigate the association of MRS metabolite ratios from a posterior cingulate (PC) gyrus voxel at baseline with the change in A β accumulation over time on serial amyloid PET in CN older adults drawn from a population-based sample. A secondary objective was to assess whether *APOE* $\epsilon 4$ modifies the relationship between MRS metabolites and the rate of A β accumulation.

METHODS Participants. Consecutive participants aged ≥ 60 years were drawn from the ongoing population-based, longitudinal Mayo Clinic Study of Aging,^{13,14} between January 2006 and May 2016. To be included in this imaging study, participants were required to be CN at baseline when MRS and amyloid PET were performed and have at least one follow-up amyloid PET. The diagnostic process and criteria for being clinically normal are described in appendix e-1 at Neurology.org. A total of 594 participants meeting inclusion criteria and passing image quality control were included in the analyses. The final cohort flowchart is provided as figure e-1.

Blood was collected to determine the *APOE* $\epsilon 4$ noncarrier or carrier status.

Change in A β accumulation over time was assessed using all available follow-up amyloid PET examinations on an individual. Consecutive participants had 1 (n = 416; 70%), 2 (n = 144; 24.6%), 3 (n = 29; 4.8%), or 4 (n = 5; 0.6%) follow-up PET scans performed approximately every 15 months.

Standard protocol approvals, registrations, and participant consents. The Mayo Clinic and Olmsted Medical Center institutional review boards approved the study. Every participant provided written informed consent.

¹H-MRS and MRI studies. Baseline MRS and MRI were performed at 3T using an 8-channel phase array coil (GE Healthcare, Waukesha, WI). A 3D high-resolution T1-weighted magnetization-prepared rapid acquisition gradient echo (MPRAGE) scan was acquired for anatomic segmentation and region labeling of PET and localization of ¹H-MRS voxel.

A point-resolved spectroscopic sequence was acquired with repetition time/echo time 2,000/30 ms with a single voxel of $2 \times 2 \times 2$ cm³ placed in the midsagittal MPRAGE image including right and left PC gyri and inferior precunei. Although the transverse relaxation time of *N*-acetylaspartate (NAA) and choline (Cho) is longer than mL, a single short echo time of 30 ms allowed measurements of all 3 metabolites in participants within the Alzheimer disease (AD) continuum.¹⁵ Metabolites were quantified using the automated proton brain examination/single-voxel package, and their intensities were scaled by creatine (Cr), a standard reference. Individual voxel placement and magnetic resonance spectra were visually evaluated by a trained image analyst for quality control. A trained image analyst reviewed the location of the MRS voxel and evaluated water suppression, baseline distortions, or lipid

contamination. Voxels that did not include the PC location according to the predetermined anatomic landmarks and spectra with poor water suppression, lipid contamination, or baseline distortions failed quality control and were excluded. Although the spectral fit was not measured quantitatively, the quantification of metabolite ratios failed if the spectral fit was poor.

PET studies. ¹¹C-Pittsburgh compound B (PiB)-PET/CT images were acquired using a GE scanner (GE Healthcare). Participants were injected with the PiB tracer (average activity 625 MBq; range 385–723) and a low-dose CT scan was acquired for attenuation correction. Forty to sixty minutes postinjection, a 20-minute dynamic PET scan consisting of four 5-minute frames was acquired. These 4 frames were averaged to create a single statistical image.

Cortical A β retention for each PiB image was calculated as a global cortical standardized uptake value ratio (SUVR).¹⁶ For measuring change over time in PiB uptake, we used a previously published SUVR measurement technique, which was demonstrated to improve reliability and plausibility for serial measurements compared to traditional cross-sectional approaches.¹⁷ This technique uses a reference region of eroded supratentorial white matter (WM) segmented using MRI, combined with the whole cerebellum and pons. In brief, each PiB scan is rigidly registered to its corresponding T1-weighted MRI. Each MRI is segmented using SPM12¹⁸ with an in-house population-specific template and several population-specific measure alterations previously described.¹⁹ These segmentations are used for locating supratentorial WM for the reference region.

The target region and the cerebellar/pons regions included as part of the reference region were each localized using a corresponding in-house atlas¹⁹ that was nonlinearly registered to each corresponding MRI using the advanced normalization tools symmetric normalization algorithm,²⁰ resampled using nearest-neighbor interpolation, and refined using the tissue segmentations described above. Automated registration and segmentation steps were each visually confirmed for acceptable quality. SUVRs were then calculated from PiB scans as the mean of all voxels in the target region normalized by the mean of all voxels in the reference region.

Statistical analysis. We used mixed-effects models to model repeated PiB SUVR values as a function of baseline MRS metabolite ratios for all participants. We incorporated random slopes and intercepts for each participant (estimating the correlation between the slopes and intercepts). The primary predictor of interest involved an interaction of baseline MRS ratio with time, because we were interested in longitudinal change in A β accumulation. Models included the nested time and MRS ratio at baseline as is proper for an evaluation of interaction with time. A significant interaction of MRS ratio at baseline with time would indicate that the increase in the rate of A β accumulation on serial PET depends upon the value of the MRS ratio at baseline. A significant association between baseline MRS ratio and A β accumulation in the model would indicate that the MRS ratio was associated with consistently higher A β accumulation across all serial PET measurements in a given participant but not with an increased rate of accumulation. The models also accounted for effects of baseline age, sex, and *APOE* $\epsilon 4$ status. We computed the 3-way interactions of baseline MRS ratios and *APOE* $\epsilon 4$ status with time to assess whether *APOE* $\epsilon 4$ modifies the relationship between baseline metabolite MRS ratios and change over time in A β accumulation on serial PET.

Analyses were performed using SAS version 9.4 (SAS Institute, Cary, NC) and R statistical software version 3.1.1 (R-

Table 1 Participants' (n = 594) characteristics at baseline

| Characteristics | Values |
|-----------------------------------|---------------------------|
| Age, y | 74.4 (7.3) |
| Male | 343 (58) |
| APOE ϵ 4 carrier | 169 (29) |
| Education, y | 14.73 (2.70) |
| Short test of mental status | 35.06 (2.24) ^a |
| NAA/Cr | 1.68 (0.11) |
| Cho/Cr | 0.63 (0.06) |
| mI/Cr | 0.51 (0.06) |
| NAA/ml | 3.35 (0.57) |
| PiB SUVR, mean (SD) | 1.50 (0.33) |
| PiB SUVR, median (range) | 1.37 (1.18-1.93) |
| Follow-up time, y, mean (SD) | 3.26 (1.50) |
| Follow-up time, y, median (range) | 2.67 (1-9.17) |

Abbreviations: Cho = choline; Cr = creatine; ml = myo-inositol; NAA = N-acetylaspartate; PiB = ¹¹C-Pittsburgh compound B; SUVR = cortical standardized uptake value ratio. APOE ϵ 4 status was missing in 1 and short test of mental status in 8 participants. Mean (SD) is listed for continuous variables unless otherwise noted and counts and proportions (%) are listed for categorical variables.

^aMaximum score is 38 points.⁴⁰

project.org) with 2-sided significance set at α 0.05 type I error rate. Because we were interested in the association of individual metabolite ratios with serial PiB measurements, and at this stage did not want to inflate type II error by declaring true associations null, we did not adjust for multiple comparisons.^{21,22}

RESULTS Participants' characteristics at baseline are listed in table 1. Although a higher mI/Cr at baseline was only borderline associated with a higher A β load across all serial PET of a given participant ($p = 0.06$), it is more important that it was significantly associated with a greater increase in rate of A β accumulation ($p = 0.011$), adjusting for baseline age, sex, APOE ϵ 4, and the interaction between APOE ϵ 4 and age (table 2). Similarly, a lower baseline NAA/ml was associated with consistently higher A β load across all serial PETs of a given participant ($p = 0.007$), but moreover, it was associated with an increased rate of A β accumulation ($p = 0.006$), adjusting for the same covariates (table 2). Figure 1 illustrates the estimated increase in rate of A β accumulation by baseline MRS ratios and by APOE ϵ 4 with specific estimated values shift according to age, sex, and APOE ϵ 4. Figure 2 shows the 3 individuals from the current cohort, their magnetic resonance spectra at baseline, and associated A β load at baseline and at follow-up.

Mixed-effect models for the remaining metabolite ratios showed that a lower baseline NAA/Cr was associated with consistently higher A β load across all

serial PET examinations in a given participant ($p = 0.02$; table e-1). However, NAA/Cr was not associated with an increased rate of A β accumulation ($p = 0.18$; figure e-2). Cho/Cr was associated neither with A β load across serial PET ($p = 0.28$) nor with rate of A β accumulation ($p = 0.47$; table e-1).

APOE ϵ 4 was associated with consistently higher A β load across all serial PiB SUVR measurements ($p < 0.001$). Furthermore, the interaction of APOE ϵ 4 with time ($p < 0.001$) was associated with an increased rate of A β accumulation, taking into account baseline age, sex, and time with baseline age interaction (table 3, model 1; figure 1). However, an accelerated rate of A β accumulation in APOE ϵ 4 carriers compared to noncarriers may be because APOE ϵ 4 carriers have higher baseline A β load.¹⁶ Nevertheless, when we compared rates of A β accumulation between a subset of our APOE ϵ 4 carriers (n = 149) and noncarriers matched on age, sex, and baseline A β load to a subset of our noncarriers (n = 149), the interaction between APOE ϵ 4 and time remained significant ($p = 0.001$; table 3, model 2) using mixed-effect model with a random block design to account for matching. Therefore, APOE ϵ 4 carriers accumulated A β at an accelerated rate compared to APOE ϵ 4 noncarriers even when they had a similar baseline A β load (figure 1).

Finally, we assessed whether APOE ϵ 4 status modified the relationship between the baseline metabolites and increased rate of A β accumulation using a 3-way interaction of baseline metabolites, APOE ϵ 4, and time among all. None of these interactions was significant, including for mI/Cr \times APOE ϵ 4 \times time ($p = 0.35$) and for NAA/ml \times APOE ϵ 4 \times time ($p = 0.90$). Therefore, longitudinally, APOE ϵ 4 status did not modify the relationship between MRS metabolites and rate of A β accumulation on serial PET.

DISCUSSION In this large cohort of CN older adults, mean age of 74, drawn from a population-based sample, we demonstrated that noninvasive and inexpensive baseline MRS metabolite levels are associated with an increased rate of A β accumulation on serial PET. Lower NAA/ml and higher mI/Cr at baseline were associated with an increased rate of A β accumulation taking into account age at baseline, sex, and APOE ϵ 4 status. APOE ϵ 4 carriers accumulated A β faster than noncarriers. APOE ϵ 4 status did not alter the relationship between baseline metabolite levels and rate of A β accumulation and both MRS metabolites and APOE ϵ 4 likely are independently associated with an increased A β accumulation over time.

An elevated mI/Cr has been consistently associated with biomarkers of elevated A β in CN adults cross-sectionally.^{7,8,23,6} Moreover, in the transgenic

Table 2 Estimated rate of β -amyloid ($A\beta$) accumulation by baseline myo-inositol (mI)/creatinine (Cr) and N-acetylaspartate (NAA)/mI ratios

| | Estimate (SE) | p Value |
|--|----------------|---------|
| mI/Cr with time interaction as primary predictor | | |
| Intercept | -0.863 (0.098) | <0.001 |
| Time, y | -0.052 (0.009) | <0.001 |
| Baseline age | 0.008 (0.001) | <0.001 |
| Male | 0.033 (0.014) | 0.017 |
| APOE ϵ 4 | 0.119 (0.016) | <0.001 |
| Baseline mI/Cr ratio | 0.223 (0.016) | 0.06 |
| APOE ϵ 4 with time interaction | 0.011 (0.002) | <0.001 |
| Baseline age with time interaction | 0.001 (0.000) | <0.001 |
| Baseline mI/Cr ratio with time interaction | 0.029 (0.011) | 0.011 |
| NAA/mI with time interaction as primary predictor | | |
| Intercept | -0.628 (0.087) | <0.001 |
| Time, y | -0.024 (0.009) | 0.003 |
| Baseline age | 0.008 (0.001) | <0.001 |
| Male | 0.034 (0.014) | 0.013 |
| APOE ϵ 4 | 0.118 (0.016) | <0.001 |
| Baseline NAA/mI ratio | -0.035 (0.013) | 0.007 |
| APOE ϵ 4 with time interaction | 0.011 (0.002) | <0.001 |
| Baseline age with time interaction | 0.001 (0.000) | <0.001 |
| Baseline NAA/mI ratio with time interaction | -0.003 (0.001) | 0.006 |

Coefficient estimates with their SE and p values are reported for the rate of $A\beta$ accumulation as the response. The predictor of primary interest is an interaction of baseline mI/Cr ratio with time and then baseline NAA/mI ratio with time, which are 2 metabolite ratios significantly associated with the change (increase and decrease) in rate of $A\beta$ accumulation. The interaction with time is illustrated in figure 1. The individual effects of other variables that contribute to the model fit are also shown.

murine AD model, a passive immunization with anti- $A\beta$ antibodies lessened the mI/Cr in the treatment arm compared to placebo.²⁴ In the current longitudinal cohort, we demonstrated findings that suggest an elevated mI/Cr as a predictor of an accelerated $A\beta$ accumulation over time on serial PET.

NAA/Cr ratio, a marker of neuronal viability and synaptic integrity, is reduced in participants with MCI²⁵ and AD,^{15,26,27} but not in CN older adults, suggesting that a decline in NAA/Cr is preceded by an increased mI/Cr during the course of AD. In line with this, an autopsy-confirmed study⁸ demonstrated an association between a lower NAA/Cr and a higher burden of tau-related pathology and loss of synaptic integrity that is believed to follow the changes in $A\beta$ biomarkers during the course of AD.²⁸ Accordingly, we observed that a lower NAA/Cr was associated with consistently higher $A\beta$ load across all serial PET examinations of a given participant but not with an increased rate of $A\beta$ accumulation. In addition to mI/Cr, significant association was observed between a lower baseline NAA/mI and an increased rate of $A\beta$

accumulation. Lower NAA/mI has predicted progression from CN to MCI in a population-based cohort²⁹ and only a lower NAA/mI among routinely examined MRS ratios correlated with both greater tau and $A\beta$ burden at autopsy.⁸ The current study supports the composite NAA/mI ratio as a marker of increased longitudinal $A\beta$ accumulation in CN older adults.

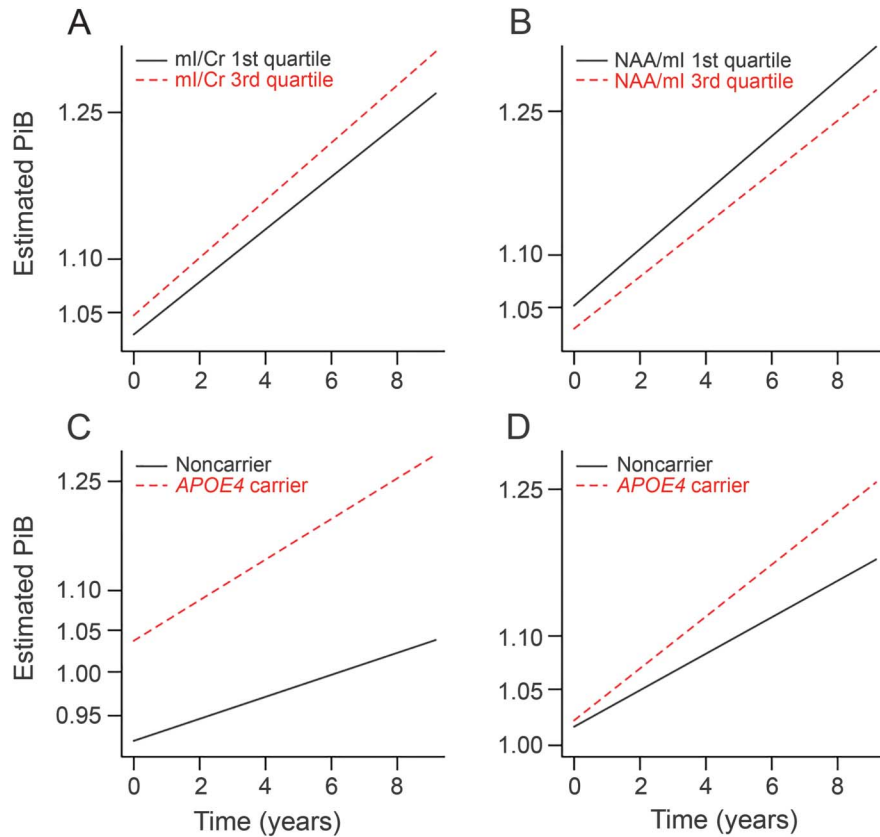
Although Cho/Cr has been associated with a higher $A\beta$ load on PET^{7,29} and a worse cognitive performance in CN older adults,^{6,9} we did not observe an association of Cho/Cr and rate of $A\beta$ accumulation. No association was found between Cho/Cr and AD-related pathology in an autopsy-confirmed cohort,⁸ and the significance of Cho/Cr during the progression of AD remains unclear.

APOE ϵ 4 status did not modify the relationship between baseline MRS metabolites and rate of $A\beta$ accumulation on serial PET. Instead, APOE ϵ 4 was independently associated with an accelerated $A\beta$ accumulation. Whereas the relationship between a higher $A\beta$ load in APOE ϵ 4 carriers has been well-established cross-sectionally,^{3,30,31} the effect of APOE ϵ 4 status on longitudinal $A\beta$ accumulation in CN older adults has not been clarified, likely due to small sample sizes, various PiB uptake measurement approaches, and different interpretation of contributing effects of baseline $A\beta$ load, age, sex, and number of available follow-up PET scans.^{5,32-34} Moreover, APOE ϵ 4 effect on longitudinal $A\beta$ accumulation may be mediated by baseline $A\beta$ load,¹⁶ which is higher in APOE ϵ 4 carriers than noncarriers. Higher baseline $A\beta$ load is a risk factor for increased $A\beta$ accumulation over time.¹⁶ However, our finding of longitudinally accelerated $A\beta$ accumulation in APOE ϵ 4 carriers with similar baseline $A\beta$ load to APOE ϵ 4 noncarriers indicates that APOE ϵ 4 carriers accumulate $A\beta$ faster than noncarriers, regardless of baseline $A\beta$ levels.

A cross-sectional study by Voevodskaya et al.⁷ demonstrated that already cognitively normal APOE ϵ 4 carriers with still normal $A\beta$ biomarker levels had elevated mI/Cr. It was suggested that mI/Cr may be an early biomarker of $A\beta$ accumulation.³⁵ Our findings support this hypothesis by showing that an elevated mI/Cr ratio in older adults is associated with an increased rate of $A\beta$ accumulation. In addition, we showed that the relationship between MRS metabolite alterations and rates of $A\beta$ accumulation is independent of APOE ϵ 4 status. Taken together, these findings suggest that cross-sectional MRS metabolite alterations may occur in APOE ϵ 4 carriers because of their risk of increased $A\beta$ accumulation over time.

Higher baseline $A\beta$ load increases the risk of cognitive decline over time in CN older adults.^{34,36} However, a recent cut point for $A\beta$ positivity on PET in CN older adults³⁷ was based on repeated

Figure 1 Estimated rate of β -amyloid ($A\beta$) accumulation on serial PET by baseline magnetic resonance spectroscopy (MRS) metabolite ratios and *APOE* $\epsilon 4$ status



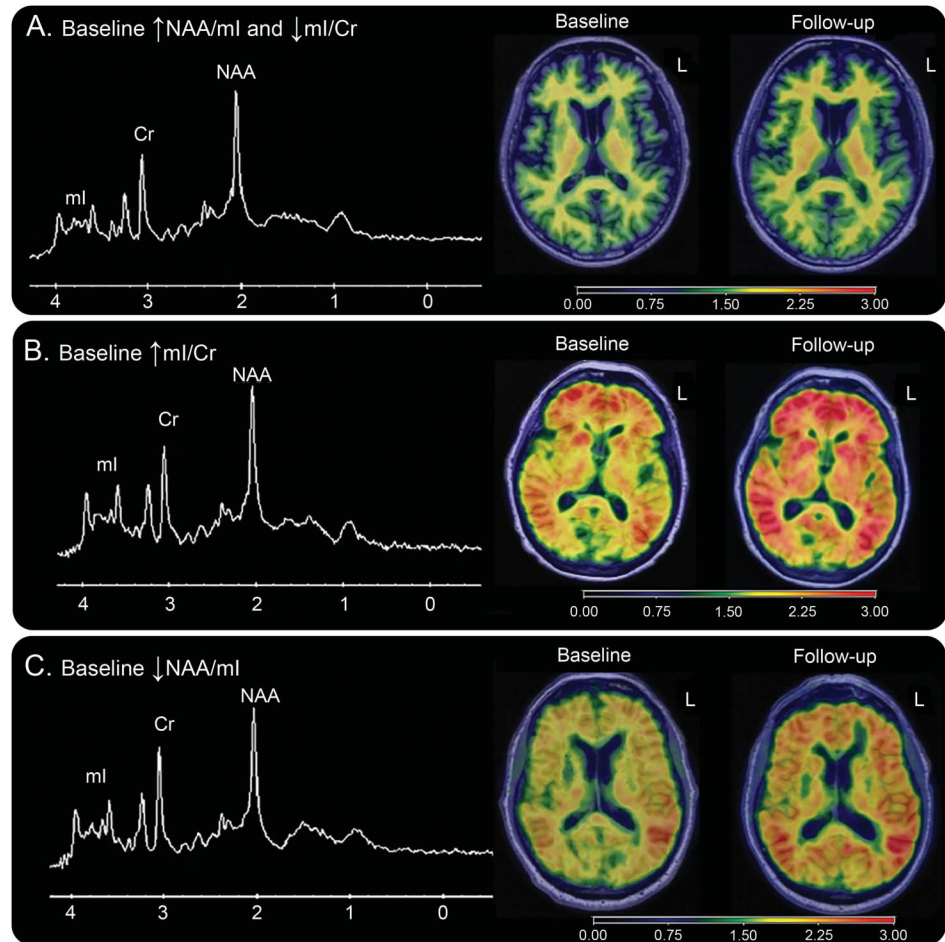
The estimates for the rate of $A\beta$ accumulation for a 75-year-old clinically normal man from the Mayo Clinic Study of Aging are shown. His rate of $A\beta$ accumulation is estimated using an interaction between his baseline MRS metabolite ratios and time as primary predictor. The 1st and 3rd quartiles of MRS ratios are based on the models in table 2. (A) With a higher baseline myo-inositol (mI)/creatine (Cr) ratio, rate of $A\beta$ accumulation increases more than it does with lower baseline mI/Cr ratio. Interaction of baseline MRS metabolites with time is visualized by gradually diverging slopes between quartiles. (B) A lower baseline *N*-acetylaspartate (NAA)/ml ratio is associated with an increase in rate of $A\beta$ accumulation, a negative association represented by inverse order of quartiles. (C) The rate of $A\beta$ accumulation is compared between a 75-year-old male *APOE* $\epsilon 4$ noncarrier and an *APOE* $\epsilon 4$ carrier of the same age and sex (table 3). The carrier slope is increasing and diverging from the noncarrier slope with time. However, note an obvious difference in baseline $A\beta$ load between the *APOE* $\epsilon 4$ carrier and noncarrier, and because of this $A\beta$ accumulation might be faster in the *APOE* $\epsilon 4$ carrier. (D) The difference in rate of $A\beta$ accumulation is shown between the *APOE* $\epsilon 4$ carrier matched on age, sex, and baseline $A\beta$ load to the noncarrier. The *APOE* $\epsilon 4$ carrier accumulates $A\beta$ faster, regardless of baseline $A\beta$ load. Note that the baseline Pittsburgh compound B (PiB) standardized uptake value ratio (SUVR) is derived using the serial PiB SUVR measurement approach.

measurements of $A\beta$ accumulation. Using repeated measurements, the reliable worsening in $A\beta$ accumulation was identified and served as cut point. Moreover, a few studies demonstrated that an increased rate of $A\beta$ accumulation on PET is associated with cognitive decline over time in CN⁴ and progression to MCI.⁵ Therefore identifying those who accumulate $A\beta$ faster over time provides additional and valuable information on at-risk individuals beyond cross-sectional measurements, which do not provide any information on disease progression. However, so far, the biomarkers that would identify such individuals have been scarce. Identifying those who accumulate $A\beta$ faster can have important implications for early diagnosis and selecting at-risk individuals for secondary preventive interventions targeted to reduce

$A\beta$ accumulation rate. It is possible that interventions might be more effective in those who are still clinically normal but on the way to higher rates of $A\beta$ accumulation. Our current findings suggest that both MRS metabolite alterations and *APOE* $\epsilon 4$ status independently are associated with accelerated rates of $A\beta$ accumulation.

We did not dichotomize the participants as amyloid-positive or -negative by a cut point, although this popular approach may have practical advantages. Instead, we treated serial PiB SUVR as continuous measures that allowed us to include the CN participants with the full range of PiB SUVR values. Cut point may create a gray zone where sub-threshold but important relationships might be obscured. For example, the biological difference

Figure 2 Magnetic resonance spectra and amyloid PET at baseline and follow-up



These are 3 individuals from the Mayo Clinic Study of Aging. (A) A 76-year-old woman with high N-acetylaspartate (NAA)/myo-inositol (ml) ratio 3.25 and low ml/creatinine (Cr) ratio 0.35 and minimal A β load (Pittsburgh compound B [PiB] standardized uptake value ratio [SUVR] 1.29) at baseline and minimal progression on follow-up 32 months later (PiB SUVR 1.30). (B) A 78-year-old man with a high ml/Cr ratio 0.63 and higher amyloid load at baseline (PiB SUVR 1.40) further shows a considerable progression on follow-up PET (PiB SUVR 1.82) 45 months later. (C) A 76-year-old woman with low NAA/ml ratio 2.74 with baseline PiB SUVR 1.35 shows progression on PET (PiB SUVR 1.58) 30 months later.

between those participants who are close to the cut point, but arbitrarily fall into opposite groups, or a minor longitudinal change that moves a participant from one group to another by a given cut point might be negligible. On the contrary, a large difference in PiB SUVR among 2 participants who are in the same PiB group and a large change in PiB SUVR in a participant over time without a change in PiB group designation by cut point may be very meaningful. Finally, the cut point for amyloid positivity for longitudinal amyloid measurements remains to be established.

Strengths of this study are the large sample of individuals drawn from a single population with serial amyloid PET including a large subset of *APOE* ϵ 4 carriers matched to noncarriers on demographics and baseline A β load. In this cohort, A β accumulation over time was measured using a modified reference region that has demonstrated an improved reliability

and plausibility for serial measurements compared to traditional cross-sectional approaches.¹⁷

The limitations of our study are similar to those of other studies using participants drawn from a population-based sample, such as the presence of various subthreshold pathologies in CN older adults, which may increase the variability of MRS metabolite measurements and weaken some of the studied relationships. However, the levels of MRS ratios in the current cohort of CN older adults were consistent with previous studies by others and by our group,^{9,29,38} including an autopsy-confirmed study on MRS correlates of A β accumulation.⁸ Our proportion of CN *APOE* ϵ 4 carriers (29%) was similar to previous reports.^{5,32,34} However, we cannot exclude the potential for participation or survival bias because more educated and generally healthier participants may be more willing to participate longitudinally in imaging studies,²⁹ and our findings may not be

Table 3 Estimated rate of β -amyloid ($A\beta$) accumulation by $APOE \epsilon 4$ status

| | Estimate (SE) | p Value |
|---|----------------|-------------------|
| Model 1: $APOE \epsilon 4$ as primary predictor in the whole cohort | | |
| Intercept | -0.747 (0.076) | <0.001 |
| Time, y | -0.037 (0.008) | <0.001 |
| Baseline age | 0.008 (0.001) | <0.001 |
| Male | 0.034 (0.014) | 0.014 |
| $APOE \epsilon 4$ | 0.117 (0.016) | <0.001 |
| Baseline age with time interaction | 0.001 (0.000) | <0.001 |
| $APOE \epsilon 4$ with time interaction | 0.011 (0.002) | <0.001 |
| Model 2: $APOE \epsilon 4$ as primary predictor in subset of $APOE \epsilon 4$ carriers matched to noncarriers | | |
| Intercept | -0.036 (0.018) | 0.043 |
| Time, y | 0.017 (0.002) | <0.001 |
| $APOE \epsilon 4$ | 0.004 (0.004) | 0.34 ^a |
| $APOE \epsilon 4$ with time interaction | 0.006 (0.002) | 0.001 |

Coefficient estimates with their SE and p values are reported for the rate of $A\beta$ accumulation on serial PET as response in the whole cohort (n = 594). The effects of individual variables contributing to the model fit are shown. Model 1 shows that $APOE \epsilon 4$ status is associated with a consistently higher $A\beta$ load across all serial PET in a given participant. However, it is an interaction of $APOE \epsilon 4$ status with time, which is associated with an increased rate of $A\beta$ accumulation (visualized in figure 1). Model 2 compares estimated rate of $A\beta$ accumulation between a subset of our $APOE \epsilon 4$ carriers (n = 149) matched on baseline age, sex, and baseline $A\beta$ load to noncarriers (n = 149), showing that $APOE \epsilon 4$ carriers accumulate $A\beta$ faster than noncarriers.

^aNote this is a matched analysis.

entirely generalizable to other populations of CN adults. Finally, an inclusion of those ≥ 60 years old does not allow studying the relationship between rate of $A\beta$ accumulation and MRS metabolites at an even earlier stage of AD pathophysiology. However, younger adults do not show sufficient increase in rate of $A\beta$ accumulation to model longitudinal process. Increase in the rate of $A\beta$ accumulation on serial PET in those younger than 60 is minimal^{33,39} and limited in capturing potential associations with baseline MRS metabolites.

MRS is a noninvasive and inexpensive technique that can be part of a standard clinical magnetic resonance examination, including in clinical trials. However, for these purposes, the standardization and optimization of multicenter MRS studies are necessary. Moreover, a longitudinal investigation of serial MRS metabolites to estimate progression of $A\beta$ in participants within the AD continuum would provide additional information on the temporal ordering between the alterations in MRS metabolites and $A\beta$ pathophysiology.

AUTHOR CONTRIBUTIONS

Dr. Nedelska: study concept and design, analysis and interpretation of the data, drafting the manuscript. S.A. Przybelski: design and analysis or interpretation of the data, critical revision of the manuscript for important intellectual content. T. Lesnick: design and analysis or interpretation

of the data, drafting manuscript, critical revision of the manuscript for important intellectual content. Dr. Lowe: acquisition of data, critical revision of the manuscript for important intellectual content. Dr. Schwarz: data analysis, critical revision of the manuscript for important intellectual content. Dr. Machulda: acquisition of data, critical revision of the manuscript for important intellectual content. Dr. Mielke: acquisition of data, critical revision of the manuscript for important intellectual content. Dr. Roberts: acquisition of data, critical revision of the manuscript for important intellectual content. Dr. Kremers: analysis or interpretation of the data, critical revision of the manuscript for important intellectual content. Dr. Boeve: acquisition of data, critical revision of the manuscript for important intellectual content. Dr. Knopman: acquisition of data, critical revision of the manuscript for important intellectual content. Dr. Petersen: acquisition of data, critical revision of the manuscript for important intellectual content. Dr. Jack: acquisition of data, critical revision of the manuscript for important intellectual content. Dr. Kantarci: study concept and design, acquisition of data, interpretation of the data, drafting the manuscript, critical revision of the manuscript for important intellectual content.

STUDY FUNDING

NIH (R01-AG040042, R01-AG11378, P50-AG16574, U01-AG006786, AG034676, C06-RR018898), Gerald A. and Henrietta Rauenhorst Foundation, Mangurian Foundation, and the Robert H. and Clarice Smith and Abigail Van Buren Alzheimer's Disease Research Program.

DISCLOSURE

Z. Nedelska was supported by a joint Research Fellowship 2016 provided by the International Brain Research Organization and the International Society for Neurochemistry. S. Przybelski, T. Lesnick, and C. Schwarz report no disclosures relevant to the manuscript. V. Lowe is a consultant for Bayer Schering Pharma and receives research support from GE Healthcare, Siemens Molecular Imaging, AVID Radiopharmaceuticals, the NIH (National Institute on Aging [NIA], National Cancer Institute), the Elsie and Marvin Dekelboum Family Foundation, the Minnesota Partnership for Biotechnology and Medical Genomics, and the Leukemia & Lymphoma Society. M. Machulda is funded by the NIH. M. Mielke receives research support from the NIH/NIA and unrestricted research grants from Biogen. R. Roberts receives research support from the NIH/NIA and from Abbott Research Laboratories. W. Kremers is funded by the NIH and has received research funding from AstraZeneca and Biogen. B. Boeve has served as an investigator for clinical trials sponsored by GE Healthcare, FORUM Pharmaceuticals, C2N Diagnostics, and Axovant; receives royalties from the publication of *Behavioral Neurology of Dementia* (Cambridge Medicine, 2009); serves on the Scientific Advisory Board of the Tau Consortium; and receives research support from the NIH (U01-AG045390, U54-NS092089, P50-AG016574, U01-AG006786, R01-AG041797), the Mayo Clinic Dorothy and Harry T. Mangurian Jr. Lewy Body Dementia Program, and the Little Family Foundation. D. Knopman served as Deputy Editor for *Neurology*[®], served on a Data Safety Monitoring Board for Lilly Pharmaceuticals, serves on a Data Safety Monitoring Board for Lundbeck Pharmaceuticals and for the DIAN study, served as a consultant to TauRx Pharmaceuticals ending in November 2012, was an investigator in clinical trials sponsored by Baxter and Elan Pharmaceuticals in the last 2 years, is currently an investigator in a clinical trial sponsored by TauRx, and receives research support from the NIH. R. Petersen serves on scientific advisory boards for Pfizer, Elan Pharmaceuticals, Wyeth Pharmaceuticals, and GE Healthcare; receives royalties from the publication of *Mild Cognitive Impairment* (Oxford University Press, 2003); and receives research support from the NIH/NIA (P50-AG16574 [PI] and U01-AG006786 [PI], R01-AG11378 [Co-I], and U01-24904 [Co-I]). C. Jack serves as a consultant for Janssen, Bristol-Meyer-Squibb, General Electric, and Johnson & Johnson; is involved in clinical trials sponsored by Allon and Baxter, Inc.; and receives research support from Pfizer, Inc., the NIA (AG11378 [PI], P50-AG16574 [Co-I], and U01-AG024904-01 [Co-I]), and the Alexander Family Alzheimer's Disease Research Fellowship of the Mayo Foundation. K. Kantarci serves on the Data Safety Monitoring Board for Takeda Global Research & Development Center,

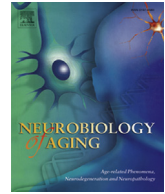
Inc., and data monitoring boards of Pfizer and Janssen Alzheimer Immunotherapy, and is funded by the NIH (R01-AG040042 [PI], R21-NS066147 [PI], P50-AG44170/Project 2 [PI], P50-AG16574/Project 1 [PI], and R01-AG11378 [Co-I]). Go to Neurology.org for full disclosures.

Received March 21, 2017. Accepted in final form July 5, 2017.

REFERENCES

1. Jansen WJ, Ossenkuppele R, Knol DL, et al. Prevalence of cerebral amyloid pathology in persons without dementia: a meta-analysis. *JAMA* 2015;313:1924–1938.
2. Jack CR Jr, Wiste HJ, Weigand SD, et al. Age-specific population frequencies of cerebral beta-amyloidosis and neurodegeneration among people with normal cognitive function aged 50–89 years: a cross-sectional study. *Lancet Neurol* 2014;13:997–1005.
3. Rowe CC, Ellis KA, Rimajova M, et al. Amyloid imaging results from the Australian Imaging, Biomarkers and Lifestyle (AIBL) study of aging. *Neurobiol Aging* 2010;31:1275–1283.
4. Leal SL, Landau SM, Bell RK, Jagust WJ. Hippocampal activation is associated with longitudinal amyloid accumulation and cognitive decline. *Elife* 2017;6:e22978.
5. Villemagne VL, Pike KE, Chetelat G, et al. Longitudinal assessment of abeta and cognition in aging and Alzheimer disease. *Ann Neurol* 2011;69:181–192.
6. Kantarci K, Lowe V, Przybelski SA, et al. Magnetic resonance spectroscopy, beta-amyloid load, and cognition in a population-based sample of cognitively normal older adults. *Neurology* 2011;77:951–958.
7. Voevodskaya O, Sundgren PC, Strandberg O, et al. Myo-inositol changes precede amyloid pathology and relate to APOE genotype in Alzheimer disease. *Neurology* 2016;86:1754–1761.
8. Murray ME, Przybelski SA, Lesnick TG, et al. Early Alzheimer's disease neuropathology detected by proton MR spectroscopy. *J Neurosci* 2014;34:16247–16255.
9. Gomar JJ, Gordon ML, Dickinson D, et al. APOE genotype modulates proton magnetic resonance spectroscopy metabolites in the aging brain. *Biol Psychiatry* 2014;75:686–692.
10. Ringman JM, Elashoff D, Geschwind DH, et al. Plasma signaling proteins in persons at genetic risk for Alzheimer disease: influence of APOE genotype. *Arch Neurol* 2012;69:757–764.
11. Gispert JD, Monte GC, Suarez-Calvet M, et al. The APOE epsilon4 genotype modulates CSF YKL-40 levels and their structural brain correlates in the continuum of Alzheimer's disease but not those of sTREM2. *Alzheimers Dement* 2017;6:50–59.
12. Kantarci K, Smith GE, Ivnik RJ, et al. ¹H magnetic resonance spectroscopy, cognitive function, and apolipoprotein E genotype in normal aging, mild cognitive impairment and Alzheimer's disease. *J Int Neuropsychol Soc* 2002;8:934–942.
13. Roberts RO, Geda YE, Knopman DS, et al. The Mayo Clinic Study of Aging: design and sampling, participation, baseline measures and sample characteristics. *Neuroepidemiology* 2008;30:58–69.
14. Petersen RC, Roberts RO, Knopman DS, et al. Prevalence of mild cognitive impairment is higher in men: The Mayo Clinic Study of Aging. *Neurology* 2010;75:889–897.
15. Kantarci K, Jack CR Jr, Xu YC, et al. Regional metabolic patterns in mild cognitive impairment and Alzheimer's disease: a ¹H MRS study. *Neurology* 2000;55:210–217.
16. Jack CR Jr, Wiste HJ, Lesnick TG, et al. Brain beta-amyloid load approaches a plateau. *Neurology* 2013;80:890–896.
17. Schwarz CG, Senjem ML, Gunter JL, et al. Optimizing PiB-PET SUVR change-over-time measurement by a large-scale analysis of longitudinal reliability, plausibility, separability, and correlation with MMSE. *Neuroimage* 2016;144:113–127.
18. Ashburner J, Friston KJ. Unified segmentation. *Neuroimage* 2005;26:839–851.
19. Schwarz CG, Gunter JL, Wiste HJ, et al. A large-scale comparison of cortical thickness and volume methods for measuring Alzheimer's disease severity. *Neuroimage Clin* 2016;11:802–812.
20. Avants BB, Epstein CL, Grossman M, Gee JC. Symmetric diffeomorphic image registration with cross-correlation: evaluating automated labeling of elderly and neurodegenerative brain. *Med Image Anal* 2008;12:26–41.
21. Rothman KJ. No adjustments are needed for multiple comparisons. *Epidemiology* 1990;1:43–46.
22. Perneger TV. What's wrong with Bonferroni adjustments? *BMJ* 1998;316:1236–1238.
23. Kantarci K, Knopman DS, Dickson DW, et al. Alzheimer disease: postmortem neuropathologic correlates of antemortem ¹H MR spectroscopy metabolite measurements. *Radiology* 2008;248:210–220.
24. Marjanska M, Weigand SD, Preboske G, et al. Treatment effects in a transgenic mouse model of Alzheimer's disease: a magnetic resonance spectroscopy study after passive immunization. *Neuroscience* 2014;259:94–100.
25. Kantarci K. Proton MRS in mild cognitive impairment. *J Magn Reson Imaging* 2013;37:770–777.
26. Catani M, Cherubini A, Howard R, et al. (1)H-MR spectroscopy differentiates mild cognitive impairment from normal brain aging. *Neuroreport* 2001;12:2315–2317.
27. Huang W, Alexander GE, Chang L, et al. Brain metabolite concentration and dementia severity in Alzheimer's disease: a (1)H MRS study. *Neurology* 2001;57:626–632.
28. Jack CR Jr, Knopman DS, Jagust WJ, et al. Tracking pathophysiological processes in Alzheimer's disease: an updated hypothetical model of dynamic biomarkers. *Lancet Neurol* 2013;12:207–216.
29. Kantarci K, Weigand SD, Przybelski SA, et al. MRI and MRS predictors of mild cognitive impairment in a population-based sample. *Neurology* 2013;81:126–133.
30. Morris JC, Roe CM, Xiong C, et al. APOE predicts amyloid-beta but not tau Alzheimer pathology in cognitively normal aging. *Ann Neurol* 2010;67:122–131.
31. Mielke MM, Wiste HJ, Weigand SD, et al. Indicators of amyloid burden in a population-based study of cognitively normal elderly. *Neurology* 2012;79:1570–1577.
32. Resnick SM, Bilgel M, Moghekar A, et al. Changes in Abeta biomarkers and associations with APOE genotype in 2 longitudinal cohorts. *Neurobiol Aging* 2015;36:2333–2339.
33. Vlassenko AG, Mintun MA, Xiong C, et al. Amyloid-beta plaque growth in cognitively normal adults: longitudinal [¹¹C]Pittsburgh compound B data. *Ann Neurol* 2011;70:857–861.
34. Petersen RC, Wiste HJ, Weigand SD, et al. Association of elevated amyloid levels with cognition and biomarkers in cognitively normal people from the community. *JAMA Neurol* 2016;73:85–92.

35. Kantarci K, Goldberg TE. MR spectroscopy, APOE genotype, and evolving beta-amyloid pathology: what is being detected and when. *Neurology* 2016;86:1750–1751.
36. Vemuri P, Lesnick TG, Przybelski SA, et al. Vascular and amyloid pathologies are independent predictors of cognitive decline in normal elderly. *Brain* 2015;138:761–771.
37. Jack CR Jr, Wiste HJ, Weigand SD, et al. Defining imaging biomarker cut points for brain aging and Alzheimer's disease. *Alzheimers Dement* 2016;13:205–216.
38. Kantarci K, Petersen RC, Boeve BF, et al. ¹H MR spectroscopy in common dementias. *Neurology* 2004;63:1393–1398.
39. Rodrigue KM, Kennedy KM, Devous MD Sr, et al. Beta-amyloid burden in healthy aging: regional distribution and cognitive consequences. *Neurology* 2012;78:387–395.
40. Kokmen E, Smith GE, Petersen RC, Tangalos E, Ivnik RC. The short test of mental status: correlations with standardized psychometric testing. *Arch Neurol* 1991;48:725–728.



Pattern of brain atrophy rates in autopsy-confirmed dementia with Lewy bodies



Zuzana Nedelska^{a,b,c}, Tanis J. Ferman^d, Bradley F. Boeve^e, Scott A. Przybelski^f, Timothy G. Lesnick^f, Melissa E. Murray^g, Jeffrey L. Gunter^a, Matthew L. Senjem^a, Prashanti Vemuri^a, Glenn E. Smith^h, Yonas E. Geda^{i,j}, Jonathan Graff-Radford^e, David S. Knopman^e, Ronald C. Petersen^e, Joseph E. Parisi^k, Dennis W. Dickson^{g,l}, Clifford R. Jack Jr^a, Kejal Kantarci^{a,*}

^a Department of Radiology, Mayo Clinic, Rochester, MN, USA

^b Department of Neurology, 2nd Faculty of Medicine and Motol University Hospital, Charles University in Prague, Prague, the Czech Republic

^c International Clinical Research Center, St. Anne's University Hospital Brno, Brno, the Czech Republic

^d Department of Psychiatry and Psychology, Mayo Clinic, Jacksonville, FL, USA

^e Department of Neurology, Mayo Clinic, Rochester, MN, USA

^f Department of Health Sciences Research, Mayo Clinic, Rochester, MN, USA

^g Department of Neuroscience, Mayo Clinic, Jacksonville, FL, USA

^h Department of Psychiatry and Psychology, Mayo Clinic, Rochester, MN, USA

ⁱ Department of Psychiatry and Psychology, Mayo Clinic, Scottsdale, AZ, USA

^j Department of Neurology, Mayo Clinic, Scottsdale, AZ, USA

^k Department of Pathology and Laboratory Medicine, Mayo Clinic, Rochester, MN, USA

^l Neuropathology Laboratory, Mayo Clinic, Jacksonville, FL, USA

ARTICLE INFO

Article history:

Received 10 April 2014

Received in revised form 16 June 2014

Accepted 8 July 2014

Available online 15 July 2014

Keywords:

Autopsy-confirmed dementia with Lewy bodies

Alzheimer's disease

Serial MRI

Atrophy rate

Braak neurofibrillary tangle stage

Sample size estimate

ABSTRACT

Dementia with Lewy bodies (DLB) is characterized by preserved whole brain and medial temporal lobe volumes compared with Alzheimer's disease dementia (AD) on magnetic resonance imaging. However, frequently coexistent AD-type pathology may influence the pattern of regional brain atrophy rates in DLB patients. We investigated the pattern and magnitude of the atrophy rates from 2 serial MRIs in autopsy-confirmed DLB patients ($n = 20$) and mixed DLB/AD patients ($n = 22$), compared with AD ($n = 30$) and elderly nondemented control subjects ($n = 15$), followed antemortem. DLB patients without significant AD-type pathology were characterized by lower global and regional rates of atrophy, similar to control subjects. The mixed DLB/AD patients displayed greater atrophy rates in the whole brain, temporoparietal cortices, hippocampus and amygdala, and ventricle expansion, similar to AD patients. In the DLB and DLB/AD patients, the atrophy rates correlated with Braak neurofibrillary tangle stage, cognitive decline, and progression of motor symptoms. Global and regional atrophy rates are associated with AD-type pathology in DLB, and these rates can be used as biomarkers of AD progression in patients with LB pathology.

© 2015 Elsevier Inc. All rights reserved.

1. Introduction

Pathologically, dementia with Lewy bodies (DLB) is characterized by unremarkable global brain atrophy on gross inspection, and microscopically by α -synuclein aggregates (Spillantini et al., 1997) in Lewy bodies (LBs) (Kosaka, 1978; Lewy, 1912) and Lewy neurites. However, a frequent concomitant finding is varying the degree of Alzheimer's disease (AD) type pathology, that is, β -amyloid in

neuritic plaques and hyperphosphorylated tau in neurofibrillary tangles (NFT) (NIA-Reagan, 1997). This overlap between the 2 most common, yet distinct neurodegenerative dementias in terms of underlying pathology and clinical characteristics, often makes antemortem diagnosis challenging. This applies particularly to DLB patients with a high Braak NFT stage (Merdes et al., 2003) who are often misdiagnosed as having AD in the clinical settings (Schneider et al., 2007). Mixed DLB/AD dementia patients are of considerable interest because of the high frequency of the mixed pathology (Hamilton, 2000; Hansen et al., 1990; Schneider et al., 2007, 2009), their hypersensitivity to neuroleptics, and most important of all, their excellent response to acetyl-cholinesterase inhibitors (Graff-Radford

* Corresponding author at: Department of Radiology, Mayo Clinic, 200 First Street SW, Rochester, MN 55905, USA. Tel.: +1 507 284 9770; fax: +1 507 284 9778.

E-mail address: kantarci.kejal@mayo.edu (K. Kantarci).

et al., 2012; McKeith et al., 2004). Accessible, preferably noninvasive biomarkers, such as those derived from magnetic resonance imaging (MRI), would have an important role in differential diagnosis, tracking of disease progression, evaluation of treatment response, and designing clinical trials with disease-specific therapeutic agents or re-designing those with the currently available treatments in patients with DLB. Moreover, usage of longitudinal MRI measurements may reduce interindividual variability and provide a better insight into the biology of the disease than a single measurement.

Patients with AD are characterized by greater rates of whole brain and hippocampus atrophy, accompanied by greater ventricle expansion over time compared with control subjects in both clinically diagnosed and autopsy-confirmed cohorts (Fox et al., 2000; Jack et al., 2000, 2004; Whitwell et al., 2007a, 2007b). Atrophy rates on MRI have been used to assess treatment response in clinical trials on patients with AD and mild cognitive impairment (MCI) (Fox et al., 2000; Jack et al., 2003, 2008). Greater rates of atrophy on antemortem MRI have been positively associated with high Braak NFT stage and NFT density at autopsy (Josephs et al., 2008a; Silbert et al., 2003).

Relatively preserved medial temporal lobe volumes characterize patients with DLB compared with patients with AD; however, whether DLB patients have sufficient gray matter loss to be distinguished from normal control subjects, remained unclear in clinically diagnosed cohorts that likely included cases with mixed DLB/AD pathology (Barber et al., 2000; Burton et al., 2002, 2004; Harvey et al., 1999; Hashimoto et al., 1998). The involvement of frontal (Ballmaier et al., 2004; Barber et al., 2000, 2002; Whitwell et al., 2007a, 2007b), temporoparietal (Ballmaier et al., 2004; Harvey et al., 1999; Whitwell et al., 2007a, 2007b), and occipital cortices (Middelkoop et al., 2001; O'Donovan et al., 2013) has been observed in patients with DLB, although the findings have been inconsistent.

In autopsy-confirmed cohorts, medial temporal lobe atrophy on cross-sectional MRI has been associated with mixed AD-type pathology in patients with DLB (Burton et al., 2009). Specifically, greater atrophy in the hippocampus and amygdala has been associated with a high Braak NFT stage (Kantarci et al., 2012) and tau-NFT density (Murray et al., 2013) in patients with LB pathology.

In longitudinal MRI studies, clinically diagnosed patients with DLB were reported to have greater whole brain atrophy rates than age-matched controls, similar to patients with AD and vascular dementia (O'Brien et al., 2001). However, greater whole brain atrophy and ventricle expansion rates were limited to patients with mixed DLB/AD pathology compared with control subjects in an autopsy-confirmed cohort (Whitwell et al., 2007a, 2007b). The differences across the studies can be attributed to different sampling schemes (clinical vs. autopsy-confirmed sample), and different methods used to measure the atrophy. Nevertheless, the regional pattern and magnitude of atrophy rates that characterize patients with autopsy confirmed DLB and mixed DLB/AD are unknown.

Our primary objective was to identify the regional pattern of gray matter atrophy rates on antemortem serial MRI in autopsy-confirmed DLB and DLB/AD compared with those with AD and elderly control subjects. We hypothesized that autopsy-confirmed patients with DLB would have similar rates of brain atrophy, compared with elderly control subjects, whereas those with mixed LB and AD-type pathology would be affected more in terms of topographic extent and magnitude of gray matter loss over the time. Our secondary objective was to correlate rates of atrophy with measures of cognitive decline and clinical progression in patients with DLB and DLB/AD; and finally, to report sample size estimates for a hypothetical clinical trial including patients with DLB only and for DLB/AD, using rates of atrophy as surrogate measures of outcome.

2. Methods

2.1. Participants

To be included in this study, participants had to have at least 2 serial 1.5 T brain MRIs approximately 2 years apart of sufficient technical quality and had to come to autopsy. We have chosen the participants exclusively based on the autopsy diagnosis and not the clinical syndrome. We included cases with LB pathology diagnosed as either high likelihood DLB (DLB group) or intermediate and low likelihood DLB (DLB/AD group) according to the Third Report of the DLB Consortium Criteria for DLB (McKeith et al., 2005). We also included cases with high likelihood AD with no LB pathology (AD group) and low likelihood AD with no LB pathology (control group) for comparison. Patients with amygdala-only Lewy bodies ($n = 2$) were included in the DLB/AD group as they had both LB and AD pathology. Patients were excluded if they had concomitant neurologic illness at the time of either one of the MRIs or conditions known to interfere with cognition such as cortical infarcts, normal pressure hydrocephalus, subdural hematoma, or tumor. Those with lacunar infarcts or white matter hyperintensities were included.

Participants were recruited consecutively and followed prospectively until their death between 1999 and 2009 at the Mayo Clinic Alzheimer's Disease Research Center (dementia clinic-based cohort) and Alzheimer's Disease Patient Registry (community-based cohort) (Petersen et al., 1990) in Rochester, MN, USA. During life, participants underwent approximately annual clinical evaluations including standard measures of cognitive and functional performance such as Mini Mental State Examination (MMSE) (Folstein et al., 1975) that has been widely used in the field, the Dementia Rating Scale (DRS) (Mattis, 1988), which has greater dynamic range than MMSE. The severity of parkinsonism was quantified with the motor subtest of Unified Parkinson Disease Rating Scale (UPDRS) (Fahn et al., 1987). Progression of the disease was measured by subtraction of baseline from follow-up score and then annualized for consistency with imaging measures. Clinical diagnosis was established by the consensus of neurologists, neuropsychologists, and nurses. The diagnosis of probable AD was made according to NINCDS-ADRDA criteria for AD (McKhann et al., 1984). The diagnosis of probable DLB was made using the third report of the DLB Consortium criteria for DLB (McKeith et al., 2005), and diagnosis of MCI was based on Petersen criteria (Petersen, 2004). Informed signed consent was obtained from all individuals or their proxies antemortem, and study was approved by the Mayo Clinic Institutional Review Board.

2.2. Neuropathologic examination and diagnosis

Brains were processed, sectioned, and sampled using standardized methods (McKeith et al., 2005; Mirra et al., 1991). In all 87 cases, the examination and diagnosis were conducted by one of 2 experts (Dennis W. Dickson or Joseph E. Parisi) using standard staining and standard criteria (Braak and Braak, 1996), and also immunohistochemistry to determine the distribution and to semi quantitatively measure NFT density with corresponding Braak NFT stage. For Lewy body disease, cases were classified as brainstem-, limbic-, or neocortical-predominant according to the distribution and counts of LBs immunostained with monoclonal antibodies to α -synuclein. Based on the findings, we defined the study groups as follows: (1) cases with AD ($n = 30$) had high-probability AD according to the National Institute of Aging-Reagan criteria (NIA-Reagan, 1997). That is, the presence of frequent neuritic plaques corresponding to probable or definite AD according to Consortium to Establish Registry for Alzheimer's Disease criteria for AD (Mirra et al., 1991), Braak NFT stage of V or VI and no LBs; (2) cases with DLB ($n = 20$) were

diagnosed according to the third report of the DLB Consortium criteria (McKeith et al., 2005) as high likelihood DLB. They had numerous transitional (limbic) or diffuse (neocortical) LBs, Braak NFT stage \leq IV, and low to intermediate likelihood AD; (3) cases with mixed DLB/AD ($n = 22$) had both pathologies; however, not severe enough to meet criteria for high likelihood DLB. Mixed DLB/AD had intermediate or low likelihood DLB with limbic or neocortical LBs, Braak NFT stage \geq V, and frequent neuritic plaques consistent with high likelihood AD. We did not have any cases with brainstem predominant LBs in our cohort. Two cases had LBs confined to the amygdala only and were included in the mixed DLB/AD group because of high likelihood AD pathology. Cases with atypical forms of AD were not observed in cases with LB pathology; (4) controls ($n = 15$) who had no LBs, they had low likelihood AD with Braak stage \geq III, and were non-demented at the time of MRIs. We have also assessed the presence of argyrophilic grain disease (AGD), a pathology frequently found in brains of cognitively healthy (Knopman et al., 2003) and nondemented elderly individuals (Barkhof et al., 2007). This pathology has been known to be associated with aging (Ferrer et al., 2008; Saito et al., 2004) and has not been associated with a greater medial temporal gray matter loss in nondemented elderly individuals (Josephs et al., 2008b). Five controls, 5 DLB cases, and 1 mixed DLB/AD case had AGD. The relatively high number of AGD cases in our series may be because of our interest in and awareness of this entity, therefore we did not exclude cases with AGD.

2.3. Imaging studies

Brain MRIs were acquired at 1.5 T using 3-dimensional T1-weighted spoiled gradient echo recalled sequence (General Electric, Milwaukee, WI, USA) with following parameters: repetition time = 7 ms, echo time = 3 ms, inversion time = 900 ms, flip angle 8° , in-plane resolution of 1.0 mm, and slice thickness of 1.2 mm. The rates of whole brain atrophy and ventricle expansion were measured using the automated boundary shift integral algorithm (BSI) (Fox et al., 1996), modified in-house and described elsewhere (Gunter et al., 2003), and were reported as annualized percentage change from baseline volume (APC %). Regional gray matter loss across the entire brain was determined with automated, in-house developed Tensor Based Morphometry-Symmetric Diffeomorphic Image Normalization method (TBM-SyN) (Gunter et al., 2012), which uses symmetrical registration of serial MRIs (Ashburner and Ridgway, 2013), and computes 3-dimensional SyN deformations between each subject's serial MRIs using preprocessed T1-weighted images. These deformations were averaged within the pathologic group and reported as annualized log Jacobian. Further, we visualized the TBM-SyN-derived differences in the regional gray matter atrophy rates in DLB and DLB/AD groups comparing them with the control and AD groups using Statistic Parametric Mapping package (SPM; version 5) (<http://www.fil.ion.ucl.ac.uk/spm/>), with 2-sided t -test at significance level $p < 0.05$, cluster extent threshold of 50 voxels, and correction for multiple comparisons with false discovery rate. To quantify the magnitude of atrophy rates in the hippocampus and amygdala, regions of interest (ROI) from an Automated Anatomical Labeling atlas (Tzourio-Mazoyer et al., 2002), modified in-house to fit our template (Kantarci et al., 2010; Vemuri et al., 2008), were applied. Mean regional annualized log Jacobian measurements for these 2 ROIs were derived. Because LB or AD-related pathologies are not considered to affect preferentially one hemisphere over another, the ROI-based rates of atrophy were calculated as averages of right and left hemispheric ROIs. The hippocampus and amygdala were chosen for ROI analysis because these structures have received reasonable attention in the literature as proxies of AD and DLB on MRI (Burton et al., 2009, 2012; Kantarci et al., 2012; Murray et al., 2013; Vemuri et al., 2011; Whitwell et al.,

2007a, 2007b) and can be consistently quantified with various softwares because of their distinct borders (Fischl et al., 2002; Patenaude et al., 2011).

2.4. Statistical analyses

Statistical analyses were performed with R statistical software package, version 2.14.0. (<http://www.R-project.org>) and SAS version 9.3, with 2-sided statistical significance set at type I error rate $\alpha < 0.05$. For continuous variables, the means with standard deviations were reported along with the p -values from analysis of variance. For binary or categorical variables, the counts and proportions (%) were reported along with p -values from χ^2 tests. There were 2 specific normalizing transformations done to the data. The annualized DRS total had left skewness, so a constant number of 59 was first added to create a positive number where it was then cubed. The interval from MRI to death was transformed with a square root because of right skewness. To evaluate groupwise differences in the magnitude of atrophy rates derived from BSI and TBM-SyN methods, we used analysis of covariance, with pathologic diagnosis treated as the main effect, whereas the age at the time of second MRI and the interval from the second MRI to death were treated as adjustment covariates and used in the remaining analyses. We report adjusted Pearson correlations to assess the effect of NFT Braak stage on the atrophy rates within 2 global and 2 atlas-based regions, and to examine the association between atrophy rates and measures of the clinical or cognitive decline and progression of motor findings. Correlation analyses were performed exclusively within DLB and DLB/AD groups combined to see the dynamic range of values within patients having LB pathology, in keeping with our hypothesis and study objectives. Finally, we estimated the sample sizes needed per treatment group to power a hypothetical clinical trial using the annualized atrophy rates as the surrogate measures of outcome to detect standard effects of 25% and 50% in terms of hypothetical reduction or cessation of the gray matter loss that would be attributed to positive treatment response and would be clinically relevant, using a 2-sided 2-sample t -test with equal variances, type I error rate < 0.05 , and power 80%.

3. Results

3.1. Subjects' characteristics

Demographic and clinical characteristics of study participants at the time of the second MRI by group is provided in Table 1. The proportion of females ($p = 0.19$), years of education ($p = 0.84$), and inter scan interval ($p = 0.20$) were similar across the groups. Controls were older at the second MRI ($p = 0.01$) compared with pathologic groups of otherwise similar age, and the interval from the second MRI to death was also longer in controls than in the rest of sample ($p = 0.01$). Therefore, both age at second MRI and time from second MRI to death were used as covariates in statistical analyses. The duration of dementia was not different across the patient groups ($p = 0.47$). The decline in MMSE and DRS scores differed markedly across the groups ($p < 0.001$); patients with autopsy-confirmed DLB/AD and AD performed equally poorly on MMSE, and scored worse on DRS than other groups. As expected, patients with autopsy-confirmed DLB and mixed DLB/AD were characterized by a high frequency of clinical features associated with DLB such as visual hallucinations, fluctuations, REM sleep behavior disorder, and parkinsonism. Of these, only frequency of REM sleep behavior disorder distinguished DLB from the DLB/AD group ($p = 0.03$). The clinical diagnosis of DLB was present in 14 of 20 (70%) cases with autopsy-confirmed DLB and in 7 of 22 (32%) cases with DLB/AD. The breakdown of relevant medication type and

Table 1
Subjects' characteristics at time of the second MRI (closer to death)

| | Controls | DLB | DLB/AD | AD | p-value ^a |
|--|-------------|---------------------------|--------------------------|-------------|----------------------|
| | n = 15 | n = 20 | n = 22 | n = 30 | |
| Number of females (%) | 10 (67) | 6 (30) | 10 (45) | 15 (50) | 0.19 |
| MRI age (y) | 85.9 (6.8) | 77.5 (7.1) | 78.0 (9.4) | 76.7 (10.7) | 0.01 |
| Education (y) | 14.7 (3.6) | 14.5 (2.5) | 13.9 (3.7) | 13.9 (2.9) | 0.84 |
| Age at death (y) | 89.9 (7.0) | 79.7 (7.6) | 80.7 (9.3) | 79.4 (10.9) | 0.003 |
| Time scan to death (y) | 4.0 (2.3) | 2.2 (1.4) | 2.7 (1.2) | 2.7 (1.5) | 0.01 ^b |
| Scan interval (y) | 2.3 (1.4) | 1.7 (0.4) | 1.8 (0.7) | 1.9 (0.6) | 0.20 ^b |
| Dementia duration (y) | — | 5.3 (2.5) | 6.2 (3.6) | 6.5 (3.2) | 0.47 ^a |
| MMSE | 28.3 (2.2) | 21.7 (5.6) ^c | 15.0 (7.0) ^c | 15.0 (5.8) | <0.001 |
| DRS | 135.1 (5.0) | 114.3 (19.1) ^c | 99.9 (21.3) ^c | 87.7 (26.4) | <0.001 |
| Visual hallucinations ^d (%) | — | 9 (45) | 9 (41) | — | 0.79 |
| Fluctuations ^d (%) | — | 7 (64) | 2 (50) | — | 0.63 |
| RBD ^d (%) | — | 14 (88) | 6 (50) | — | 0.03 |
| UPDRS motor subscale | — | 14.1 (7.7) ^c | 12.4 (8.1) ^c | — | 0.55 |
| Clinical diagnosis (%) | | | | | |
| Cognitively normal | 11 (73) | 0 (0) | 0 (0) | 0 (0) | — |
| MCI | 3 (20) | 2 (10) | 1 (5) | 0 (0) | — |
| Probable DLB | 0 (0) | 14 (70) | 7 (32) | 0 (0) | — |
| Probable AD | 0 (0) | 4 (20) | 14 (64) | 28 (93) | — |
| Other ^e | 1 (7) | 0 (0) | 0 (0) | 2 (7) | — |
| Medication ^f (%) | | | | | |
| ACHEI only | — | 7 (35) | 11 (50) | 23 (76) | — |
| Dopaminergic agent only | — | 3 (15) | 1 (5) | 0 | — |
| No treatment | — | 4 (20) | 5 (22.5) | 6 (20) | — |
| ACHEI + dopaminergic agent | — | 6 (30) | 4 (17.5) | 0 | — |
| Memantine + ACHEI | — | 0 | 1 (5) | 1 (4) | — |

Means (SD) are reported for continuous variables.

Key: AD, Alzheimer's disease; DLB, dementia with Lewy bodies; DRS, Dementia Rating Scale; MCI, mild cognitive impairment; MRI, magnetic resonance imaging; RBS, REM sleep behavior disorder; SD, standard deviation; UPDRS, Unified Parkinson's Disease Rating Scale.

^a From analysis of variance for the continuous variables and from a χ^2 test for differences in proportions.

^b Based on a square root transformation to normalize the distribution.

^c Missing data: MMSE was available in 18 DLB and 21 DLB/AD patients; DRS was available in 15 DLB and 13 DLB/AD patients; UPDRS was available in 15 DLB and 13 DLB/AD patients.

^d A majority of control and AD subjects have not had clinical features associated with DLB assessed. The proportions (%) of these features are based on the available data which were incomplete due to the retrospective design and the disease severity limiting completion of certain tasks.

^e One control subject was clinically diagnosed as uncertain (cognitively normal or MCI), one patient with AD was clinically diagnosed as having probable corticobasal syndrome, and one patient with AD as having probable fronto-temporal dementia.

^f Medication: the agents were administered in standard doses, that is, acetyl-cholinesterase inhibitors (ACHEI) 10 mg once a day; memantine 10 mg up to twice a day and dopaminergic agents titrated as needed.

dosage is also reported in Table 1. Main autopsy findings by group are listed in Table 2.

3.2. Rates of whole brain and ventricle volume change

Global measures from BSI (Table 3) were available in 87 of the autopsied participants; however, 1 case from the mixed DLB/AD group was excluded from this analysis because of BSI failure. In patients with DLB, the whole brain atrophy rate was not different from that in controls ($p = 0.92$) but was lower than the rate in patients with mixed DLB/AD ($p = 0.01$) and AD ($p < 0.001$). In the

mixed DLB/AD group, the whole brain atrophy rate was greater compared with controls ($p = 0.04$) and was similar to that seen in AD ($p = 0.36$). Similarly, the ventricle expansion rate in DLB group was consistent with the rate in control group but was lower compared with DLB/AD and AD groups ($p < 0.001$). Patients with DLB/AD were characterized by greater ventricle expansion rate compared with controls ($p = 0.003$), indistinguishable from those with AD ($p = 0.55$) (Fig. 1).

3.3. Regional pattern of the differences in cortical atrophy rates

Three participants (2 controls and 1 AD case) were excluded because of the failure of TBM-SyN analysis. Between-group differences in gray matter atrophy rates are displayed in Fig. 2. We did not

Table 2
Main autopsy findings

| | Controls | DLB | DLB/AD | AD | p-value ^a |
|---|----------|---------|----------|----------|----------------------|
| | n = 15 | n = 20 | n = 22 | n = 30 | |
| Braak staging (% of cases) | | | | | |
| I | 3 (20) | 4 (20) | — | — | <0.001 |
| II | 4 (27) | 6 (30) | — | — | |
| III | 8 (53) | 6 (30) | — | — | |
| IV | — | 4 (20) | — | — | |
| V | — | — | 5 (23) | 2 (7) | |
| VI | — | — | 17 (77) | 28 (93) | |
| AD likelihood ^b (% of cases) | | | | | |
| Low likelihood | 15 (100) | 16 (80) | — | — | <0.001 |
| Intermediate likelihood | — | 4 (20) | — | — | |
| High likelihood | — | — | 22 (100) | 30 (100) | |

^a From a χ^2 test for differences in proportions.

^b According to the NIA-Reagan criteria, 1997.

Table 3

Global rates of change with the mean (SD) for the annualized percentage change

| | Controls | DLB | DLB/AD | AD | ANCOVA |
|-------------|------------|------------|---------------------|------------|----------------------|
| | n = 15 | n = 20 | n = 22 ^a | n = 30 | p-value [*] |
| Whole brain | -0.3 (0.5) | -0.4 (0.5) | -1.1 (1.2) | -1.4 (0.9) | 0.001 |
| Ventricle | 3.6 (1.4) | 4.8 (3.3) | 8.7 (3.5) | 9.4 (4.4) | <0.001 |

Key: AD, Alzheimer's disease; ANCOVA, analysis of covariance; DLB, dementia with Lewy bodies; MRI, magnetic resonance imaging; SD, standard deviation.

^{*} p-values are from ANCOVA adjusting for age at the time of the second MRI and the time from the second MRI to death.

^a One patient with DLB/AD was excluded from this analysis because of the boundary shift integral algorithm failure. Results for the whole brain atrophy were therefore available for 21 DLB/AD patients.

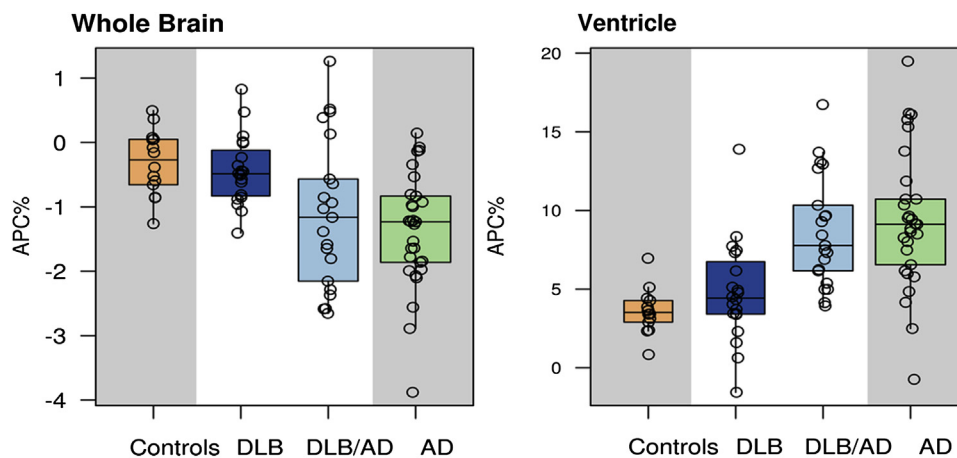


Fig. 1. Rates of the whole brain and ventricle volume change. Boxplots are depicting atrophy rate in the whole brain and expansion in the ventricle. Boxes indicate the lower quartile, the median, and the upper quartile of the distributions with whiskers extending to the furthestmost data point within the distance of 1.5 times the interquartile range.

find any differences in terms of increased gray matter loss between control and DLB or between the mixed DLB/AD and AD groups. These negative findings were consistent with the BSI-based whole brain atrophy and ventricle expansion rates as described above. Patients with DLB/AD had significantly greater atrophy rates in the temporoparietal neocortex (i.e., parahippocampal, middle and inferior temporal, inferior parietal, fusiform, and lingual gyrus), the hippocampus and amygdala as compared with control and DLB groups. Patients with DLB were characterized by generally preserved gray matter compared with DLB/AD and AD groups. The differences in atrophy rates within the hippocampus and amygdala ROIs by pathologic group are depicted in Fig. 3. In patients with DLB, the atrophy rate in the hippocampus was similar to control subjects ($p = 0.83$), and was markedly lower compared with both DLB/AD ($p < 0.001$) and AD ($p < 0.001$) groups. In the mixed DLB/AD group, the atrophy rate was greater compared with controls ($p < 0.001$) and was not different from that in AD group ($p = 0.71$). Similarly, those with DLB did not differ from controls in the amygdala atrophy rate ($p = 0.23$) and were characterized by preserved amygdala compared with AD ($p = 0.01$). Greater atrophy rate in the amygdala distinguished DLB/AD group from both DLB ($p < 0.001$) and controls ($p < 0.001$), whereas DLB/AD and AD groups were affected similarly ($p = 0.09$).

3.4. Atrophy rates and NFT Braak stage in patients with LB pathology

Greater atrophy rates in the whole brain, hippocampus, and amygdala, and expansion in the ventricle on antemortem MRI were associated with a higher Braak NFT stage at autopsy in patients with LB pathology (DLB and DLB/AD). The Pearson adjusted correlations between atrophy or expansion rates and Braak NFT stage are listed in Table 4.

3.5. Atrophy rates and measures of disease progression in patients with LB pathology

Adjusted Pearson correlations between atrophy rates and MMSE, DRS, and UPDRS as measures of cognitive decline and progression of motor impairment in patients with a range of LB pathology (DLB and DLB/AD combined) are displayed in Fig. 4. Greater whole brain atrophy rates were associated with a greater decline in cognitive function as measured by MMSE, $r = 0.54$ (95% CI = 0.25, 0.73; $p < 0.001$) and with a greater progression of the motor impairment on UPDRS, $r = -0.49$ (95% CI = -0.73, -0.13; $p = 0.0091$). There was borderline association with DRS, $r = 0.38$, (95% CI = -0.03, 0.67; $p = 0.063$). Similarly, a greater atrophy rate in the

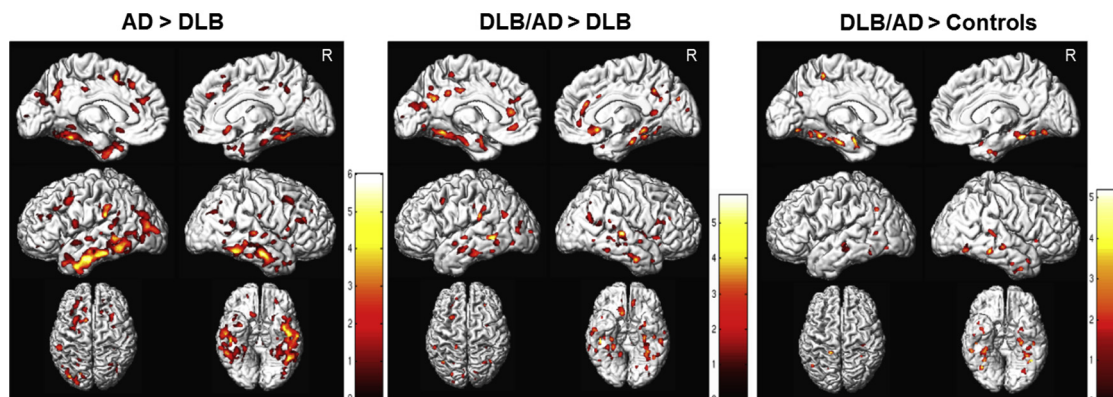


Fig. 2. Regional pattern of the differences in cortical atrophy rates. Voxel-level maps are showing the pattern of between-group differences in the annualized atrophy rates at $p < 0.05$, cluster extent threshold $k = 50$ and corrected for multiple comparisons with false discovery rate. Side T-score bars indicate magnitude of the differences. Pattern of greater atrophy rates in temporoparietal regions characterizes AD compared with DLB group (left). Similar pattern with smaller magnitude of differences characterizes mixed DLB/AD compared with DLB group (middle). More subtle differences between DLB/AD and controls (right) are potentially because of smaller control group sample size ($n = 13$) who were part of this analysis. No significant differences were found between DLB and control or DLB/AD and AD groups. Abbreviations: AD, Alzheimer's disease; DLB, dementia with Lewy bodies; R, right.

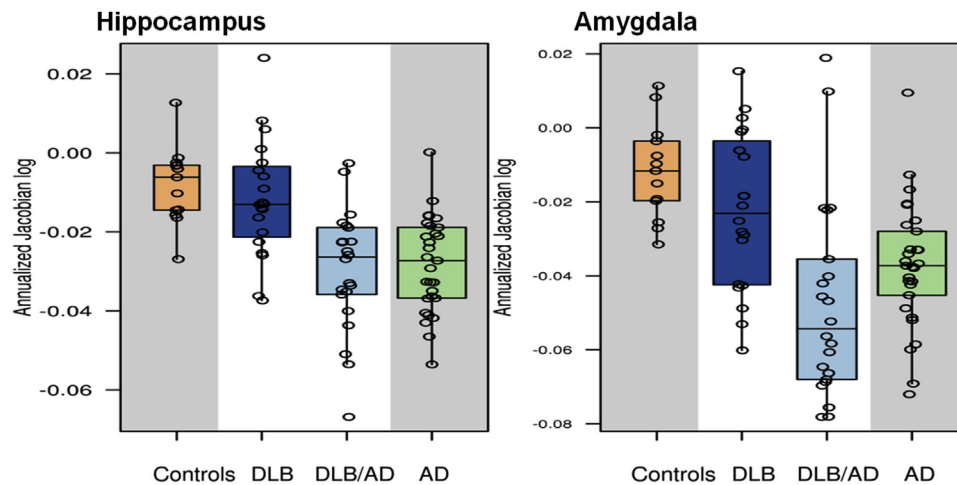


Fig. 3. Atrophy rates in the hippocampus and the amygdala. Boxplots are depicting atrophy rates in the hippocampus and amygdala. Boxes indicate the lower quartile, the median, and the upper quartile of the distributions with whiskers extending to the furthestmost data point within the distance of 1.5 times the interquartile range.

hippocampus was associated with a greater cognitive decline on MMSE, $r = 0.61$ (95% CI = 0.35, 0.77; $p < 0.001$) and DRS, $r = 0.55$ (95% CI = 0.20, 0.77; $p = 0.0036$); and also with progression of motor impairment, $r = -0.69$ (95% CI = -0.84 , -0.41 ; $p < 0.001$). Finally, the findings in the amygdala were consistent with the findings in the whole brain and the hippocampus; the amygdala atrophy rate correlated with decline in MMSE, $r = 0.40$ (95% CI = 0.09, 0.64; $p = 0.012$), DRS, $r = 0.57$ (95% CI = 0.23, 0.78; $p = 0.0022$) and the progression of motor impairment, $r = -0.55$ (95% CI = -0.77 , -0.21 ; $p = 0.0027$). Neither measures of cognitive decline nor progression of motor impairment correlated with the ventricle expansion rate.

3.6. Sample size estimates for an hypothetical clinical trial

Global (the whole brain and ventricle), and regional (the hippocampus and amygdala) atrophy rates from autopsied patients were used to calculate sample size estimates per treatment group for a hypothetical clinical trial to detect an effect of 25% and 50% in terms of the reduction in rates of atrophy. The sample size estimates by fixed effect size and brain region are listed in Table 5. In DLB/AD group, the ventricle expansion rate followed by hippocampal atrophy rate required the smallest sample sizes to measure the desirable effect. For comparison, to detect a fixed effect size in the autopsy-confirmed AD group, rates of change in the hippocampus, followed by ventricle and the amygdala required smaller sample sizes than the whole brain atrophy rate. Because rates of atrophy (or ventricular expansion) were not different in DLB patients compared with normal control subjects, we did not report on sample size estimates for the DLB group.

Table 4

Correlations (95% CI) between rates of volume change and Braak NFT stage in subjects with a range of LB-pathology

| | Pearson correlation ^a | <i>p</i> -value |
|-------------|----------------------------------|-----------------|
| Whole brain | -0.33 (-0.58, -0.01) | 0.041 |
| Ventricle | 0.43 (0.13, 0.65) | 0.006 |
| Hippocampus | -0.63 (-0.79, -0.40) | <0.001 |
| Amygdala | -0.49 (-0.69, -0.20) | 0.001 |

Key: CI, confidence interval; LB, Lewy body; MRI, magnetic resonance imaging; NFT, neurofibrillary tangles.

^a The correlations are adjusted for the age at the second MRI and the time from the second MRI to death.

4. Discussion

In this study, we demonstrated the pattern and the magnitude of atrophy rates across the entire brain gray matter in a cohort of prospectively studied patients with autopsy-confirmed DLB and mixed DLB/AD as compared with those with AD patients and control subjects. Our findings showed that patients with DLB had rates of the whole brain atrophy and ventricle expansion similar to controls and did not display any region-specific increases in atrophy rates to be distinguishable from elderly controls. On the contrary, those with mixed DLB/AD had markedly greater rates of brain atrophy, and the topography of changes consistent with that seen in AD, affecting predominantly temporoparietal cortices, hippocampus, and amygdala. Greater atrophy rates not only correlated with high Braak NFT stage, but also with measures of disease progression in patients with LB pathology.

Our findings of minimal global atrophy rates in patients with DLB compared with normal control subjects are in agreement with previous longitudinal MRI study in a smaller sample of autopsy-confirmed DLB subjects from our group (Whitwell et al., 2007a, 2007b). In addition, we found no specific pattern of regional atrophy rates in patients with autopsy-confirmed DLB compared with normal controls, unlike the cross-sectional studies from clinically diagnosed patients with DLB (Ballmaier et al., 2004; Burton et al., 2002, 2004). In these cross-sectional studies, the hippocampus and the amygdala were atrophic in DLB patients compared with normal controls, although the atrophy in DLB was less prominent than in AD patients (Burton et al., 2002, 2004). Similarly, a greater atrophy was measured in temporal and parietal cortices in DLB compared with normal control subjects (Ballmaier et al., 2004). In this study, AD patients exhibited more atrophy in temporal and also orbitofrontal cortices than DLB patients which agreed with our results. Our findings also differ from reports on clinically diagnosed patients with DLB (O'Brien et al., 2001) who were found to have similar rates of whole brain atrophy compared to AD and other dementias groups. We attribute the differences largely to the fact these studies likely included cases with mixed DLB/AD pathology.

Both, global and regional atrophy rates in patients with mixed DLB/AD pathology were similar to patients with AD demonstrating that the presence of AD pathology probably drives the atrophy rates regardless of LB pathology. In keeping with this, we found greater atrophy rates in the mixed DLB/AD pathology group compared with

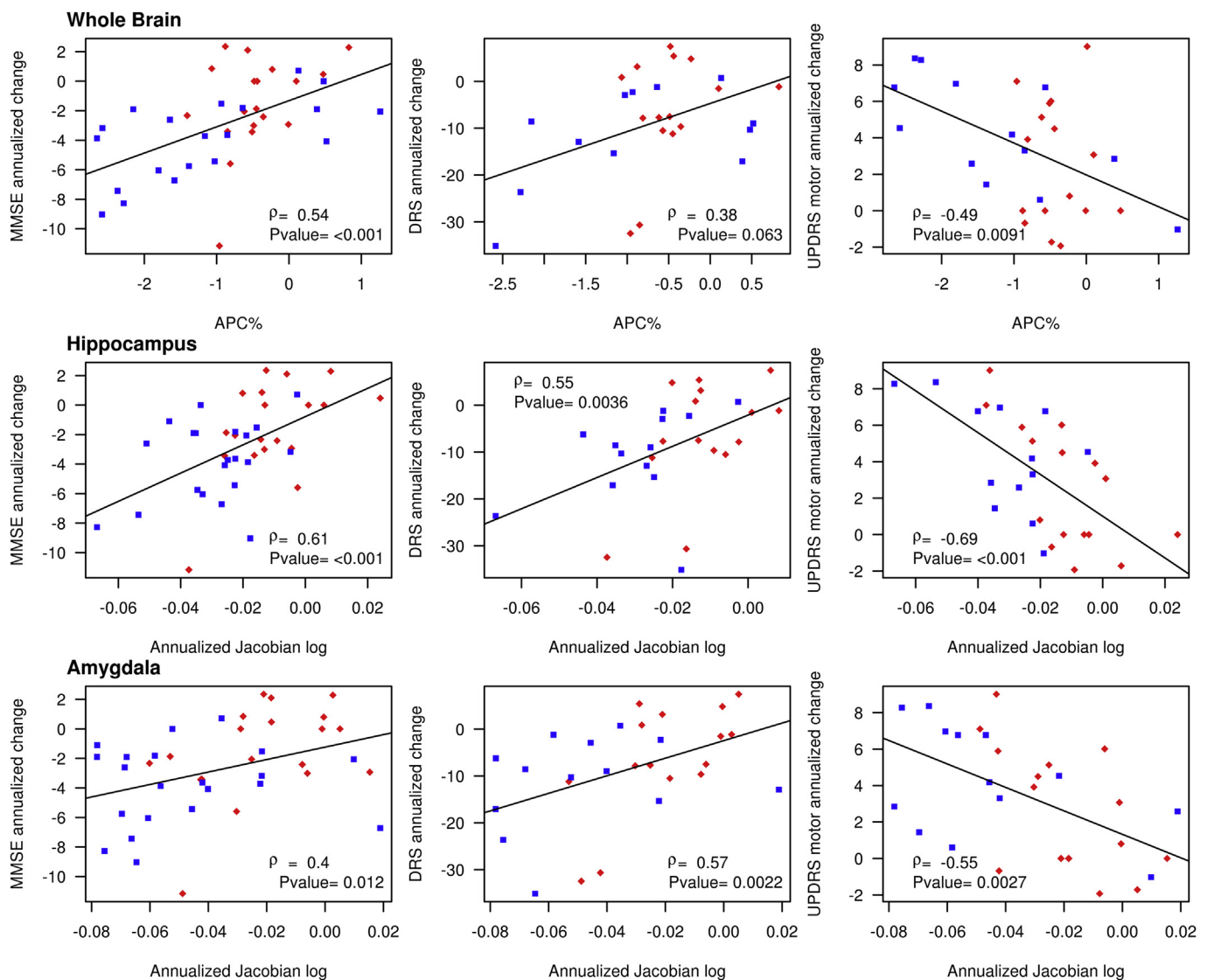


Fig. 4. Correlations between atrophy rates and measures of disease progression in patients with a range of LB pathology. Scatter plots show adjusted Pearson correlations between annualized atrophy rates in the whole brain (top row), hippocampus (middle row), and amygdala (bottom row), and annualized measures of cognitive decline on MMSE and DRS, and progression of motor findings on UPDRS. Correlation coefficient (ρ) and corresponding p -value is included within each scatterplot. Red diamonds represent patients with DLB; blue squares represent patients with mixed DLB/AD. Abbreviations: AD, Alzheimer's disease; DLB, dementia with Lewy bodies; DRS, Dementia Rating Scale; MMSE, Mini Mental State Examination; UPDRS, Unified Parkinson's Disease Rating Scale.

DLB. The mixed DLB/AD patients had higher rates of atrophy in temporoparietal regions, hippocampus, and amygdala compared with normal control subjects, a pattern consistent with the rates of atrophy in AD (Jack et al., 2004; Ridha et al., 2006; Schill et al., 2002; Thompson et al., 2003), corresponding to the progression

Table 5
Sample size estimates (95% CI) per treatment group for a clinical trial

| Effect size | DLB/AD | | AD | |
|-------------|-----------------|--------------|---------------|-------------|
| | 25% | 50% | 25% | 50% |
| Whole brain | 274 (104, 1407) | 70 (27, 354) | 111 (62, 216) | 29 (16, 54) |
| Ventricle | 43 (27, 70) | 12 (8, 18) | 57 (34, 117) | 15 (9, 28) |
| Hippocampus | 69 (39, 145) | 18 (10, 34) | 47 (30, 99) | 13 (8, 25) |
| Amygdala | 81 (31, 283) | 21 (8, 67) | 53 (29, 135) | 15 (9, 36) |

Sample sizes are estimated to detect a fixed effect of 25% or 50% in reduction of atrophy or expansion rates based on a 2-sided 2-sample t -test with equal variances, $p < 0.05$ and 80% power.

Key: AD, Alzheimer's disease; DLB, dementia with Lewy bodies.

of neurofibrillary tangles (Braak and Braak, 1996). We found a positive correlation between greater global atrophy rates and a high Braak NFT stage in patients with a range of LB pathology (DLB and mixed DLB/AD), consistent with previous longitudinal MRI studies with pathologic confirmation (Josephs et al., 2008a; Silbert et al., 2003). These studies demonstrated that high NFT Braak stage and density have been associated with greater atrophy rates in patients with AD pathology. Similarly, in our study, greater atrophy rates in the hippocampus and amygdala positively correlated with higher Braak NFT stage in patients with a range of LB pathology (DLB and DLB/AD). Our results agree with previous cross-sectional findings in autopsy-confirmed DLB (Burton et al., 2009; Kantarci et al., 2012; Murray et al., 2013), indicating that greater medial temporal atrophy rates are associated with NFT pathology.

In patients with DLB who do not have sufficient and significant NFT pathology (low or intermediate likelihood AD and Braak stage up to IV in our cases), rate of cortical gray matter loss is minimal over the time, and appears not to be associated with α -synuclein

accumulation, which likely has other deleterious effects on neuronal integrity. On the other hand, there may be a synergistic influence of tau-NFT and α -synucleinopathy, and perhaps also β -amyloid, particularly on clinical disease severity in patients with mixed DLB/AD (Jellinger et al., 2007; Horvath et al., 2013; Lashley et al., 2008). Given that the dementia duration was not different across the patient groups, differences in clinical measures between DLB and DLB/AD patients could be attributed to the synergistic effects of the 2 underlying pathologies. However, we found a positive correlation between a greater cognitive decline measured by MMSE and DRS and greater atrophy rates in the hippocampus, the amygdala, and also the whole brain in the DLB and DLB/AD groups, which agrees with a previous study from our group in patients with MCI and AD (Jack et al., 2004), demonstrating the correlations between brain atrophy rates and cognitive decline.

Age-related ventricular expansion is observed in cognitively normal elderly individuals (Sowell et al., 2003), thus ventricular expansion may also be age-related in patients with LB pathology, explaining lack of a correlation between ventricular expansion rate and the disease progression in patients with LB pathology. However, an unexpected finding was the association of LB-related motor progression on UPDRS and rates of the whole brain, hippocampal, and amygdala atrophy in patients with DLB and DLB/AD. Potentially, the AD and LB-related pathologies can either independently progress, perhaps at similar rates, or can interact with each other influencing the disease progression. Our data suggest that the relationship between the atrophy rates, driven by AD-type pathology, and progression of motor impairment is an indirect association.

So far, structural MRI is not accepted as the primary outcome measure for monitoring effect size in clinical trials. However, in patients with AD, imaging measures may provide adequate power to considerable smaller sample sizes than are required when cognitive or functional measures are used (Fox et al., 2000; Hua et al., 2009; Jack et al., 2004). In the present study, we demonstrate that the pathologic underpinnings of atrophy rates on structural MRI are proxies of AD-type pathology, in particular tau-NFT pathology in patients with mixed DLB/AD pathology. The global and regional measures we suggested for powering the clinical trial are relatively well defined regions with distinct borders, measurable by various automated softwares (Fischl et al., 2002; Gunter et al., 2003; Patenaude et al., 2011) and different field strengths (Ho et al., 2010), therefore, these measures can be used as outcomes for AD-related treatment effects and should be sufficiently comparable across the trials. The sample sizes we calculated for patients with mixed DLB/AD were comparable with estimates for patients with AD both with regional and global measures, further supporting our findings that patients with mixed DLB/AD pathologies could be monitored by rates of atrophy in the clinical trials targeting AD-type pathology, which they may benefit from.

A major strength of the present study was the availability of serial MRIs in cases with pathologic diagnosis, clarifying the inconsistencies in the literature on whether or not patients with DLB are affected by marked brain atrophy rates. Usage of longitudinal measurement from serial scans with similar inter-scan interval, not requiring additional statistical adjustment was a strength as the inter-individual variability was lessened. The limitation to our study, as with most imaging-autopsy studies, was the interval between MRI and autopsy, which was approximately 2.5 years in patients and 4 years in control subjects. We assumed a linear relationship between atrophy rates and accumulation of brain pathology during this interval and controlled for this effect in statistical analysis. This was not a significant concern for control subjects who by definition had limited pathology; however, the assumption of linear progression of disease pathology may not be true in

patients with dementia. Furthermore, we did not measure longitudinal change in dorsal midbrain or basal forebrain gray matter, the regions that are known to atrophy in patients with clinically (Brenneis et al., 2004; Hanyu et al., 2005; Vemuri, et al., 2011; Whitwell et al., 2007a, 2007b) or pathologically confirmed DLB (Kantarci et al., 2012). At this time, we were not able to conduct longitudinal measurement of these relatively small and deeply localized structures because of a high test-retest variability, and these analyses should be considered in future studies.

Overall, our findings have multiple clinical implications for using serial MRI as a tool in differential diagnosis of dementia, disease progression tracking, and designing clinical trials targeting specific pathologies that would use atrophy rates as the surrogate measures of outcome. The minimal change in volumes on structural MRI in autopsy-confirmed high-likelihood DLB reflects the fact that the pathologic progression of Lewy body pathology is not indexed by cortical gray matter volume loss, unlike AD and underscores the ongoing need for other biomarkers of disease progression for future trials in DLB. This implies that either the changes induced by α -synucleinopathy could be predominantly subcortical or cortical but predominantly biochemical and not structural. On the contrary, structural MRI is useful in tracking progression of AD-related pathology and would be an appropriate biomarker in clinical trials targeting the co-existing AD-related pathology in patients with DLB.

Disclosure statement

Dr Nedelska, Mr. Przybelski, Mr. Lesnick, Dr Gunter, Dr Senjem, Dr Graff-Radford, and Dr Geda report no disclosures. Dr Ferman is funded by the NIH (Mayo Clinic Alzheimer's Disease Research Center/Project 1-P50-AG16574/P1 [Co-I]). Dr Boeve has served as an investigator for a clinical trial sponsored by Cephalon. He has received honoraria from the American Academy of Neurology. He receives research support from the National Institute on Aging (P50-AG16574 [Co-I], U01 AG06786 [Co-I], R01-AG15866 [Co-I], and U24-AG26395 [Co-I]) and the Alzheimer's Association (IIRG-05–14,560 [PI]). Dr Murray is funded by P50-NS72187-03 (Co-I) and Robert H. and Clarice Smith and Abigail van Buren Alzheimer Disease Research Fellowship. Dr Vemuri is funded by NIH R00-AG37573. Dr Knopman serves as Deputy Editor for Neurology; served on a Data Safety Monitoring Board for Lilly Pharmaceuticals; served as a consultant to TauRx, was an investigator in clinical trials sponsored by Baxter, Elan Pharmaceuticals, and Forest Pharmaceuticals for the past 2 years; and receives research support from the NIH. Dr Smith is funded by the NIH (P50-AG16574). Dr Parisi receives publishing royalties for Principles & Practice of Neuropathology, 2nd edition. Dr Petersen serves on scientific advisory boards for Elan Pharmaceuticals, Wyeth Pharmaceuticals, and GE Healthcare and receives research support from the NIH (P50-AG16574 [PI] and U01-AG06786 [PI], R01-AG11378 [Co-I], and U01–24904 [Co-I]). Dr Dickson is funded by the NIH (P50-AG16574/Neuropathology Core [PI], P01AG017216 [PI], P50-NS072187 [PI], and R01-AG040042 [Co-I]). Dr Jack serves as a consultant for Janssen, Bristol-Meyer-Squibb, General Electric, Siemens, and Johnson and Johnson and is involved in clinical trials sponsored by Allon and Baxter, Inc. He receives research funding from the National Institutes of Health (R01-AG011378, R01-AG037551, U01-HL096917, U01-AG032438, and U01-AG024904), and the Alexander Family Alzheimer's Disease Research Professorship of the Mayo Foundation Family. Dr Kantarci serves on the data safety monitoring board for Pfizer Inc and Takeda Global Research & Development Center, Inc; and she is funded by the NIH (R01AG040042 [PI], R21 NS066147 [PI], P50 AG44170/Project 2 [PI], P50 AG16574/Project 1 [PI], and R01 AG11378 [Co-I]).

Acknowledgements

The study was funded by the National Institutes of Health P50-AG16574/P1 and R01AG040042 (to Kejal Kantarci), R01-AG015866 (to Tanis J. Ferman), R01-AG11378 (to Clifford R. Jack), and P50-AG16574 (to Ronald C. Petersen), Mangurian Foundation, and the Robert H. and Clarice Smith and Abigail Van Buren Alzheimer's Disease Research Program. Zuzana Nedelska is supported by the CTSA grant number UL1 TR000135 from the National Center for Advancing Translational Sciences, United States, a component of the NIH (its contents are solely the responsibility of the authors and do not necessarily represent the official view of NIH), Grant Agency of Charles University in Prague (doctoral student grant 624012), and European Regional Development Fund—Project FNUSA-ICRC CZ.1.05/1.1.00/02.0123, European Social Fund within the project Young Talent Incubator II (reg. CZ.1.07/2.3.00/20.0117) and the State Budget of the Czech Republic.

References

- Ashburner, J., Ridgway, G.R., 2013. Symmetric diffeomorphic modeling of longitudinal structural MRI. *Front. Neurosci.* 5, 197 eCollection 2012.
- Ballmaier, M., O'Brien, J.T., Burton, E.J., Thompson, P.M., Rex, D.E., Narr, K.L., McKeith, I.G., DeLuca, H., Toga, A.W., 2004. Comparing gray matter loss profiles between dementia with Lewy bodies and Alzheimer's disease using cortical pattern matching: diagnosis and gender effects. *Neuroimage* 23, 25–35.
- Barber, R., Ballard, C., McKeith, I.G., Gholkar, A., O'Brien, J.T., 2000. MRI volumetric study of dementia with Lewy bodies: a comparison with AD and vascular dementia. *Neurology* 54, 1304–1309.
- Barkhof, F., Polvikoski, T.M., van Straaten, E.C., Kalaria, R.N., Sulkava, R., Aronen, H.J., Niinistö, L., Rastas, S., Oinas, M., Scheltens, P., Erkinjuntti, T., 2007. The significance of medial temporal lobe atrophy: a postmortem MRI study in the very old. *Neurology* 69, 1521–1527.
- Braak, H., Braak, E., 1996. Evolution of the neuropathology of Alzheimer's disease. *Acta Neurol. Scand. Suppl.* 165, 3–12.
- Brenneis, C., Wenning, G.K., Egger, K.E., Schocke, M., Trieb, T., Seppi, K., Marksteiner, J., Ransmayr, G., Benke, T., Poewe, W., 2004. Basal forebrain atrophy is a distinctive pattern in dementia with Lewy bodies. *Neuroreport* 15, 1711–1714.
- Burton, E.J., Karas, G., Paling, S.M., Barber, R., Williams, E.D., Ballard, C.G., McKeith, I.G., Scheltens, P., Barkhof, F., O'Brien, J.T., 2002. Patterns of cerebral atrophy in dementia with Lewy bodies using voxel-based morphometry. *Neuroimage* 17, 618–630.
- Burton, E.J., McKeith, I.G., Burn, D.J., Williams, E.D., O'Brien, J.T., 2004. Cerebral atrophy in Parkinson's disease with and without dementia: a comparison with Alzheimer's disease, dementia with Lewy bodies and controls. *Brain* 127 (Pt 4), 791–800.
- Burton, E.J., Barber, R., Mukaetova-Ladinska, E.B., Robson, J., Perry, R.H., Jaros, E., Kalaria, R.N., O'Brien, J.T., 2009. Medial temporal lobe atrophy on MRI differentiates Alzheimer's disease from dementia with Lewy bodies and vascular cognitive impairment: a prospective study with pathological verification of diagnosis. *Brain* 132 (Pt 1), 195–203.
- Burton, E.J., Mukaetova-Ladinska, E.B., Perry, R.H., Jaros, E., Barber, R., O'Brien, J.T., 2012. Neuropathological correlates of volumetric MRI in autopsy-confirmed Lewy body dementia. *Neurobiol. Aging* 33, 1228–1236.
- Fahn, S., Elton, R.L., UPDRS program members, 1987. Unified Parkinson's disease rating scale. In: Fahn, S., Marsden, C.D., Goldstein, M., Calne, D.B. (Eds.), *Recent Developments in Parkinson's Disease*, 2. Macmillan Healthcare Information, Florham Park, NJ, pp. 153–163, 293–304.
- Ferrer, I., Santpere, G., van Leeuwen, F.W., 2008. Argypophilic grain disease. *Brain* 131 (Pt6), 1416–1432.
- Fischl, B., Salat, D.H., Busa, E., Albert, M., Dieterich, M., Haselgrove, C., van der Kouwe, A., Killiany, R., Kennedy, D., Klaveness, S., Montillo, A., Makris, N., Rosen, B., Dale, A.M., 2002. Whole brain segmentation: automated labeling of neuroanatomical structures in the human brain. *Neuron* 33, 341–355.
- Folstein, M.F., Folstein, S.E., McHugh, P.R., 1975. "Mini-mental state". A practical method for grading the cognitive state of patients for the clinician. *J. Psychiatr. Res.* 12, 189–198.
- Fox, N.C., Freeborough, P.A., Rossor, M.N., 1996. Visualisation and quantification of rates of atrophy in Alzheimer's disease. *Lancet* 348, 94–97.
- Fox, N.C., Cousens, S., Scathill, R., Harvey, R.J., Rossor, M.N., 2000. Using serial registered brain magnetic resonance imaging to measure disease progression in Alzheimer disease: power calculations and estimates of sample size to detect treatment effects. *Arch. Neurol.* 57, 339–344.
- Graff-Radford, J., Boeve, B.F., Pedraza, O., Ferman, T.J., Przybelski, S., Lesnick, T.G., Vemuri, P., Senjem, M.L., Smith, G.E., Knopman, D.S., Lowe, V., Jack Jr., C.R., Petersen, R.C., Kantarci, K., 2012. Imaging and acetylcholinesterase inhibitor response in dementia with Lewy bodies. *Brain* 135 (Pt 8), 2470–2477.
- Gunter, J.L., Shiung, M.M., Manduca, A., Jack Jr., C.R., 2003. Methodological considerations for measuring rates of brain atrophy. *J. Magn. Reson. Imaging* 18, 16–24.
- Gunter, J.L., Senjem, M.L., Vemuri, P., Jack Jr., C.R., 2012. Comparison of mask-based differences, boundary shift integral and symmetric normalization Jacobian integration. In: *MICCAI 2012 Workshop on Novel Imaging Biomarkers for Alzheimer's Disease and Related Disorders*. Nice, France.
- Hamilton, R.L., 2000. Lewy bodies in Alzheimer's disease: a neuropathological review of 145 cases using alpha-synuclein immunohistochemistry. *Brain Pathol.* 10, 378–384.
- Hansen, L., Salmon, D., Galasko, D., Masliah, E., Katzman, R., DeTeresa, R., Thal, J., Pay, M.M., Hofstetter, R., Klauber, M., Rice, V., Butters, N., Alford, M., 1990. The Lewy body variant of Alzheimer's disease: a clinical and pathologic entity. *Neurology* 40, 1–8.
- Hanyu, H., Tanaka, Y., Shimizu, S., Sakurai, H., Iwamoto, T., Abe, K., 2005. Differences in MR features of the substantia innominata between dementia with Lewy bodies and Alzheimer's disease. *J. Neurol.* 252, 482–484.
- Harvey, G.T., Hughes, J., McKeith, I.G., Briel, R., Ballard, C., Gholkar, A., Scheltens, P., Perry, R.H., Ince, P., O'Brien, J.T., 1999. Magnetic resonance imaging differences between dementia with Lewy bodies and Alzheimer's disease: a pilot study. *Psychol. Med.* 29, 181–187.
- Hashimoto, M., Kitagaki, H., Imamura, T., Hirono, N., Shimomura, T., Kazui, H., Tanimukai, S., Hanihara, T., Mori, E., 1998. Medial temporal and whole-brain atrophy in dementia with Lewy bodies: a volumetric MRI study. *Neurology* 51, 357–362.
- Ho, A.J., Hua, X., Lee, S., Leow, A.D., Yanovsky, I., Gutman, B., Dinov, I.D., Lepore, N., Stein, J.L., Toga, A.W., Jack Jr., C.R., Bernstein, M.A., Reiman, E.M., Harvey, D.J., Kornak, J., Schuff, N., Alexander, G.E., Weiner, M.W., Thompson, P.M., Alzheimer's Disease Neuroimaging Initiative, 2010. Comparing 3 T and 1.5 T MRI for tracking Alzheimer's disease progression with tensor-based morphometry. *Hum. Brain Mapp.* 31, 499–514.
- Horvath, J., Hermann, F.R., Burkhard, P.R., Bouras, C., Kovari, C., 2013. Neuropathology of dementia in a large cohort of patients with Parkinson's disease. *Parkinsonism Relat. Disord.* 19, 864–868.
- Hua, X., Lee, S., Yanovsky, I., Leow, A.D., Chou, Y.Y., Ho, A.J., Gutman, B., Toga, A.W., Jack Jr., C.R., Bernstein, M.A., Reiman, E.M., Harvey, D.J., Kornak, J., Schuff, N., Alexander, G.E., Weiner, M.W., Thompson, P.M., Alzheimer's Disease Neuroimaging Initiative, 2009. Optimizing power to track brain degeneration in Alzheimer's disease and mild cognitive impairment with tensor-based morphometry: an ADNI study of 515 subjects. *Neuroimage* 48, 668–681.
- Jack Jr., C.R., Petersen, R.C., Xu, Y., O'Brien, P.C., Smith, G.E., Ivnik, R.J., Boeve, B.F., Tangalos, E.G., Kokmen, E., 2000. Rates of hippocampal atrophy correlate with change in clinical status in aging and AD. *Neurology* 55, 484–489.
- Jack Jr., C.R., Slomkowski, M., Gracon, S., Hoover, T.M., Felmlee, J.P., Stewart, K., Xu, Y., Shiung, M.M., O'Brien, P.C., Cha, R., Knopman, D.S., Petersen, R.C., 2003. MRI as a biomarker of disease progression in a therapeutic trial of milameline for AD. *Neurology* 60, 253–260.
- Jack Jr., C.R., Shiung, M.M., Gunter, J.L., O'Brien, P.C., Weigand, S.D., Knopman, D.S., Boeve, B.F., Ivnik, R.J., Smith, G.E., Cha, R.H., Tangalos, E.G., Petersen, R.C., 2004. Comparison of different MRI brain atrophy rate measures with clinical disease progression in AD. *Neurology* 62, 591–600.
- Jack Jr., C.R., Petersen, R.C., Grundman, M., Jin, S., Gamst, A., Ward, C.P., Sencakova, D., Doody, R.S., Thal, L.J., Members of the Alzheimer's Disease Cooperative Study (ADCS), 2008. Longitudinal MRI findings from the vitamin E and donepezil treatment study for MCI. *Neurobiol. Aging* 29, 1285–1295.
- Jellinger, K.A., Wenning, G.K., Seppi, K., 2007. Predictors of survival in dementia with Lewy bodies and Parkinson dementia. *Neurodegener. Dis.* 4, 428–430.
- Josephs, K.A., Whitwell, J.L., Ahmed, Z., Shiung, M.M., Weigand, S.D., Knopman, D.S., Boeve, B.F., Parisi, J.E., Petersen, R.C., Dickson, D.W., Jack Jr., C.R., 2008a. Beta-amyloid burden is not associated with rates of brain atrophy. *Ann. Neurol.* 63, 204–212.
- Josephs, K.A., Whitwell, J.L., Parisi, J.E., Knopman, D.S., Boeve, B.F., Geda, Y.E., Jack Jr., C.R., Petersen, R.C., Dickson, D.W., 2008b. Argypophilic grains: a distinct disease or an additive pathology? *Neurobiol. Aging* 29, 566–573.
- Kantarci, K., Senjem, M.L., Lowe, V.J., Wiste, H.J., Weigand, S.D., Kemp, B.J., Frank, A.R., Shiung, M.M., Boeve, B.F., Knopman, D.S., Petersen, R.C., Jack Jr., C.R., 2010. Effects of age on the glucose metabolic change in mild cognitive impairment. *AJNR Am. J. Neuroradiol.* 31, 1247–1253.
- Kantarci, K., Ferman, T.J., Boeve, B.F., Weigand, S.D., Przybelski, S., Vemuri, P., Murray, M.E., Senjem, M.L., Smith, G.E., Knopman, D.S., Petersen, R.C., Jack Jr., C.R., Parisi, J.E., Dickson, D.W., 2012. Focal atrophy on MRI and neuropathologic classification of dementia with Lewy bodies. *Neurology* 79, 553–560.
- Knopman, D.S., Parisi, J.E., Salviati, A., Floriach-Robert, M., Boeve, B.F., Ivnik, R.J., Smith, G.E., Dickson, D.W., Johnson, K.A., Petersen, L.E., McDonald, W.C., Braak, H., Petersen, R.C., 2003. Neuropathology of cognitively normal elderly. *J. Neuropathol. Exp. Neurol.* 62, 1087–1095.
- Kosaka, K., 1978. Lewy bodies in cerebral cortex, report of three cases. *Acta Neuropathol.* 42, 127–134.
- Lashley, T., Holton, J.L., Gray, E., Kirkham, K., O'Sullivan, S.S., Hilbig, A., Wood, N.W., Lees, A.J., Revesz, T., 2008. *Acta Neuropathol.* 115, 417–425.
- Levy, F., 1912. Paralysis agitans. I. Pathologische Anatomie. In: Lewandowsky, M., Abelsdorff, G. (Eds.), *Handbuch der Neurologie*, 3. Springer-Verlag, Berlin, pp. 920–933.

- Mattis, S., 1988. Dementia Rating Scale (DRS). Psychological Assessment Resources, Odessa, FL.
- McKeith, I.G., Mintzer, J., Aarsland, D., Burn, D., Chiu, H., Cohen-Mansfield, J., Dickson, D., Dubois, B., Duda, J.E., Feldman, H., Gauthier, S., Halliday, G., Lawlor, B., Lippa, C., Lopez, O.L., Carlos Machado, J., O'Brien, J., Playfer, J., Reid, W., International Psychogeriatric Association Expert Meeting on DLB, 2004. Dementia with Lewy bodies. *Lancet Neurol.* 3, 19–28.
- McKeith, I.G., Dickson, D.W., Lowe, J., Emre, M., O'Brien, J.T., Feldman, H., Cummings, J., Duda, J.E., Lippa, C., Perry, E.K., Aarsland, D., Arai, H., Ballard, C.G., Boeve, B., Burn, D.J., Costa, D., Del Ser, T., Dubois, B., Galasko, D., Gauthier, S., Goetz, C.G., Gomez-Tortosa, E., Halliday, G., Hansen, L.A., Hardy, J., Iwatsubo, T., Kalaria, R.N., Kaufer, D., Kenny, R.A., Korczyn, A., Kosaka, K., Lee, V.M., Lees, A., Litvan, I., Londos, E., Lopez, O.L., Minoshima, S., Mizuno, Y., Molina, J.A., Mukaetova-Ladinska, E.B., Pasquier, F., Perry, R.H., Schulz, J.B., Trojanowski, J.Q., Yamada, M., Consortium on DLB, 2005. Diagnosis and management of dementia with Lewy bodies: third report of the DLB Consortium. *Neurology* 65, 1863–1872.
- McKhann, G., Drachman, D., Folstein, M., Katzman, R., Price, D., Stadlan, E.M., 1984. Clinical diagnosis of Alzheimer's disease: report of the NINCDS-ADRDA Work Group under the auspices of Department of Health and Human Services Task Force on Alzheimer's Disease. *Neurology* 34, 939–944.
- Merdes, A.R., Hansen, L.A., Jeste, D.V., Galasko, D., Hofstetter, C.R., Ho, G.J., Thal, L.J., Corey-Bloom, J., 2003. Influence of Alzheimer pathology on clinical diagnostic accuracy in dementia with Lewy bodies. *Neurology* 60, 1586–1590.
- Middelkoop, H.A., van der Flier, W.M., Burton, J., Lloyd, A.J., Paling, S., Barber, R., Ballard, C., McKeith, I.G., O'Brien, J.T., 2001. Dementia with Lewy bodies and AD are not associated with occipital lobe atrophy on MRI. *Neurology* 57, 2117–2120.
- Mirra, S.S., Heyman, A., McKeel, D., Sumi, S.M., Crain, B.J., Brownlee, L.M., Vogel, F.S., Hughes, J.P., van Belle, G., Berg, L., 1991. The Consortium to Establish a Registry for Alzheimer's Disease (CERAD). Part II. Standardization of the neuropathologic assessment of Alzheimer's disease. *Neurology* 41, 479–486.
- Murray, M.E., Ferman, T.J., Boeve, B.F., Przybelski, S.A., Lesnick, T.G., Liesinger, A.M., Senjem, M.L., Gunter, J.L., Preboske, G.M., Lowe, V.J., Vemuri, P., Dugger, B.N., Knopman, D.S., Smith, G.E., Parisi, J.E., Silber, M.H., Graff-Radford, N.R., Petersen, R.C., Jack Jr., C.R., Dickson, D.W., Kantarci, K., 2013. MRI and pathology of REM sleep behavior disorder in dementia with Lewy bodies. *Neurology* 81, 1681–1689.
- Consensus recommendations for the postmortem diagnosis of Alzheimer's disease, 1997. The National Institute on Aging and Reagan Institute Working Group on diagnostic criteria for the neuropathological assessment of Alzheimer's disease. *Neurobiol. Aging* 18 (4 Suppl), S1–S2.
- O'Brien, J.T., Paling, S., Barber, R., Williams, E.D., Ballard, C., McKeith, I.G., Gholkar, A., Crum, W.R., Rossor, M.N., Fox, N.C., 2001. Progressive brain atrophy on serial MRI in dementia with Lewy bodies, AD, and vascular dementia. *Neurology* 56, 1386–1388.
- O'Donovan, J., Watson, R., Colloby, S.J., Firbank, M.J., Burton, E.J., Barber, R., Blamire, A.M., O'Brien, J.T., 2013. Does posterior cortical atrophy on MRI discriminate between Alzheimer's disease, dementia with Lewy bodies, and normal aging? *Int. Psychogeriatr.* 25, 111–119.
- Patenaude, B., Smith, S.M., Kennedy, D.N., Jenkinson, M., 2011. A Bayesian model of shape and appearance for subcortical brain segmentation. *Neuroimage* 56, 907–922.
- Petersen, R.C., 2004. Mild cognitive impairment as a diagnostic entity. *J. Intern. Med.* 256, 183–194.
- Petersen, R.C., Kokmen, E., Tangalos, E., Ivnik, R.J., Kurland, L.T., 1990. Mayo clinic Alzheimer's disease patient registry. *Aging (Milano)* 2, 408–415.
- Ridha, B.H., Barnes, J., Bartlett, J.W., Godbolt, A., Pepple, T., Rossor, M.N., Fox, N.C., 2006. Tracking atrophy progression in familial Alzheimer's disease: a serial MRI study. *Lancet Neurol.* 5, 828–834.
- Saito, Y., Ruberu, N.N., Sawabe, M., Arai, T., Tanaka, N., Kakuta, Y., Yamanouchi, H., Murayama, S., 2004. Staging of argyrophilic grains: an age-associated tauopathy. *J. Neuropathol. Exp. Neurol.* 63, 911–918.
- Scahill, R.I., Schott, J.M., Stevens, J.M., Rossor, M.N., Fox, N.C., 2002. Mapping the evolution of regional atrophy in Alzheimer's disease: unbiased analysis of fluid-registered serial MRI. *Proc. Natl. Acad. Sci. U.S.A.* 99, 4703–4707.
- Schneider, J.A., Arvanitakis, Z., Bang, W., Bennett, D.A., 2007. Mixed brain pathologies account for most dementia cases in community-dwelling older persons. *Neurology* 69, 2197–2204.
- Schneider, J.A., Arvanitakis, Z., Leurgans, S.E., Bennett, D.A., 2009. The neuropathology of probable Alzheimer disease and mild cognitive impairment. *Ann. Neurol.* 66, 200–208.
- Silbert, L.C., Quinn, J.F., Moore, M.M., Corbridge, E., Ball, M.J., Murdoch, G., Sexton, G., Kaye, J.A., 2003. Changes in prefrontal brain volume predict Alzheimer's disease pathology. *Neurology* 61, 487–492.
- Sowell, E.R., Peterson, B.S., Thompson, P.M., Welcome, S.E., Henkenius, A.L., Toga, A.W., 2003. Mapping cortical change across the human life span. *Nat. Neurosci.* 6, 309–315.
- Spillantini, M.G., Schmidt, M.L., Lee, V.M., Trojanowski, J.Q., Jakes, R., Goedert, M., 1997. Alpha-synuclein in Lewy bodies. *Nature* 388, 839–840.
- Thompson, P.M., Hayashi, K.M., de Zubicaray, G., Janke, A.L., Rose, S.E., Semple, J., Herman, D., Hong, M.S., Dittmer, S.S., Doddrell, D.M., Toga, A.W., 2003. Dynamics of gray matter loss in Alzheimer's disease. *J. Neurosci.* 23, 994–1005.
- Tzourio-Mazoyer, N., Landeau, B., Papathanassiou, D., Crivello, F., Etard, O., Delcroix, N., Mazoyer, B., Joliot, M., 2002. Automated anatomical labeling of activations in SPM using a macroscopic anatomical parcellation of the MNI MRI single-subject brain. *Neuroimage* 15, 273–289.
- Vemuri, P., Whitwell, J.L., Kantarci, K., Josephs, K.A., Parisi, J.E., Shiung, M.S., Knopman, D.S., Boeve, B.F., Petersen, R.C., Dickson, D.W., Jack Jr., C.R., 2008. Antemortem MRI based Structural Abnormality iNdex (STAND)-scores correlate with postmortem Braak neurofibrillary tangle stage. *Neuroimage* 42, 559–567.
- Vemuri, P., Simon, G., Kantarci, K., Whitwell, J.L., Senjem, M.L., Przybelski, S.A., Gunter, J.L., Josephs, K.A., Knopman, D.S., Boeve, B.F., Ferman, T.J., Dickson, D.W., Parisi, J.E., Petersen, R.C., Jack Jr., C.R., 2011. Antemortem differential diagnosis of dementia pathology using structural MRI: differential-STAND. *Neuroimage* 55, 522–531.
- Whitwell, J.L., Jack Jr., C.R., Parisi, J.E., Knopman, D.S., Boeve, B.F., Petersen, R.C., Ferman, T.J., Dickson, D.W., Josephs, K.A., 2007a. Rates of cerebral atrophy differ in different degenerative pathologies. *Brain* 130 (Pt 4), 1148–1158.
- Whitwell, J.L., Weigand, S.D., Shiung, M.M., Boeve, B.F., Ferman, T.J., Smith, G.E., Knopman, D.S., Petersen, R.C., Benarroch, E.E., Josephs, K.A., Jack Jr., C.R., 2007b. Focal atrophy in dementia with Lewy bodies on MRI: a distinct pattern from Alzheimer's disease. *Brain* 130 (Pt 3), 708–719.

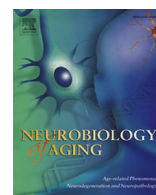
Web references

- Statistical Parametric Mapping software and documentation to be found at: <http://www.fil.ion.ucl.ac.uk/spm/> Recently viewed April 9, 2014.
- R statistical software to be found at: <http://www.R-project.org> Recently viewed April 9, 2014.



Contents lists available at ScienceDirect

Neurobiology of Aging

journal homepage: www.elsevier.com/locate/neuaging

White matter integrity in dementia with Lewy bodies: a voxel-based analysis of diffusion tensor imaging

Zuzana Nedelska^{a,b,c}, Christopher G. Schwarz^a, Bradley F. Boeve^d, Val J. Lowe^a, Robert I. Reid^e, Scott A. Przybelski^f, Timothy G. Lesnick^f, Jeffrey L. Gunter^e, Matthew L. Senjem^e, Tanis J. Ferman^g, Glenn E. Smith^h, Yonas E. Geda^{c,i,j}, David S. Knopman^d, Ronald C. Petersen^d, Clifford R. Jack Jr^a, Kejal Kantarci^{a,*}

^a Department of Radiology, Mayo Clinic, Rochester, MN, USA

^b Department of Neurology, Charles University in Prague, 2nd Faculty of Medicine and Motol University Hospital, Prague, The Czech Republic

^c International Clinical Research Center, St. Anne's University Hospital Brno, Brno, The Czech Republic

^d Department of Neurology, Mayo Clinic, Rochester, MN, USA

^e Department of Information Technology, Mayo Clinic, Rochester, MN, USA

^f Department of Health Sciences Research, Mayo Clinic, Rochester, MN, USA

^g Department of Psychiatry and Psychology, Mayo Clinic, Jacksonville, FL, USA

^h Department of Psychiatry and Psychology, Mayo Clinic, Rochester, MN, USA

ⁱ Department of Psychiatry and Psychology, Mayo Clinic, Scottsdale, AZ, USA

^j Department of Neurology, Mayo Clinic, Scottsdale, AZ, USA

ARTICLE INFO

Article history:

Received 22 September 2014

Received in revised form 27 February 2015

Accepted 3 March 2015

Keywords:

Dementia with Lewy bodies
Diffusion tensor imaging
White matter integrity
Amyloid-beta load
Voxel-based analysis
Cortical hypometabolism

ABSTRACT

Many patients with dementia with Lewy bodies (DLB) have overlapping Alzheimer's disease (AD)-related pathology, which may contribute to white matter (WM) diffusivity alterations on diffusion tensor imaging (DTI). Consecutive patients with DLB ($n = 30$), age- and sex-matched AD patients ($n = 30$), and cognitively normal controls ($n = 60$) were recruited. All subjects underwent DTI, 18F 2-fluoro-deoxy-D-glucose, and ¹¹C Pittsburgh compound B positron emission tomography scans. DLB patients had reduced fractional anisotropy (FA) in the parietooccipital WM but not elsewhere compared with cognitively normal controls, and elevated FA in parahippocampal WM compared with AD patients, which persisted after controlling for β -amyloid load in DLB. The pattern of WM FA alterations on DTI was consistent with the more diffuse posterior parietal and occipital glucose hypometabolism of 2-fluoro-deoxy-D-glucose positron emission tomography in the cortex. DLB is characterized by a loss of parietooccipital WM integrity, independent of concomitant AD-related β -amyloid load. Cortical glucose hypometabolism accompanies WM FA alterations with a concordant pattern of gray and WM involvement in the parietooccipital lobes in DLB.

© 2015 Elsevier Inc. All rights reserved.

1. Introduction

Diffusion tensor imaging (DTI) provides information on white matter (WM) microstructure, using the anisotropic nature of water diffusion, which is impeded perpendicularly to WM fibers. Fractional anisotropy (FA) is a robust DTI-derived measure (Pierpaoli and Basser, 1996) of the directionality of water diffusion, which decreases with the degeneration of WM. Hence, FA is often used as a proxy of WM integrity (Carmichael and Lockhart, 2012; Douaud et al., 2011).

DTI studies in dementia with Lewy bodies (DLB) have reported varying extents of WM involvement, ranging from widespread reduced FA in the corpus callosum, frontal, parietal, occipital, and temporal WM (Bozzali et al., 2005; Lee et al., 2010) to involvement confined to temporoparietal limbic and occipital pathways (Firbank et al., 2007, 2011; Kiuchi et al., 2011; Watson et al., 2012). Reduced FA in the occipital WM, specifically in the inferior longitudinal fasciculus, a pathway important for visuospatial processing, was a common finding in DLB patients (Bozzali et al., 2005; Kantarci et al., 2010; Kiuchi et al., 2011; Lee et al., 2010; Ota et al., 2008; Watson et al., 2012). Many DLB patients who fulfill the clinical criteria for probable DLB have overlapping Alzheimer's disease (AD)-related pathology, which may have contributed to the variation in WM diffusivity alterations in DLB.

* Corresponding author at: Mayo Clinic, 200 First Street SW, Rochester, MN 55905, USA. Tel.: +1 507 284 9770; fax: +1 507 284 9778.

E-mail address: kantarci.kejal@mayo.edu (K. Kantarci).

^{11}C Pittsburgh compound B (PiB) on positron emission tomography (PET) imaging traces β -amyloid ($\text{A}\beta$) plaques which are present in both AD and DLB patients (Foster et al., 2010; Rowe et al., 2007). Although PiB binds to $\text{A}\beta$ in both the neuritic and diffuse plaques (Klunk et al., 2001; Mathis et al., 2002), it has a higher affinity to neuritic plaques. Further, PiB does not bind to α -synuclein in Lewy bodies (Burack et al., 2010; Fodero-Tavoletti et al., 2007; Kantarci et al., 2012c). Therefore, PiB uptake on PET can serve as a marker of AD-related $\text{A}\beta$ pathology in DLB.

[^{18}F]2-fluoro-deoxy-D-glucose (18F-FDG) PET findings in DLB are characterized by hypometabolism in the occipital and posterior temporoparietal cortex (Imamura et al., 1997; Minoshima et al., 2001). However, cortical atrophy has not been observed in these posterior brain regions, neither in cross-sectional magnetic resonance imaging (MRI) studies in clinically diagnosed DLB patients (Middelkoop et al., 2001; Whitwell et al., 2007), nor in a longitudinal MRI study that investigated the pattern of cortical atrophy rates on antemortem MRI in an autopsy-confirmed cohort (Nedelska et al., 2014). Since DLB patients show a specific pattern of reduced cortical metabolism, FDG-PET is particularly useful to examine the neurodegenerative changes in the cortical gray matter, and to assess whether hypometabolism in the cortex relates to a loss of WM integrity in DLB.

It remains unknown whether AD-related $\text{A}\beta$ pathology is responsible for the alterations in WM microstructure in patients with DLB. Further, it is unclear whether the WM alterations on DTI topographically coincide with cortical hypometabolism observed on FDG-PET in DLB. First, we determined the pattern of WM diffusivity alterations in DLB compared with cognitively normal controls (CN) and AD patients using voxel-based analysis (VBA) across the WM of the entire brain. Second, we examined the contribution of $\text{A}\beta$ load to the disruption of WM integrity in patients with DLB, and finally, we compared the pattern of WM alterations on DTI and cortical glucose hypometabolism on FDG-PET in DLB.

2. Methods

2.1. Subjects and clinical evaluations

We identified 30 consecutive patients with probable DLB (McKeith et al., 2005) from a prospective, longitudinally followed

cohort at the Mayo Clinic Alzheimer's Disease Research Center (ADRC; a dementia clinic-based cohort) in Rochester, MN during a 3-year period 2010–2013. For comparison, we included 30 patients with probable AD (McKhann et al., 1984) and 60 CN either from the ADRC or from the Mayo Clinic Study on Aging (a community-based cohort) who were (1:1 or 2:1, respectively) age- and sex-matched with DLB patients. Eligibility was defined as the absence of any major abnormality on structural MRI that could confound the results such as tumors or large hemispheric infarcts, the absence of primary neurological illness affecting cognition other than DLB or AD, and sufficient scan quality to conduct analysis. The study was approved by the Mayo Clinic Institutional Review Board. All subjects or their proxies provided the informed consent on study participation.

Global measures of Clinical Dementia Rating Sum of Boxes (CDR-SOB; Hughes et al., 1982), Mini-Mental State Examination (MMSE; Folstein et al., 1975), and Dementia Rating Scale (DRS; Morris, 1993) were used to assess clinical disease severity at the time of the study. The presence, duration, and severity of DLB clinical features, and the duration of dementia were ascertained. Visual hallucinations (VH) had to be fully formed, recurring, and unlikely to be the consequence of causes other than DLB. VH severity was coded as mild, moderate, or severe. Fluctuations were considered present if patients scored 3 or 4 points on the Mayo Clinic Fluctuations questionnaire (Ferman et al., 2004). Motor impairment was scored using motor subscale of the Unified Parkinson's Disease Rating Scale (Fahn, 1987). Probable rapid eye movement sleep behavior disorder (pRBD) was diagnosed using the International Classification of Sleep Disorders-II diagnostic criteria B for pRBD (AASM, 2005).

2.2. MRI acquisition

MRIs were performed at 3T using an 8-channel phased array coil (GE, Milwaukee, WI, USA) and parallel imaging with an acceleration factor of 2. A 3D T1-weighted high-resolution magnetization prepared rapid gradient echo acquisition with repetition time = 7 ms, echo time = 3 ms, inversion time = 900 ms, flip angle = 8° , a slice thickness of 1.2 mm, and in plane resolution of 1.0 mm was obtained for anatomic segmentation and labeling. DTI was acquired using a single-shot echo-planar T2-weighted sequence in the axial plane with the following acquisition parameters: TR = 10,200 ms;

Table 1
Subjects' characteristics

| | CN n = 60 | DLB n = 30 | AD n = 30 | p-Value ^a |
|--------------------------------|-------------------|--------------------|-------------------|----------------------|
| Females (%) | 10 (17) | 5 (17) | 5 (17) | 1.0 |
| Age (y) | 68.5 (63, 76) | 69 (63, 76) | 72.5 (64, 79) | 0.48 |
| Education (y) | 15.5 (12.5, 18) | 15 (12, 18) | 16 (12, 18) | 0.69 |
| APOE ϵ 4 carriers (%) | 11 (18) | 13 (43) | 23 (77) | <0.001 |
| CDR sum of boxes | 0.0 (0.0, 0.0) | 5.75 (4.0, 7.0) | 4.75 (2.5, 7.0) | <0.001 |
| MMSE | 29 (28, 29) | 20.5 (15, 24) | 21 (14, 23) | <0.001 |
| DRS | — | 125.5 (114, 131) | 111 (85, 127) | 0.03 |
| PiB SUVR | 1.31 (1.27, 1.37) | 1.43 (1.30, 1.88) | 2.35 (2.17, 2.52) | <0.001 |
| VH present (%) | — | 23 (77) | 2 (8) | <0.001 |
| Fluctuations present (%) | — | 27 (90) | 2 (8) | <0.001 |
| Motor UPDRS | — | 12 (7, 14) | 0 (0, 2) | <0.001 |
| RBD present (%) | — | 28 (93) | 4 (15) | <0.001 |
| Dementia duration (y) | — | 5.04 (3.75, 7.17) | 5.21 (3.50, 7.00) | 0.88 |
| VH duration (y) | — | 1.91 (0.75, 3.59) | — | — |
| Fluctuations duration (y) | — | 2.25 (1.49, 3.67) | — | — |
| Parkinsonism duration (y) | — | 3.50 (1.17, 5.75) | — | — |
| RBD duration (y) | — | 9.21 (4.16, 14.08) | — | — |

Medians (interquartile ranges) are listed for the continuous and the proportions (%) are for the categorical variables.

Key: AD, Alzheimer's disease; APOE, apolipoprotein; CDR, Clinical Dementia Rating; CN, cognitively normal control; DLB, dementia with Lewy bodies; DRS, Dementia Rating Scale; MMSE, Mini-Mental State Examination; PiB, ^{11}C Pittsburgh compound B; RBD, rapid eye movement sleep behavior disorder; SUVR, standardized uptake value ratio; UPDRS, Unified Parkinson's Disease Rating Scale; VH, visual hallucinations (probable and definite combined together).

^a p-Values are from the Wilcoxon rank sum for the continuous variables, and a χ^2 test for differences in proportions.

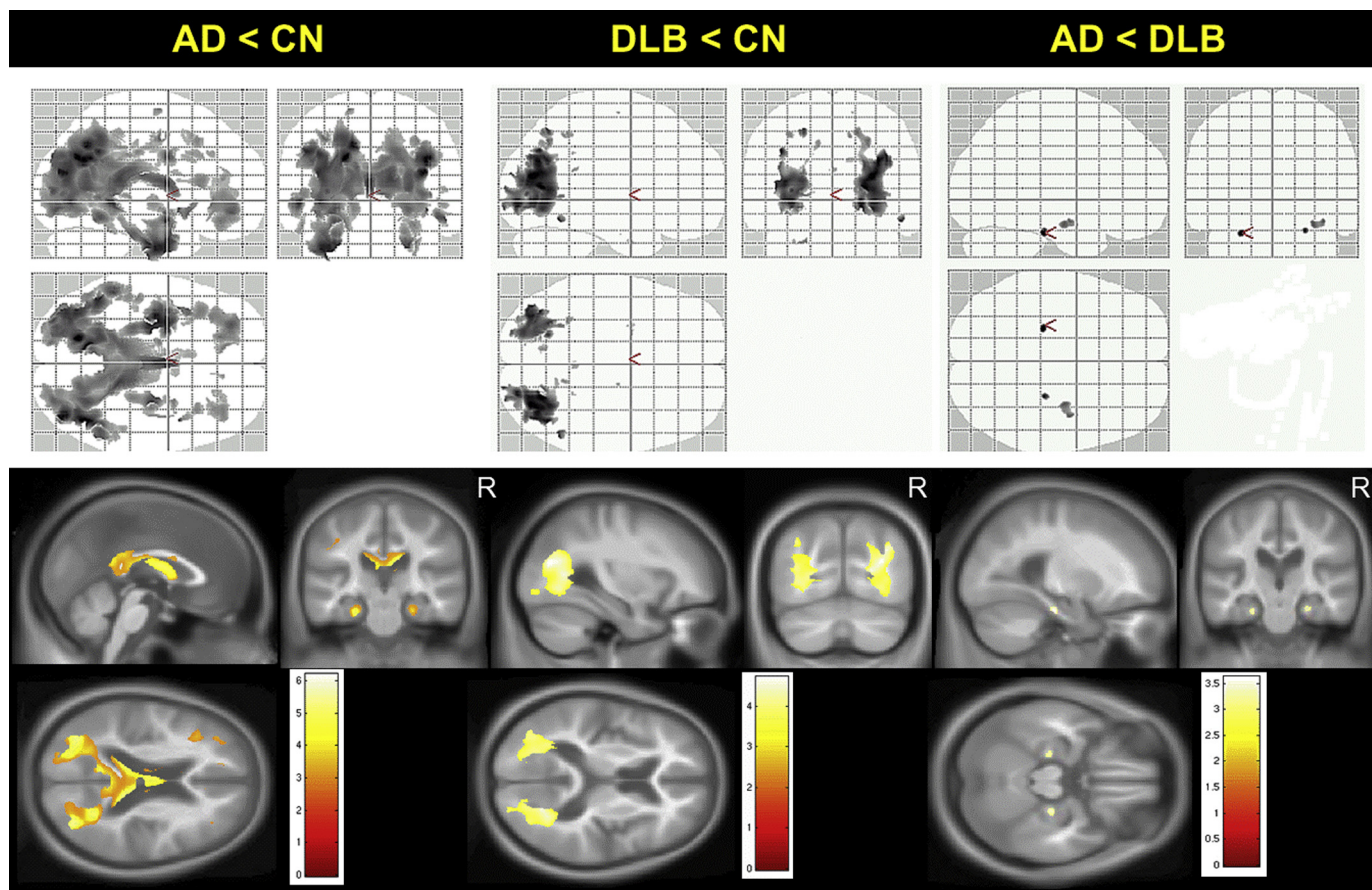


Fig. 1. Patterns of differences in FA between clinical groups on VBA. Voxel-level maps show topographic pattern of between-group differences in FA. FA maps overlaid on glass brain from SPM (top row) or anatomical sections (bottom row) show magnitude of the differences in FA using side T-statistic bars, $p < 0.001$ (uncorrected). AD patients have widespread FA decreases in temporoparietal, occipital, and frontal WM compared with CN (left column). DLB patients have reduced FA confined to parietooccipital WM compared with CN (middle column). In AD, reduced FA in parahippocampal WM is observed compared with DLB patients (right column). Abbreviations: AD, Alzheimer's disease; CN, cognitively normal control; DLB, dementia with Lewy bodies; FA, fractional anisotropy; SPM, Statistical Parametric Mapping; VBA, voxel-based analysis; WM, white matter.

in-plane matrix 128/128; field of view 35 cm; phase field of view 0.66. DTI volumes included 41 diffusion-encoding directions, and 4 non-diffusion weighted T2 images with 2.7-mm slice thickness and 2.7-mm isotropic resolution.

2.3. ^{11}C -PiB and ^{18}F -FDG-PET studies

^{11}C -PiB and ^{18}F -FDG-PET scans were performed within a median time of 7 days before or after DTI. Images were acquired using a PET/CT scanner (DRX, GE, Milwaukee, WI) in 3D on the same day with 1 hour interval between each other. Each subject was injected with ^{11}C -PiB and later with ^{18}F -FDG. Following a 40 minutes of PiB uptake period, a 20-minute PiB scan consisting of 4 dynamic frames each of 5 minute was obtained. Following a 30-minute ^{18}F -FDG uptake interval, an 8-minute FDG scan was acquired. PiB and FDG individual scans were affine co-registered to corresponding T1-weighted MRI scan. PiB and FDG images were parcellated into regions of interest (Tzourio-Mazoyer et al., 2002) using an in-house modified automatic anatomical labeling atlas (Vemuri et al., 2008), and partial volume correction was applied using a brain versus cerebrospinal fluid (CSF) model (Meltzer et al., 1999). The global cortical PiB standardized uptake value ratio (SUVR) was calculated as the median uptake in the bilateral parietal, temporal, prefrontal, orbito-frontal, cingulate precuneus, and anterior cingulate cortical uptake divided by uptake in the cerebellar gray matter (Jack et al., 2008). The cortical FDG uptake in each voxel was divided by the median pons

FDG uptake. Differences in glucose metabolism between CN and DLB patients were displayed using Statistical Parametric Mapping 5 (<http://www.fil.ion.ucl.ac.uk/spm>), at $p < 0.001$ and corrected for multiple comparisons using family-wise error. We used pons normalized FDG uptake values from those VBA-derived cortical regions, where FDG uptake was significantly reduced in DLB compared with CN, to determine the correlations among the focal abnormalities in FDG uptake and DTI findings in DLB.

2.3.1. DTI analysis

Each of the 41 diffusion-weighted images was affine co-registered to the non-diffusion weighted b_0 images to minimize head motion and eddy current-related distortions. Images were brain-extracted using FSL Brain Extraction Tool (<http://fsl.fmrib.ox.ac.uk/fsl/fslwiki/BET>). Tensors were fit using a least squares model, and FA maps were generated (Behrens et al., 2003). A VBA across the whole brain was conducted using the FA images according to previously published technique (Schwarz et al., 2014). Briefly, FA images of all subjects were nonlinearly co-registered via an iterative, group-wise registration algorithm Advanced Normalization Tools (Avants et al., 2010) and normalized to a 1-mm isotropic MNI 152 standard space via the FMRIB58_FA template (Jenkinson et al., 2012). The images were smoothed using an 8-mm full-width-half-maximum Gaussian kernel. Non-WM regions were removed by masking out voxels where the mean FA across co-registered subjects' images was < 0.2 .

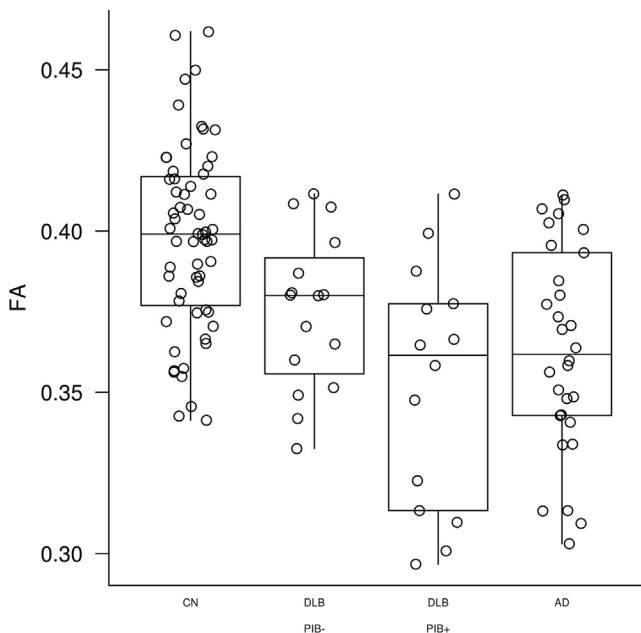


Fig. 2. Parietooccipital FA in PiB positive and PiB negative DLB. FA values from VBA-derived WM regions, where FA was significantly reduced in DLB compared with CN are displayed in PiB positive (SUVR < 1.5) and PiB negative (SUVR \geq 1.5) DLB subjects compared with AD and CN subjects. Abbreviations: AD, Alzheimer's disease; CN, cognitively normal control; DLB, dementia with Lewy bodies; FA, fractional anisotropy; PiB, ^{11}C Pittsburgh compound B; VBA, voxel-based analysis; WM, white matter.

We first examined the topographic pattern of FA differences between each of the 2 clinical groups on VBA using Statistical Parametric Mapping 5 at $p < 0.001$ corrected and uncorrected for multiple comparisons to capture the whole range of differences across the DLB spectrum with varying degrees of PiB retention compared with AD and CN groups. Second, we included the individual PiB SUVR as a continuous covariate in regression model to examine the contribution of A β load to WM diffusivity alterations in DLB compared with CN. Third, we used FA values from those VBA-derived WM regions, where FA was significantly reduced in DLB compared with CN, to determine the associations of focal abnormalities in FA with clinical features and focal abnormalities in FDG-PET in patients with DLB.

2.4. Statistics

Analyses on subjects' characteristics and correlations were performed using SAS version 9.3 and R statistical software package, version 2.14.0 (<http://www.R-project.org>) with 2-sided significance set at type-I error rate $\alpha < 0.05$. For continuous variables, the medians with interquartile ranges were reported along with the p -values from either the Kruskal-Wallis or Wilcoxon 2-sample rank-sum test. For binary or categorical variables, the proportions (%) were reported along with the p -values from χ^2 test. The associations between FA values and the duration or severity of clinical features in DLB patients were examined using the Spearman rank correlations. Correlations between duration of VH, severity of VH, and FA values were determined by likelihood ratio test.

3. Results

3.1. Subjects' characteristics

Subjects' characteristics are listed in Table 1. Groups were well matched on sex and age. We treated apolipoprotein (APOE) $\epsilon 4/2$

carriers as APOE $\epsilon 4/\epsilon 4$ or APOE $\epsilon 3/\epsilon 4$ carriers. The proportion of APOE $\epsilon 4$ carriers was highest in AD group ($p < 0.001$). Patients with DLB did not differ from AD in the estimated dementia duration ($p = 0.88$), or in measures of CDR-SOB ($p = 0.15$) or MMSE ($p = 0.99$). AD patients had a greater A β burden than DLB patients ($p < 0.001$) on ^{11}C -PiB PET. As expected, the frequencies of VH, pRBD, fluctuations and parkinsonism were higher in DLB compared with AD group ($p < 0.001$). Of the 30 DLB patients 16 (53%) were PiB negative (SUVR < 1.5) and 14 (47%) were PiB positive (SUVR \geq 1.5).

3.2. Patterns of WM FA alteration on VBA

Topographical patterns of between-group differences in FA are displayed in Fig. 1. We found no differences across the clinical groups after correction for multiple comparisons; therefore, we present uncorrected data ($p < 0.001$). Patients with AD had markedly reduced FA in temporal and parietal WM and less so in occipital and frontal WM compared with CN. Patients with DLB had FA decreases confined solely to posterior parietal and occipital WM compared with CN. Patients with DLB had a higher FA in the parahippocampal WM compared with AD patients. Median FA values derived from the voxels that have lower FA compared with CN are plotted in Fig. 2 demonstrating that PiB positivity may have influenced the findings, justifying the A β load-adjusted analysis.

3.3. Effect of A β load on WM integrity in DLB

Adjustment for A β load did not have a substantial effect on the FA alterations in DLB in the parietooccipital WM. The topographical pattern and magnitude of reduced FA in DLB remained similar between unadjusted and A β load-adjusted VBA; the only difference was that the extent of WM involvement shrunk from diffuse parietooccipital to a well-circumscribed area lying on parietal and occipital WM border (Fig. 3).

3.4. Association of WM FA alterations with clinical measures in DLB

From DLB-related features, we observed a marginally significant negative association with severity of VH (Spearman's $r = -0.36$; $p = 0.07$) and the parietooccipital WM FA abnormality on VBA. None of global clinical measures of CDR-SOB, MMSE, or DRS correlated with reduced FA in parietooccipital WM.

3.5. Cortical glucose hypometabolism and WM FA alterations in DLB

Fig. 4 overlays the VBA of glucose hypometabolism and FA decreases in patients with DLB compared with the CN group. Patterns of WM alteration and cortical glucose hypometabolism involved similar brain regions in DLB. Although changes on ^{18}F -FDG-PET were more diffuse, affecting inferior temporal, posterior parietal, and occipital cortices, an overlap with WM FA decreases was obvious in the parietooccipital lobes. However, we did not find an association between parietooccipital WM FA reduction and cortical glucose metabolism derived from regions that differed from CN subjects on VBA ($p = 0.14$).

4. Discussion

This study demonstrates how patients with DLB differ on the pattern of WM integrity disruption from age- and sex-matched CN and AD patients using a voxel-based algorithm examining the WM of the entire brain. DLB patients are characterized by reduced FA confined to the posterior parietal and occipital WM. Controlling for A β load, estimated by a global PiB retention, does not alter this finding and a similar, but more circumscribed pattern of reduced

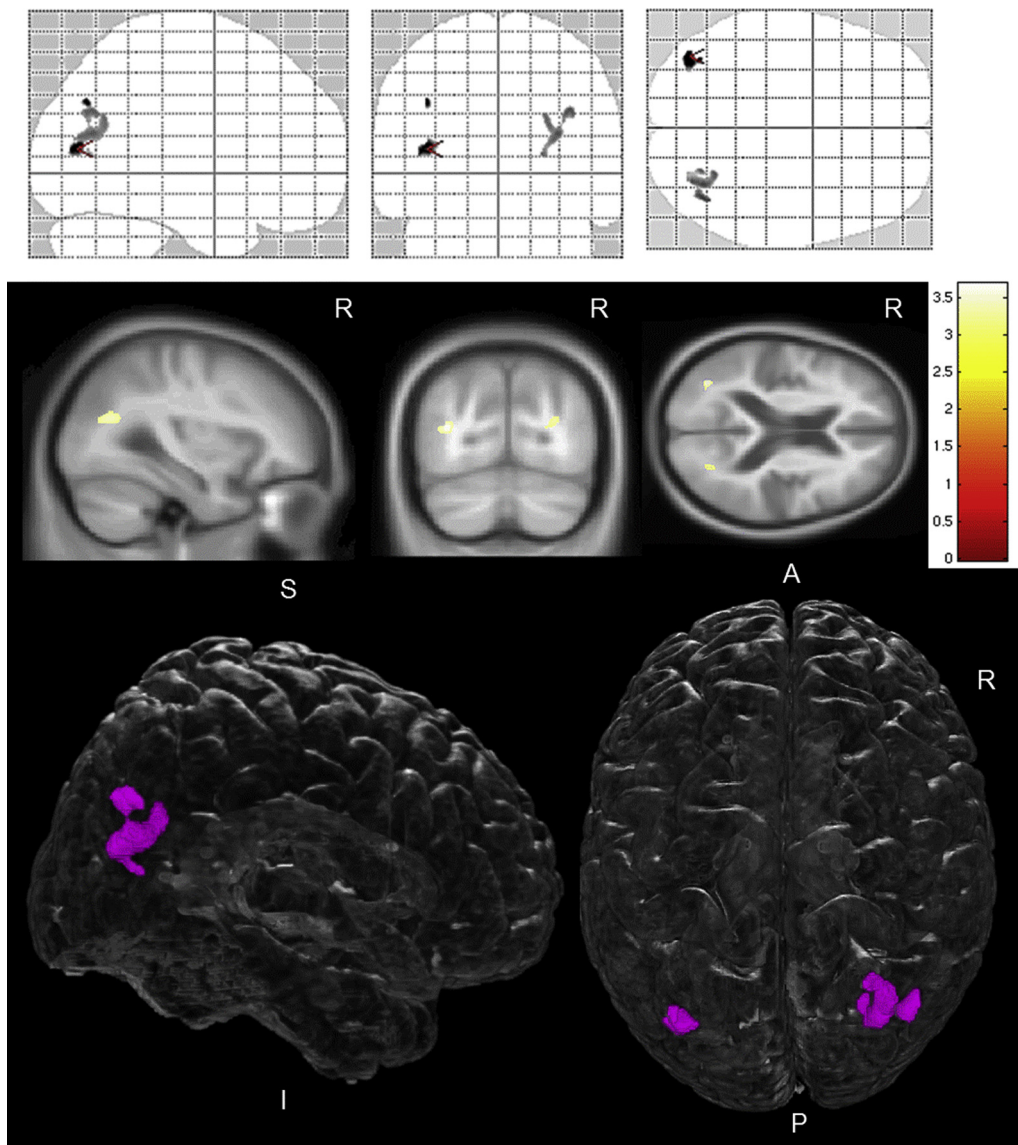


Fig. 3. Pattern of reduced FA in DLB patients compared with CN, adjusted for $A\beta$ load. Voxel-level maps show pattern of reduced FA in DLB patients compared with CN. FA maps overlaid on glass brain from SPM (top row) or anatomical sections (middle row) show magnitude of the FA differences between these 2 groups using side T-bars, $p < 0.001$ (uncorrected) on voxel-based analysis. Bottom row shows FA differences overlaid on a 3D glass-brain render from MRicroGL (<http://www.mccauslandcenter.sc.edu/mricrogl/>), with FA decreases confined to a well circumscribed region in parietooccipital WM. Abbreviations: CN, cognitively normal control; DLB, dementia with Lewy bodies; FA, fractional anisotropy; SPM, statistical parametric mapping.

FA is observed in the parietal and occipital WM border in DLB. This suggests WM integrity disruption in this region is only in-part dependent on $A\beta$ load, and is a typical feature of DLB. Comparing the pattern of cortical glucose hypometabolism on 18F-FDG-PET and WM FA alterations on DTI, cortical hypometabolic changes were more widespread than WM disruption in DLB. However, these abnormalities overlapped in the parietooccipital lobes.

In DLB patients, loss of posterior WM integrity has been a consistent finding across a number of DTI studies (Bozzali et al., 2005; Kantarci et al., 2010; Kiuchi et al., 2011; Lee et al., 2010; Ota et al., 2008; Watson et al., 2012) when compared with CN. Whereas we observed reduced FA in the posterior parietal and occipital WM compared with CN, we did not find differences elsewhere, unlike previous studies demonstrating more widespread WM involvement of temporal areas (Bozzali et al., 2005; Lee et al., 2010), varying severity of frontal (Bozzali et al., 2005; Lee et al., 2010; Watson et al., 2012), or pontine WM involvement

(Watson et al., 2012). Adjustment for $A\beta$ load led to a shrinkage of the regions where posterior parietooccipital WM FA was significantly reduced, but these were topographically consistent with unadjusted analysis. Patients with DLB commonly have mixed AD pathology, which may be responsible for hippocampal atrophy (Kantarci et al., 2012a; Murray et al., 2013) and greater medial temporal lobe atrophy rates (Nedelska et al., 2014) in these patients. While we do not have autopsy confirmation on a majority of our subjects, adjustment for $A\beta$ load reduced the impact of AD-related pathology on DTI findings. In fact, the occipital FA values derived from the VBA analysis were slightly lower in PiB positive DLB than the PiB negative DLB subjects, although both had reduced FA in this region compared with CN. It is likely that the widespread WM involvement in DLB, particularly in the temporal lobes, is associated with mixed AD pathology, which may not be apparent clinically.

Occipital and posterior parietal WMs comprise fibers connecting primary and association visual cortices to other brain regions, as

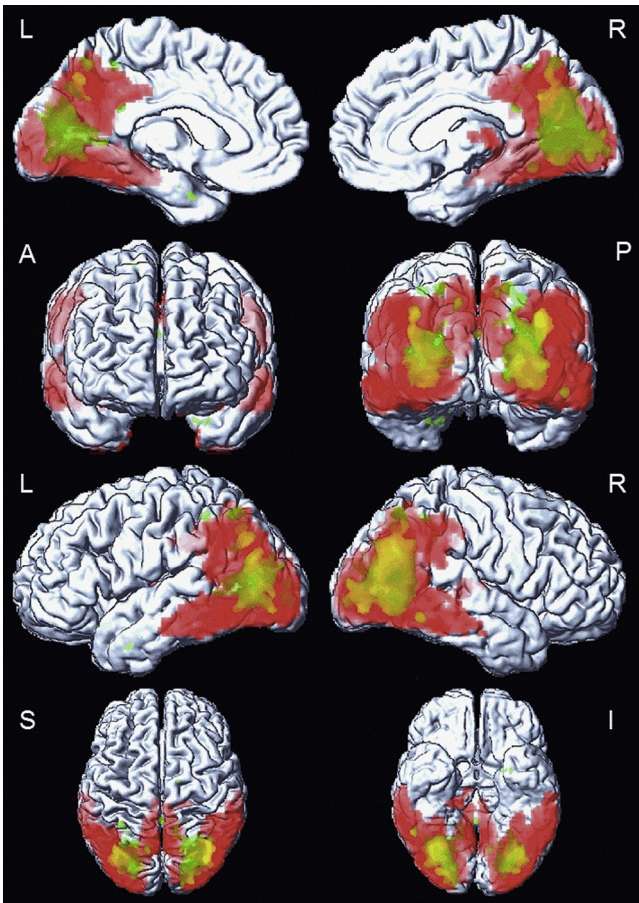


Fig. 4. Overlapping patterns of WM and cortical gray matter alterations in DLB patients on VBA. Cortical glucose hypometabolism on 18F-FDG-PET is overlapping with reduced FA in WM on DTI in DLB patients compared with CN. The overlap is displayed on a surface render using SPM5. The WM alteration (green color) is confined to parietooccipital region, $p < 0.001$ (uncorrected). The alteration in cortical glucose metabolism (red color) is more diffuse in posterior temporal, parietal, and in occipital cortices, $p < 0.001$ (family-wise error corrected). Abbreviations: CN, cognitively normal control; DLB, dementia with Lewy bodies; DTI, diffusion tensor imaging; FDG-PET, 2-fluoro-deoxy-D-glucose positron emission tomography; FA, fractional anisotropy; SPM5, Statistical Parametric Mapping 5; VBA, voxel-based analysis; WM, white matter.

well as 'what' and 'where' distinction pathways (Mesulam, 1998). In keeping with the functional anatomy, and considering that most of our DLB patients had VH, an association between VH and FA was expected. However, we found only a marginally significant association between FA and the severity of VH (coded as mild, moderate, or severe). We previously reported an association between presence of VH (present vs. absent) and reduced FA in the inferior longitudinal fasciculus that connects occipital visual cortex to temporal lobe (Kantarci et al., 2010). It is possible that the relationship between reduced FA and VH is confined to the inferior longitudinal fasciculus and not the entire occipital WM FA abnormality we analyzed in this study. Occipital WM has been investigated in autopsy-confirmed cohort DLB patients (Higuchi et al., 2000), where microvacuolation and gliosis were more frequent and severe in the occipital WM in DLB compared with AD patients. Such changes in control brains were minimal. Antemortem occipital hypometabolism on FDG-PET characterized those DLB patients with the most severe microvacuolation. Furthermore, microvacuolation was thought to be a substrate for mean diffusivity elevation in the amygdala in DLB (Fujino and Dickson, 2008;

Higuchi et al., 2000; Jellinger, 2004; Kantarci et al., 2010). Similarly, WM microvacuolation may be the substrate underlying reduced FA we observed in the parietooccipital WM of patients with DLB.

We observed that the cortical hypometabolism was largely overlying the disruption in WM integrity in the parietooccipital lobes. This posterior pattern of glucose hypometabolism, primarily involving the occipital cortex, is a characteristic feature of DLB (Minoshima et al., 2001) and is independent of AD-related A β load (Graff-Radford et al., 2014; Kantarci et al., 2012b). It is thought that the glucose hypometabolism in DLB is related to synaptic dysfunction because of presynaptic α -synuclein deposition with loss of postsynaptic dendritic spines (Kramer and Schulz-Schaeffer, 2007; Zaja-Milatovic et al., 2006), which may contribute to degeneration in the connecting tracts in the WM. Based on this topographic concordance, which was not statistically significant on quantitative analysis, the relationship between reduced WM FA and cortical hypometabolism in the occipital lobe should be further investigated by identifying the cortical connections of WM tracts involved in this region.

When we compared AD patients with CN, we observed reduced FA particularly in the temporoparietal WM, in agreement with previous DTI studies (Bozzali et al., 2002; Damoiseaux and Greicius, 2009; Huang et al., 2007; Kantarci et al., 2010; Medina et al., 2006; Mielke et al., 2009; Salat et al., 2010). DLB patients had elevated FA in a small but clearly bilateral and symmetric parahippocampal WM compared with AD patients. We found no other differences between these 2 groups, in agreement with a previous study reporting more asymmetrically reduced FA in the parahippocampal WM in AD patients (Watson et al., 2012). A relative preservation of parahippocampal WM integrity in DLB compared with AD patients is consistent with the preservation of hippocampal volumes on MRI in DLB compared with AD in autopsy-confirmed studies (Burton et al., 2009; Kantarci et al., 2012a; Murray et al., 2013). Dementia duration measured by clinical testing did not differ between our DLB and AD patients, and severity of dementia measured by DRS differed only slightly between these 2 groups. Our finding suggests that a hippocampal connectivity, which is in part carried by the cingulum tract that runs in the parahippocampal WM, is disrupted in AD but relatively preserved in DLB patients.

A limitation of our study is a lack of autopsy confirmation that could elucidate the role of WM microvacuolation on FA reduction and cortical glucose hypometabolism in DLB. We did not analyze the data on mean diffusivity, which is significantly affected by partial volume averaging of CSF. Although the influence of partial volume averaging of CSF is less on FA, up to 16% of the difference among subjects with mild cognitive impairment and CN has been attributed to macrostructural changes and associated partial volume averaging of CSF (Berlot et al., 2014). Development of robust methods for correction of partial volume averaging of CSF may improve the specificity of DTI findings in both GM and WM. Finally, we did not correct for multiple comparisons when reporting the VBA findings, which is common in AD DTI literature perhaps because of the effect sizes observed in DTI studies (Keihaninejad et al., 2012). In fact, correcting for multiple comparisons with family-wise error correction completely diminished the group differences.

In conclusion, current data indicate that loss of parietooccipital WM integrity is a characteristic feature of DLB, independent of AD-related A β deposition. This pattern of WM degeneration is consistent with the overlying reduction in glucose metabolism in the parietooccipital cortex. Although we cannot draw inferences on any causal or temporal relationship between loss of WM and GM integrity, our findings demonstrate that microstructural changes in the WM coincide with the GM hypometabolism in the

parietooccipital lobes in DLB patients. Longitudinal imaging studies may reveal the temporal course of GM and WM alterations in DLB.

Disclosure statement

Z. Nedelska, C. Schwarz, R. Reid, S. Przybelski, T. Lesnick, J. Gunter, and M. Senjem report no disclosures. B. Boeve has served as an investigator for a clinical trial sponsored by Cephalon, Inc. He has received honoraria from the American Academy of Neurology. He receives research support from the National Institute on Aging (P50-AG16574 [Co-I], U01 AG06786 [Co-I], R01-AG15866 [Co-I], and U24-AG26395 [Co-I]), and the Alzheimer's Association (IIRG-05-14,560 [PI]). T. Ferman is funded by the NIH (Mayo Clinic Alzheimer's Disease Research Center/Project 1-P50-AG16574/P1 [Co-I]). G. Smith is funded by the NIH (P50-AG16574). D. Knopman serves as Deputy Editor for *Neurology*; serves on a Data Safety Monitoring Board for Lundbeck Pharmaceuticals and for the Dominantly Inherited Alzheimer's Disease Treatment Unit. He is participating in clinical trials sponsored by Lilly Pharmaceuticals and TauRx Pharmaceuticals. He receives research support from the NIH. R. Petersen serves on scientific advisory boards for Elan Pharmaceuticals, Wyeth Pharmaceuticals, and GE Healthcare and receives research support from the NIH (P50-AG16574 [PI] and U01-AG06786 [PI], R01-AG11378 [Co-I], and U01-24904 [Co-I]). C. Jack serves as a consultant for Janssen, Bristol-Meyer-Squibb, General Electric, Siemens, and Johnson and Johnson and is involved in clinical trials sponsored by Allon and Baxter, Inc. He receives research funding from the National Institutes of Health (R01-AG011378, R01-AG037551, U01-HL096917, U01-AG032438, U01-AG024904), and the Alexander Family Alzheimer's Disease Research Professorship of the Mayo Foundation Family. K. Kantarci serves on the data safety monitoring board for Pfizer Inc and Takeda Global Research & Development Center, Inc; and she is funded by the NIH (R01AG040042 [PI], P50 AG44170/Project 2 [PI], P50 AG16574/Project 1 [PI], R01 AG11378[Co-I], U19 AG10483[Co-I], U01 AG042791[Co-I]), and Minnesota Partnership for Biotechnology and Medical Genomics (PO03590201[PI]).

Acknowledgements

Funding: Financial support for the conduct of the research was provided by the NIH (R01 AG040042, P50 AG016574, U01 AG06786, R01 AG11378, C06 RR018898), the Mangurian Foundation, and the Robert H. and Clarice Smith and Abigail Van Buren Alzheimer's Disease Research Program. Sponsors did not have any role in study design; in the collection, analysis, and interpretation of data; in the writing of the report; and in the decision to submit the article for publication.

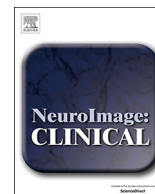
Yonas E. Geda is in part supported by AG-16574, Edli Foundation, RWJ Foundation and European Regional Development Fund-Project FNUSA-ICRC (CZ.1.05/1.1.00/02.0123). Zuzana Nedelska is supported by CTSA Grant Number UL1 TR000135 from the National Center for Advancing Translational Sciences (NCATS), a component of the National Institutes of Health (NIH). Its contents are solely the responsibility of the authors and do not necessarily represent the official view of NIH; Grant Agency of Charles University in Prague (doctoral student grant 624012); by European Regional Development Fund—Project FNUSA-ICRC (CZ.1.05/1.1.00/02.0123), European Social Fund (CZ.1.07/2.3.00/20.0117), and the State Budget of the Czech Republic.

References

AASM, 2005. *International Classification of Sleep Disorders—2: Diagnostic and Coding Manual*. American Academy of Sleep Medicine, Chicago.

- Avants, B.B., Yushkevich, P., Pluta, J., Minkoff, D., Korczynski, M., Detre, J., Gee, J.C., 2010. The optimal template effect in hippocampus studies of diseased populations. *Neuroimage* 49, 2457–2466.
- Behrens, T.E., Woolrich, M.W., Jenkinson, M., Johansen-Berg, H., Nunes, R.G., Clare, S., Matthews, P.M., Brady, J.M., Smith, S.M., 2003. Characterization and propagation of uncertainty in diffusion-weighted MR imaging. *Magn. Reson. Med.* 50, 1077–1088.
- Berlot, R., Metzler-Baddeley, Jones, D.K., O'Sullivan, M.J., 2014. CSF contamination contributes to apparent microstructural alterations in mild cognitive impairment. *Neuroimage* 92, 27–35.
- Bozzali, M., Falini, A., Cercignani, M., Baglio, F., Farina, E., Alberoni, M., Vezzulli, P., Olivetto, F., Mantovani, F., Shallice, T., Scotti, G., Canal, N., Nemni, R., 2005. Brain tissue damage in dementia with Lewy bodies: an in vivo diffusion tensor MRI study. *Brain* 128, 1595–1604.
- Bozzali, M., Falini, A., Franceschi, M., Cercignani, M., Zuffi, M., Scotti, G., Comi, G., Filippi, M., 2002. White matter damage in Alzheimer's disease assessed in vivo using diffusion tensor magnetic resonance imaging. *J. Neurol. Neurosurg. Psychiatry* 72, 742–746.
- Burack, M.A., Hartlein, J., Flores, H.P., Taylor-Reinwald, L., Perlmutter, J.S., Cairns, N.J., 2010. In vivo amyloid imaging in autopsy-confirmed Parkinson disease with dementia. *Neurology* 74, 77–84.
- Burton, E.J., Barber, R., Mukaetova-Ladinska, E.B., Robson, J., Perry, R.H., Jaros, E., Kalaria, R.N., O'Brien, J.T., 2009. Medial temporal lobe atrophy on MRI differentiates Alzheimer's disease from dementia with Lewy bodies and vascular cognitive impairment: a prospective study with pathological verification of diagnosis. *Brain* 132, 195–203.
- Carmichael, O., Lockhart, S., 2012. The role of diffusion tensor imaging in the study of cognitive aging. *Curr. Top. Behav. Neurosci.* 11, 289–320.
- Damoiseaux, J.S., Greicius, M.D., 2009. Greater than the sum of its parts: a review of studies combining structural connectivity and resting-state functional connectivity. *Brain Struct. Funct.* 213, 525–533.
- Douaud, G., Jbabdi, S., Behrens, T.E., Menke, R.A., Gass, A., Monsch, A.U., Rao, A., Whitcher, B., Kindlmann, G., Matthews, P.M., Smith, S., 2011. DTI measures in crossing-fibre areas: increased diffusion anisotropy reveals early white matter alteration in MCI and mild Alzheimer's disease. *Neuroimage* 55, 880–890.
- Fahn, S., Elton, R.L., UPDRS program members, 1987. Unified Parkinson's disease rating scale. In: Fahn, S., Marsden, C.D., Goldstein, M., Calne, D.B. (Eds.), *Recent Developments in Parkinson's Disease*, 2. Macmillan Healthcare Information, Florham Park, NJ, p. 153e163, 293e304.
- Ferman, T.J., Smith, G.E., Boeve, B.F., Ivnik, R.J., Petersen, R.C., Knopman, D., Graff-Radford, N., Parisi, J., Dickson, D.W., 2004. DLB fluctuations: specific features that reliably differentiate DLB from AD and normal aging. *Neurology* 62, 181–187.
- Firbank, M.J., Blamire, A.M., Krishnan, M.S., Teodorczuk, A., English, P., Gholkar, A., Harrison, R., O'Brien, J.T., 2007. Atrophy is associated with posterior cingulate white matter disruption in dementia with Lewy bodies and Alzheimer's disease. *Neuroimage* 36, 1–7.
- Firbank, M.J., Blamire, A.M., Teodorczuk, A., Teper, E., Mitra, D., O'Brien, J.T., 2011. Diffusion tensor imaging in Alzheimer's disease and dementia with Lewy bodies. *Psychiatry Res.* 194, 176–183.
- Fodero-Tavoletti, M.T., Smith, D.P., McLean, C.A., Adlard, P.A., Barnham, K.J., Foster, L.E., Leone, L., Perez, K., Cortes, M., Culvenor, J.G., Li, Q.X., Loughton, K.M., Rowe, C.C., Masters, C.L., Cappai, R., Villemagne, V.L., 2007. In vitro characterization of Pittsburgh compound-B binding to Lewy bodies. *J. Neurosci.* 27, 10365–10371.
- Folstein, M.F., Folstein, S.E., McHugh, P.R., 1975. "Mini-mental state": A practical method for grading the cognitive state of patients for the clinician. *J. Psychiatr. Res.* 12, 189–198.
- Foster, E.R., Campbell, M.C., Burack, M.A., Hartlein, J., Flores, H.P., Cairns, N.J., Hershey, T., Perlmutter, J.S., 2010. Amyloid imaging of Lewy body-associated disorders. *Mov. Disord.* 25, 2516–2523.
- Fujino, Y., Dickson, D.W., 2008. Limbic lobe microvacuolation is minimal in Alzheimer's disease in the absence of concurrent Lewy body disease. *Int. J. Clin. Exp. Pathol.* 1, 369–375.
- Graff-Radford, J., Murray, M.E., Lowe, V.J., Boeve, B.F., Ferman, T.J., Przybelski, S.A., Lesnick, T.G., Senjem, M.L., Gunter, J.L., Smith, G.E., Knopman, D.S., Jack, C.R., Dickson, D.W., Petersen, R.C., Kantarci, K., 2014. Dementia with Lewy bodies: basis of cingulate island sign. *Neurology* 83, 801–809.
- Higuchi, M., Tashiro, M., Arai, H., Okamura, N., Hara, S., Higuchi, S., Itoh, M., Shin, R.W., Trojanowski, J.Q., Sasaki, H., 2000. Glucose hypometabolism and neuropathological correlates in brains of dementia with Lewy bodies. *Exp. Neurol.* 162, 247–256.
- Huang, J., Friedland, R.P., Auchus, A.P., 2007. Diffusion tensor imaging of normal-appearing white matter in mild cognitive impairment and early Alzheimer disease: preliminary evidence of axonal degeneration in the temporal lobe. *AJNR Am. J. Neuroradiol.* 28, 1943–1948.
- Hughes, C.P., Berg, L., Danziger, W.L., Coben, L.A., Martin, R.L., 1982. A new clinical scale for the staging of dementia. *Br. J. Psychiatry* 140, 566–572.
- Imamura, T., Ishii, K., Sasaki, M., Kitagaki, H., Yamaji, S., Hirono, N., Shimomura, T., Hashimoto, M., Tanimukai, S., Kazui, H., Mori, E., 1997. Regional cerebral glucose metabolism in dementia with Lewy bodies and Alzheimer's disease: a comparative study using positron emission tomography. *Neurosci. Lett.* 235, 49–52.
- Jack Jr., C.R., Lowe, V.J., Senjem, M.L., Weigand, S.D., Kemp, B.J., Shiung, M.M., Knopman, D.S., Boeve, B.F., Klunk, W.E., Mathis, C.A., Petersen, R.C., 2008. ¹¹C PiB and structural MRI provide complementary information in imaging of

- Alzheimer's disease and amnesic mild cognitive impairment. *Brain* 131, 665–680.
- Jellinger, K.A., 2004. Lewy body-related alpha-synucleinopathy in the aged human brain. *J. Neural Transm.* 111, 1219–1235.
- Jenkinson, M., Beckmann, C.F., Behrens, T.E., Woolrich, M.W., Smith, S.M., 2012. *Fsl*. *Neuroimage* 62, 782–790.
- Kantarci, K., Avula, R., Senjem, M.L., Samikoglu, A.R., Zhang, B., Weigand, S.D., Przybelski, S.A., Edmonson, H.A., Vemuri, P., Knopman, D.S., Ferman, T.J., Boeve, B.F., Petersen, R.C., Jack Jr., C.R., 2010. Dementia with Lewy bodies and Alzheimer disease: neurodegenerative patterns characterized by DTI. *Neurology* 74, 1814–1821.
- Kantarci, K., Ferman, T.J., Boeve, B.F., Weigand, S.D., Przybelski, S., Vemuri, P., Murray, M.E., Senjem, M.L., Smith, G.E., Knopman, D.S., Petersen, R.C., Jack Jr., C.R., Parisi, J.E., Dickson, D.W., 2012a. Focal atrophy on MRI and neuropathologic classification of dementia with Lewy bodies. *Neurology* 79, 553–560.
- Kantarci, K., Lowe, V.J., Boeve, B.F., Weigand, S.D., Senjem, M.L., Przybelski, S.A., Dickson, D.W., Parisi, J.E., Knopman, D.S., Smith, G.E., Ferman, T.J., Petersen, R.C., Jack Jr., C.R., 2012b. Multimodality imaging characteristics of dementia with Lewy bodies. *Neurobiol. Aging* 33, 2091–2105.
- Kantarci, K., Yang, C., Schneider, J.A., Senjem, M.L., Reyes, D.A., Lowe, V.J., Barnes, L.L., Aggarwal, N.T., Bennett, D.A., Smith, G.E., Petersen, R.C., Jack Jr., C.R., Boeve, B.F., 2012c. Antemortem amyloid imaging and beta-amyloid pathology in a case with dementia with Lewy bodies. *Neurobiol. Aging* 33, 878–885.
- Keihaninejad, S., Ryan, N.S., Malone, I.B., Modat, M., Cash, D., Ridgway, G.R., Zhang, H., Fox, N.C., Ourselin, S., 2012. The Importance of Group-Wise Registration in Tract Based Spatial Statistics Study of Neurodegeneration: A Simulation Study in Alzheimer's Disease. *PLoS One* 7, e45996.
- Kiuchi, K., Morikawa, M., Taoka, T., Kitamura, S., Nagashima, T., Makinodan, M., Nakagawa, K., Fukusumi, M., Ikeshita, K., Inoue, M., Kichikawa, K., Kishimoto, T., 2011. White matter changes in dementia with Lewy bodies and Alzheimer's disease: a tractography-based study. *J. Psychiatr. Res.* 45, 1095–1100.
- Klunk, W.E., Wang, Y., Huang, G.F., Debnath, M.L., Holt, D.P., Mathis, C.A., 2001. Uncharged thioflavin-T derivatives bind to amyloid-beta protein with high affinity and readily enter the brain. *Life Sci.* 69, 1471–1484.
- Kramer, M.L., Schulz-Schaeffer, W.J., 2007. Presynaptic alpha-synuclein aggregates, not Lewy bodies, cause neurodegeneration in dementia with Lewy bodies. *J. Neurosci.* 27, 1405–1410.
- Lee, J.E., Park, H.J., Park, B., Song, S.K., Sohn, Y.H., Lee, J.D., Lee, P.H., 2010. A comparative analysis of cognitive profiles and white-matter alterations using voxel-based diffusion tensor imaging between patients with Parkinson's disease dementia and dementia with Lewy bodies. *J. Neurol. Neurosurg. Psychiatry* 81, 320–326.
- Mathis, C.A., Bacskai, B.J., Kajdasz, S.T., McLellan, M.E., Frosch, M.P., Hyman, B.T., Holt, D.P., Wang, Y., Huang, G.F., Debnath, M.L., Klunk, W.E., 2002. A lipophilic thioflavin-T derivative for positron emission tomography (PET) imaging of amyloid in brain. *Bioorg. Med. Chem. Lett.* 12, 295–298.
- McKeith, I.G., Dickson, D.W., Lowe, J., Emre, M., O'Brien, J.T., Feldman, H., Cummings, J., Duda, J.E., Lippa, C., Perry, E.K., Aarsland, D., Arai, H., Ballard, C.G., Boeve, B., Burn, D.J., Costa, D., Del Ser, T., Dubois, B., Galasko, D., Gauthier, S., Goetz, C.G., Gomez-Tortosa, E., Halliday, G., Hansen, L.A., Hardy, J., Iwatsubo, T., Kalaria, R.N., Kaufer, D., Kenny, R.A., Korczyn, A., Kosaka, K., Lee, V.M., Lees, A., Litvan, I., Londos, E., Lopez, O.L., Minoshima, S., Mizuno, Y., Molina, J.A., Mukaetova-Ladinska, E.B., Pasquier, F., Perry, R.H., Schulz, J.B., Trojanowski, J.Q., Yamada, M., 2005. Diagnosis and management of dementia with Lewy bodies: third report of the DLB Consortium. *Neurology* 65, 1863–1872.
- McKhann, G., Drachman, D., Folstein, M., Katzman, R., Price, D., Stadlan, E.M., 1984. Clinical diagnosis of Alzheimer's disease: report of the NINCDS-ADRDA Work Group under the auspices of Department of Health and Human Services Task Force on Alzheimer's disease. *Neurology* 34, 939–944.
- Medina, D., DeToledo-Morrell, L., Urresta, F., Gabrieli, J.D., Moseley, M., Fleischman, D., Bennett, D.A., Leurgans, S., Turner, D.A., Stebbins, G.T., 2006. White matter changes in mild cognitive impairment and AD: a diffusion tensor imaging study. *Neurobiol. Aging* 27, 663–672.
- Meltzer, C.C., Kinahan, P.E., Greer, P.J., Nichols, T.E., Comtat, C., Cantwell, M.N., Lin, M.P., Price, J.C., 1999. Comparative evaluation of MR-based partial-volume correction schemes for PET. *J. Nucl. Med.* 40, 2053–2065.
- Mesulam, M.M., 1998. From sensation to cognition. *Brain* 121, 1013–1052.
- Middelkoop, H.A., van der Flier, W.M., Burton, E.J., Lloyd, A.J., Paling, S., Barber, R., Ballard, C., McKeith, I.G., O'Brien, J.T., 2001. Dementia with Lewy bodies and AD are not associated with occipital lobe atrophy on MRI. *Neurology* 57, 2117–2120.
- Mielke, M.M., Kozauer, N.A., Chan, K.C., George, M., Toroney, J., Zerrate, M., Bandeen-Roche, K., Wang, M.C., Vanzijl, P., Pekar, J.J., Mori, S., Lyketsos, C.G., Albert, M., 2009. Regionally-specific diffusion tensor imaging in mild cognitive impairment and Alzheimer's disease. *Neuroimage* 46, 47–55.
- Minoshima, S., Foster, N.L., Sima, A.A., Frey, K.A., Albin, R.L., Kuhl, D.E., 2001. Alzheimer's disease versus dementia with Lewy bodies: cerebral metabolic distinction with autopsy confirmation. *Ann. Neurol.* 50, 358–365.
- Morris, J.C., 1993. The Clinical Dementia Rating (CDR): current version and scoring rules. *Neurology* 43, 2412–2414.
- Murray, M.E., Ferman, T.J., Boeve, B.F., Przybelski, S.A., Lesnick, T.G., Liesinger, A.M., Senjem, M.L., Gunter, J.L., Preboske, G.M., Lowe, V.J., Vemuri, P., Dugger, B.N., Knopman, D.S., Smith, G.E., Parisi, J.E., Silber, M.H., Graff-Radford, N.R., Petersen, R.C., Jack Jr., C.R., Dickson, D.W., Kantarci, K., 2013. MRI and pathology of REM sleep behavior disorder in dementia with Lewy bodies. *Neurology* 81, 1681–1689.
- Nedelska, Z., Ferman, T.J., Boeve, B.F., Przybelski, S.A., Lesnick, T.G., Murray, M.E., Gunter, J.L., Senjem, M.L., Vemuri, P., Smith, G.E., Geda, Y.E., Graff-Radford, J., Knopman, D.S., Petersen, R.C., Parisi, J.E., Dickson, D.W., Jack Jr., C.R., Kantarci, K., 2015. Pattern of brain atrophy rates in autopsy-confirmed dementia with Lewy bodies. *Neurobiol. Aging* 36, 452–461.
- Ota, M., Sato, N., Saitoh, Y., Endo, F., Murata, M., Asada, T., 2008. Diffusion tensor imaging in familial spastic paraplegia with mental impairment and thin corpus callosum. *Magn. Reson. Med. Sci.* 7, 163–167.
- Pierpaoli, C., Basser, P.J., 1996. Toward a quantitative assessment of diffusion anisotropy. *Magn. Reson. Med.* 36, 893–906.
- Rowe, C.C., Ng, S., Ackermann, U., Gong, S.J., Pike, K., Savage, G., Cowie, T.F., Dickinson, K.L., Maruff, P., Darby, D., Smith, C., Woodward, M., Merory, J., Tochon-Danguy, H., O'Keefe, G., Klunk, W.E., Mathis, C.A., Price, J.C., Masters, C.L., Villemagne, V.L., 2007. Imaging beta-amyloid burden in aging and dementia. *Neurology* 68, 1718–1725.
- Salat, D.H., Tuch, D.S., van der Kouwe, A.J., Greve, D.N., Pappu, V., Lee, S.Y., Hevelone, N.D., Zaleta, A.K., Growdon, J.H., Corkin, S., Fischl, B., Rosas, H.D., 2010. White matter pathology isolates the hippocampal formation in Alzheimer's disease. *Neurobiol. Aging* 31, 244–256.
- Schwarz, C.G., Reid, R.I., Gunter, J.L., Senjem, M.L., Przybelski, S.A., Zuk, S.M., Whitwell, J.L., Vemuri, P., Josephs, K.A., Kantarci, K., Thompson, P.M., Petersen, R.C., Jack Jr., C.R., 2014. Improved DTI registration allows voxel-based analysis that outperforms tract-based spatial statistics. *Neuroimage* 94, 65–78.
- Tzourio-Mazoyer, N., Landeau, B., Papathanassiou, D., Crivello, F., Etard, O., Delcroix, N., Mazoyer, B., Joliot, M., 2002. Automated anatomical labeling of activations in SPM using a macroscopic anatomical parcellation of the MNI MRI single-subject brain. *Neuroimage* 15, 273–289.
- Vemuri, P., Gunter, J.L., Senjem, M.L., Whitwell, J.L., Kantarci, K., Knopman, D.S., Boeve, B.F., Petersen, R.C., Jack Jr., C.R., 2008. Alzheimer's disease diagnosis in individual subjects using structural MR images: validation studies. *Neuroimage* 39, 1186–1197.
- Watson, R., Blamire, A.M., Colloby, S.J., Wood, J.S., Barber, R., He, J., O'Brien, J.T., 2012. Characterizing dementia with Lewy bodies by means of diffusion tensor imaging. *Neurology* 79, 906–914.
- Whitwell, J.L., Weigand, S.D., Shiung, M.M., Boeve, B.F., Ferman, T.J., Smith, G.E., Knopman, D.S., Petersen, R.C., Benaroch, E.E., Josephs, K.A., Jack Jr., C.R., 2007. Focal atrophy in dementia with Lewy bodies on MRI: a distinct pattern from Alzheimer's disease. *Brain* 130, 708–719.
- Zaja-Milatovic, S., Keene, C.D., Montine, K.S., Leverenz, J.B., Tsuang, D., Montine, T.J., 2006. Selective dendritic degeneration of medium spiny neurons in dementia with Lewy bodies. *Neurology* 66, 1591–1593.



Regional cortical perfusion on arterial spin labeling MRI in dementia with Lewy bodies: Associations with clinical severity, glucose metabolism and tau PET

Zuzana Nedelska^{a,b}, Matthew L. Senjem^{a,c}, Scott A. Przybelski^d, Timothy G. Lesnick^d, Val J. Lowe^a, Bradley F. Boeve^e, Arvin Arani^a, Prashanthi Vemuri^a, Jonathan Graff-Radford^e, Tanis J. Ferman^f, David T. Jones^e, Rodolfo Savica^e, David S. Knopman^e, Ronald C. Petersen^e, Clifford R. Jack^a, Kejal Kantarci^{a,*}

^a Department of Radiology, Mayo Clinic, Rochester, MN, United States

^b Department of Neurology, Charles University, 2nd Faculty of Medicine, Motol University Hospital, Prague, Czech Republic

^c Department of Information Technology, Mayo Clinic, Rochester, MN, United States

^d Department of Health Sciences, Mayo Clinic, Rochester, MN, United States

^e Department of Neurology, Mayo Clinic, Rochester, MN, United States

^f Department of Psychiatry and Psychology, Mayo Clinic, Jacksonville, FL, United States

ARTICLE INFO

Keywords:

Dementia with Lewy bodies
Cingulate island sign ratio
Cortical perfusion
Arterial spin labeling MRI
Or AV1–1451 tau PET
FDG PET

ABSTRACT

Visually preserved metabolism in posterior cingulate cortex relative to hypometabolism in precuneus and cuneus, the *cingulate island sign*, is a feature of dementia with Lewy bodies (DLB) on FDG-PET. Lower *cingulate island sign ratio* (posterior cingulate cortex/cuneus + precuneus; FDG-CISr) values have been associated with a higher Braak neurofibrillary tangle stage in autopsied DLB. Using voxel-wise analysis, we assessed the patterns of regional cortical perfusion and metabolism, and using an atlas-based approach, we measured perfusion cingulate island sign ratio on arterial spin labeling MRI (ASL-CISr), and its associations with FDG-CISr, uptake on tau-PET and clinical severity in DLB. Our study sample ($n = 114$) included clinically probable DLB patients ($n = 19$), age-matched patients with probable Alzheimer's disease dementia (AD; $n = 19$) and matched controls ($n = 76$) who underwent MRI with 3-dimensional pseudo-continuous arterial spin labeling, 18F-FDG-PET and 18F-AV-1451 tau PET. Patterns of cortical perfusion and metabolism were derived from quantitative maps using Statistical Parametric Mapping. DLB patients showed hypoperfusion on ASL-MRI in precuneus, cuneus and posterior parieto-occipital cortices, compared to controls, and relatively spared posterior cingulate gyrus, similar to pattern of hypometabolism on FDG-PET. DLB patients had higher ASL-CISr and FDG-CISr than AD patients ($p < 0.001$). ASL-CISr correlated with FDG-CISr in DLB patients ($r = 0.67$; $p = 0.002$). Accuracy of distinguishing DLB from AD patients was 0.80 for ASL-CISr and 0.91 for FDG-CISr. Lower ASL-CISr was moderately associated with a higher composite medial temporal AV-1451 uptake ($r = -0.50$; $p = 0.03$) in DLB. Lower perfusion in precuneus and cuneus was associated with worse global clinical scores. In summary, the pattern of cortical hypoperfusion on ASL-MRI is similar to hypometabolism on FDG-PET, and respective cingulate island sign ratios correlate with each other in DLB. Non-invasive and radiotracer-free ASL-MRI may be further developed as a tool for the screening and diagnostic evaluation of DLB patients in a variety of clinical settings where FDG-PET is not accessible.

1. Introduction

Although dementia with Lewy bodies (DLB) is the second most common neurodegenerative dementia in older adults, the diagnostic accuracy has been suboptimal (Nelson et al., 2010) and DLB remains

underdiagnosed (Mok et al., 2004) in the clinical setting. In addition, pathology underlying clinically diagnosed patients with DLB is often mixed with AD pathology (Irwin et al., 2017; Merdes et al., 2003; Mckeith et al., 2017; Halliday et al., 2011) and these can be misdiagnosed as having AD. Diagnostic accuracy needs to improve because

* Corresponding author at: Mayo Clinic, 200 First Street SW, Rochester, MN 55905, United States.
E-mail address: kantarci.kejal@mayo.edu (K. Kantarci).

the spectrum of DLB clinical symptoms is variable and wide, and DLB patients are sensitive to atypical neuroleptics that are commonly prescribed to the elderly.

DLB patients are characterized by parieto-occipital hypometabolism on 18F-fluorodeoxyglucose PET (FDG-PET) (Minoshima et al., 2001; Kantarci et al., 2012; Imamura et al., 1997), and visually preserved metabolism in the posterior cingulate cortex relative to hypometabolism in cuneus and precuneus, known as *cingulate island sign* (CIS) (Imamura et al., 1997; Lim et al., 2009). The quantitative measure of metabolism in posterior cingulate gyrus divided by metabolism in precuneus and cuneus is *CIS ratio* (Lim et al., 2009) (henceforth FDG-CISr). A lower FDG-CISr has been associated with a higher Braak neurofibrillary tangle stage at autopsy (Graff-Radford et al., 2014) and a greater medial temporal atrophy on MRI (Iizuka and Kameyama, 2016), but was not influenced by β -amyloid load on PET (Graff-Radford et al., 2014). FDG-CISr has been considered highly specific for the diagnosis of probable DLB (Lim et al., 2009), and has been recently included as a supportive biomarker in the fourth consensus report of the DLB Consortium (Mckeith et al., 2017). However, unlike MRI, FDG-PET is less available in many clinical facilities.

Arterial spin labeling (ASL) (Williams et al., 1992; Detre et al., 2009) is an MRI technique for quantitative measurement of the regional cerebral blood flow at the tissue level using the water molecules in the blood as endogenous magnetically labeled tracers. ASL can be included in a routine MRI examination and does not require injection of a radiotracer or contrast agent. Various ASL-MRI techniques have been used to evaluate patients within the AD spectrum (Musiek et al., 2012; Wolk and Detre, 2012; Chen et al., 2011). The pseudo-continuous ASL (Dai et al., 2008) has demonstrated a very good reliability and precision compared to a gold standard perfusion ^{15}O -water PET in elderly and patients with AD dementia (Xu et al., 2010) where a short acquisition time is important (Dai et al., 2008; Xu et al., 2010).

It remains unclear whether regional changes in cortical perfusion on ASL-MRI, particularly in CIS regions (Imabayashi et al., 2017; Imabayashi et al., 2016) are similar to hypometabolic changes on FDG-PET in DLB patients, and whether measuring the cortical perfusion on ASL MRI, particularly in regions that make up CIS, can be potentially useful for differentiating DLB patients from those with AD dementia.

Our objectives were first to assess the pattern of regional cortical perfusion using ASL-MRI in DLB patients and compare this pattern of regional cortical perfusion to regional metabolism on FDG-PET using voxel-wise approach. Second, to measure the perfusion and metabolism in the regions making up the CISr (henceforth ASL-CISr and FDG-CISr) using an atlas-based approach. Third, to determine the associations of ASL-CISr with composite medial temporal 18F-AV-1451 uptake on tau-PET which was chosen as proxy of an additional AD-related neurofibrillary tangle pathology in DLB patients, and associations of ASL-CISr with severity of the clinical impairment in DLB patients.

2. Materials and methods

2.1. Participants

This prospective study was approved by the Mayo Clinic Institutional Review Board in compliance with Health Insurance Portability and Accountability Act. All participants or their proxies provided a written informed consent prior to their participation. We included consecutive patients with clinically probable DLB ($n = 19$) (Mckeith et al., 2005) who were evaluated at the Mayo Clinic Alzheimer's Disease Research Center between June 2015 and March 2017. For comparison, we included concurrent patients with clinically probable AD dementia ($n = 19$) (Mckhann et al., 2011), matched 1:1 on age to DLB patients. As another comparison group, we selected clinically unimpaired older adults (CN; $n = 76$), matched 4:1 to DLB patients on age and sex from the Mayo Clinic Study of Aging, a population-based study of aging (Roberts et al., 2008). Patients with DLB and AD dementia

were treated with acetylcholinesterase inhibitors in a standard dosing regimen and with additional medications if needed.

All patients underwent comprehensive evaluations including neurological examination, interview with patient and his/her caregiver and neuropsychological tests covering four cognitive domains (memory, language, executive, visuospatial). Global measures of Clinical Dementia Rating Sum of Boxes (CDR-SOB); Dementia Rating Scale (DRS) and short test of mental status (Kokmen et al., 1991) were used to assess the global cognition and clinical disease severity of patients with dementia.

2.2. Ascertainment of DLB features

The presence, duration and severity of DLB clinical features, and the duration of dementia were evaluated. Visual hallucinations were considered present if they were well-formed and recurrent images of people, animals or objects. Fluctuations were considered as present if patients scored 3 or 4 points on the Mayo Clinic Fluctuations questionnaire (Ferman et al., 2004). Parkinsonism was rated using the Unified Parkinson's Disease Rating Scale part III (UPDRS-III). Probable REM sleep behavior disorder (RBD) was diagnosed using the International Classification of Sleep Disorders-II diagnostic criteria B for probable RBD (AASM, 2005).

2.3. Ascertainment of clinically unimpaired controls

Criteria for being clinically unimpaired were independent functioning and normal performance on tests covering four cognitive domains (memory, language, executive, visuospatial). The raw score from each test was transformed into age-adjusted score using previously established normative data from the Mayo Clinic's Older Americans Normative Studies (Ivnik et al., 1992) on the participants from the same population. Participants scoring 1.0 SD or more than the age-specific mean in the general population were considered for possible cognitive impairment (Petersen et al., 2010). The final decision on normal cognition was established during a panel consensus after taking into account education, prior occupation, visual or hearing deficits, and reviewing all other participant's information.

To be included in the current study, all participants needed to undergo MRI with pseudo-continuous ASL. All participants underwent FDG-PET except for one DLB patient. All DLB patients were requested to undergo AV-1451 tau PET. Only participants with scans of sufficient technical quality and without comorbidities that could interfere with cognitive functioning (brain tumor, large cortical infarct, normal pressure hydrocephalus, traumatic brain injury, alcoholism) were included. We excluded two DLB, two AD patients and four controls due to excessive head motion prior to image analysis.

2.4. Imaging studies

To investigate the patterns of cortical hypoperfusion, cortical metabolism and similarities between the two patterns in DLB patients as compared to controls, we used voxel-wise analysis. We further used an atlas-based approach to measure the perfusion and metabolism in regions that make up the ASL-CISr and FDG-CISr. CIS ratio denotes that the atlas-based measurement of perfusion or metabolism from the posterior cingulate cortex is divided by the perfusion or metabolism in cuneus+precuneus combined. An atlas-based approach was used to compare the magnitude of FDG-CISr and ASL-CISr to each other, and measure the associations between ASL-CISr and composite medial temporal AV-1451 uptake on tau PET and measures of clinical severity in DLB patients.

The relationship between the magnitude of ASL-CISr and severity of AD tau-related pathology in DLB patients was assessed using the AV-1451 uptake in a composite medial temporal region of the entorhinal cortex, parahippocampal gyrus and hippocampus. A study on

differences in tau deposition by AV-1451 between DLB and AD patients (Kantarci et al., 2017) showed that a composite meta-ROI consisting of these regions distinguished patients with DLB from those with AD using AV-1451 tau PET. Thus, medial temporal AV-1451 uptake can be considered to reflect AD-related tau pathology in patients with DLB.

2.5. ASL-MRI acquisition

For anatomical segmentation and labeling, a T1-weighted 3-dimensional high resolution magnetization prepared rapid acquisition gradient echo sequence was performed on a 3 Tesla MRI scanner (GE Healthcare; Waukesha, Wisconsin) with an eight channel phased array head coil. During the acquisition, participants were wearing ear plugs and were asked to relax but were not asked to close their eyes.

Cerebral blood flow of the entire cerebral cortex was acquired using a product 3-dimensional fast spin echo (FSE) pseudo-continuous ASL sequence with an interleaved stack-of-spiral readout and background suppression (Dai et al., 2008). The imaging parameters used were a labeling duration of 1450 ms, post labeling delay of 2025 ms, repetition time/echo time of 4800/10 milliseconds, refocusing flip angle 111.1 degrees, FOV 240 mm, acquisition matrix 512/8 samples re-gridded to a 128 × 128 matrix with an in-plane reconstructed resolution of 1.875 × 1.875 cm²; 40 slices with slice thickness 4 mm, no gap. Using the same readout scheme, 3 excitation averages of label and control volume pairs were acquired, a proton density (PD) weighted volume, and 4 discarded acquisitions to reach steady state were acquired, resulting in an overall scan duration of 4 min 48 s. The mean ASL difference image and the PD-weighted image were combined to calculate quantitative cerebral blood flow maps. Scans were visually inspected to ensure the whole brain coverage, and checked for image artefacts and only scans with sufficient quality were used for analysis.

2.6. Analysis of cortical perfusion on ASL-MRI

Individual pseudo-continuous ASL acquisitions were converted from DICOM to nifti-1 format, resulting in a single 4-dimensional nifti-1 volume where the first 3-dimensional volume was the PD and the second 3-dimensional volume was the PW - a difference between tag and control volumes. This was split into one 3-dimensional PD nifti-1 volume and one 3-dimensional PW nifti-1 volume. Each was co-registered to the participant's own T1-weighted volume using Statistical Parametric Mapping registration module, with the PD as the source and the T1-weighted volume as the target, and this transformation was also applied to move the PW volume into the T1 space. The quantitative cerebral blood flow maps were generated by fitting a derivative of the general kinetic model based on PW and PD volumes, using the formula provided in the recommendations for implementation of ASL (Alsop et al., 2015).

We used 2-class partial volume correction in ASL analysis (Meltzer et al., 1999).

Atlas-based parcellation of quantitative cerebral blood flow maps into regions of interest was performed by propagating an in-house modified version of the automated anatomic labeling atlas (Tzourio-Mazoyer et al., 2002) from template space into participant's T1 space, using the inverse spatial normalization parameters obtained from Statistical Parametric Mapping unified segmentation.

To reduce the subject-to-subject variability of ASL cerebral blood flow, the mean blood flow of the whole cerebellum gray matter was chosen as an internal reference in both voxel- and atlas-based analyses. The mean blood flow in the numerator (posterior cingulate cortex) and denominator (precuneus + cuneus) components of the CISr were divided by the mean flow in the whole cerebellum gray matter. Since CISr was measured as perfusion in posterior cingulate region divided by perfusion in precuneus + cuneus, the internal reference was not needed in this measurement.

2.7. Acquisition and analysis of 18F-FDG-PET and 18F-AV1451 tau PET

Scans were acquired using PET/CT scanner (DRX; GE Healthcare; Milwaukee, Wisconsin) operating in 3-dimensional mode. Briefly, FDG-PET was performed after 30 min of uptake, with four 2-minute dynamic frames. A 20-minute AV-1451 PET scan was performed after 80 min of uptake. During the acquisition, participants were wearing ear plugs and were asked to relax but were not asked to close their eyes. Individual FDG-PET and AV-1451 PET scans were co-registered to the participant's own T1-weighted MRI with a subsequent atlas-based parcellation.

For AV-1451 PET used in the current study solely as a proxy of an additional AD-related pathology in DLB, the median standardized uptake value in left + right cerebellar crus was used as a reference (Kantarci et al., 2017).

For FDG-PET and for a consistency with ASL-MRI analysis, the mean standardized uptake in the cerebellar gray matter has been chosen as a reference.

2-class partial volume correction was used in tau-PET and FDG-PET analysis (Meltzer et al., 1999).

The patterns of hypoperfusion on ASL-MRI and hypometabolism on FDG-PET in DLB patients were derived from an exploratory voxel-based analysis of the cortical gray matter using multiple regressions in Statistic Parametric Mapping. Smoothing was not applied. DLB patients were compared to controls using *t*-test and cluster size *k* of minimum 100 voxels. Comparisons were displayed as uncorrected for multiple comparisons (*p* < 0.001) to show the full range of differences, and applying the voxel-wise family wise error correction for multiple comparisons (FWE; *p* < 0.05).

2.8. Statistical analysis

Participants' characteristics were summarized using means and standard deviations (SD) or proportions (%). Continuous variables were compared across clinical groups using analysis of variance with a random block design to account for matching, followed by a priori chosen contrasts for pair-wise comparisons. The dummy (0, 1) variables (or blocks) were included as predictors in the models to account for the matching. Associations between continuous variables (FDG-CISr and ASL-CISr) among all were expressed as the partial correlations and were calculated after adjustment for the blocks. Categorical variables were compared between DLB and AD groups and between DLB and controls using either conditional logistic regression or exact conditional logistic regression. Associations between continuous variables in DLB patients where appropriate were assessed using Pearson correlations and their associated *p*-values. Medial temporal composite AV-1451 standardized uptake value ratio was log-transformed to meet the model assumptions.

Area under the receiver operating characteristic curve statistics with 95% confidence intervals (CI) was calculated to measure the performance of ASL-CISr and FDG-CISr when distinguishing between DLB and AD patients. Analyses were performed using SAS version 9.4 and R statistical software version 3.1.1 <http://www.R-project.org> with significance set at type I error rate α < 0.05.

3. Results

3.1. Participants' characteristics

Demographic and clinical characteristics are summarized in Table 1. Due to matching, no differences in age were observed between DLB and AD dementia patients. As expected, there were more women in AD than DLB group due to sex-based differences between the two disorders. No differences in the education or functional measures of clinical impairment were observed between DLB and AD group by CDR-SOB and DRS; however MMSE was lower in AD than in DLB group (*p* = 0.003). *APOE* ϵ 4 carriers were more prevalent in AD group (*p* = 0.016).

Table 1
Participants' demographic and clinical characteristics.

| | CN n = 76 | DLB n = 19 | AD n = 19 | DLB vs CN p-value* | DLB vs AD p-value* |
|------------------------------------|--------------|---------------|--------------|-----------------------|-----------------------|
| Age, years | 68.9 (6.7) | 68.9 (6.4) | 69.1 (6.8) | 0.96 | 0.77 |
| Male, no. (%) | 72 (95%) | 18 (95%) | 15 (79%) | 1.00 | 0.09 |
| APOE ϵ 4 carrier, no. (%) | 14 (19%) | 7 (37%) | 14 (82%) | < 0.001 | < 0.001 |
| Education, years | 14.8 (2.2) | 15.8 (2.5) | 16.3 (3.0) | 0.11 | 0.54 |
| MMSE | 28.7 (0.9) | 24.7 (4.3) | 21.8 (5.8) | < 0.001 | 0.003 |
| CDR-SOB | 0.0 (0.1) | 5.5 (4.6) | 4.1 (2.9) | < 0.001 | 0.07 |
| Motor UPDRS | 0.3 (1.0) | 13.0 (7.8) | 0.3 (0.6) | < 0.001 | < 0.001 |
| DRS | NA | 122.4 (26.0) | 124.7 (10.1) | < 0.001 | 0.81 |
| Visual hallucination, no. (%) | NA | 10 (53%) | 0 (0%) | – | – |
| Fluctuations, no. (%) | NA | 15 (79%) | 1 (6%) | – | – |
| Parkinsonism, no. (%) | NA | 19 (100%) | 1 (6%) | – | – |
| RBD, no. (%) | NA | 19 (100%) | 3 (17%) | – | – |
| ACHEI medication, no (%) | NA | 19 (100%) | 19 (100%) | – | – |

The mean (SD) is listed for the continuous variables and count (%) for the categorical variables.

Abbreviations: CN – clinically normal; DLB – dementia with Lewy bodies; AD – Alzheimer's disease dementia; APOE – apolipoprotein E; MMSE – Mini Mental State Examination; CDR-SOB – Clinical Dementia Rating – Sum of boxes; UPDRS – Unified Parkinson Disease Rating Scale; DRS – Dementia Rating Scale; RBD – REM sleep behavior disorder; ACHEI – acetylcholinesterase inhibitor.

* *p*-values for continuous variables are from analysis of variance with a random block design to account for matching, followed by a priori chosen contrasts for pair-wise comparisons of the clinical groups of interest (CN compared to DLB patients and AD patients compared to CN. *p*-values for categorical variables are either from conditional logistic regression or exact conditional logistic regression.

3.2. Pattern of hypoperfusion in DLB patients

Fig. 1 illustrates the voxel-wise pattern of cortical hypoperfusion side by side with cortical hypometabolism in DLB patients when compared to controls. Overall, the hypoperfusion was the most severe in the posterior parieto-temporal and occipital cortices that included precuneus and cuneus and supramarginal and angular gyrus, whereas the posterior cingulate gyrus was relatively spared. Moreover, the pattern of cortical hypoperfusion was similar with hypometabolism, although hypometabolism was slightly more wide-spread and included also voxels in the frontal cortices. No voxels with a higher perfusion in DLB than in controls were found.

3.3. Magnitude of ASL-CISr and FDG-CISr by clinical group

CISr were consistently highest in DLB and lowest in AD dementia patients on both ASL and FDG-PET (Fig. 2). On pair-wise comparisons of ASL-CISr, DLB had higher ASL-CISr than AD dementia patients ($p < 0.001$) and controls ($p = 0.007$). On pair-wise comparisons of FDG-CISr, DLB patients also had higher FDG-CISr than both AD dementia patients and controls ($p < 0.001$). The magnitude of ASL-CISr was slightly higher than FDG-CISr for a given clinical group.

3.4. Correlation between ASL-CISr and FDG-CISr

The ASL-CISr correlated with FDG-CISr among all participants using partial correlations accounting for the matching and in DLB patients using Pearson correlation (Fig. 3).

3.5. Relationship between medial temporal AV-1451 uptake and ASL-CISr in DLB

As expected, AD dementia patients had the highest whereas controls had the lowest medial temporal AV-1451 uptake ($p < 0.001$). DLB patients had higher medial temporal AV-1451 uptake than controls ($p = 0.022$). A higher medial temporal AV-1451 uptake correlated with lower ASL-CISr in DLB patients ($r = -0.50$; $p = 0.03$; Fig. 4).

Fig. 5 shows images of the individuals with DLB and AD dementia from our cohort which demonstrate CIS as a visually recognizable finding on ASL MRI and FDG-PET along with the corresponding AV-1451 uptake in medial temporal regions.

3.6. Regional perfusion in CISr regions and clinical impairment in DLB

Associations between ASL-CISr and MMSE, DRS, CDR-SOB or motor UPDRS were not observed. However, a lower perfusion in precuneus + cuneus (relative to perfusion in cerebellum) which make up the denominator of the CISr correlated with a higher CDR-SOB ($r = -0.57$; $p = 0.012$) and with lower DRS ($r = 0.54$; $p = 0.038$) and lower MMSE ($r = 0.50$; $p = 0.043$) corresponding to a worse global cognitive or functional impairment in DLB patients.

3.7. Utilizing CIS ratios to distinguish the DLB from AD patients

The receiver operating characteristics (ROC) curves with associated area under the ROC (AUROC) were calculated for ASL-CISr and for FDG-CISr used to distinguish between DLB and AD dementia patients. Although FDG-CISr performed better (AUROC 0.91; 95% CI 0.79–1.00), the accuracy of ASL-CISr was also good (0.80; 95% CI 0.65–0.95), Fig. 6.

4. Discussion

In this study, we demonstrated that patients with DLB had relatively spared regional perfusion in the posterior cingulate cortex in contrast with a hypoperfusion in precuneus and cuneus on ASL-MRI. Voxel-wise findings of hypoperfusion on ASL-MRI were similar to hypometabolism on FDG-PET in DLB, especially in posterior parietal and occipital regions, and the magnitude of ASL-CISr correlated with FDG-CISr. Conversely, AD dementia patients had severe hypoperfusion in posterior cingulate cortex; therefore ASL-CISr was higher in DLB than in AD dementia patients. Lower ASL-CISr in DLB patients was associated with a higher medial temporal AV-1451 uptake, a proxy of additional AD tau-related pathology in DLB patients. Lower perfusion in precuneus and cuneus that make up the denominator of ASL-CISr was associated with a greater clinical impairment by global cognitive and functional scores. Although the accuracy of FDG-CISr for distinguishing between DLB and AD dementia patients was higher, the accuracy of ASL-CISr was also good.

Only a few recent studies investigated ASL-MRI perfusion in a smaller number of DLB patients compared to controls (Binnewijzend et al., 2014; Taylor et al., 2012; Roquet et al., 2016). The severity and distribution of hypoperfusion in DLB patients varied, likely due to various methods used for ASL-MRI acquisition (sometimes not covering

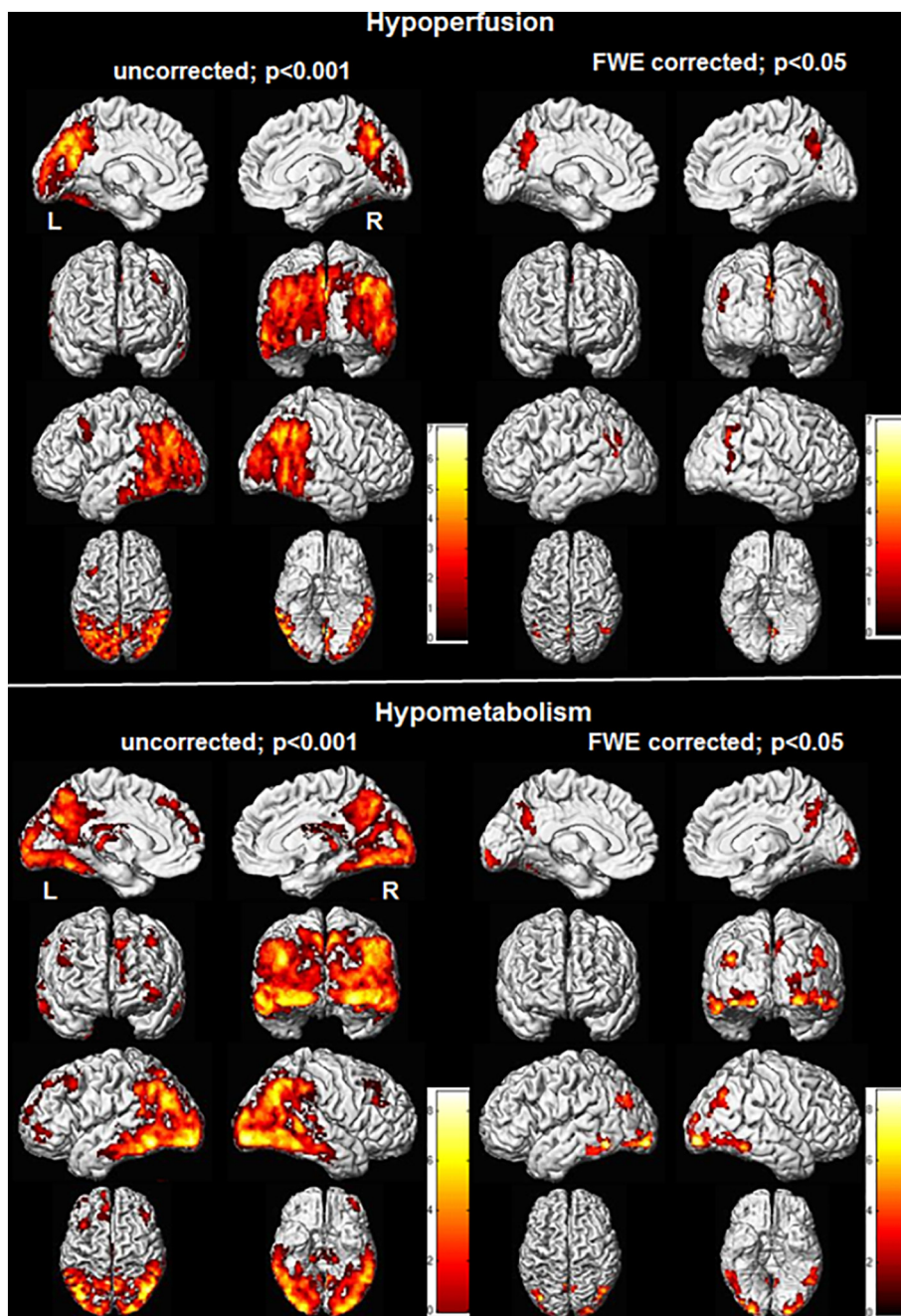


Fig. 1. Cortical hypoperfusion on ASL-MRI and hypometabolism on FDG-PET in DLB patients.

Regional cortical hypoperfusion on ASL is compared voxel-wise between DLB patients and CN (top panels). Pattern of cortical hypometabolism on FDG-PET is shown in the bottom panels. In the uncorrected analysis ($p < 0.001$, top left), DLB patients have hypoperfusion in the medial parieto-occipital cortices, specifically in precuneus and cuneus and in the lateral occipital and temporo-parietal cortex (e.g. angular, supramarginal and middle and inferior temporal gyrus) compared to CN. The perfusion in posterior cingulate gyrus is relatively spared. Pattern of hypoperfusion is similar to hypometabolism (bottom left), although the hypometabolism is more wide-spread involving voxels in temporo-parietal and frontal cortices. The posterior cingulate gyrus is only marginally involved. After voxel-wise correction for multiple comparisons with family-wise error (FWE) ($p < 0.05$, top right), the hypoperfusion remains confined to precuneus and cuneus and also supramarginal and angular gyrus. Hypometabolic areas overlap with hypoperfusion, although hypometabolism extends more into lateral temporo-parietal and to a lesser degree into frontal cortices (bottom right).

the entire brain or covering only a selected section), post-processing, and utilizing various voxel cluster thresholds at various significance levels. One of more consistent finding across these studies (Binnewijzend et al., 2014; Taylor et al., 2012) was hypoperfusion in precuneus and cuneus. Recently, a pattern of relatively preserved perfusion in the posterior cingulate cortex and cingulate island sign in DLB patients was also confirmed on perfusion SPECT imaging (Imabayashi et al., 2017; Imabayashi et al., 2016; Iizuka et al., 2017). Comparison of ASL-MRI with FDG-PET, a well-established functional method included as supportive feature for DLB diagnosis (Mckeith et al., 2017; Mckeith et al., 2005) has not been performed.

The pattern of hypoperfusion in our cohort of DLB patients was similar to the hypometabolic pattern on FDG-PET (Minoshima et al., 2001; Imamura et al., 1997; Kantarci et al., 2012) although the involvement on FDG-PET was more severe, especially in cuneus, and included voxels in lingual and frontal cortices. Similarly, highly

correlated patterns have been observed in early phase perfusion of AV-1451 PET and glucose hypometabolism on FDG-PET in a variety of neurodegenerative diseases (Hammes et al., 2017).

The consistent findings of relatively spared perfusion in posterior cingulate gyrus, hypoperfusion in precuneus and cuneus, and particularly their ratio ASL-CISr that we investigated in the current study, may be of added value for assessment of patients for DLB. ASL-CISr was highest in DLB and lowest in AD dementia patients, a finding consistent with FDG-CISr, although two AD dementia patients had higher ASL-CISr than expected (Fig. 2). Patients with atypical AD such as posterior cortical atrophy can have higher FDG-CISr (and potentially also higher ASL-CISr), although CISr and occipital involvement would be typically asymmetrical in posterior cortical atrophy (Whitwell et al., 2017).

ASL-MRI and FDG-PET are measuring two interrelated processes; perfusion and metabolism (Buxton and Frank, 1997). We found a good correlation between the FDG-PET and ASL findings in DLB patients.

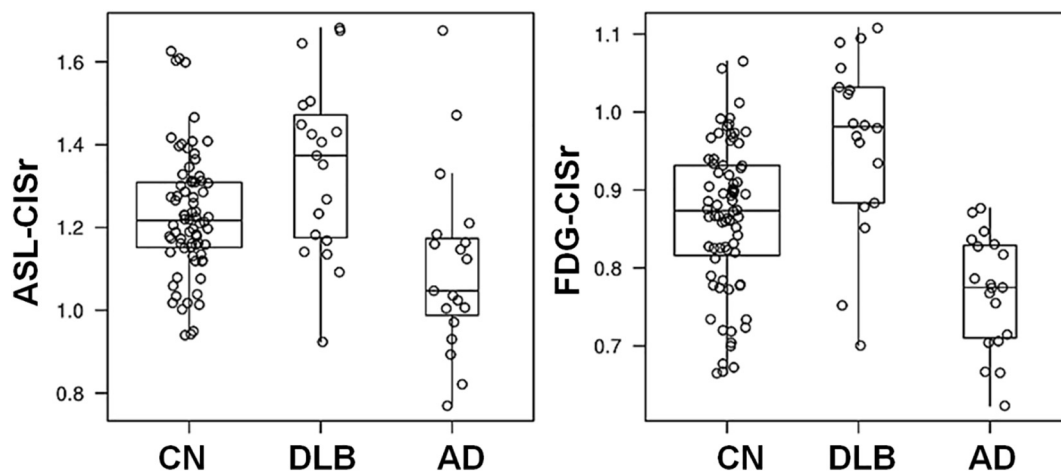


Fig. 2. Differences in ASL-CISr and FDG-CISr by clinical group.

Box-and-whisker plots show differences in magnitude of ASL-CISr and FDG-CISr; DLB patients have the highest CIS ratios whereas AD dementia patients have the lowest CIS ratios.

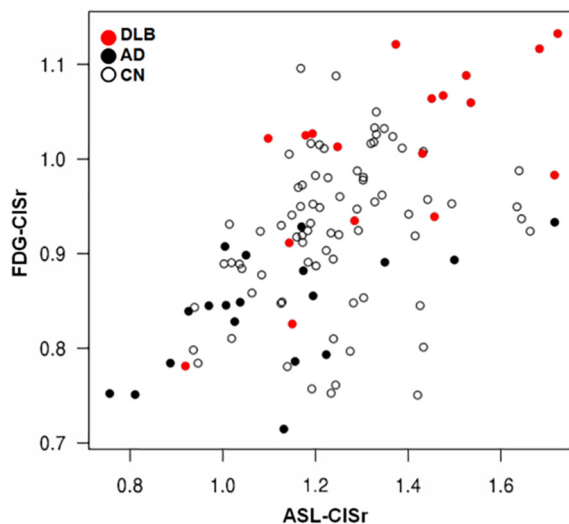


Fig. 3. Correlation between ASL-CISr and FDG-CISr.

Scatter plot shows Pearson correlation between FDG-CISr and ASL-CISr in DLB patients (red dots; $r_p = 0.67$; $p = 0.002$) and among all ($r_p = 0.52$; $p < 0.001$).

However, the magnitude of ASL-CISr was slightly higher than FDG-CISr in a given clinical group. This may be explained by potential regional (posterior cingulate versus cuneus and precuneus) differences in perfusion and metabolism (Chen et al., 2011) on ASL and FDG-PET, although the pattern of hypoperfusion overlapped with hypometabolism.

Higher composite medial temporal AV-1451 uptake on tau PET was associated with lower ASL-CISr, in agreement with a previous finding of a higher neurofibrillary tangle Braak stage at autopsy correlating with a lower FDG-CISr (Lim et al., 2009; Graff-Radford et al., 2014). This relationship is likely a reflection of greater AD-related neurofibrillary tangle pathology in the limbic network of those patients who have overlapping AD and Lewy body pathology. Posterior cingulate cortex is a part of the limbic network that is affected by AD-related neurofibrillary tangle pathology since the early stage of the disease (Minoshima et al., 1997; Reiman et al., 1996), and may be less targeted by Lewy body pathology (Lim et al., 2009). The relationship between a higher composite medial temporal AV-1451 uptake and lower ASL-CISr, however, needs to be interpreted with a caution since there were a few DLB patients with low medial temporal AV-1451 uptake who also had lower ASL-CISr values where higher ASL-CISr values would be expected instead. Other underlying pathologies than neurofibrillary tangle tau

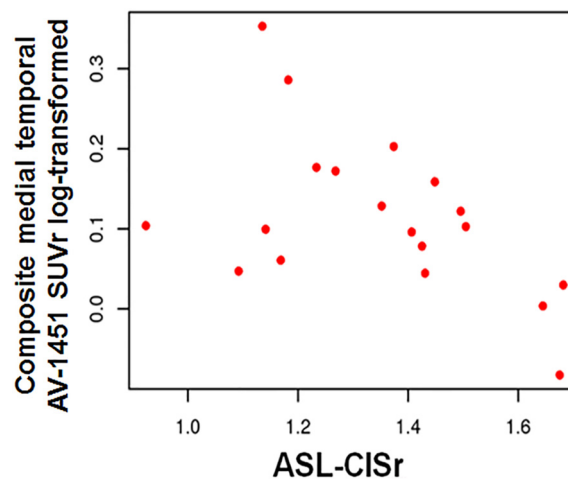


Fig. 4. Correlation between perfusion cingulate island sign ratio and medial temporal tau AV-1451 uptake in DLB.

Pearson correlation between a higher composite medial temporal AV-1451 uptake as a proxy of AD-related tau pathology and lower ASL-CISr in DLB patients ($r = -0.50$; $p = 0.03$). The SUVR of AV-1451 uptake is log-transformed.

pathology, such as hippocampal sclerosis, TAR DNA-binding protein 43 or cerebrovascular disease could contribute to this. Presence of these pathologies could explain lower AV-1451 uptake in DLB patients with lower ASL-CISr, in whom higher ASL-CISr values were expected in the presumed absence of neurofibrillary tangle tau pathology.

Among DLB patients, neuroimaging markers of AD-related pathology such as hippocampal volumes predict the treatment response with acetylcholinesterase inhibitors (Graff-Radford et al., 2012), therefore, ASL-CISr which is associated with neurofibrillary tangle pathology may serve as a prognostic biomarker but further research will be required.

Our consecutive DLB patients were mildly demented. We did not include DLB patients with more severe clinical disease as it has been challenging to acquire multimodality imaging of sufficient quality from DLB patients with moderate to severe dementia, a frequent problem in multimodality imaging studies in DLB patients. At this milder stage, a lower perfusion in precuneus and cuneus, relative to perfusion in cerebellar gray matter, correlated with greater clinical impairment by higher CDR-SOB, lower DRS and lower MMSE. However, there was no correlation between ASL-CISr as such and clinical disease severity; or between perfusion in the posterior cingulate cortex relative to

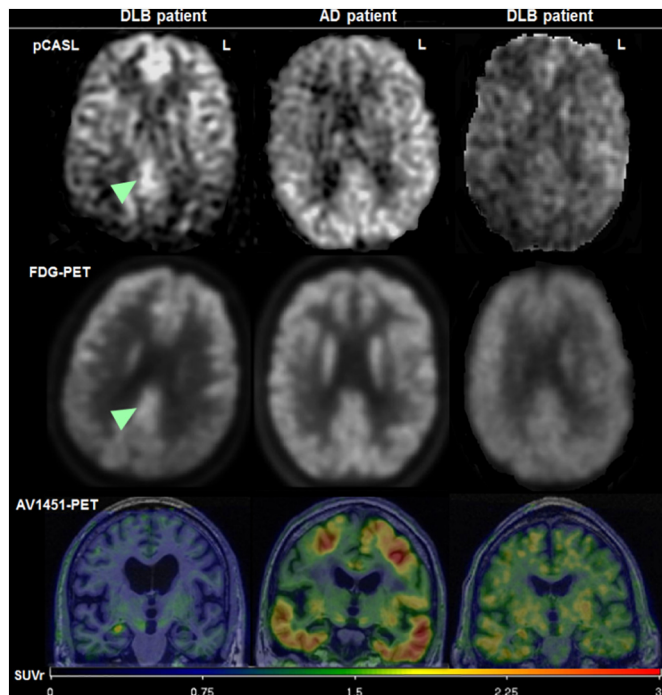


Fig. 5. Individual imaging findings in DLB and AD patients. Left: a 70 years old male DLB patient who has visually preserved CIS on ASL and FDG-PET: the arrow head points to the relatively preserved perfusion in the posterior cingulate cortex, when compared to a lower signal in precuneus and cuneus. He has a minimal medial temporal AV-1451 uptake (the bright spot on the right side is a non-specific uptake in the choroid plexus and not in the hippocampus itself). Middle: A 74 years old male AD dementia patient who does not have visually preserved CIS on ASL or FDG-PET. He has a considerable AV-1451 uptake including the medial temporal cortex. Right: an 82 years old male DLB patient who does not have visually preserved CIS on either ASL or FDG-PET and he has higher medial temporal AV-1451 uptake than DLB patient to the left.

cerebellum and the clinical measures of disease severity. This may be due to the relatively lower amount of AD-related tau pathology in posterior cingulate cortex in our DLB patients, or because the perfusion in precuneus and cuneus (as opposed to perfusion in posterior cingulate cortex) may reflect the severity of underlying pathologies, their interactions and associated clinical impairment more optimally. The Lewy body and AD-related pathologies may also progress at the different rates in these regions; a recent study using serial SPECT (Iizuka et al., 2017) reported that CISr was initially low in prodromal DLB patients, then high in mild DLB patients and again lower on follow up SPECT in DLB patients, potentially due to the progression of AD-related pathology.

AUROC statistics is commonly used to compare the diagnostic imaging methods. Using AUROC statistics, FDG-CISr was more accurate than ASL in distinguishing DLB and AD dementia patients possibly due to lower signal-to-noise ratio of the ASL acquisition. However, ASL-CISr also performed favorably with good sensitivity. Using a head array receiver coil with a higher number of channels, or increasing the number of averages could potentially increase the diagnostic accuracy for ASL-CISr measurement. Given the practical advantages of ASL, ASL-CISr may be considered as a potential screening tool for DLB in the clinical settings.

An internal reference region is needed in the quantitative analysis of cerebral blood flow because of the wide subject-to-subject variability in cerebral perfusion. We chose the whole cerebellar gray matter as an internal reference for ASL, and for consistency for FDG-PET, for the following reasons: 1) The ASL acquisition covered the entire cerebral and cerebellar hemispheres and signal-to-noise ratio in the cerebellum

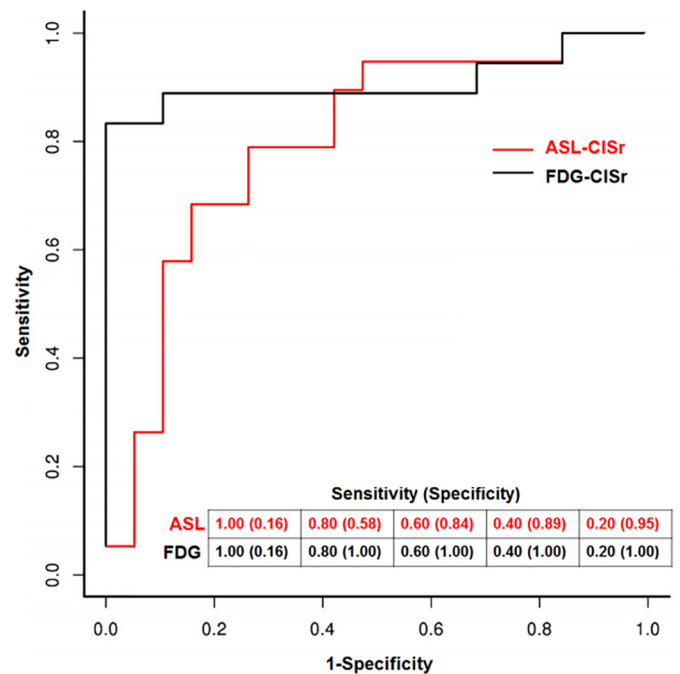


Fig. 6. Discrimination between DLB and AD patients using CISr. The receiver operating characteristics (ROC) curves are shown for ASL-CISr and for FDG-CISr for distinguishing DLB and AD dementia patients. The overall accuracy for ASL-CISr corresponds to area under the ROC (AUROC) of 0.80 (95% CI 0.79–1.00) and for FDG-CISr to AUROC of 0.91 (95% CI 0.65–0.95). Various sensitivities and associated specificities for both measures are listed.

was on par with that of the cerebrum; 2) cerebellum has not been preferentially affected by either Lewy body or AD pathology.

ASL-MRI is a non-invasive and radiotracer-free imaging modality that may be considered and further developed as tool for screening and diagnosis of DLB in a wide range of the clinical facilities where FDG-PET is not accessible.

Study funding

This study was funded by the NIH (R01-AG040042, R01-AG11378, P50-AG16574, U01-AG06786, U01-AG024904, R01-AG041851 and C06-RR018898), Foundation Dr. Corinne Schulerand, the Mangurian Foundation for Lewy Body Research, The Elsie and Marvin Dekelboun Family Foundation, and the Robert H. and Clarice Smith and Abigail Van Buren Alzheimer's Disease Research Program.

Acknowledgements and disclosures

We would like to greatly thank AVID Radiopharmaceuticals, Inc., for their support in supplying AV-1451 precursor, chemistry production advice and oversight, and FDA regulatory cross-filing permission and documentation needed for this work.

M. Senjem, S. Przybelski, T. Lesnick, C. Schwarz, D. Jones and R. Savica report no disclosures. Z. Nedelska was supported by a joint Research Fellowship 2016 provided by the International Brain Research Organization (IBRO) and the International Society for Neurochemistry (ISN), Czech Alzheimer Foundation and by CTSA Grant Number UL1 TR002377 from the National Center for Advancing Translational Sciences (NCATS), a component of the National Institutes of Health (NIH); its contents are solely the responsibility of the authors and do not necessarily represent the official view of NIH. V. Lowe is a consultant for Bayer Schering Pharma and receives research support from GE Healthcare, Siemens Molecular Imaging, AVID Radiopharmaceuticals, the NIH (National Institute on Aging [NIA],

National Cancer Institute), the Elsie and Marvin Deikelbom Family Foundation, the MN Partnership for Biotechnology and Medical Genomics, and the Leukemia & Lymphoma Society. B. Boeve has served as an investigator for clinical trials sponsored by GE Healthcare, FORUM Pharmaceuticals, C2N Diagnostics and Axovant. He receives royalties from the publication of a book entitled Behavioral Neurology of Dementia (Cambridge Medicine, 2009). He serves on the Scientific Advisory Board of the Tau Consortium. He receives research support from the NIH (U01-AG045390, U54-NS092089, P50-AG016574, U01-AG006786, and R01-AG041797), the Mayo Clinic Dorothy and Harry T. Mangurian Jr. Lewy Body Dementia Program and the Little Family Foundation. Dr. Vemuri receives support from the NIH (R01-NS097495 and P50-AG16574 [PI]). Dr. Graff-Radford receives research support from the NIH-NIA under Award Number K76AG057015. D. Knopman served as Deputy Editor for *Neurology*[®]; served on a Data Safety Monitoring Board for Lilly Pharmaceuticals; serves on a Data Safety Monitoring Board for Lundbeck Pharmaceuticals and for the DIAN study; served as a consultant to TauRx Pharmaceuticals ending in November 2012; was an investigator in clinical trials sponsored by Baxter and Elan Pharmaceuticals in the past 2 years; is currently an investigator in a clinical trial sponsored by TauRx; and receives research support from the NIH. R. Petersen serves on scientific advisory boards for Pfizer, Elan Pharmaceuticals, Wyeth Pharmaceuticals, and GE Healthcare, receives royalties from the publication of *Mild Cognitive Impairment* (Oxford University Press, 2003); and receives research support from the NIH/NIA and receives research support from the NIH (P50-AG16574 [PI] and U01-AG06786 [PI], R01-AG11378 [Co-I], and U01-24904 [Co-I]). C. Jack serves as a consultant for Janssen, Bristol-Meyer-Squibb, General Electric, and Johnson & Johnson; is involved in clinical trials sponsored by Allon and Baxter, Inc.; and receives research support from Pfizer, Inc., the NIA (AG11378 [PI], P50-AG16574 [Co-I], and U01-AG024904-01 [Co-I]), and the Alexander Family Alzheimer's Disease Research Professorship of the Mayo Foundation. K. Kantarci serves on the Data Safety Monitoring Board for Takeda Global Research & Development Center, Inc.; data monitoring boards of Pfizer and Janssen Alzheimer Immunotherapy; and is funded by the NIH (R01-AG040042 [PI], R21-NS066147 [PI], P50-AG44170/Project 2 [PI], P50-AG16574/Project 1 [PI], and R01-AG11378 [Co-I]).

References

- AASM, 2005. International Classification of Sleep Disorders—2: Diagnostic and Coding Manual. American Academy of Sleep Medicine, Chicago.
- Alsop, D.C., Detre, J.A., Golay, X., Gunther, M., Hendrikse, J., Hernandez-Garcia, L., et al., 2015. Recommended implementation of arterial spin-labeled perfusion MRI for clinical applications: a consensus of the ISMRM perfusion study group and the European consortium for ASL in dementia. *Magn. Reson. Med.* 73 (1), 102–116.
- Binnewijzend, M.A., Kuijter, J.P., van der Flier, W.M., Benedictus, M.R., Moller, C.M., Pijnenburg, Y.A., et al., 2014. Distinct perfusion patterns in Alzheimer's disease, frontotemporal dementia and dementia with Lewy bodies. *Eur. Radiol.* 24 (9), 2326–2333.
- Buxton, R.B., Frank, L.R., 1997. A model for the coupling between cerebral blood flow and oxygen metabolism during neural stimulation. *J. Cereb. Blood Flow Metab.* 17 (1), 64–72.
- Chen, Y., Wolk, D.A., Reddin, J.S., Korczykowski, M., Martinez, P.M., Musiek, E.S., et al., 2011. Voxel-level comparison of arterial spin-labeled perfusion MRI and FDG-PET in Alzheimer disease. *Neurology* 77 (22), 1977–1985.
- Dai, W., Garcia, D., de Bazelaire, C., Alsop, D.C., 2008. Continuous flow-driven inversion for arterial spin labeling using pulsed radio frequency and gradient fields. *Magn. Reson. Med.* 60 (6), 1488–1497.
- Detre, J.A., Wang, J., Wang, Z., Rao, H., 2009. Arterial spin-labeled perfusion MRI in basic and clinical neuroscience. *Curr. Opin. Neurol.* 22 (4), 348–355.
- Ferman, T.J., Smith, G.E., Boeve, B.F., Ivnik, R.J., Petersen, R.C., Knopman, D., et al., 2004. DLB fluctuations: specific features that reliably differentiate DLB from AD and normal aging. *Neurology* 62 (2), 181–187.
- Graff-Radford, J., Boeve, B.F., Pedraza, O., Ferman, T.J., Przybelski, S., Lesnick, T.G., et al., 2012. Imaging and acetylcholinesterase inhibitor response in dementia with Lewy bodies. *Brain* 135 (Pt 8), 2470–2477.
- Graff-Radford, J., Murray, M.E., Lowe, V.J., Boeve, B.F., Ferman, T.J., Przybelski, S.A., et al., 2014. Dementia with Lewy bodies: basis of cingulate island sign. *Neurology* 83 (9), 801–809.
- Halliday, G.M., Holton, J.L., Revesz, T., Dickson, D.W., 2011. Neuropathology underlying clinical variability in patients with synucleinopathies. *Acta Neuropathol.* 122 (2), 187–204.
- Hammes, J., Bischof, G.N., Giehl, K., Faber, J., Drzezga, A., Klockgether, T., et al., 2017. Elevated in vivo [18F]-AV-1451 uptake in a patient with progressive supranuclear palsy. *Mov. Disord.* 32 (1), 170–171.
- Iizuka, T., Kameyama, M., 2016. Cingulate island sign on FDG-PET is associated with medial temporal lobe atrophy in dementia with Lewy bodies. *Ann. Nucl. Med.* 30 (6), 421–429.
- Iizuka, T., Iizuka, R., Kameyama, M., 2017. Cingulate island sign temporally changes in dementia with Lewy bodies. *Sci. Rep.* 7 (1), 14745.
- Imabayashi, E., Yokoyama, K., Tsukamoto, T., Sone, D., Sumida, K., Kimura, Y., et al., 2016. The cingulate island sign within early Alzheimer's disease-specific hypoperfusion volumes of interest is useful for differentiating Alzheimer's disease from dementia with Lewy bodies. *EJNMMI Res.* 6 (1), 67.
- Imabayashi, E., Soma, T., Sone, D., Tsukamoto, T., Kimura, Y., Sato, N., et al., 2017. Validation of the cingulate island sign with optimized ratios for discriminating dementia with Lewy bodies from Alzheimer's disease using brain perfusion SPECT. *Ann. Nucl. Med.* 31 (7), 536–543.
- Imamura, T., Ishii, K., Sasaki, M., Kitagaki, H., Yamaji, S., Hirono, N., et al., 1997. Regional cerebral glucose metabolism in dementia with Lewy bodies and Alzheimer's disease: a comparative study using positron emission tomography. *Neurosci. Lett.* 235 (1–2), 49–52.
- Irwin, D.J., Grossman, M., Weintraub, D., Hurtig, H.I., Duda, J.E., Xie, S.X., et al., 2017. Neuropathological and genetic correlates of survival and dementia onset in synucleinopathies: a retrospective analysis. *Lancet Neurol.* 16 (1), 55–65.
- Ivnik, R.J., Malec, J.F., Smith, G.E., Tangalos, E.G., Petersen, R.C., Kokmen, E., et al., 1992. Mayo's Older Americans Normative Studies: WAIS-R, WMS-R and AVL-T norms for ages 56 through 97. *Clin. Neuropsychol.* 6 (Suppl. 2), 1–104.
- Kantarci, K., Lowe, V.J., Boeve, B.F., Weigand, S.D., Senjem, M.L., Przybelski, S.A., et al., 2012. Multimodality imaging characteristics of dementia with Lewy bodies. *Neurobiol. Aging* 33 (9), 2091–2105 Sep 21, 2012.
- Kantarci, K., Lowe, V.J., Boeve, B.F., Senjem, M.L., Tosakulwong, N., Lesnick, T.G., et al., 2017. AV-1451 tau and beta-amyloid positron emission tomography imaging in dementia with Lewy bodies. *Ann. Neurol.* 81 (1), 58–67.
- Kokmen, E., Smith, G.E., Petersen, R.C., Tangalos, E., Ivnik, R.C., 1991. The short test of mental status. Correlations with standardized psychometric testing. *Arch. Neurol.* 48 (7), 725–728.
- Lim, S.M., Katsifis, A., Villemagne, V.L., Best, R., Jones, G., Saling, M., et al., 2009. The 18F-FDG PET cingulate island sign and comparison to 123I-beta-CIT SPECT for diagnosis of dementia with Lewy bodies. *J. Nucl. Med.* 50 (10), 1638–1645.
- Mckeith, I.G., Dickson, D.W., Lowe, J., Emre, M., O'Brien, J.T., Feldman, H., et al., 2005. Diagnosis and management of dementia with Lewy bodies: third report of the DLB consortium. *Neurology* 65 (12), 1863–1872.
- Mckeith, I.G., Boeve, B.F., Dickson, D.W., Halliday, G., Taylor, J.P., Weintraub, D., et al., 2017. Diagnosis and management of dementia with Lewy bodies: fourth consensus report of the DLB consortium. *Neurology* 89 (1), 88–100.
- Mckhann, G.M., Knopman, D.S., Chertkow, H., Hyman, B.T., Jack Jr., C.R., Kawas, C.H., et al., 2011. The diagnosis of dementia due to Alzheimer's disease: recommendations from the National Institute on Aging-Alzheimer's Association workgroups on diagnostic guidelines for Alzheimer's disease. *Alzheimers Dement.* 7 (3), 263–269.
- Meltzer, C.C., Kinahan, P.E., Greer, P.J., Nichols, T.E., Comtat, C., Cantwell, M.N., et al., 1999. Comparative evaluation of MR-based partial-volume correction schemes for PET. *J. Nucl. Med.* 40 (12), 2053–2065.
- Merdes, A.R., Hansen, L.A., Jeste, D.V., Galasko, D., Hofstetter, C.R., Ho, G.J., et al., 2003. Influence of Alzheimer pathology on clinical diagnostic accuracy in dementia with Lewy bodies. *Neurology* 60 (10), 1586–1590.
- Minoshima, S., Giordani, B., Berent, S., Frey, K.A., Foster, N.L., Kuhl, D.E., 1997. Metabolic reduction in the posterior cingulate cortex in very early Alzheimer's disease. *Ann. Neurol.* 42 (1), 85–94.
- Minoshima, S., Foster, N.L., Sima, A.A., Frey, K.A., Albin, R.L., Kuhl, D.E., 2001. Alzheimer's disease versus dementia with Lewy bodies: cerebral metabolic distinction with autopsy confirmation. *Ann. Neurol.* 50 (3), 358–365.
- Mok, W., Chow, T.W., Zheng, L., Mack, W.J., Miller, C., 2004. Clinicopathological concordance of dementia diagnoses by community versus tertiary care clinicians. *Am. J. Alzheimers Dis. Other Dement* 19 (3), 161–165.
- Musiek, E.S., Chen, Y., Korczykowski, M., Saboury, B., Martinez, P.M., Reddin, J.S., et al., 2012. Direct comparison of fluorodeoxyglucose positron emission tomography and arterial spin labeling magnetic resonance imaging in Alzheimer's disease. *Alzheimers Dement.* 8 (1), 51–59.
- Nelson, P.T., Jicha, G.A., Kryscio, R.J., Abner, E.L., Schmitt, F.A., Cooper, G., et al., 2010. Low sensitivity in clinical diagnoses of dementia with Lewy bodies. *J. Neurol.* 257 (3), 359–366.
- Petersen, R.C., Roberts, R.O., Knopman, D.S., Geda, Y.E., Cha, R.H., Pankratz, V.S., et al., 2010. Prevalence of mild cognitive impairment is higher in men. The Mayo Clinic study of aging. *Neurology* 75 (10), 889–897.
- Reiman, E.M., Caselli, R.J., Yun, L.S., Chen, K., Bandy, D., Minoshima, S., et al., 1996. Preclinical evidence of Alzheimer's disease in persons homozygous for the epsilon 4 allele for apolipoprotein E. *N. Engl. J. Med.* 334 (12), 752–758.
- Roberts, R.O., Geda, Y.E., Knopman, D.S., Cha, R.H., Pankratz, V.S., Boeve, B.F., et al., 2008. The Mayo Clinic study of aging: design and sampling, participation, baseline measures and sample characteristics. *Neuroepidemiology* 30 (1), 58–69.
- Roquet, D., Sourty, M., Botzung, A., Armspach, J.P., Blanc, F., 2016. Brain perfusion in dementia with Lewy bodies and Alzheimer's disease: an arterial spin labeling MRI study on prodromal and mild dementia stages. *Alzheimers Res. Ther.* 8, 29.
- Taylor, J.P., Ffrench, M.J., He, J., Barnett, N., Pearce, S., Livingstone, A., et al., 2012. Visual cortex in dementia with Lewy bodies: magnetic resonance imaging study. *Br. J. Psychiatry* 200 (6), 491–498.

- Tzourio-Mazoyer, N., Landeau, B., Papathanassiou, D., Crivello, F., Etard, O., Delcroix, N., et al., 2002. Automated anatomical labeling of activations in SPM using a macroscopic anatomical parcellation of the MNI MRI single-subject brain. *NeuroImage* 15 (1), 273–289.
- Whitwell, J.L., Graff-Radford, J., Singh, T.D., Drubach, D.A., Senjem, M.L., Spsychalla, A.J., et al., 2017. 18F-FDG PET in posterior cortical atrophy and dementia with Lewy bodies. *J. Nucl. Med.* 58 (4), 632–638.
- Williams, D.S., Detre, J.A., Leigh, J.S., Koretsky, A.P., 1992. Magnetic resonance imaging of perfusion using spin inversion of arterial water. *Proc. Natl. Acad. Sci. U. S. A.* 89 (1), 212–216.
- Wolk, D.A., Detre, J.A., 2012. Arterial spin labeling MRI: an emerging biomarker for Alzheimer's disease and other neurodegenerative conditions. *Curr. Opin. Neurol.* 25 (4), 421–428.
- Xu, G., Rowley, H.A., Wu, G., Alsop, D.C., Shankaranarayanan, A., Dowling, M., et al., 2010. Reliability and precision of pseudo-continuous arterial spin labeling perfusion MRI on 3.0 T and comparison with 15O-water PET in elderly subjects at risk for Alzheimer's disease. *NMR Biomed.* 23 (3), 286–293.



Original Investigation | Neurology

Association of Longitudinal β -Amyloid Accumulation Determined by Positron Emission Tomography With Clinical and Cognitive Decline in Adults With Probable Lewy Body Dementia

Zuzana Nedelska, MD, MS; Christopher G. Schwarz, PhD; Timothy G. Lesnick, MS; Bradley F. Boeve, MD; Scott A. Przybelski, BS; Val J. Lowe, MD; Walter K. Kremers, PhD; Jeffrey L. Gunter, PhD; Matthew L. Senjem, MS; Jonathan Graff-Radford, MD; Tanis J. Ferman, PhD; Julie A. Fields, PhD; David S. Knopman, MD; Ronald C. Petersen, MD; Clifford R. Jack Jr, MD; Kejal Kantarci, MD, MS

Abstract

IMPORTANCE In patients with probable dementia with Lewy bodies (DLB), overlapping Alzheimer disease pathology is frequent and is associated with faster decline and shorter survival. More than half of patients with DLB have elevated β -amyloid levels on carbon-11 labeled Pittsburgh compound B (PiB) positron emission tomography, but the trajectory of longitudinal β -amyloid accumulation and its associations with clinical and cognitive decline in DLB are not known.

OBJECTIVES To determine the trajectory of β -amyloid accumulation in patients with probable DLB and to investigate the associations of β -amyloid accumulation with measures of clinical and cognitive decline over time in DLB.

DESIGN, SETTING, AND PARTICIPANTS This cohort study included 35 consecutive patients with probable DLB from the Mayo Clinic Alzheimer Disease Research Center and matched them by age, sex, and apolipoprotein e4 status with 140 cognitively unimpaired participants from the population-based Mayo Clinic Study of Aging. Participants were observed from April 2010 to September 2017. Data analysis was conducted from January 2018 to January 2019.

EXPOSURE Baseline and follow-up PiB positron emission tomography and comprehensive clinical evaluations.

MAIN OUTCOMES AND MEASURES Rate of change in PiB standardized uptake value ratios (SUVRs) by PiB SUVR and time in years; the associations between baseline PiB SUVR, change in PiB SUVR, and change in several measures of clinical and cognitive decline.

RESULTS A total of 175 participants were evaluated (35 [20.0%] with probable DLB; mean [SD] age, 69.6 [7.3] years; 16 [45.7%] apolipoprotein e4 carriers; 31 [88.6%] men; and 140 [80.0%] cognitively unimpaired adults; mean [SD] age, 69.7 [7.2] years; 64 [45.7%] apolipoprotein e4 carriers; 124 [88.6%] men). In both groups, the rates of change in PiB SUVR showed an initial acceleration at lower baseline PiB SUVR followed by a deceleration at higher baseline PiB SUVR, thus forming an inverted-U shape. The trajectories of the rates of change in PiB SUVR did not differ between participants with probable DLB and cognitively unimpaired participants in terms of shape ($P = .59$) or vertical shift (coefficient [SE] 0.007 [0.006]; $P = .22$). The integral association of cumulative PiB SUVR with time in years showed a sigmoid-shaped functional form in both groups. In participants with probable DLB, higher baseline PiB SUVR and change in PiB SUVR were associated with more rapid clinical decline, as measured by the Clinical Dementia Rating, sum of boxes (baseline PiB SUVR: regression coefficient [SE], 1.90 [0.63]; $P = .005$; $R^2 = 0.215$; change in PiB SUVR, regression coefficient [SE], 16.17 [7.47]; $P = .04$; $R^2 = 0.124$) and the Auditory Verbal Learning Test, delayed

(continued)

Key Points

Question What is the trajectory of β -amyloid accumulation over time, and how is it associated with clinical and cognitive decline among patients with probable dementia with Lewy bodies?

Findings This cohort study of 175 participants found that the cumulative density of β -amyloid accumulation by time in years followed a sigmoid-shaped form among patients with probable dementia with Lewy bodies as well as among cognitively unimpaired participants who were matched by age, sex, and apolipoprotein e4 status. In dementia with Lewy bodies, both baseline and longitudinal β -amyloid load accumulation were associated with measures of clinical and cognitive decline over time.

Meaning The results of this study suggest that longitudinal β -amyloid accumulation among patients with dementia with Lewy bodies could be used to track the clinical progression of dementia with Lewy bodies and potentially to design clinical trials targeting β -amyloid in dementia with Lewy bodies.

Author affiliations and article information are listed at the end of this article.

Open Access. This is an open access article distributed under the terms of the CC-BY License.

Abstract (continued)

recall (baseline PiB SUVR, regression coefficient [SE], -2.09 [0.95]; $P = .04$; $R^2 = 0.182$; change in PiB SUVR, regression coefficient [SE], -25.05 [10.04]; $P = .02$; $R^2 = 0.221$).

CONCLUSIONS AND RELEVANCE In this study, the rate of change in PiB SUVR among participants with probable DLB increased, peaked, and then decreased, which was similar to the trajectory in cognitively unimpaired participants and the Alzheimer disease dementia continuum. Higher baseline PiB SUVR and change in PiB SUVR were associated with more rapid clinical and cognitive decline over time. Measuring the change in PiB SUVR has implications for designing anti- β -amyloid randomized clinical trials for individuals with probable DLB.

JAMA Network Open. 2019;2(12):e1916439. doi:10.1001/jamanetworkopen.2019.16439

Introduction

Dementia with Lewy bodies (DLB) is a common neurodegenerative dementia associated with Lewy body disease pathology. Patients with probable DLB frequently have varying levels of Alzheimer disease (AD) pathology, β -amyloid, and neurofibrillary tangles (NFT), in addition to Lewy body disease pathology.^{1,2} In DLB, concomitant AD pathology has been associated with a faster clinical progression and a shorter survival in autopsy-confirmed cohorts.³⁻⁷

Positron emission tomography (PET) imaging with carbon-11 labeled Pittsburgh compound B (PiB) is a well-established biomarker of β -amyloid in vivo.⁸⁻¹⁰ Approximately two-thirds of patients with DLB have elevated PiB uptake on PET.¹¹ However, the association of a higher PiB uptake with greater clinical or cognitive impairment has been equivocal in DLB cross-sectionally.¹² Longitudinal studies in DLB are needed to understand the trajectory of PiB uptake over time and to determine its association with clinical progression. Monitoring these aspects will be important for identifying the most eligible candidates for emerging targeted treatments and for assessing the response to such treatments.

Using serial PiB PET, prospective studies¹³⁻¹⁵ in cognitively unimpaired (CU) and in cognitively impaired individuals within the AD continuum with a range of baseline PiB standardized uptake value ratios (SUVRs) demonstrated that the rate of change in PiB SUVR is not linear. At lower baseline PiB SUVR, the rate of change in PiB SUVR accelerates and then decelerates at a higher baseline PiB SUVR,¹³⁻¹⁵ thus forming an inverted-U shaped curve as a function of baseline PiB SUVR.^{13,15} Consequentially, cumulative PiB SUVR as a function of time follows a sigmoid-shaped trajectory,^{13,15} reaching a plateau at high baseline PiB SUVR within the AD continuum,^{13,15} with implications for the timing of treatment strategies.

In DLB, the trajectory of the change in PiB SUVR is not known. Nor is it known whether accelerated rates of change in PiB SUVR are associated with faster clinical declines in DLB. In this longitudinal PiB PET cohort study, our objective was to determine the change in PiB SUVR and the cumulative PiB SUVR over time in patients with probable DLB compared with CU adults with similar demographic characteristics. Our second objective was to evaluate the associations of baseline PiB SUVR and change in PiB SUVR with measures of longitudinal clinical and cognitive decline in probable DLB. A final objective was to calculate sample size estimates for a hypothetical randomized clinical trial targeting β -amyloid in DLB.

Methods

Data Source, Study Design, and Population

The probable DLB group included 35 consecutive patients observed through the Mayo Clinic Alzheimer Disease Research Center between April 2010 and September 2017, of whom 32 met

clinical criteria for probable DLB at baseline¹⁶ and 3 had mild cognitive impairment (MCI) at baseline and developed probable DLB by the first follow up. To compare the trajectory of change in PiB SUVR, we included 140 CU participants observed through the Mayo Clinic Study of Aging, a longitudinal, population-based cohort study.¹⁷ Cognitively unimpaired individuals were matched 4:1 with patients with probable DLB on age, sex, and apolipoprotein (APOE) e4 status; they remained CU throughout the study duration.

Baseline and Follow-up Visits

All participants were required to have a baseline PiB PET coupled with a comprehensive clinical evaluation and an identical follow-up within 12 to 15 months for the probable DLB group and within 15 to 30 months for the CU group. Baseline and follow-up visits incorporated a medical history review, informant interview, neurologic examination, neuropsychological assessment, and a series of informant questionnaires.^{3,17-19} After each visit, a consensus panel, composed of the study nurse, neurologist (B.F.B, J.G.-R., D.S.K., or R.C.P.), and neuropsychologist (T.J.F. or J.A.F.) who evaluated the participant, established the clinical diagnosis after accounting for visual or hearing deficits, education, and prior level of functioning.

Clinical and Cognitive Measures

Clinical severity and progression were determined using global cognitive assessments (ie, Mini-Mental State Examination [MMSE] and Dementia Rating Scale [DRS]) and noncognitive functional assessments (Clinical Dementia Rating scale, sum of boxes [CDR-SOB] and motor impairment by Unified Parkinson Disease Rating Scale part III [UPDRS-III]). Neuropsychological evaluations included the Auditory Verbal Learning Test (AVLT) for memory, the Boston Naming Test (BNT) for object naming, the Trail Making Test, part A (TMT-A) for divided attention, and the Rey Complex Figure (RCF) test for visual-perceptual processing.

The study was approved by the Mayo Clinic institutional review board, and informed consent on participation was obtained from every participant or an appropriate surrogate. The study followed Strengthening the Reporting of Observational Studies in Epidemiology (STROBE) reporting guideline.

Imaging Study

Baseline and follow-up PiB PET imaging was performed on PET-computed tomography systems operating in a 3-dimensional mode (GE Medical Systems). Scans consisted of four 5-minute dynamic frames acquired from 40 to 60 minutes after injection of PiB; detailed descriptions have been published elsewhere.^{15,20} For anatomic segmentation and labeling of PiB PET images, 3-dimensional, high-resolution, magnetization-prepared rapid gradient echo T1-weighted magnetic resonance imaging (MRI) scans, performed during the same visit cycle as the PiB PET, were acquired with a 3-T MRI scanner with 1 mm³ resolution (GE Medical Systems).²¹ Baseline and follow-up MRI images were automatically segmented and bias corrected using unified segmentation²² in statistical parametric mapping 12. We rigidly aligned PET images to MRI images, using statistical parametric mapping 12 (baseline-to-baseline and follow-up-to-follow-up), and MRI segmentations were used to perform 2-class partial volume correction.²³ For consistency, we also performed analyses with no partial volume correction of PiB SUVR. Regions were automatically located using advanced normalization tools²⁴ with the Mayo Clinic Adult Lifespan Template.^{25,26} For each PiB image, PiB uptake was calculated as the SUVR in a standard composite region consisting of voxels in the parietal, posterior cingulate, precuneus, prefrontal, orbitofrontal, temporal, and anterior cingulate cortices.¹⁵ To maximize the reliability and plausibility of measurements, we used 2 reference regions: 1 for baseline PiB SUVR and 1 for longitudinal change in PiB SUVR. For the baseline PiB SUVR measurement, we used a standard cerebellar crus reference region.²⁷ To measure the change in PiB SUVR, we used a composite reference region of eroded supratentorial white matter, whole cerebellum, and pons; this technique was developed by our group, has been extensively tested and compared with multiple

alternative approaches, and has been shown to improve reliability and plausibility for serial measurements compared with cross-sectional approaches.²⁰

Statistical Analysis

Demographic, clinical, and cognitive characteristics of participants with probable DLB and CU participants at baseline were summarized using means with SDs or proportions. A log transformation or a square root transformation was performed to normalize the distribution of baseline PiB SUVR, MMSE score, and CDR-SOB score. Continuous variables were compared between probable DLB and CU groups using analysis of variance with a random block design with an added predictor to account for matching. The change in PiB SUVR for probable DLB and CU groups was constructed from partial volume-corrected serial PiB SUVR. Changes in PiB SUVR and in clinical and cognitive measures were annualized. We chose generalized additive models (GAMs) with 95% CIs to model the change in PiB SUVR as a function of baseline PiB SUVR. We used 4-*df* penalized splines in GAMs as our primary analysis to estimate the shapes of change in PiB SUVR vs baseline PiB SUVR for probable DLB and CU groups separately. Subsequently, we tested for a type of interaction between group (probable DLB or CU) and change in PiB SUVR by fitting fixed 4-*df* regression splines (to control the smooths and produce nested models) within each group and then by fitting a 4-*df* regression spline without differentiating the groups. We used an approximate F test from the analysis of deviance table comparing the models to test the interaction. We used GAMs to estimate the cumulative PiB SUVR as a function of time in years in the probable DLB and CU groups; GAMs accounted for matching between the groups. We used linear regression models to determine the association of baseline PiB SUVR and rate of change in PiB SUVR with rate of change in measures of clinical and cognitive decline. We reported results of models without adjustment for any covariates. We investigated regression models, adjusting for combinations of age, sex, education, and *APOE* e4 carrier status but found that no covariates were statistically significant nor did inclusion of the covariates produce qualitatively different results for PiB SUVR or change in PiB SUVR. Finally, in the probable DLB group, we estimated sample size for a hypothetical anti- β -amyloid clinical trial in patients with probable DLB. Mixed-effect models and the jackknife-based resampling method were used to estimate the sample sizes expressed as mean values with asymptotic confidence intervals. Change in PiB SUVR, CDR-SOB score, DRS score, and MMSE score were used for these calculations, assuming 1-sided tests, 80% power, $\alpha = 0.05$, and readings at 12, 18, and 24 months of follow-up. Analyses were performed using SAS statistical software version 9.4 (SAS Institute) and R statistical software version 3.1.1 (R Foundation for Statistical Computing) with $P < .05$ considered statistically significant. All tests were 2-tailed, except for tests for sample size estimates, which were 1-tailed.

Results

Baseline Cohort Characteristics

Baseline characteristics of participants in the probable DLB and CU groups, matched on age, sex, and *APOE* e4 status, are listed in **Table 1**. In total, 175 participants were evaluated. Of these, 35 (20.0%) had probable DLB, with mean (SD) age of 69.6 (7.3) years; 16 (45.7%) were *APOE* e4 carriers; and 31 (88.6%) were men. A total of 140 CU participants (80.0%) were matched on age (mean [SD] age 69.7 [7.2] years), *APOE* e4 status (64 [45.7%] carriers), and sex (124 [88.6%] men) to patients with probable DLB. Dementia severity of participants with probable DLB was mild based on MMSE, DRS, and CDR-SOB scores. Mean (SD) baseline PiB SUVR, reported with partial volume correction, was higher among participants with probable DLB than among CU participants (1.58 [0.41] vs 1.36 [0.22]; $P < .001$; range, 1.17-2.57 vs 1.11-2.36). We obtained similar results on baseline PiB SUVR and findings in this study when we analyzed PiB SUVR data with no partial volume correction (mean [SD] baseline PiB SUVR 1.44 [0.36] vs 1.26 [0.20]; $P < .001$; range, 1.05-2.23 vs 1.01-2.21). The interval between baseline and follow-up visit was shorter among the probable DLB group than the CU group because of recruitment from 2 sources; therefore, change in PiB SUVR and changes in clinical and cognitive

measures were annualized. Compared with patients with probable DLB who did not carry *APOE* e4, *APOE* e4 carriers had higher mean (SD) baseline PiB SUVR (1.40 [0.27] vs 1.79 [0.46]; $P = .005$) and lower mean (SD) UPDRS-III motor score (11.1 [5.5] vs 6.5 [5.7]; $P = .02$). In clinical and cognitive measures and frequencies of probable DLB, *APOE* e4 carriers vs noncarriers did not differ (ie, all $P > .05$). We did not examine differences in the change in PiB SUVR between participants with probable DLB who were *APOE* e4 carriers vs noncarriers because of relatively small subgroups.

Trajectories of Change in PiB SUVR

Change in PiB SUVR by baseline PiB SUVR did not differ between the probable DLB and CU groups (Figure 1A); the regression-based smooth curves for rate of change in PiB SUVR did not differ between DLB and CU ($P = .59$). Moreover, we observed no difference in the shape (vertical shift) of

Table 1. Participants' Baseline Characteristics

| Characteristic | Mean (SD) | | P Value ^a |
|--|---------------------------|-------------------------------------|----------------------|
| | CU Participants (n = 140) | Patients With Probable DLB (n = 35) | |
| Men, No. (%) | 124 (88.6) | 31 (88.6) | >.99 |
| Age, y | 69.7 (7.2) | 69.6 (7.3) | .68 |
| <i>APOE</i> e4 carrier, No. (%) | 64 (45.7) | 16 (45.7) | >.99 |
| Education, y | 15.3 (2.4) | 15.7 (2.9) | .44 |
| Interscan interval, y | 2.4 (1.0) | 1.2 (0.4) | <.001 |
| PiB SUVR | | | |
| Baseline, mean (SD) [range] | 1.36 (0.22) [1.11-2.36] | 1.58 (0.41) [1.17-2.57] | <.001 ^b |
| Slope, baseline to follow-up | 0.016 (0.024) | 0.020 (0.037) | .45 |
| CDR-SOB score ^c | 0.0 (0.2) | 3.4 (1.8) | <.001 ^b |
| MMSE score ^c | 28.5 (1.1) | 24.3 (4.7) | <.001 ^b |
| UPDRS-III motor score ^d | 0.4 (1.2) | 9.1 (6.0) | <.001 |
| AVLT, delayed recall score ^e | 8.2 (2.9) | 3.2 (3.4) | <.001 |
| TMT-A score ^f | 33.6 (9.0) | 69.0 (38.4) | <.001 |
| BNT score ^g | NA | 25.3 (4.7) | NA |
| RCF copy, total score ^g | NA | 17.9 (10.5) | NA |
| DRS score ^h | NA | 128.6 (8.9) | NA |
| Visual hallucination, No. (%) ⁱ | NA | 17 (50.0) | NA |
| Fluctuations, No. (%) ⁱ | NA | 22 (64.7) | NA |
| Parkinsonism, No. (%) ⁱ | NA | 29 (85.3) | NA |
| RBD, No. (%) ^{j,i} | NA | 33 (97.1) | NA |
| Cognitive impairment, y ⁱ | NA | 5.58 (3.32) | NA |

Abbreviations: *APOE*, apolipoprotein; AVLT, Auditory Verbal Learning Test; BNT, Boston Naming Test; CDR-SOB, Clinical Dementia Rating Scale, sum of boxes; CU, cognitively unimpaired; DLB, dementia with Lewy bodies; DRS, Dementia Rating Scale; MMSE, Mini-Mental State Examination; PiB SUVR, carbon-11 labeled Pittsburgh compound B, standardized uptake value ratio; RCF, Rey Complex Figure; RBD, REM Sleep Behavior Disorder; TMT-A, Trail Making Test, part A; UPDRS-III, Unified Parkinson Disease Rating Scale, part III.

^a P values for differences between groups came from an analysis of variance using a random block design with an added predictor for the matching ID.

^b Either a log transformation or square root transformation was performed to normalize the distribution.

^c Data missing for 1 CU participant.

^d Data missing for 1 CU participant and 1 participant with probable DLB.

^e Data missing for 1 CU participant and 6 participants with probable DLB.

^f Data missing for 1 CU participant and 2 participants with probable DLB.

^g Data missing for 5 participants with probable DLB.

^h Data missing for 6 participants with probable DLB.

ⁱ Data missing for 1 participant with probable DLB.

^j A total of 25 of 34 patients (73.5%) with probable DLB had probable RBD confirmed by polysomnography; 8 (23.5%) had possible RBD confirmed by Mayo Clinic Sleep Questionnaire¹⁸; and 1 (2.9%) did not have RBD.

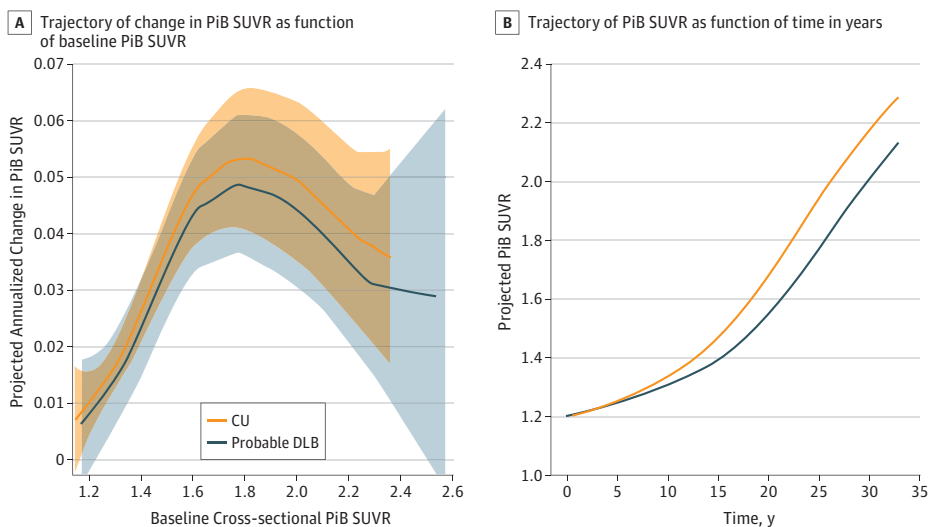
trajectories between the probable DLB and CU groups (regression spline model, approximate $P = .07$; penalized spline model, coefficient [SE] 0.007 [0.006]; $P = .22$) (Figure 1A). The association between change in PiB SUVR and baseline PiB SUVR was nonlinear (test of linearity, $P < .001$) in both PDLB and CU groups. In both probable DLB and CU groups, change in PiB SUVR accelerated at lower baseline PiB SUVR, peaked at a PiB SUVR of approximately 1.8, and then decelerated at higher baseline PiB SUVR, forming an inverted U-shaped curve as a function of baseline PiB SUVR. Subsequently, the associations of change in PiB SUVR as a function of baseline PiB SUVR were integrated into PiB SUVR as a function of time associations in probable DLB and CU groups (ie, the cumulative density function) (Figure 1B). The integral association of PiB SUVR by time rendered sigmoid-shaped trajectories for both probable DLB and CU groups (Figure 1B).

Association of Baseline and Change in PiB SUVR With Clinical and Cognitive Decline in Patients With Probable DLB

In patients with probable DLB, the associations of baseline PiB SUVR and change in PiB SUVR with measures of clinical progression are summarized in **Table 2** and **Figure 2**. Higher baseline PiB SUVR was associated with a greater longitudinal decline, as measured by the DRS (regression coefficient [SE], -22.40 [6.53]; $P = .002$; $R^2 = 0.312$), the CDR-SOB (regression coefficient [SE], 1.90 [0.63]; $P = .005$; $R^2 = 0.215$), the AVLT, delayed recall (regression coefficient [SE], -2.09 [0.95]; $P = .04$; $R^2 = 0.182$), the BNT (regression coefficient [SE], -2.39 [0.84]; $P = .009$; $R^2 = 0.245$), and the TMT-A (regression coefficient [SE], 43.43 [12.96]; $P = .002$; $R^2 = 0.286$). Similarly, greater change in PiB SUVR was associated with greater decline as measured by the CDR-SOB (regression coefficient [SE], 16.17 [7.47]; $P = .04$; $R^2 = 0.124$) and the AVLT, delayed recall (regression coefficient [SE], -25.05 [10.04]; $P = .02$; $R^2 = 0.221$). Baseline PiB SUVR and change in PiB SUVR were not associated with changes in MMSE score, UPDRS-III score, or visual-perceptual processing (Table 2).

The nature of the selection of the CU participants resulted in a restricted range of change in cognition and clinical scales. For example, only 8 CU participants (5.7%) had nonzero values for change in CDR-SOB score. Thus, the findings from only 8 influential participants would have to be interpreted with extreme caution. In addition, since we selected CU participants to match patients with probable DLB on age, sex, and APOE e4 status, we could only make inferences about this CU sample, which does not fully represent the CU population.

Figure 1. Trajectories of Change in Carbon-11 Labeled Pittsburgh Compound B Standardized Uptake Value Ratio (PiB SUVR) and Baseline PiB SUVR



A, Regardless of clinical group, change in PiB SUVR increases, peaks at a baseline PiB SUVR of approximately 1.8, and then decreases, forming an inverted U-shaped curve. Change in PiB SUVR did not differ between the probable dementia with Lewy bodies (DLB) and cognitively unimpaired (CU) groups in the shape or vertical shift between the trajectories; confidence bands, indicated by shaded areas, largely overlap. The widening of the confidence bands on the right side of the panel reflects the lower number of participants ($n = 11$) with higher baseline PiB SUVR values (ie, >1.7). B, The inverted U-shaped curves were integrated into the sigmoid-shaped trajectory of cumulative PiB SUVR as a function of time in years.

Sample Size Estimates for Hypothetical Clinical Trial in DLB

The sample size estimates for a hypothetical clinical trial in patients with DLB showed that using the change in PiB SUVR to measure therapeutic effect would require the smallest sample size. Change in PiB SUVR was followed by change in CDR-SOB score, whereas using the measurements of changes in DRS and MMSE scores would require larger samples (Table 3).

Discussion

In this longitudinal cohort PiB PET study, we determined the trajectories of change in PiB SUVR in patients with mild probable DLB compared with CU participants, matched on demographic variables and *APOE* e4 status. The trajectories of change in PiB SUVR did not differ between probable DLB and CU groups. In both groups, the trajectories were nonlinear, with an initial acceleration at lower baseline PiB SUVR followed by a deceleration at higher baseline PiB SUVR. The integral association between cumulative PiB SUVR and time showed a sigmoid-shaped functional form in both probable DLB and CU groups, very similar to the trajectories reported in AD continuum cohorts, which included CU participants with a range of baseline PiB SUVRs.¹³⁻¹⁵ Furthermore, the rate of clinical progression in probable DLB was associated with both baseline PiB SUVR and change in PiB SUVR. We showed that measuring change in PiB SUVR and change in CDR-SOB score would require a smaller sample size in a hypothetical clinical trial among patients with probable DLB. Altogether, our findings suggest that measuring change in PiB SUVR is a valid biomarker of longitudinal β -amyloid accumulation in individuals with probable DLB and that progression of β -amyloid pathology in probable DLB is associated with functional and cognitive decline.

Table 2. Associations of Baseline PiB SUVR and Change in PiB SUVR With Clinical and Cognitive Decline in Probable Dementia with Lewy Bodies

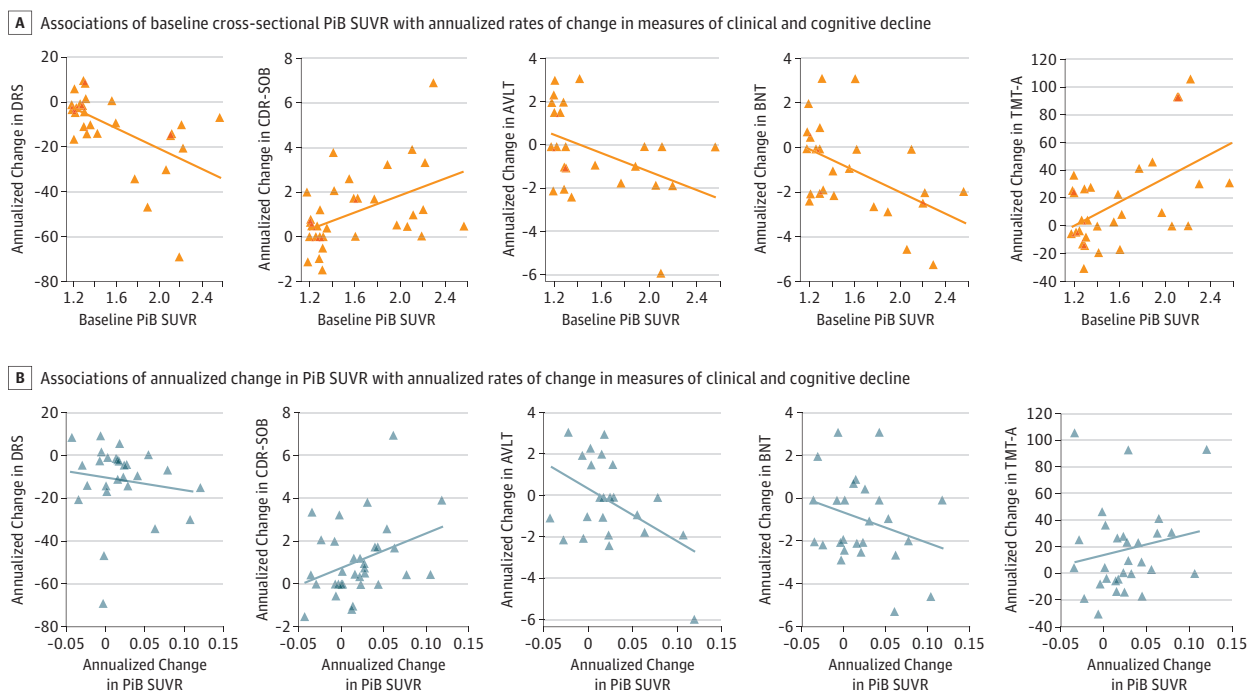
| Change in Measure | Regression Coefficient (SE) ^a | P Value | R ² |
|---------------------------|--|---------|----------------|
| Baseline PiB SUVR | | | |
| DRS | -22.40 (6.53) | .002 | 0.312 |
| CDR-SOB | 1.90 (0.63) | .005 | 0.215 |
| MMSE | -2.25 (1.78) | .22 | 0.046 |
| UPDRS-III | -0.93 (1.74) | .60 | 0.009 |
| AVLT | -2.09 (0.95) | .04 | 0.182 |
| BNT | -2.39 (0.84) | .009 | 0.245 |
| TMT-A | 43.43 (12.96) | .002 | 0.286 |
| ROCFT | -4.26 (3.76) | .27 | 0.047 |
| Change in PiB SUVR | | | |
| DRS | -62.09 (86.67) | .48 | 0.019 |
| CDR-SOB | 16.17 (7.47) | .04 | 0.124 |
| MMSE | -28.40 (19.78) | .16 | 0.059 |
| UPDRS-III | 6.66 (19.39) | .73 | 0.004 |
| AVLT | -25.05 (10.04) | .02 | 0.221 |
| BNT | -13.81 (9.80) | .17 | 0.074 |
| TMT-A | 153.42 (167.73) | .37 | 0.029 |
| ROCFT | 30.08 (39.88) | .46 | 0.021 |

Abbreviations: AVLT, Auditory Verbal Learning Test, delayed recall; BNT, Boston Naming Test; CDR-SOB, Clinical Dementia Rating, sum of boxes; DRS, Dementia Rating Scale; MMSE, Mini-Mental State Examination; PiB SUVR, carbon-11 labeled Pittsburgh compound B, standardized uptake value ratio; TMT-A, Trail Making Test, part A; UPDRS-III, Unified Parkinson Disease Rating Scale, part III, motor score.

^a Regression coefficients for these associations are from simple linear regression models.

We compared change in PiB SUVR between participants with probable DLB and CU participants who were matched by age, sex, and APOE e4 status. We hypothesized that such matching could allow for an indirect evaluation of the effect of α-synuclein on the change in PiB SUVR in participants with probable DLB. Interestingly, we found that change in PiB SUVR in the probable DLB group did not diverge from the CU group. However, the trajectories of change in PiB SUVR seen in our study closely resembled the trajectories of change in PiB SUVR in previous longitudinal studies on change in PiB SUVR among CU patients, patients with MCI, and patients with AD.¹³⁻¹⁵ These similarities across large cohorts and studies would suggest a relatively uniform progression of β-amyloid pathology with respect to baseline β-amyloid load in various neurodegenerative syndromes (ie, AD and DLB) and individuals with no cognitive impairment.

Figure 2. Rate of Change in Clinical and Cognitive Measures by Baseline Carbon-11 Labeled Pittsburgh Compound B Standardized Uptake Value Ratios (PiB SUVR) and Change in PiB SUVR Among Patients with Probable Dementia with Lewy Bodies



A, Scatterplots show significant associations of the baseline cross-sectional PiB SUVR with the annualized rates of change in measures of clinical and cognitive decline in patients with probable DLB. B, Scatterplots show associations of change in PiB SUVR with changes in measures of clinical and cognitive decline; associations with change in

Clinical Dementia Rating, sum of boxes (CDR-SOB) score and Auditory Verbal Learning Test (AVLT), delayed recall are significant. The estimates for these associations are from simple linear regression models (Table 2). BNT indicates Boston Naming Test; DRS, Dementia Rating Scale; and TMT-A, Trail Making Test, part A.

Table 3. Sample Size Estimates for Hypothetical Clinical Trial in Dementia with Lewy Bodies^a

| Measure | Participants, No. (95% CI) | | | | | | | |
|-----------------------|----------------------------|---------------|---------------|---------------|---------------|-------------|---------------|------------|
| Follow-up, mo | 12 | 12 | 18 | 18 | 24 | 24 | 36 | |
| Reduction in slope, % | 25 | 50 | 25 | 50 | 25 | 50 | 25 | 50 |
| PiB SUVR | 602 (521-682) | 151 (131-170) | 258 (224-292) | 65 (57-73) | 151 (131-171) | 38 (33-43) | 61 (53-69) | 16 (14-17) |
| CDR-SOB | 768 (655-882) | 193 (164-221) | 328 (280-377) | 83 (71-95) | 193 (164-222) | 49 (42-56) | 77 (66-89) | 20 (17-22) |
| DRS | 867 (735-1000) | 215 (181-251) | 370 (309-431) | 94 (79-108) | 218 (185-250) | 55 (46-63) | 87 (75-100) | 22 (19-26) |
| MMSE | 1583 (1262-1904) | 397 (321-472) | 681 (543-820) | 170 (138-203) | 395 (313-477) | 99 (79-118) | 159 (127-190) | 40 (32-48) |

Abbreviations: CDR-SOB, Clinical Dementia Rating, sum of boxes; DRS, Dementia Rating Scale; MMSE, Mini-Mental State Examination; PiB SUVR, carbon-11 labeled Pittsburgh compound B, standardized uptake value ratio.

^a Slope estimates and variances are from mixed models. Sample sizes are estimated using jackknife resampling as mean values along with asymptotic confidence intervals.

We note that the primary underlying pathology contributing to cognitive impairment in probable DLB patients is α -synuclein, with additional β -amyloid, NFT-tau, and possibly other pathologies, such as vascular disease or TAR DNA-binding protein-43. There is growing evidence of complex interactions between α -synuclein, β -amyloid, and NFT-tau,^{4,28,29} such that individuals with higher α -synuclein levels also tend to have higher β -amyloid and NFT-tau burdens. However, our findings suggest that the likely presence of α -synuclein in patients with mild probable DLB does not significantly alter the trajectory of β -amyloid accumulation as measured by PET.

The associations of baseline PiB SUVR with clinical and cognitive impairment have been ambiguous in probable DLB,¹² which may be because of discrepancies in study design, small sample sizes of generally cross-sectional cohorts, and discrepancies in the interpretation of findings because observing an association is not equal to finding a causal association. Many studies combined patients with probable DLB, Parkinson disease dementia, or even MCI with Parkinson disease in 1 group. Some reported an association of higher PiB SUVR with lower MMSE scores,³⁰ worse semantic memory,^{30,31} or lower CDR scores,³² whereas others did not find an association with MMSE³³ or CDR scores.²¹ A study performed by our group³⁴ observed an association of higher baseline PiB SUVR with worsening in CDR-SOB score over time. In the current study, we showed associations of baseline PiB SUVR with measures of longitudinal clinical and cognitive decline in patients with DLB. We found that a higher baseline PiB SUVR was associated with a more rapid decline as measured by DRS, CDR-SOB, AVLT, BNT, and TMT-A. Moreover, longitudinally, a greater change in PiB SUVR was associated with greater changes in CDR-SOB and AVLT scores. Thus, these 2 measures may be more sensitive and optimal for monitoring the cooccurrence of β -amyloid progression and clinical progression in probable DLB. The association of memory decline with PiB SUVR in probable DLB is interesting because, early in the AD continuum, many studies did not confirm associations of baseline PiB SUVR or change in PiB SUVR with memory decline.^{35,36} This could be owing to floor effect in AD and MCI studies, in which baseline memory performance is already moderately to severely impaired, but in DLB, baseline memory scores are less impaired. Aside from methodological issues, a potential biological explanation has been that β -amyloid alone is insufficient to influence cognitive impairment directly and rather constitutes an early event causing a chain of downstream pathologic changes leading to cognitive decline.^{35,37,38} We have shown that a higher PiB SUVR in patients with probable DLB was associated with higher fluoride-18 flortaucipir (AV-1451) uptake.³⁹ It remains to be seen whether the associations of baseline PiB SUVR and change in PiB SUVR with clinical and cognitive decline in probable DLB are direct effects of the progression of β -amyloid accumulation or whether it is the progression of α -synuclein or NFT-tau that influences cognitive decline, thus making the association of β -amyloid progression with clinical and cognitive decline indirect.

There was no association of PiB SUVR or change in PiB SUVR with changes in MMSE score, UPDRS-III score, or RCF-measured visual-perceptual performance. A potential explanation is lower statistical power or relatively narrow range of values in a probable DLB group of this size. Additionally, cognitive fluctuations may contribute to both short-term and long-term variability in clinical and cognitive evaluations. Moreover, the MMSE might not be an optimal measure of global cognitive decline in probable DLB,⁴⁰ although some studies have suggested otherwise.⁴¹ Most importantly, these clinical and cognitive measures may be influenced by other pathologies, such as NFT-tau or α -synuclein, or by other neurologic and functional factors, such as mood or daytime sleepiness.

Sample size calculations for a hypothetical clinical trial in patients with probable DLB showed that measuring change in PiB SUVR followed by change in CDR-SOB score required the smallest sample size compared with the most often-used global cognitive and functional measures. Favorable sample size estimates using change in CDR-SOB score may again suggest that global functional measures may be more optimal for tracking overall impairment in probable DLB and may track better with complex symptoms, such as cognitive, motor, sleep-related, affective, and psychiatric symptoms. Conversely, a large sample size by change in MMSE score indicated that the MMSE may not be an optimal measure for global cognitive decline in probable DLB in a clinical trial setting.

Limitations

Our study has some limitations. Although this longitudinal study sample was larger than most cross-sectional β -amyloid PET studies among individuals with probable DLB, it may still not have the sufficient power to detect subtle associations or conduct subgroup analyses, such as change in PiB SURV by *APOE* e4 status or by sex. The differences in change in PiB SUVR between CU *APOE* e4 carriers vs noncarriers were previously investigated⁴² but need to be investigated among individuals with probable DLB. A recent meta-analysis did not show greater prevalence of β -amyloid pathology by PET in women vs men within the AD continuum,⁴³ but the sex effects need to be investigated further in probable DLB. Furthermore, CU participants may have various subthreshold pathologies owing to their population-based origin.⁴⁴ Approximately 30% of CU participants have elevated baseline PiB SUVR.⁴³ Some of them develop cognitive impairment and dementia,³⁵ whereas others remain without cognitive impairment. It is likely that some of the CU participants in this study will later develop cognitive impairment. To mitigate this, CU participants had to remain clinically unimpaired during the follow-up period.

Conclusions

In this cohort study, the sigmoid trajectory of cumulative PiB SUVR by time observed in patients with probable DLB was consistent with the trajectories in the AD continuum, including the CU participants with lower baseline PiB SUVR. This finding suggests that, at sufficiently high baseline PiB SUVR, PiB uptake would reach equilibrium. This has potential implications for the timing of potential anti- β -amyloid strategies in probable DLB. Whereas the consequences of anti- β -amyloid approaches among patients with probable DLB are unknown at this time, associations of PiB SUVR and change in PiB SUVR with clinical and cognitive decline suggest that anti- β -amyloid strategies may have a place in clinical trials involving patients with probable DLB. However, how an anti- β -amyloid treatment would affect the progression of α -synuclein and NFT-tau in probable DLB remains to be seen. Because of the interactions among β -amyloid, α -synuclein, and NFT-tau,^{3,4} it is possible that targeting β -amyloid alone might contribute to overall pathologic progression and functional improvement in probable DLB patients. However, owing to the heterogeneity and complexity of underlying proteinopathies and clinical symptoms in probable DLB, individualized combination therapies with acetyl-cholinesterase inhibitors,⁴⁵ lifestyle interventions, treatment of age-related comorbidities, and anti-tau treatments will need to be considered.

ARTICLE INFORMATION

Accepted for Publication: October 4, 2019.

Published: December 2, 2019. doi:10.1001/jamanetworkopen.2019.16439

Open Access: This is an open access article distributed under the terms of the [CC-BY License](#). © 2019 Nedelska Z et al. *JAMA Network Open*.

Corresponding Author: Kejal Kantarci, MD, MS, Department of Radiology, Mayo Clinic, 200 First St SW, Rochester, MN 55905 (kantarci.kejal@mayo.edu).

Author Affiliations: Department of Radiology, Mayo Clinic, Rochester, Minnesota (Nedelska, Lowe, Gunter, Senjem, Jack, Kantarci); Department of Health Sciences, Mayo Clinic, Rochester, Minnesota (Schwarz, Lesnick, Przybelski, Kremers); Department of Neurology, Mayo Clinic, Rochester, Minnesota (Boeve, Graff-Radford, Knopman, Petersen); Department of Psychiatry and Psychology, Mayo Clinic, Jacksonville, Florida (Ferman); Department of Psychiatry and Psychology, Mayo Clinic, Rochester, Minnesota (Fields).

Author Contributions: Dr Kantarci had full access to all of the data in the study and takes responsibility for the integrity of the data and the accuracy of the data analysis.

Concept and design: Nedelska, Kremers, Kantarci.

Acquisition, analysis, or interpretation of data: All authors.

Drafting of the manuscript: Nedelska, Lesnick, Kantarci.

Critical revision of the manuscript for important intellectual content: All authors.

Statistical analysis: Nedelska, Schwarz, Lesnick, Przybelski, Kremers.

Obtained funding: Lowe, Kantarci.

Administrative, technical, or material support: Boeve, Lowe, Senjem, Graff-Radford, Jack, Jr, Kantarci.

Supervision: Nedelska, Lowe, Kantarci.

Conflict of Interest Disclosures: Dr Schwarz reporting receiving grants from the National Institutes of Health outside the submitted work. Dr Boeve reported receiving grants from the National Institutes of Health, the Little Family Foundation, and the Turner Foundation during the conduct of the study; and receiving grants from Alector and Biogen; serving as an investigator for clinical trials sponsored by Axovant Gene Therapies and Biogen; receiving personal fees from the Tau Consortium for serving on its advisory board; and receiving royalties from Cambridge Medicine for *Behavioral Neurology of Dementia* outside the submitted work. Dr Lowe reported receiving grants from GE Healthcare, Siemens Healthcare, Avid Radiopharmaceuticals, the Minnesota Partnership for Biotechnology and Medical Genomics, and the Leukemia and Lymphoma Society; receiving research support from the National Institutes of Health, and serving as a consultant for Bayer Pharmaceuticals and Piramal Inc outside the submitted work. Dr Kremers reported receiving grants from the National Institutes of Health during the conduct of the study and grants from AstraZeneca, Biogen, and Roche outside the submitted work. Mr Senjem reported receiving grants from the National Institutes of Health during the conduct of the study; having stock options in Align Technology, CRISPR Therapeutics, Gilead Sciences, Globus Medical Inc, Inovio Pharmaceuticals, Ionis Pharmaceuticals, Johnson and Johnson, LHC Group Inc, Medtronic, Mesa Labs, Natus Medical Incorporated, Parexel International, and Varex Imaging outside the submitted work. Dr Graff-Radford reported receiving research support from the National Institutes of Health outside of the submitted work. Dr Fields reported receiving grants from the National Institutes of Health during the conduct of the study. Dr Knopman reported serving as deputy editor of *Neurology*; serving on the data and safety monitoring boards for Eli Lilly and Co, Lundbeck Pharmaceuticals, and the Dominantly Inherited Alzheimer Disease Network Trials Unit; being an investigator in clinical trials supported by Baxter, Elan Pharmaceuticals, and the Tau Consortium; and receiving grants from the National Institutes of Health outside the submitted work. Dr Petersen reported receiving grants from the National Institutes of Health during the conduct of the study; and serving as a consultant for Roche Holding, Merck, Biogen, Eli Lilly and Company, Pfizer, Elan Pharmaceuticals, Wyeth Pharmaceuticals, GE Healthcare, and Eisai; receiving royalties from Oxford University Press for *Mild Cognitive Impairment*; serving on the data and safety monitoring board for Genentech; and presenting at GE Healthcare outside the submitted work. Dr Jack reported serving as a consultant for Eli Lilly and Co, serving on an independent data monitoring board for Roche Holding, and speaking for Eisai, but he received no personal compensation from any commercial entity; and receiving research support from the National Institutes of Health and the Alexander Family Alzheimer Disease Research Professorship of the Mayo Clinic outside the submitted work. Dr Kantarci reported serving on the data and safety monitoring board for Takeda Pharmaceutical Company; receiving research support from Avid Radiopharmaceuticals and Eli Lilly and Co; and receiving funding from the National Institutes of Health, the Bluefield Project to Cure Frontotemporal Dementia, the National Center for Advancing Translational Sciences, and the Alzheimer's Drug Discovery Foundation outside the submitted work. No other disclosures were reported.

Funding/Support: This study was supported by grants U01-NS100620, P50-AG016574, U01-AG006786, R01-AG011378, R01-AG041851, R01-AG040042, C06-RR018898, and R01-NS080820 from the National Institutes of Health, by the Fondation Dr Corinne Schuler, the Mangurian Foundation for Lewy Body Research, the Elsie and Marvin Dekelboum Family Foundation, and the Robert H. and Clarice Smith and Abigail Van Buren Alzheimer Disease Research Program. Dr Nedelska was supported by Clinical and Translational Science Awards grant UL1 TRO02377 from the National Center for Advancing Translational Sciences.

Role of the Funder/Sponsor: The funders had no role in the design and conduct of the study; collection, management, analysis, and interpretation of the data; preparation, review, or approval of the manuscript; and decision to submit the manuscript for publication.

Disclaimer: The National Center for Advancing Translational Sciences is a component of the National Institutes of Health; the article's contents are solely the responsibility of the authors and do not necessarily represent the official view of the National Institutes of Health.

REFERENCES






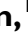

1. McKeith IG, Dickson DW, Lowe J, et al; Consortium on DLB. Diagnosis and management of dementia with Lewy bodies: third report of the DLB Consortium. *Neurology*. 2005;65(12):1863-1872. doi:10.1212/01.wnl.0000187889.17253.b1
2. Schneider JA, Arvanitakis Z, Bang W, Bennett DA. Mixed brain pathologies account for most dementia cases in community-dwelling older persons. *Neurology*. 2007;69(24):2197-2204. doi:10.1212/01.wnl.0000271090.28148.24

3. Ferman TJ, Aoki N, Crook JE, et al. The limbic and neocortical contribution of α-synuclein, tau, and amyloid β to disease duration in dementia with Lewy bodies. *Alzheimers Dement*. 2018;14(3):330-339. doi:10.1016/j.jalz.2017.09.014
4. Irwin DJ, Grossman M, Weintraub D, et al. Neuropathological and genetic correlates of survival and dementia onset in synucleinopathies: a retrospective analysis. *Lancet Neurol*. 2017;16(1):55-65. doi:10.1016/S1474-4422(16)30291-5
5. Wakisaka Y, Furuta A, Tanizaki Y, Kiyohara Y, Iida M, Iwaki T. Age-associated prevalence and risk factors of Lewy body pathology in a general population: the Hisayama study. *Acta Neuropathol*. 2003;106(4):374-382. doi:10.1007/s00401-003-0750-x
6. Mueller C, Soysal P, Rongve A, et al. Survival time and differences between dementia with Lewy bodies and Alzheimer's disease following diagnosis: a meta-analysis of longitudinal studies. *Ageing Res Rev*. 2019;50:72-80. doi:10.1016/j.arr.2019.01.005
7. Graff-Radford J, Aakre J, Savica R, et al. Duration and pathologic correlates of Lewy body disease. *JAMA Neurol*. 2017;74(3):310-315. doi:10.1001/jamaneurol.2016.4926
8. Klunk WE, Engler H, Nordberg A, et al. Imaging brain amyloid in Alzheimer's disease with Pittsburgh compound-B. *Ann Neurol*. 2004;55(3):306-319. doi:10.1002/ana.20009
9. Fodero-Tavoletti MT, Smith DP, McLean CA, et al. In vitro characterization of Pittsburgh compound-B binding to Lewy bodies. *J Neurosci*. 2007;27(39):10365-10371. doi:10.1523/JNEUROSCI.0630-07.2007
10. Kantarci K, Yang C, Schneider JA, et al. Antemortem amyloid imaging and β-amyloid pathology in a case with dementia with Lewy bodies. *Neurobiol Aging*. 2012;33(5):878-885. doi:10.1016/j.neurobiolaging.2010.08.007
11. Petrou M, Dwamena BA, Foerster BR, et al. Amyloid deposition in Parkinson's disease and cognitive impairment: a systematic review. *Mov Disord*. 2015;30(7):928-935. doi:10.1002/mds.26191
12. Donaghy P, Thomas AJ, O'Brien JT. Amyloid PET imaging in Lewy body disorders. *Am J Geriatr Psychiatry*. 2015;23(1):23-37. doi:10.1016/j.jagp.2013.03.001
13. Villemagne VL, Burnham S, Bourgeat P, et al; Australian Imaging Biomarkers and Lifestyle (AIBL) Research Group. Amyloid β deposition, neurodegeneration, and cognitive decline in sporadic Alzheimer's disease: a prospective cohort study. *Lancet Neurol*. 2013;12(4):357-367. doi:10.1016/S1474-4422(13)70044-9
14. Villain N, Chételat G, Grassiot B, et al; AIBL Research Group. Regional dynamics of amyloid-β deposition in healthy elderly, mild cognitive impairment and Alzheimer's disease: a voxelwise PiB-PET longitudinal study. *Brain*. 2012;135(Pt 7):2126-2139. doi:10.1093/brain/aws125
15. Jack CR Jr, Wiste HJ, Lesnick TG, et al. Brain β-amyloid load approaches a plateau. *Neurology*. 2013;80(10):890-896. doi:10.1212/WNL.0b013e3182840bbe
16. McKeith IG, Boeve BF, Dickson DW, et al. Diagnosis and management of dementia with Lewy bodies: fourth consensus report of the DLB Consortium. *Neurology*. 2017;89(1):88-100. doi:10.1212/WNL.0000000000004058
17. Roberts RO, Geda YE, Knopman DS, et al. The Mayo Clinic Study of Aging: design and sampling, participation, baseline measures and sample characteristics. *Neuroepidemiology*. 2008;30(1):58-69. doi:10.1159/000115751
18. Boeve BF, Molano JR, Ferman TJ, et al. Validation of the Mayo Sleep Questionnaire to screen for REM sleep behavior disorder in an aging and dementia cohort. *Sleep Med*. 2011;12(5):445-453. doi:10.1016/j.sleep.2010.12.009
19. Ferman TJ, Smith GE, Boeve BF, et al. DLB fluctuations: specific features that reliably differentiate DLB from AD and normal aging. *Neurology*. 2004;62(2):181-187. doi:10.1212/WNL.62.2.181
20. Schwarz CG, Senjem ML, Gunter JL, et al. Optimizing PiB-PET SUVR change-over-time measurement by a large-scale analysis of longitudinal reliability, plausibility, separability, and correlation with MMSE. *Neuroimage*. 2017;144(Pt A):113-127.
21. Kantarci K, Lowe VJ, Boeve BF, et al. Multimodality imaging characteristics of dementia with Lewy bodies. *Neurobiol Aging*. 2012;33(9):2091-2105. doi:10.1016/j.neurobiolaging.2011.09.024
22. Ashburner J, Friston KJ. Unified segmentation. *Neuroimage*. 2005;26(3):839-851. doi:10.1016/j.neuroimage.2005.02.018
23. Meltzer CC, Leal JP, Mayberg HS, Wagner HN Jr, Frost JJ. Correction of PET data for partial volume effects in human cerebral cortex by MR imaging. *J Comput Assist Tomogr*. 1990;14(4):561-570. doi:10.1097/00004728-199007000-00011

24. Avants BB, Epstein CL, Grossman M, Gee JC. Symmetric diffeomorphic image registration with cross-correlation: evaluating automated labeling of elderly and neurodegenerative brain. *Med Image Anal*. 2008;12(1):26-41. doi:10.1016/j.media.2007.06.004
25. Schwarz CG, Gunter JL, Ward CP, et al. The Mayo Clinic Adult Lifespan Template (MCALT): better quantification across the lifespan. Paper presented at: Alzheimer's Association International Conference; July 15, 2017; London, UK.
26. Neuroimaging Tool and Resources Collaboratory. Mayo Clinic Adult Lifespan Template and atlases. <https://www.nitrc.org/projects/mcalt/>. Accessed October 21, 2019.
27. Jack CR Jr, Wiste HJ, Weigand SD, et al. Defining imaging biomarker cut points for brain aging and Alzheimer's disease. *Alzheimers Dement*. 2017;13(3):205-216. doi:10.1016/j.jalz.2016.06.077
28. Clinton LK, Blurton-Jones M, Myczek K, Trojanowski JQ, LaFerla FM. Synergistic interactions between abeta, tau, and alpha-synuclein: acceleration of neuropathology and cognitive decline. *J Neurosci*. 2010;30(21):7281-7289. doi:10.1523/JNEUROSCI.0490-10.2010
29. Halliday GM, Song YJ, Harding AJ. Striatal β -amyloid in dementia with Lewy bodies but not Parkinson's disease. *J Neural Transm (Vienna)*. 2011;118(5):713-719. doi:10.1007/s00702-011-0641-6
30. Gomperts SN, Locascio JJ, Marquie M, et al. Brain amyloid and cognition in Lewy body diseases. *Mov Disord*. 2012;27(8):965-973. doi:10.1002/mds.25048
31. Lee SH, Cho H, Choi JY, et al. Distinct patterns of amyloid-dependent tau accumulation in Lewy body diseases. *Mov Disord*. 2018;33(2):262-272. doi:10.1002/mds.27252
32. Foster ER, Campbell MC, Burack MA, et al. Amyloid imaging of Lewy body-associated disorders. *Mov Disord*. 2010;25(15):2516-2523. doi:10.1002/mds.23393
33. Gomperts SN, Rentz DM, Moran E, et al. Imaging amyloid deposition in Lewy body diseases. *Neurology*. 2008;71(12):903-910. doi:10.1212/01.wnl.0000326146.60732.d6
34. Sarro L, Senjem ML, Lundt ES, et al. Amyloid- β deposition and regional grey matter atrophy rates in dementia with Lewy bodies. *Brain*. 2016;139(Pt 10):2740-2750. doi:10.1093/brain/aww193
35. Villemagne VL, Pike KE, Ch  telat G, et al. Longitudinal assessment of A β and cognition in aging and Alzheimer disease. *Ann Neurol*. 2011;69(1):181-192. doi:10.1002/ana.22248
36. Rowe CC, Ellis KA, Rimajova M, et al. Amyloid imaging results from the Australian Imaging, Biomarkers and Lifestyle (AIBL) study of aging. *Neurobiol Aging*. 2010;31(8):1275-1283. doi:10.1016/j.neurobiolaging.2010.04.007
37. Xiong C, Jasielc MS, Weng H, et al. Longitudinal relationships among biomarkers for Alzheimer disease in the Adult Children Study. *Neurology*. 2016;86(16):1499-1506. doi:10.1212/WNL.0000000000002593
38. Donohue MC, Sperling RA, Petersen R, Sun CK, Weiner MW, Aisen PS; Alzheimer's Disease Neuroimaging Initiative. Association between elevated brain amyloid and subsequent cognitive decline among cognitively normal persons. *JAMA*. 2017;317(22):2305-2316. doi:10.1001/jama.2017.6669
39. Kantarci K, Lowe VJ, Boeve BF, et al. AV-1451 tau and β -amyloid positron emission tomography imaging in dementia with Lewy bodies. *Ann Neurol*. 2017;81(1):58-67. doi:10.1002/ana.24825
40. Smits LL, van Harten AC, Pijnenburg YA, et al. Trajectories of cognitive decline in different types of dementia. *Psychol Med*. 2015;45(5):1051-1059. doi:10.1017/S0033291714002153
41. Kramberger MG, Auestad B, Garcia-Ptacek S, et al; E-DLB. Long-term cognitive decline in dementia with Lewy bodies in a large multicenter, international cohort. *J Alzheimers Dis*. 2017;57(3):787-795. doi:10.3233/JAD-161109
42. Nedelska Z, Przybelski SA, Lesnick TG, et al. ¹H-MRS metabolites and rate of β -amyloid accumulation on serial PET in clinically normal adults. *Neurology*. 2017;89(13):1391-1399. doi:10.1212/WNL.0000000000004421
43. Jansen WJ, Ossenkoppele R, Knol DL, et al; Amyloid Biomarker Study Group. Prevalence of cerebral amyloid pathology in persons without dementia: a meta-analysis. *JAMA*. 2015;313(19):1924-1938. doi:10.1001/jama.2015.4668
44. Rahimi J, Kovacs GG. Prevalence of mixed pathologies in the aging brain. *Alzheimers Res Ther*. 2014;6(9):82. doi:10.1186/s13195-014-0082-1
45. Graff-Radford J, Boeve BF, Pedraza O, et al. Imaging and acetylcholinesterase inhibitor response in dementia with Lewy bodies. *Brain*. 2012;135(Pt 8):2470-2477. doi:10.1093/brain/aww173

BRAIN COMMUNICATIONS

Longitudinal atrophy in prodromal dementia with Lewy bodies points to cholinergic degeneration

 Kejal Kantarci,¹  Zuzana Nedelska,^{1,2}  Qin Chen,^{1,3}  Matthew L. Senjem,¹  Christopher G. Schwarz,¹  Jeffrey L. Gunter,¹  Scott A. Przybelski,⁴ Timothy G. Lesnick,⁴ Walter K. Kremers,⁴ Julie A. Fields,⁵ Jonathan Graff-Radford,⁶ Rodolfo Savica,⁶ David Jones,⁶ Hugo Botha,⁶ David S. Knopman,⁶ Val Lowe,¹ Neill R. Graff-Radford,⁷ Melissa M. Murray,⁸ Dennis W. Dickson,⁸ R. Ross Reichard,⁹ Clifford R. Jack Jr,¹ Ronald C. Petersen,⁶ Tanis J. Ferman¹⁰ and Bradley F. Boeve⁶

Mild cognitive impairment with the core clinical features of dementia with Lewy bodies is recognized as a prodromal stage of dementia with Lewy bodies. Although grey matter atrophy has been demonstrated in prodromal dementia with Lewy bodies, longitudinal rates of atrophy during progression to probable dementia with Lewy bodies are unknown. We investigated the regional patterns of cross-sectional and longitudinal rates of grey matter atrophy in prodromal dementia with Lewy bodies, including those who progressed to probable dementia with Lewy bodies. Patients with mild cognitive impairment with at least one core clinical feature of dementia with Lewy bodies (mean age = 70.5; 95% male), who were enrolled in the Mayo Clinic Alzheimer's Disease Research Center and followed for at least two clinical evaluations and MRI examinations, were included ($n = 56$). A cognitively unimpaired control group ($n = 112$) was matched 2:1 to the patients with mild cognitive impairment by age and sex. Patients either remained stable ($n = 28$) or progressed to probable dementia with Lewy bodies ($n = 28$) during a similar follow-up period and pathologic confirmation was available in a subset of cases ($n = 18$). Cross-sectional and longitudinal rates of grey matter atrophy were assessed using voxel-based and atlas-based region of interest analyses. At baseline, prodromal dementia with Lewy bodies was characterized by atrophy in the nucleus basalis of Meynert both in those who remained stable and those who progressed to probable dementia with Lewy bodies ($P < 0.05$ false discovery rate corrected). Increase in longitudinal grey matter atrophy rates were widespread, with greatest rates of atrophy observed in the entorhinal and parahippocampal cortices, temporoparietal association cortices, thalamus and the basal ganglia, in mild cognitive impairment patients who progressed to probable dementia with Lewy bodies at follow-up ($P < 0.05$ false discovery rate corrected). Rates of inferior temporal atrophy were associated with greater rates of worsening on the clinical dementia rating–sum of boxes. Seventeen of the 18 (94%) autopsied cases had Lewy body disease. Results show that atrophy in the nucleus basalis of Meynert is a feature of prodromal dementia with Lewy bodies regardless of proximity to progression to probable dementia with Lewy bodies. Longitudinally, grey matter atrophy progresses in regions with significant cholinergic innervation, in alignment with clinical disease progression, with widespread and accelerated rates of atrophy in patients who progress to probable dementia with Lewy bodies. Given the prominent neurodegeneration in the cholinergic system, patients with prodromal dementia with Lewy bodies may be candidates for cholinesterase inhibitor treatment.

1 Department of Radiology, Mayo Clinic, Rochester, MN, USA

2 Department of Neurology, Charles University, Prague, Czech Republic

3 Department of Neurology, West China Hospital of Sichuan University, Chengdu, Sichuan, China

4 Department of Health Sciences Research, Mayo Clinic, Rochester, MN, USA

5 Department of Psychology and Psychiatry, Mayo Clinic, Rochester, MN, USA

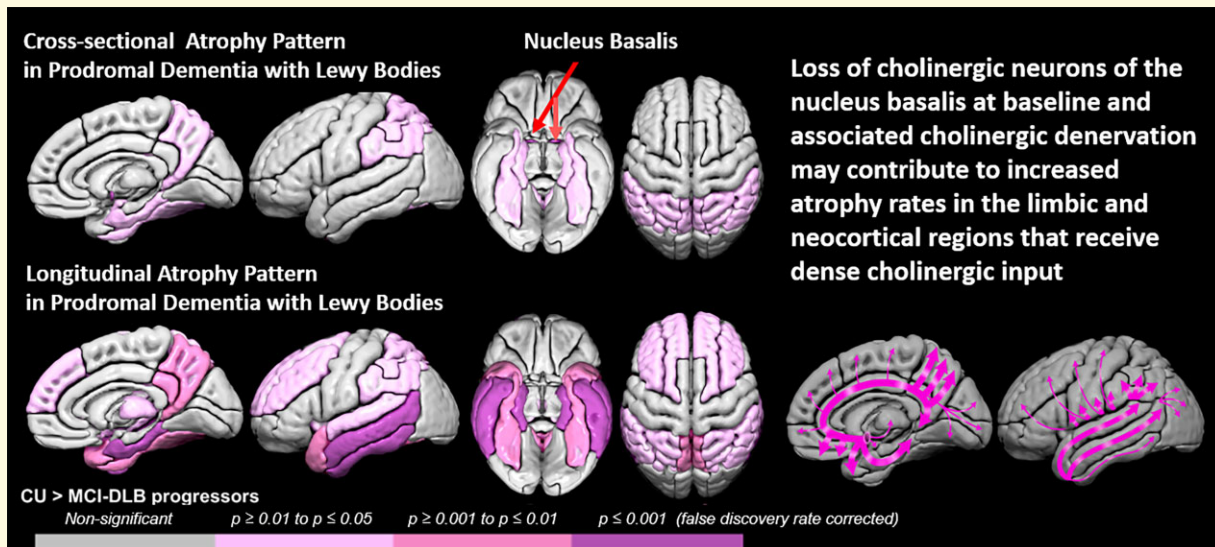
- 6 Department of Neurology, Mayo Clinic, Rochester, MN, USA
 7 Department of Neurology, Mayo Clinic, Jacksonville, FL, USA
 8 Department of Laboratory Medicine and Pathology, Mayo Clinic, Rochester, MN, USA
 9 Department of Laboratory Medicine and Pathology, Mayo Clinic, Jacksonville, FL, USA
 10 Department of Psychology and Psychiatry, Mayo Clinic, Jacksonville, FL, USA

Correspondence to: Kejal Kantarci, MD, MS
 Department of Radiology
 Mayo Clinic
 200 First Street SW
 Rochester, MN 55905, USA
 E-mail: kantarci.kejal@mayo.edu

Keywords: mild cognitive impairment; dementia with Lewy bodies; MRI; atrophy; prodromal DLB

Abbreviations: ADRC = Alzheimer's Disease Research Center; CDR = Clinical Dementia Rating Scale; CU = cognitively unimpaired; DLB = dementia with Lewy bodies; MCALT = Mayo Clinic Adult Lifespan Template; MCI-LB = mild cognitive impairment with core clinical features of DLB; MCSA = Mayo Clinic Study of Aging; pRBD = probable rapid eye movement sleep behaviour disorder; SPM = statistical parametric mapping; TBM-Syn = tensor-based morphometry with symmetric normalization; UPDRS-III = Unified Parkinson's Disease Rating Scale part III

Graphical Abstract



Introduction

Based on the evidence that was available in 2020, the prodromal dementia with Lewy bodies (DLB) Diagnostic Study Group published the research criteria for the diagnosis of prodromal DLB.¹ The prodromal phase of DLB includes three categories of presentations: (i) mild cognitive impairment (MCI)-onset, (ii) delirium-onset and (iii) psychiatric-onset, whereas evidence from the MCI-onset category of prodromal DLB was sufficient to propose formal criteria for prodromal DLB, the evidence from the delirium-onset and psychiatric-onset presentations were found to be insufficient.¹ Thus, MCI with the core clinical features of DLB is now recognized as a prodromal stage of DLB (MCI-LB).

MCI-LB may be present years before probable DLB becomes evident. Non-amnesic MCI along with hippocampal

preservation on MRI has been shown to be a strong predictor of progression from MCI-LB to probable DLB versus Alzheimer's disease dementia.^{2,3} Cross-sectional structural MRI studies have demonstrated atrophy in insula, temporal and cingulate cortices, and the nucleus basalis of Meynert in MCI-LB;⁴⁻⁸ however, clinical progression of MCI patients to probable DLB, as well as rates of longitudinal of atrophy during progression to probable DLB are unknown.

Patients with probable DLB are characterized by increased rates of global brain atrophy and cortical atrophy on longitudinal structural MRI compared to their cognitively unimpaired (CU) peers.⁹⁻¹² Furthermore, regional grey matter atrophy rates are associated with clinical disease progression in both patients with clinically diagnosed probable DLB¹³ and autopsy-confirmed Lewy body disease,¹² indicating that neurodegeneration is an important component of DLB

pathophysiology. Determining the cross-sectional and longitudinal patterns of atrophy in MCI-LB and particularly in MCI-LB who progressed to probable DLB would provide an opportunity for detection of early neurodegeneration in patients with DLB at the prodromal stage. In addition, determining the topographic pattern and time course of structural MRI changes in MCI-LB may provide insights into the clinical evolution of DLB starting from the earliest stages.

Objectives of the present study were 2-fold: (i) to assess the pattern of cross-sectional and longitudinal rates of grey matter atrophy in MCI patients with at least one clinical core feature of DLB, (i.e. MCI-LB) compared with CU controls; (ii) to determine whether the rates of grey matter atrophy are associated with clinical disease progression in MCI-LB.

Materials and methods

Participants

Patients included those with MCI and at least one core clinical feature of DLB (i.e. parkinsonism, fluctuations, visual hallucinations, RBD), enrolled in the Mayo Clinic Alzheimer's Disease Research Center (ADRC) between October 2005 and December 2017 and followed with at least two clinical evaluations and MRI exams ($n = 56$). Although the recently published research criteria for prodromal DLB¹ was not used for inclusion at the time of enrolment to this prospective study, in retrospect 47 (84%) of the patients with MCI met the research criteria for probable prodromal DLB and the remaining 9 (16%) met the research criteria for possible prodromal DLB.

Mayo Clinic ADRC participants are followed prospectively with approximately annual clinical evaluations and MRI. To include all MCI-DLB participants and to keep the follow-up interval consistent between the MCI-DLB patients who remained stable (MCI-LB stable) and MCI-DLB patients who progressed to probable DLB (MCI-LB progressor), we included the last two evaluations prior to and at the time of progression to DLB in MCI-LB progressors ($n = 28$) and last two evaluations in MCI-LB stables ($n = 28$). The CU adults included as controls (CU; $n = 112$) were participants of the Mayo Clinic Study of Aging (MCSA), a prospective population-based study of aging.¹⁴ CU had at least two clinical evaluations and MRI examinations and were matched to MCI-LB 2:1 on age at baseline and sex.

Clinical evaluation

Diagnosis of MCI was made according to the criteria by Petersen *et al.*,^{15,16} and diagnosis of probable DLB was made according to the DLB Consortium Criteria.^{17,18} Clinical Dementia Rating–Sum of Boxes (CDR–SOB) was used to determine clinical disease severity. Assessments for the clinical features of DLB were detailed in previous reports from the ADRC cohorts.^{14,19} Briefly, the 4-item Mayo Fluctuations Scale scores of 3 or 4²⁰ were used to identify

the presence of fluctuations. Visual hallucinations were characterized by being fully formed and not restricted to a single episode or related to another medical issue, or treatment. A history of probable REM sleep behaviour disorder (pRBD) was based on the International Classification of Sleep Disorders-II diagnostic criteria.²¹ Presence of parkinsonism was based on two of the four cardinal features (bradykinesia, rigidity, tremor and postural instability). The Unified Parkinson's Disease Rating Scale-III (UPDRS-III) score²² was used to quantify the severity of motor impairment.

Informed consent was obtained from all participants and/or their proxies for participation in this study. All procedures were approved by the Mayo Clinic Institutional Review Board.

MRI acquisition and analysis

All MRIs were performed at 3T with an 8-channel phased array head coil (GE Healthcare, Milwaukee, WI, USA). A 3D high-resolution T₁-weighted magnetization-prepared rapid gradient echo acquisition was performed with repetition time/echo time/inversion time = 2300/3/900 ms, flip angle 8°, voxel resolution 1.2 × 1 × 1 mm.

T₁-weighted MRI were tissue-class segmented and corrected for B0 inhomogeneities using Unified Segmentation²³ in SPM12 (www.fil.ion.ucl.ac.uk/spm) with population-optimized templates and settings from the Mayo Clinic Adult Lifespan Template (MCALT; <https://www.nitrc.org/projects/mcalt/>). Tissue volumes were calculated by summing voxel-wise probabilities within each of 28 cortical and subcortical region of interest (ROI) labels from the an in-house atlas of the substantia innominata, propagated using ANTS Symmetric Normalization,²⁴ with right and left hemispheric values averaged as previously described.²⁵ We then estimated cortical thickness from these segmentations using ANTS DiReCT, also as previously described.²⁶

We used a fully automated in-house developed image processing pipeline, named tensor-based morphometry with symmetric normalization (TBM-SyN), to compute the changes in cortical volume over time in each participant.^{27,28} Briefly, the steps in the TBM-SyN pipeline were as follows. First, for each participant, both of their longitudinal T₁-weighted structural MRI scans were iteratively co-registered to their mean, using a 6 degrees-of-freedom, followed by 9 degrees-of-freedom rigid body registration using SPM12. Next, image intensity histograms across each participant's time series of images were normalized using an in-house developed differential bias correction algorithm,²⁸ and the SyN diffeomorphic registration algorithm from ANTs software²⁴ was used to compute deformations between each pair of images in each direction, producing the Jacobian determinant images and the 'annualized' log of the Jacobian determinant from the deformation in each direction. The voxel values of the Jacobian determinant image represent the expansion or contraction of each voxel over time, and those of the annualized log Jacobian determinant image can be thought of as analogous to an annualized per cent change at each voxel. The SyN deformations

were applied in each direction, respectively, to the original bias corrected late and early images, to get the early image warped to the late, and the late image warped to the early image, and average them with their respective originals, resulting in a ‘synthetic late image’ and a ‘synthetic early image’. Then, we segmented the synthetic early and late images each using the same segmentation pipeline described previously.

To assess the cross-sectional and longitudinal atrophy at the voxel level, the baseline tissue-class segmented images and the annualized log of the Jacobian determinant for each voxel in each participant were smoothed with a 6 mm full-width at half maximum Gaussian smoothing kernel. Between-group voxel-based comparisons were computed using SPM12 and displayed after correcting for multiple comparisons with false discovery rate (FDR; $P < 0.05$). Our main analysis was voxel-based analysis to investigate group differences. However, because our secondary objective was to determine whether the rates of grey matter atrophy are associated with clinical disease progression in MCI-LB, we employed a secondary atlas-based ROI analysis. Data from the atlas-based ROI analysis was utilized for investigating the associations between atrophy rates and clinical disease progression.

Pathologic examination

We used standardized methods for the neuropathologic assessment by expert neuropathologists (MEM, DWD and RRR) blinded to MRI results. Sampling was done according to the CERAD protocol²⁹ and the fourth report of the DLB Consortium.¹⁷ Immunohistochemistry to detect Lewy-related pathology was performed using monoclonal antibody to alpha-synuclein (LB509; 1:200; Zymed, San Francisco, CA, USA) using a protocol (formic acid pretreatment and DAKO DAB polymer signal detection) as previously described.³⁰ The presence, density, semiquantitative scores and distribution of Lewy body-related pathology were based on recommendations of the fourth report of the DLB Consortium.¹⁷ Amyloid-beta plaques and neurofibrillary tangles were staged according to the National Institute on Aging-Alzheimer’s Association (NIA-AA) criteria.^{31,32}

Cases with intermediate or high likelihood DLB (according to the fourth report of the DLB Consortium Criteria) who had low Alzheimer’s disease pathology (according to the NIA-AA criteria) were classified as Lewy body disease; cases with intermediate or high likelihood DLB and intermediate or high Alzheimer’s disease were classified as having mixed Lewy body disease–Alzheimer’s disease pathology and cases with intermediate or high Alzheimer’s disease and no Lewy body disease pathology or low likelihood DLB were classified as Alzheimer’s disease.

Statistical analysis

Baseline demographic and clinical characteristics were summarized with means and standard deviations for continuous variables, and with counts and percentages for categorical

variables. Baseline characteristics were compared between MCI-LB and controls using conditional logistic regression models to account for the matching. MMSE and CDR–SOB scores had fitting problems resulting in lack of convergence, and in those instances the comparisons came from an exact conditional logistic model. The differences in the characteristics of MCI-LB stables and MCI-LB progressors were analysed with *t*-tests for continuous variables and χ^2 tests for categorical variables. Assessments of atlas-based ROI findings were corrected for multiple comparisons by requiring the corrected FDR to be $P < 0.05$. Findings from atlas-based ROI analysis were used to determine regions used for partial Pearson correlation analysis with CDR–SOB. These correlations were adjusted for age.

Data availability

The Mayo Clinic Study of Aging and Alzheimer’s Disease Research Center make data available to qualified researchers upon reasonable request.

Results

Characteristics of the cohort

Baseline demographic and clinical characteristics of MCI-LB and CU participants and subgroups of MCI-LB stables and MCI-LB progressors are listed in [Table 1](#). MCI-LB patients did not differ in age and sex from the CU controls, owing to matching. The median time interval between serial MRI sessions was 2.2 years for CU and 1.3 years for MCI-LB (1.4 years for MCI-LB stables and 1.3 years for MCI-LB progressors) due to the differences in follow-up time intervals among the MCSA and ADRC cohorts. To account for the longer MRI time intervals in CU compared with MCI-LB patients, all longitudinal measurements were annualized. Higher CDR–SOB ($P < 0.001$), UPDRS-III ($P < 0.001$), and lower MMSE scores ($P < 0.001$), and a higher frequency of *APOE* $\epsilon 4$ carriers ($P = 0.029$) were observed in the MCI-LB group compared with the CU at baseline.

Characteristics of MCI-LB stables were similar to the MCI-LB progressors in age, sex, education and *APOE* $\epsilon 4$ status at baseline and scan time interval at follow-up. Compared with MCI-LB stables, MCI-LB progressors were clinically more impaired at baseline with lower MMSE scores ($P = 0.005$), higher CDR–SOB scores ($P < 0.001$), UPDRS-III scores ($P = 0.016$) and had a higher number of DLB core clinical features. The frequency of visual hallucinations, fluctuations and parkinsonism were higher in the MCI-LB progressors compared with the MCI-LB stables, while the frequency of pRBD was the same (89%) among the MCI-LB stables and MCI-LB progressors. Of the 56 MCI-LB participants, 46 (82%) were taking cholinesterase inhibitor treatments during follow-up. There were no differences in anticholinesterase use among MCI-LB stables (79%) and MCI-LB progressors (86%; $P = 0.49$).

Table 1 Characteristics of participants

| | CU (n = 112) | MCI-LB (n = 56) | P-value* | MCI-LB stable (n = 28) | MCI-LB progressor (n = 28) | P-value** |
|--------------------------------|--------------|-----------------|----------|------------------------|----------------------------|-----------|
| Age, years | 70.5 (7.1) | 70.5 (7.1) | 0.99 | 70.8 (7.8) | 70.1 (6.4) | 0.73 |
| Males, no. (%) | 106 (95%) | 53 (95%) | 1.00 | 26 (93%) | 27 (96%) | 0.55 |
| APOE ϵ 4, no. (%) | 21 (19%) | 19 (35%) | 0.029* | 7 (26%) | 12 (43%) | 0.19 |
| Education, years | 15.3 (2.7) | 16.1 (2.6) | 0.093 | 16.2 (2.4) | 16.0 (2.8) | 0.76 |
| Scan interval, years | 2.2 (0.8) | 1.3 (0.9) | <0.001* | 1.4 (1.1) | 1.3 (0.5) | 0.61 |
| MMSE | 28.4 (1.2) | 26.6 (2.5) | <0.001* | 27.5 (1.8) | 25.7 (2.8) | 0.005** |
| CDR–Sum of Boxes | 0.0 (0.2) | 1.7 (0.9) | <0.001† | 1.3 (0.8) | 2.1 (0.9) | <0.001** |
| UPDRS-III | 0.7 (2.2) | 6.2 (4.4) | <0.001* | 4.7 (4.5) | 7.5 (3.9) | 0.016** |
| Visual hallucinations, no. (%) | — | 13 (24%) | | 3 (11%) | 10 (36%) | 0.032** |
| Fluctuations, no. (%) | — | 22 (40%) | | 6 (22%) | 16 (57%) | 0.008** |
| Parkinsonism, no. (%) | — | 44 (80%) | | 18 (67%) | 26 (93%) | 0.015** |
| pRBD, no. (%) | — | 49 (89%) | | 24 (89%) | 25 (89%) | 0.96 |
| Cognitive impairment, years | — | 5.3 (3.7) | | 5.4 (3.9) | 5.2 (3.5) | 0.84 |
| Cholinesterase, no. (%) | — | 46 (82%) | | 22 (79%) | 24 (86%) | 0.49 |
| DLB features | | | | | | |
| One, no. (%) | — | 12 (21%) | | 9 (32%) | 3 (11%) | 0.002 |
| Two, no. (%) | — | 20 (36%) | | 14 (50%) | 6 (21%) | |
| Three, no. (%) | — | 18 (32%) | | 4 (14%) | 14 (50%) | |
| Four, no. (%) | — | 6 (11%) | | 1 (4%) | 5 (18%) | |

Mean (SD) listed for the continuous variables and count (%) for the categorical variables.

*P-values come from a conditional logistic model.

†The P-value is from an exact conditional logistic model.

**P-values come from a t-test for the continuous variables or a χ^2 test for the categorical variables.

Cortical atrophy at baseline

Voxel-based analysis shows the pattern of grey matter atrophy at baseline comparing MCI-LB and CU (Fig. 1). The atrophy in MCI-LB was observed in the amygdala, inferior temporal lobe and basal forebrain region that localized to the nucleus basalis of Meynert. Notably, nucleus basalis of Meynert bilaterally was the most significant region of grey matter atrophy in MCI-LB compared with CU after correcting for multiple comparisons (FDR; $P < 0.05$). No differences in cortical thickness were found between MCI-LB stables and MCI-LB progressors at baseline. Neither did we find greater atrophy in CU compared with MCI-LB.

Atlas-based ROI differences between MCI-LB and CU are shown in Supplementary Fig. 1. Consistent with the voxel-based analysis, the greatest grey matter atrophy in MCI-LB patients was observed in the substantia innominata ROI which includes the nucleus basalis of Meynert compared to CU (FDR corrected $P = 0.001$). In addition, grey matter atrophy included the amygdala, fusiform, lateral parietal precuneus, supramarginal angular, entorhinal and parahippocampal cortices in MCI-LB compared with CU (FDR corrected $P < 0.05$). Because several regions were involved, we grouped the differences based on their magnitude into the three levels thresholded as shown with a colour scale in Supplementary Fig. 1. No differences in cortical thickness were found between MCI-LB stables and MCI-LB progressors at baseline using atlas-based analysis (FDR corrected $P > 0.05$). The box plots in Fig. 2 displays the substantia innominata volumes in CU, MCI-LB stables and MCI-LB progressors. Both MCI-LB stables (FDR corrected $P = 0.007$) and MCI-LB progressors (FDR corrected $P = 0.028$) had smaller substantia innominata volumes compared with CU.

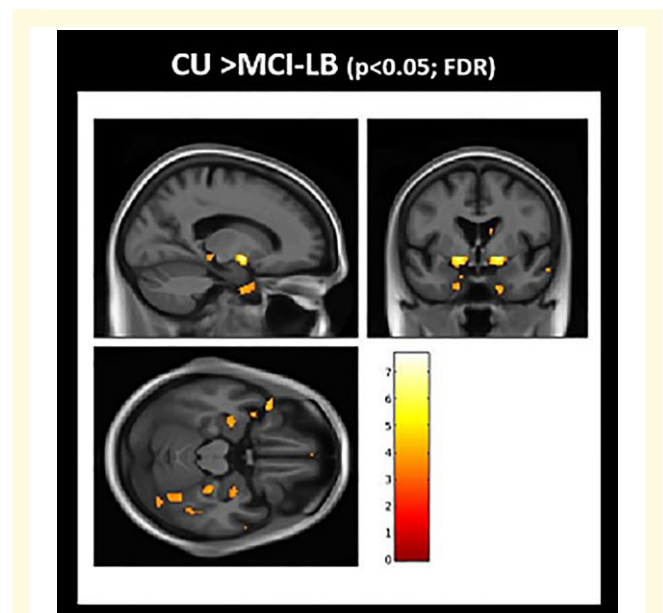


Figure 1 Grey matter atrophy in MCI-LB at baseline: voxel-based analysis. Voxel-based analysis show differences in grey matter atrophy in MCI-LB compared to CU projected to the 3D brain surface. Greater atrophy in the basal forebrain, inferior temporal and amygdala regions are seen in MCI-LB compared with the CU group (FDR; $P < 0.05$). T-score bar indicate magnitude of the differences.

Longitudinal rates of atrophy

Greater rates of longitudinal grey matter atrophy were observed in the lateral and inferior temporal cortices and

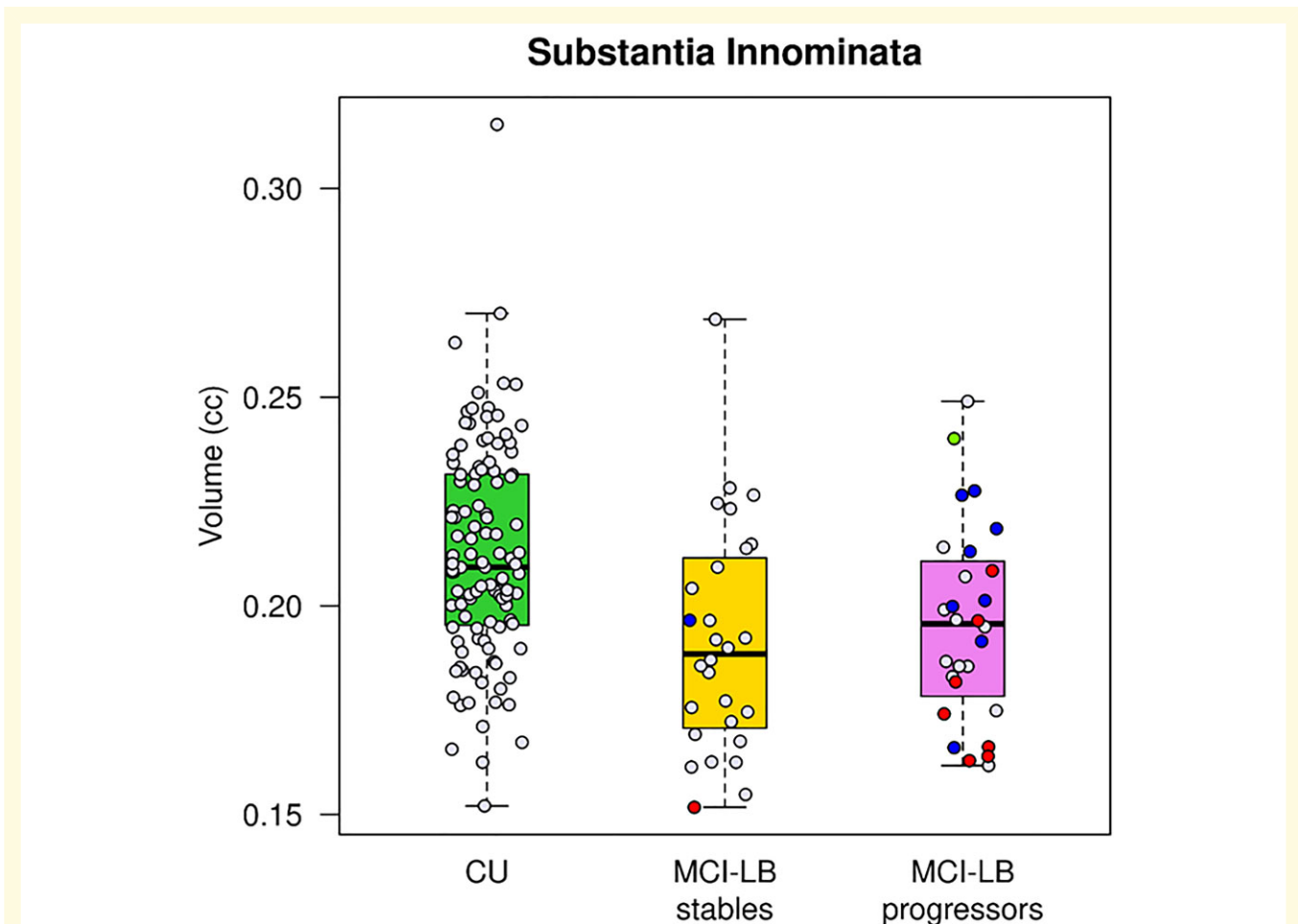


Figure 2 Substantia innominata volumes. Box plots show that MCI-LB stables (FDR corrected $P = 0.007$) and MCI-LB progressors (FDR corrected $P = 0.028$) had smaller substantia innominata volumes compared to CU. The pathologically confirmed cases were colour coded based on the pathologic diagnosis after a median (range) of 5.3 (2.4–10.6) years. Blue labels represent cases with intermediate or high likelihood DLB (according to the fourth report of the DLB Consortium Criteria) who had low Alzheimer's disease pathology (according to the NIA-AA criteria) classified as Lewy body disease. Red labels represent cases with intermediate or high likelihood DLB and intermediate or high Alzheimer's disease, classified as having mixed Lewy body disease–Alzheimer's disease pathology. The single green label represents a case with high Alzheimer's disease and no Lewy body disease pathology classified as Alzheimer's disease.

temporal pole, as well as medial and lateral parietal cortices, thalamus and insula in both the MCI-LB and the DLB-progressor groups compared with CU on voxel-based analysis (Fig. 3). No differences in the annualized atrophy rates were observed between MCI-LB stables and CU or between MCI-LB stables and MCI-LB progressors on voxel-based analysis. Neither did we find greater atrophy in CU compared with MCI-LB.

Atlas-based ROI differences in rates of grey matter atrophy between MCI-LB patients and CU, and between MCI-LB progressors and CU, are shown in Supplementary Fig. 2. Consistent with voxel-based analysis, MCI-LB patients showed greater rates of grey matter atrophy in the temporoparietal cortices and these changes were more pronounced in those who progressed to DLB. Patients in the MCI-LB group showed the greatest rates of grey matter atrophy in the entorhinal and parahippocampal cortices, inferior

and middle temporal cortices (FDR corrected $P < 0.001$) and also greater rates of grey matter atrophy in the posterior cingulate, precuneus, fusiform, supramarginal, angular, temporal pole, superior temporal, superior and middle frontal, lateral parietal and insular cortices, as well as thalamus, compared with CU (FDR corrected $P < 0.05$). Similarly, MCI-LB progressors showed greater rates of cortical atrophy in the inferior, middle and superior temporal, temporal pole, precuneus, supramarginal, angular, entorhinal and parahippocampal, lateral parietal, fusiform, and posterior cingulate cortex and thalamus (FDR corrected $P < 0.001$), as well as greater rates of atrophy in the lateral occipital, superior and middle frontal, insula, sensory motor, cuneus cortices, hippocampus, amygdala and caudate (FDR corrected $P < 0.05$), compared with CU. The only region that showed greater rates of atrophy in MCI-LB stables compared with CU was the entorhinal and parahippocampal cortices

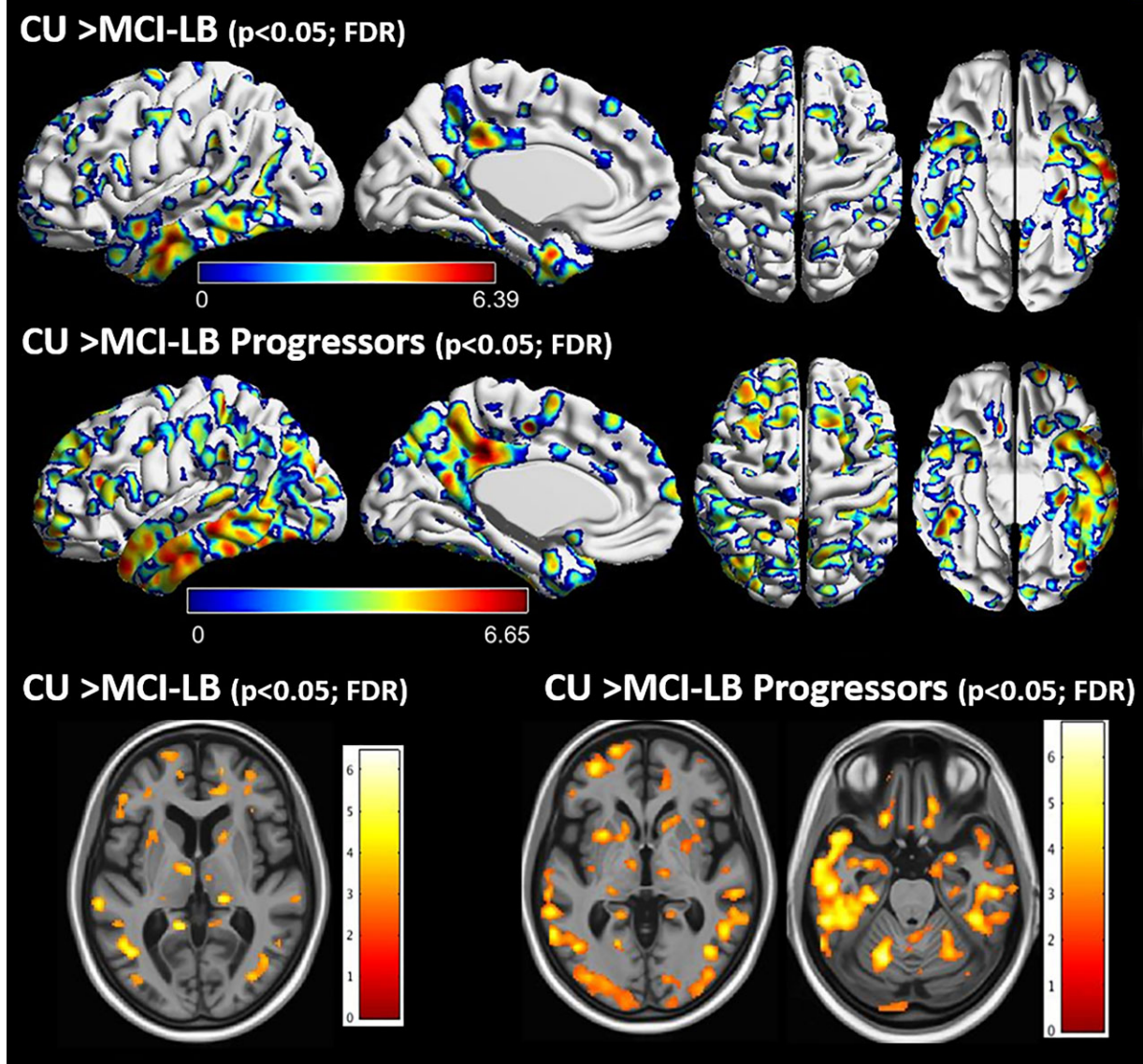


Figure 3 Regional pattern of group differences in longitudinal rates of cortical atrophy: voxel-based analysis. Voxel-based analyses show differences in the annualized rates of grey matter atrophy in MCI-LB compared to CU projected to the 3D brain surface. Greater rates of atrophy in the lateral and inferior temporal cortices and temporal pole, as well as medial and lateral parietal cortices is observed in MCI-LB compared with CU in the upper row, and in MCI-LB progressors compared with CU in the middle row (FDR; $P < 0.05$). Individual sections demonstrating differences in longitudinal rates of atrophy in the thalamus, amygdala and insula is shown in the bottom row. The blue colours around the FDR corrected $P < 0.05$ clusters are due to interpolation of edge voxels. T -score bars indicate magnitude of the differences.

(FDR corrected $P = 0.014$). No difference in rates of atrophy was found between the MCI-LB stables and MCI-LB progressors after FDR correction for multiple comparisons (Supplementary Fig. 3).

Correlation with disease progression

Among the ROIs with greater atrophy rates in MCI-LB compared with CU, decline in cortical volumes correlated with disease progression in only two of the ROIs (inferior temporal and fusiform). Correlations of longitudinal change in CDR-SOB and longitudinal change in cortical volumes are

listed in Supplementary Table 1. In MCI-LB, longitudinal increase in CDR-SOB correlated with longitudinal rates of volume loss in the inferior temporal ($r = -0.35$; $P = 0.011$) and fusiform ($r = -0.44$; $P < 0.001$) cortices after adjusting for age at baseline (Fig. 4). Number of core clinical features at baseline was not associated with the rates of atrophy in any of the ROIs in MCI-LB ($P > 0.05$).

Pathologic confirmation

Pathologic diagnosis was available in the autopsied MCI-LB cases ($n = 18$). Cases were classified either as Lewy body

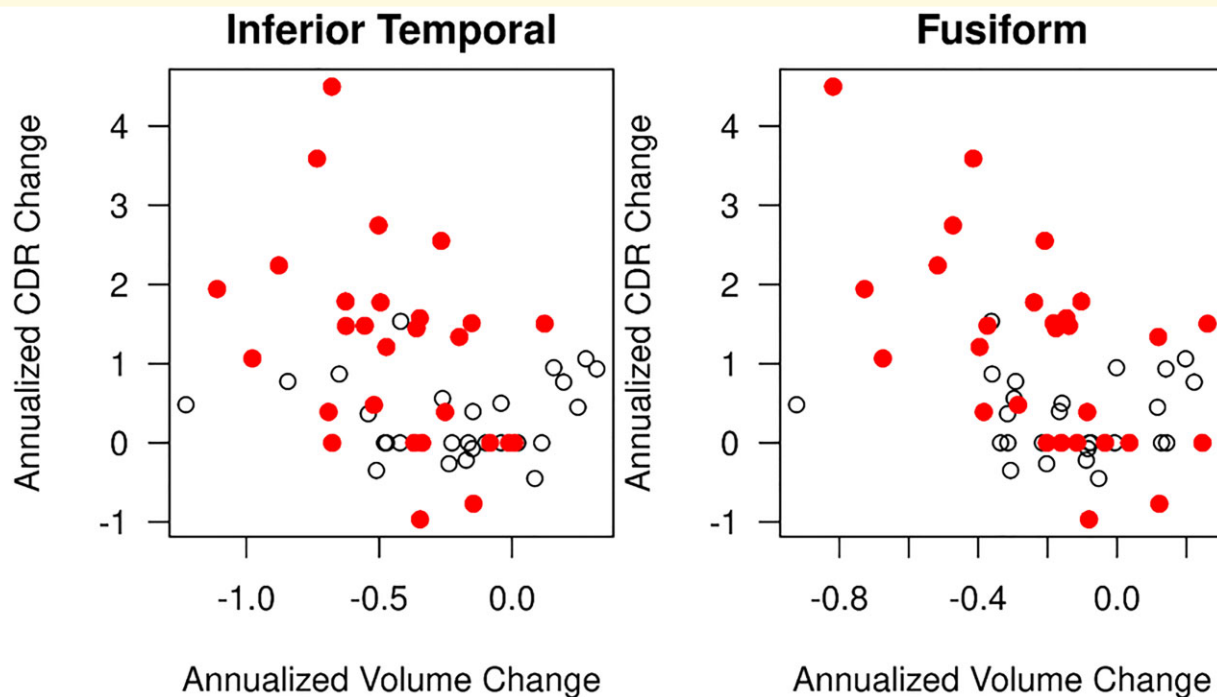


Figure 4 Longitudinal decline in inferior temporal and fusiform gyrus grey matter correlates with clinical disease progression in MCI-LB. In MCI-LB, longitudinal increase in CDR-SOB correlated with longitudinal rates of volume loss in the inferior temporal ($r = -0.35$; $P = 0.011$) and fusiform ($r = -0.44$; $P < 0.001$) cortices after adjusting for age at baseline. The open circles represent MCI-LB stablers and the red circles represent MCI-LB progressors.

disease ($n = 8$; MCI-LB stable $n = 1$; MCI-LB progressor $n = 7$) or Lewy body disease–Alzheimer’s disease ($n = 9$; MCI-LB stable $n = 1$; MCI-LB progressor $n = 8$). One of the MCI-LB patients with parkinsonism and RBD at the time of baseline MRI progressed to probable DLB during follow-up and was found to have high likelihood Alzheimer’s disease and no Lewy body disease at autopsy. Thus, 17 of the 18 (94%) pathologically confirmed cases had Lewy body disease. The median (range) time from baseline MRI to death was 5.3 (2.4–10.6) years. Because of the wide range and variability in time from baseline MRI to death, pathologic diagnosis may not fully represent the extent of pathology at the time of baseline MRI. Therefore, we did not investigate the MRI findings in association with pathologic diagnosis. However, we present the substantia innominata volumes of the pathologically confirmed cases in Fig. 2 using diagnosis-based colour codes. Interestingly, the MCI-LB patient who was pathologically classified as Alzheimer’s disease had one of the largest substantia innominata volumes among the MCI-LB patients.

Discussion

In this longitudinal structural MRI study, we demonstrated a baseline and longitudinal pattern of atrophy in MCI patients with one or more core DLB features (i.e. MCI-LB) and in those who progressed to probable DLB (i.e. MCI-LB

progressors) at follow-up. At baseline, we found grey matter atrophy in the nucleus basalis of Meynert in MCI-LB compared with CU. Longitudinally, increased rates of grey matter atrophy were widespread in both cortical and subcortical grey matter with the greatest rates of atrophy in the entorhinal and parahippocampal gyri, temporoparietal association cortices, thalamus and the basal ganglia compared with CU. This pattern was most pronounced for the MCI-LB progressors, and greater rates of atrophy were associated with greater rates of clinical progression.

At baseline, MCI-LB patients had atrophy in the basal forebrain and specifically in the cholinergic nucleus basalis of Meynert. Inferior and medial temporal and parietal cortices were involved to a lesser extent but did not statistically differ from CU on voxel-based analysis after correction for multiple comparisons. Nucleus basalis of Meynert consists primarily of large acetylcholinesterase-positive neurons that innervate the cerebral cortex. Early LB-related pathology involves the basal forebrain cholinergic nuclei³³ with significant loss of cholinergic neurons particularly in the nucleus basalis of Meynert.^{33,34} Atrophy in the substantia innominata region that includes the nucleus basalis of Meynert has been demonstrated in DLB and Alzheimer’s disease patients, but this was more prominent in patients with DLB.^{11,35,36} Substantia innominata atrophy was also reported in patients with mild probable DLB who were likely at the early stages of DLB and in MCI-LB.^{8,37} Moreover, substantia innominata atrophy on MRI was associated with a

better response to cholinesterase inhibitors in both patients with DLB and Alzheimer's disease.³⁸ Our findings provide evidence of neurodegeneration in the nucleus basalis of Meynert in prodromal DLB. We observed smaller volumes in the substantia innominata region both in MCI-LB stables and MCI-LB progressors and did not observe differences in grey matter atrophy at baseline between these two groups. Furthermore, seventeen of the eighteen (94%) MCI-LB patients had pathologically confirmed Lewy body disease at autopsy. Therefore, atrophy of the nucleus basalis of Meynert appears to be a feature of MCI-LB regardless of proximity to progression to probable DLB. These findings support the concept that cholinergic deficit plays an important role in prodromal DLB.

Although atrophy in the temporal and parietal cortical regions in MCI-LB were not statistically significant after correction for multiple comparisons on voxel-based analysis, there was evidence of smaller amygdala, inferior temporal and parietal cortex volumes in MCI-LB compared to CU using atlas-based ROI analysis evaluating 28 cortical and subcortical regions, even after correcting for multiple comparisons. This difference in findings using different analytic approaches may be due to the relatively small sample size and diminished power to detect smaller differences using voxel-based analysis versus atlas-based ROI analysis.

When investigating atrophy in patients with probable DLB, it is important to consider that many patients with Lewy body disease or probable DLB have additional Alzheimer's disease pathology at autopsy.^{39–41} Amyloid- β and/or tau biomarker positivity was demonstrated in 61% of probable DLB patients from a large multinational cohort ($n=417$).⁴² On the other hand, only 35% patients with MCI-LB showed amyloid- β positivity on PET,⁴³ suggesting that amyloid- β pathology accumulates as MCI-LB patients progress to DLB and continues to increase thereafter.⁴⁴ Amyloid- β deposition is associated with increased rates of atrophy,¹³ and tau pathology influences cortical volumes in

probable DLB.⁴⁵ Similarly, in MCI-LB, Alzheimer's disease pathology may influence neurodegeneration in regions that are affected during the evolution of Alzheimer's disease such as the nucleus basalis of Meynert and the medial temporal lobe, but the nucleus basalis of Meynert in Alzheimer's disease is not affected until later in Alzheimer's disease compared to DLB,³⁷ and a more prominent atrophy in the nucleus basalis of Meynert region was observed in MCI-LB compared to MCI due to Alzheimer's disease.⁸ We also note that the MCI-LB patient with pure Alzheimer's disease pathology at autopsy had one of the most preserved substantia innominata volumes among MCI-LB. In addition, among the medial temporal lobe regions, we did not identify hippocampal atrophy in MCI-LB compared with CU. Hippocampal atrophy is a feature of additional co-occurring Alzheimer's disease pathology in DLB,¹⁹ and hippocampal preservation in MCI predicts future progression to probable DLB versus Alzheimer's disease dementia.^{3,46} Thus, preservation of hippocampal volumes in the MCI-LB patients we studied suggest that contribution of Alzheimer's disease to neurodegeneration in MCI-LB was not substantial.

Longitudinal analysis of serial MRIs demonstrated increased rates of atrophy in MCI-LB throughout the limbic and the neocortical regions, particularly in the temporoparietal cortices and the insula. Atrophy in the insula has been reported in MCI-LB in cross-sectional studies, which likely included a subset of patients who later progressed to probable DLB.^{5,6} Increased rates of atrophy were pronounced in MCI-LB progressors, but they were only observed in the entorhinal and parahippocampal cortices in MCI-LB stables compared with CU, suggesting that atrophy rates in MCI-LB could be non-linear and accelerate as MCI-LB patients progress to probable DLB. Most cortical and subcortical regions with greater rates of atrophy were the brain regions that receive dense cholinergic inputs from the nucleus basalis of Meynert⁴⁷ such as the amygdala and the temporal and parietal association cortex as demonstrated in Fig. 5. Hence, degeneration of cholinergic

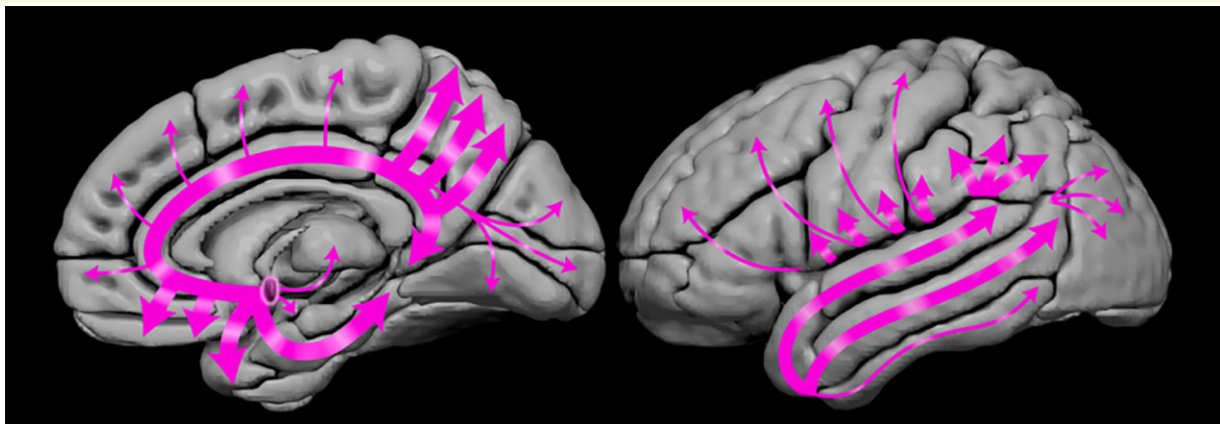


Figure 5 Cholinergic projections from the nucleus basalis of Meynert. Schematic showing the projections from nucleus basalis of Meynert to the cortex, amygdala, thalamus and caudate. Thicker arrows suggest more dense projections from this cholinergic nucleus to limbic and temporoparietal association cortices and the amygdala where the greatest rates of atrophy were observed in MCI-LB compared with CU.

neurons of the nucleus basalis of Meynert at baseline and associated cholinergic denervation may have contributed to increased atrophy rates in the limbic and neocortical regions in MCI-LB. We did not observe increased rates of atrophy in the substantia innominata region. It is possible that atrophy of nucleus basalis of Meynert occurs very early during the evolution of Lewy body disease and reaches a plateau at the symptomatic stages such as in MCI-LB.

Consistent with the widespread increased rates of atrophy in MCI-LB progressors but not in MCI-LB stables, higher rates of atrophy in the inferior temporal and fusiform gyri were associated with greater increase (worsening) in CDR-SOB scores. Cortical atrophy has been associated with clinical disease progression in probable DLB,⁹ and here we demonstrate a similar finding in MCI-LB localized to the inferior temporal lobe. Inferior temporal lobe is impacted by both α -synuclein and neurofibrillary tangle tau pathologies in transitional and diffuse Lewy body disease.⁴⁸ Increased tau deposition in the inferior temporal lobes at much higher levels than the medial temporal lobe regions has been demonstrated on PET in probable DLB.^{49,50} Altogether, these findings suggest that the inferior temporal lobe may be particularly vulnerable to neurodegeneration either due to α -synuclein or neurofibrillary tangle tau pathologies, or both early in the course of DLB with accelerated atrophy rates and associated clinical progression in MCI-LB.

A strength of this study is that we measured the baseline cross-sectional and longitudinal rates of atrophy in MCI-LB who either progressed to probable DLB or remained as MCI-LB during a similar length of follow-up. Findings in the MCI-LB stable and progressor groups reveal the time course of neurodegeneration in prodromal DLB demonstrating that neurodegeneration is associated with clinical progression with slower rates of atrophy during a stable clinical course and accelerated rates of atrophy as MCI-LB patients progress to dementia. This study also has several limitations. First, the sample sizes were modest, which may be one of the reasons for relatively weaker findings using voxel-based analysis compared to atlas-based ROI analysis. Second, to keep the follow-up interval consistent between the MCI-DLB patients who remained stable and progressed to DLB, the last two evaluations prior to and at the time of progression to DLB were assessed for MCI-LB progressors, while the last two evaluations were considered for MCI-LB stables. As reported in [Table 1](#), baseline clinical characteristics of MCI-LB stable and MCI-LB progressor groups were different with greater disease severity observed in MCI-LB progressors. Although we did not find statistically significant differences in the rates of atrophy between MCI-LB stables and MCI-LB progressors, disease severity could have potentially influenced the higher number of regions impacted in MCI-progressors than MCI-LB stables. Third, we assumed linearity in the rates of change when annualizing the longitudinal measurements that occurred within 1–2 years, which may have introduced error when comparing groups with different follow-up intervals. Finally, we did not have autopsy confirmation of Lewy body disease and presence of additional Alzheimer's disease

pathology in the entire cohort, and the pathologic examination occurred many years after the baseline MRI making it difficult to associate MRI findings with pathologic diagnosis. Therefore, it is not possible to attribute findings in MCI-LB to Lewy body disease and/or Alzheimer's disease pathology. Investigations into the prevalence of and Alzheimer's disease biomarkers and their contribution to neurodegeneration in prodromal DLB is warranted.

MCI-LB is characterized by atrophy in the nucleus basalis of Meynert, making neurodegeneration in the cholinergic system a prominent feature of MCI-LB. Grey matter atrophy progresses in alignment with clinical disease progression in MCI-LB with accelerated rates of atrophy observed in MCI-LB patients who progress to probable DLB within approximately a year. Although additional Alzheimer's disease pathology may be responsible for accelerated neurodegeneration during the progression of MCI-LB patients to dementia, the cholinergic deficits at baseline may also be contributing to the widespread accelerated atrophy rates in MCI-LB. Patients with probable DLB, particularly those with negative Alzheimer's disease biomarkers show the best response to cholinesterase inhibitors.⁵¹ Because neurodegeneration in the nucleus basalis of Meynert is a characteristic of MCI-LB, patients with MCI-LB should be considered as candidates for cholinesterase inhibitor treatment. An intriguing possibility to examine is whether such treatment given during the prodromal stage of DLB serves to slow the neurodegeneration that is due to cholinergic denervation.

Acknowledgements

The authors are grateful to their patients and informants for their participation in their detailed annual assessments and for their involvement in the present study.

Funding

This study was supported by the National Institutes of Health grants (U01 NS100620, P50 AG16574, U01 AG06786, R01 AG11378); Foundation Dr Corinne Schulerand, Mayo Clinic Dorothy and Harry T. Mangurian Jr Foundation for the Lewy Body Disease Research; the Lewy Body Dementia Association; the Little Family Foundation; the Turner Family Foundation and the Katherine B. Andersen Foundation.

Competing interests

The authors report no competing interests.

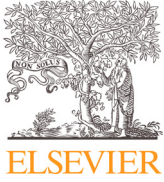
Supplementary material

[Supplementary material](#) is available at *Brain Communications* online.

References

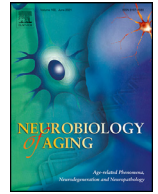
- McKeith IG, Ferman TJ, Thomas AJ, *et al.* Research criteria for the diagnosis of prodromal dementia with Lewy bodies. *Neurology*. 2020;94:743–755.
- Ferman TJ, Smith GE, Kantarci K, *et al.* Nonamnesic mild cognitive impairment progresses to dementia with Lewy bodies. *Neurology*. 2013;81:2032–2038.
- Kantarci K, Lesnick T, Ferman TJ, *et al.* Hippocampal volumes predict risk of dementia with Lewy bodies in mild cognitive impairment. *Neurology*. 2016;87:2317–2323.
- Durcan R, Donaghy P, Osborne C, Taylor JP, Thomas AJ. Imaging in prodromal dementia with Lewy bodies: Where do we stand? *Int J Geriatr Psychiatry*. 2019;34:635–646.
- Blanc F, Colloby SJ, Philippi N, *et al.* Cortical thickness in dementia with Lewy bodies and Alzheimer's disease: A comparison of prodromal and dementia stages. *PLoS One*. 2015;10:e0127396.
- Blanc F, Colloby SJ, Cretin B, *et al.* Grey matter atrophy in prodromal stage of dementia with Lewy bodies and Alzheimer's disease. *Alzheimers Res Ther*. 2016;8:31.
- Roquet D, Noblet V, Anthony P, *et al.* Insular atrophy at the prodromal stage of dementia with Lewy bodies: A VBM DARTEL study. *Sci Rep*. 2017;7:9437.
- Schumacher J, Taylor JP, Hamilton CA, *et al.* In vivo nucleus basalis of Meynert degeneration in mild cognitive impairment with Lewy bodies. *Neuroimage Clin*. 2021;30:102604.
- Mak E, Su L, Williams GB, *et al.* Progressive cortical thinning and subcortical atrophy in dementia with Lewy bodies and Alzheimer's disease. *Neurobiol Aging*. 2015;36:1743–1750.
- Mak E, Su L, Williams GB, *et al.* Longitudinal assessment of global and regional atrophy rates in Alzheimer's disease and dementia with Lewy bodies. *Neuroimage Clin*. 2015;7:456–462.
- Whitwell JL, Jack CR Jr, Parisi JE, *et al.* Rates of cerebral atrophy differ in different degenerative pathologies. *Brain*. 2007;130(Pt 4):1148–1158.
- Nedelska Z, Ferman TJ, Boeve BF, *et al.* Pattern of brain atrophy rates in autopsy-confirmed dementia with Lewy bodies. *Neurobiol Aging*. 2015;36:452–461.
- Sarro L, Senjem ML, Lundt ES, *et al.* Amyloid-beta deposition and regional grey matter atrophy rates in dementia with Lewy bodies. *Brain*. 2016;139(Pt 10):2740–2750.
- Roberts RO, Geda YE, Knopman DS, *et al.* The Mayo Clinic Study of Aging: Design and sampling, participation, baseline measures and sample characteristics. *Neuroepidemiology*. 2008;30:58–69.
- Petersen RC, Smith GE, Waring SC, Ivnik RJ, Tangalos EG, Kokmen E. Mild cognitive impairment: Clinical characterization and outcome. *Arch Neurol*. 1999;56:303–308.
- Petersen RC, Roberts RO, Knopman DS, *et al.* Mild cognitive impairment: Ten years later. *Arch Neurol*. 2009;66:1447–1455.
- McKeith IG, Boeve BF, Dickson DW, *et al.* Diagnosis and management of dementia with Lewy bodies: Fourth consensus report of the DLB Consortium. *Neurology*. 2017;89:88–100.
- McKeith IG, Dickson DW, Lowe J, *et al.* Diagnosis and management of dementia with Lewy bodies: Third report of the DLB Consortium. *Neurology*. 2005;65:1863–1872.
- Kantarci K, Ferman TJ, Boeve BF, *et al.* Focal atrophy on MRI and neuropathologic classification of dementia with Lewy bodies. *Neurology*. 2012;79:553–560.
- Ferman TJ, Smith GE, Boeve BF, *et al.* DLB fluctuations: Specific features that reliably differentiate DLB from AD and normal aging. *Neurology*. 2004;62:181–187.
- AAoS. *International classification of sleep disorders. Diagnostic and coding manual*. American Academy of Sleep Medicine. 2005: 51–55.
- Fahn S. *Recent developments in Parkinson's disease*. Vol. 2. Macmillan Health Care Information; 1987:293–304.
- Ashburner J, Friston KJ. Unified segmentation. *Neuroimage*. 2005;26:839–851.
- Avants BB, Epstein CL, Grossman M, Gee JC. Symmetric diffeomorphic image registration with cross-correlation: Evaluating automated labeling of elderly and neurodegenerative brain. *Med Image Anal*. 2008;12:26–41.
- Schwarz CG, Gunter JL, Wiste HJ, *et al.* A large-scale comparison of cortical thickness and volume methods for measuring Alzheimer's disease severity. *Neuroimage Clin*. 2016;11:802–812.
- Das SR, Avants BB, Grossman M, Gee JC. Registration based cortical thickness measurement. *Neuroimage*. 2009;45:867–879.
- Cash DM, Frost C, Iheme LO, *et al.* Assessing atrophy measurement techniques in dementia: Results from the MIRIAD atrophy challenge. *Neuroimage*. 2015;123:149–164.
- Vemuri P, Senjem ML, Gunter JL, *et al.* Accelerated vs. unaccelerated serial MRI based TBM-SyN measurements for clinical trials in Alzheimer's disease. *Neuroimage*. 2015;113:61–69.
- Mirra SS, Heyman A, McKeel D, *et al.* The Consortium to Establish a Registry for Alzheimer's Disease (CERAD). Part II. Standardization of the neuropathologic assessment of Alzheimer's disease. *Neurology*. 1991;41:479–486.
- Beach TG, White CL, Hamilton RL, *et al.* Evaluation of alpha-synuclein immunohistochemical methods used by invited experts. *Acta Neuropathol*. 2008;116:277–288.
- Hyman BT, Phelps CH, Beach TG, *et al.* National Institute on Aging-Alzheimer's Association guidelines for the neuropathologic assessment of Alzheimer's disease. *Alzheimers Dement*. 2012;8:1–13.
- Montine TJ, Phelps CH, Beach TG, *et al.* National Institute on Aging-Alzheimer's Association guidelines for the neuropathologic assessment of Alzheimer's disease: A practical approach. *Acta Neuropathol*. 2012;123:1–11.
- Braak H, Ghebremedhin E, Rub U, Braatzke H, Del Tredici K. Stages in the development of Parkinson's disease-related pathology. *Cell Tissue Res*. 2004;318:121–134.
- Schmeichel AM, Buchhalter LC, Low PA, *et al.* Mesopontine cholinergic neuron involvement in Lewy body dementia and multiple system atrophy. *Neurology*. 2008;70:368–373.
- Hanyu H, Tanaka Y, Sakurai H, Takasaki M, Abe K. Atrophy of the substantia innominata on magnetic resonance imaging and response to donepezil treatment in Alzheimer's disease. *Neurosci Lett*. 2002;319:33–36.
- Teipel SJ, Fritz HC, Grothe MJ, Alzheimer's Disease Neuroimaging Initiative. Neuropathologic features associated with basal forebrain atrophy in Alzheimer disease. *Neurology*. 2020;95:e1301–e1311.
- Tiraboschi P, Hansen LA, Alford M, *et al.* Early and widespread cholinergic losses differentiate dementia with Lewy bodies from Alzheimer disease. *Arch Gen Psychiatry*. 2002;59:946–951.
- Hanyu H, Shimizu S, Tanaka Y, Hirao K, Iwamoto T, Abe K. MR features of the substantia innominata and therapeutic implications in dementias. *Neurobiol Aging*. 2007;28:548–554.
- Galasko D, Hansen LA, Katzman R, *et al.* Clinical-neuropathological correlations in Alzheimer's disease and related dementias. *Arch Neurol*. 1994;51:888–895.
- Gomez-Isla T, Growdon WB, McNamara M, *et al.* Clinicopathologic correlates in temporal cortex in dementia with Lewy bodies. *Neurology*. 1999;53:2003–2009.
- Schneider JA, Arvanitakis Z, Bang W, Bennett DA. Mixed brain pathologies account for most dementia cases in community-dwelling older persons. *Neurology*. 2007;69:2197–2204.
- Ferreira D, Przybelski SA, Lesnick TG, *et al.* beta-Amyloid and tau biomarkers and clinical phenotype in dementia with Lewy bodies. *Neurology*. 2020;95:e3257–e3268.
- Chen Q, Lowe VJ, Boeve BF, *et al.* beta-Amyloid PET and ¹²³I-FP-CIT SPECT in mild cognitive impairment at risk for lewy body dementia. *Neurology*. 2021;96:e1180–e1189.
- Nedelska Z, Schwarz CG, Lesnick TG, *et al.* Association of longitudinal beta-amyloid accumulation determined by positron emission

- tomography with clinical and cognitive decline in adults with probable lewy body dementia. *JAMA Netw Open*. 2019;2:e1916439.
45. Spotorno N, Coughlin DG, Olm CA, *et al.* Tau pathology associates with in vivo cortical thinning in Lewy body disorders. *Ann Clin Transl Neurol*. 2020;7:2342–2355.
 46. Siddiqui TG, Whitfield T, Praharaaju SJ, *et al.* Magnetic resonance imaging in stable mild cognitive impairment, prodromal Alzheimer's disease, and prodromal dementia with lewy bodies. *Dement Geriatr Cogn Disord*. 2020;49:583–588.
 47. Oswal A, Gratwicke J, Akram H, *et al.* Cortical connectivity of the nucleus basalis of Meynert in Parkinson's disease and Lewy body dementias. *Brain*. 2020;144(3):781–788.
 48. Ferman TJ, Aoki N, Crook JE, *et al.* The limbic and neocortical contribution of alpha-synuclein, tau, and amyloid beta to disease duration in dementia with Lewy bodies. *Alzheimers Dement*. 2018;14:330–339.
 49. Kantarci K, Lowe VJ, Boeve BF, *et al.* AV-1451 tau and beta-amyloid positron emission tomography imaging in dementia with Lewy bodies. *Ann Neurol*. 2017;81:58–67.
 50. Gomperts SN, Locascio JJ, Makaretz SJ, *et al.* Tau positron emission tomographic imaging in the Lewy body diseases. *JAMA Neurol*. 2016;73:1334–1341.
 51. Graff-Radford J, Boeve BF, Pedraza O, *et al.* Imaging and acetylcholinesterase inhibitor response in dementia with Lewy bodies. *Brain*. 2012;135(Pt 8):2470–2477.



Contents lists available at ScienceDirect

Neurobiology of Aging

journal homepage: www.elsevier.com/locate/neuaging.org

Cerebrovascular disease, neurodegeneration, and clinical phenotype in dementia with Lewy bodies

Daniel Ferreira^{a,b}, Zuzana Nedelska^{b,c}, Jonathan Graff-Radford^d, Scott A. Przybelski^e, Timothy G. Lesnick^e, Christopher G. Schwarz^b, Hugo Botha^d, Matthew L. Senjem^{b,f}, Julie A. Fields^g, David S. Knopman^d, Rodolfo Savica^d, Tanis J. Ferman^h, Neill R. Graff-Radfordⁱ, Val J. Lowe^b, Clifford R. Jack^b, Ronald C. Petersen^d, Afina W. Lemstra^j, Marleen van de Beek^j, Frederik Barkhof^{k,l}, Frederic Blanc^{m,n}, Paulo Loureiro de Sousa^{m,n}, Nathalie Philippi^{m,n}, Benjamin Cretin^{m,n}, Catherine Demuyne^{m,n}, Jakub Hort^{c,o}, Ketil Oppedal^{p,q,r}, Bradley F. Boeve^d, Dag Aarsland^{p,s}, Eric Westman^{a,t}, Kejal Kantarci^{b,*}

^a Division of Clinical Geriatrics, Center for Alzheimer Research, Department of Neurobiology, Care Sciences, and Society, Karolinska Institutet, Stockholm, Sweden

^b Department of Radiology, Mayo Clinic, Rochester, MN, USA

^c Department of Neurology, Charles University, 2nd Faculty of Medicine, Motol University Hospital, Prague, Czech Republic

^d Department of Neurology, Mayo Clinic, Rochester, MN, USA

^e Department of Health Sciences, Mayo Clinic, Rochester, MN, USA

^f Department of Information Technology, Mayo Clinic, Rochester, MN, USA

^g Department of Psychiatry and Psychology, Mayo Clinic, Rochester, MN, USA

^h Department of Psychiatry and Psychology, Mayo Clinic, Jacksonville, FL

ⁱ Department of Neurology, Mayo Clinic, Jacksonville, FL, USA

^j Department of Neurology and Alzheimer Center, VU University Medical Center, Amsterdam, Netherlands

^k Department of Radiology and Nuclear Medicine, VU University Medical Center, Amsterdam, Netherlands

^l Queen Square Institute of Neurology, University College London, London, UK

^m Day Hospital of Geriatrics, Memory Resource and Research Centre (CM2R) of Strasbourg, Department of Geriatrics, Hopitaux Universitaires de Strasbourg, Strasbourg, France

ⁿ University of Strasbourg and French National Centre for Scientific Research (CNRS), ICube Laboratory and Federation de Medecine Translationnelle de Strasbourg (FMTS), Team Imagerie Multimodale Integrative en Sante (IMIS)/ICONE, Strasbourg, France

^o International Clinical Research Center, St. Anne's University Hospital Brno, Brno, Czech Republic

^p Centre for Age-Related Medicine, Stavanger University Hospital, Stavanger, Norway

^q Stavanger Medical Imaging Laboratory (SMIL), Department of Radiology, Stavanger University Hospital, Stavanger, Norway

^r Department of Electrical Engineering and Computer Science, University of Stavanger, Stavanger, Norway

^s Institute of Psychiatry, Psychology and Neuroscience, King's College London, London, UK

^t Department of Neuroimaging, Centre for Neuroimaging Sciences, Institute of Psychiatry, Psychology and Neuroscience, King's College London, London, UK

ARTICLE INFO

Article history:

Received 16 December 2020

Revised 26 April 2021

Accepted 28 April 2021

Available online 14 May 2021

ABSTRACT

We investigated whether cerebrovascular disease contributes to neurodegeneration and clinical phenotype in dementia with Lewy bodies (DLB). Regional cortical thickness and subcortical gray matter volumes were estimated from structural magnetic resonance imaging (MRI) in 165 DLB patients. Cortical and subcortical infarcts were recorded and white matter hyperintensities (WMHs) were assessed. Subcortical only infarcts were more frequent (13.3%) than cortical only infarcts (3.1%) or both subcortical

* Corresponding author at: Kejal Kantarci, Department of Radiology, Mayo Clinic, 200 First Street Southwest, Rochester, MN 55905. Tel.: 507 2849770; Fax: 507 2849778. E-mail address: kantarci.kejal@mayo.edu (K. Kantarci).

Keywords:

Dementia with Lewy bodies (DLB)
 Cerebrovascular disease
 Magnetic resonance imaging
 White matter hyperintensities
 infarcts
 Neurodegeneration

and cortical infarcts (2.4%). Infarcts, irrespective of type, were associated with WMHs. A higher WMH volume was associated with thinner orbitofrontal, retrosplenial, and posterior cingulate cortices, smaller thalamus and pallidum, and larger caudate volume. A higher WMH volume was associated with the presence of visual hallucinations and lower global cognitive performance, and tended to be associated with the absence of probable rapid eye movement sleep behavior disorder. Presence of infarcts was associated with the absence of parkinsonism. We conclude that cerebrovascular disease is associated with gray matter neurodegeneration in patients with probable DLB, which may have implications for the multifactorial treatment of probable DLB.

© 2021 Elsevier Inc. All rights reserved.

1. Introduction

Although Lewy bodies are the main pathological hallmark of dementia with Lewy bodies (DLB), recent neuropathological and magnetic resonance imaging (MRI) studies have recognized the potential role of cerebrovascular disease in DLB pathogenesis (Donaghy et al., 2020; Jellinger, 2018; Watson and Colloby, 2016).

Two common MRI markers of cerebrovascular disease are white matter hyperintensities (WMHs) and infarcts (Wardlaw et al., 2013). Whereas several studies showed that the WMH burden is higher in patients with probable DLB than in healthy controls (Barber et al., 1999; Joki et al., 2018; Kim et al., 2015; Koikkalainen et al., 2016; Sarro et al., 2017), no differences in WMH burden have also been reported (Burton et al., 2006; De Reuck et al., 2016; Oppedal et al., 2012). Further, it is unclear whether the WMH burden in DLB is due to primary vascular pathology or is secondary to neurodegeneration (Barber et al., 2000; Chimowitz et al., 1992; Fazekas et al., 1996). Two studies showed that WMH burden in DLB is associated with increased global brain atrophy and atrophy in the medial temporal lobes (Barber et al., 2000; Joki et al., 2018). Moreover, investigations into the association between WMHs and cognitive functioning have also provided mixed results. No associations have been reported in several studies (Barber et al., 1999; Burton et al., 2006; Fukui et al., 2013; Oppedal et al., 2012), while other reports suggested that the association of WMHs with cognition may depend on the *APOE* genotype and/or the location of the lesions. For instance, Mirza et al. (2019) reported an association exclusively in *APOE* $\epsilon 4$ carriers, and Park et al. (2015) showed that increased WMHs in cholinergic white matter pathways is associated with lower cognitive performance. Very few studies investigated the association of WMHs with clinical features of DLB. Sarro et al. (2017) showed no associations with visual hallucinations, parkinsonism, or cognitive fluctuations. However, Barber et al. (1999) reported that although periventricular WMHs were not associated with visual hallucinations, occipital WMHs were associated with the absence of visual hallucinations; while Fukui et al. (2013) showed that periventricular WMHs were associated with the presence of visual hallucinations in DLB. Further, increased WMHs have been associated with a lower frequency of rapid eye movement sleep behavior disorder (RBD) (Sarro et al., 2017). Finally, the WMH burden may increase with age in probable DLB (Barber et al., 1999; Sarro et al., 2017), although some studies did not replicate that finding (Burton et al., 2006; Park et al., 2015), and the WMH burden may be higher in women but not in *APOE* $\epsilon 4$ carriers (Sarro et al., 2017).

Even less is known about infarcts in DLB. Their frequency seems to be comparable to that in healthy controls (Kim et al., 2015; Koikkalainen et al., 2016; Sarro et al., 2017), and may be associated with older age, but not with *APOE* genotype, sex, or severity of dementia (Sarro et al., 2017).

Therefore, the current knowledge on how cerebrovascular disease contributes to neurodegeneration and clinical phenotype in

DLB is limited and inconclusive. This may be partially explained by the lack of longitudinal studies specifically designed to investigate associations between cerebrovascular disease and neurodegeneration and clinical phenotype in DLB. Further, methodological variability and the use of relatively small samples, has made replication and generalization of findings difficult. In the current multicenter study, we investigated WMHs and cortical and subcortical infarcts in 165 patients with probable DLB, the largest cohort so far in an MRI study of cerebrovascular disease in DLB. We hypothesized that there would be a positive association between WMHs and infarcts, and that a higher burden of cerebrovascular disease would be associated with reduced cortical thickness and volume of subcortical gray matter structures, as MRI markers of neurodegeneration. We also hypothesized that a higher burden of cerebrovascular disease would be associated with a lower frequency of clinical features of DLB and a lower cognitive performance.

2. Methods

2.1. Participants

We used data from the European DLB consortium (E-DLB) (Oppedal et al., 2019) and the Mayo Clinic DLB cohort (Kantarci et al., 2017), from Rochester, Minnesota, the United States.

The E-DLB consortium archives data from 40 centers across Europe (Kramberger et al., 2017), including patients with probable DLB, Parkinson's disease with dementia, or AD. For the current study, we included patients with probable DLB from the E-DLB centers that had collected more than 20 DLB patients each and had high-resolution T1-weighted and fluid attenuation inversion recovery (FLAIR) MRI data (see below). Three E-DLB centers satisfied such criteria, including the Day Hospital of Geriatrics, Memory Resource and Research Centre (CMRR, Strasbourg, France, $n = 34$), the Motol University Hospital (Prague, Czech Republic, $n = 29$), and the VU University Medical Center (VUmc, Amsterdam, the Netherlands, $n = 34$). The diagnostic procedure and clinical examinations are described elsewhere (Kramberger et al., 2017). Briefly, diagnosis was made according to the 2005 International Consensus Criteria for probable DLB (McKeith et al., 2005), based on detailed history and clinical examinations including physical, neurological, and psychiatric examinations performed by a licensed neurologist. Exclusion criteria were patients with acute delirium, terminal illness, previous major stroke, psychotic or bipolar disorder, craniocerebral trauma, a major neurological illness other than dementia.

The Mayo Clinic DLB cohort is a prospective study of consecutive cases assessed through the Mayo Clinic Alzheimer's Disease Research Center and the Mayo Clinic Study of Aging. For the current study we included patients assessed between May 2007 and September 2017 who had high-resolution T1-weighted and FLAIR MRI data (see below). All patients underwent a medical history review, informant interview, neurologic examination, and neuropsychological assessment (Ferman et al., 2018). For the current study,

patients with a diagnosis of probable DLB according to the 2005 International Consensus Criteria (McKeith et al., 2005) were included ($n = 68$).

All centers recorded whether patients fulfilled criteria for parkinsonism, visual hallucinations (VH), fluctuating cognition, and a clinical history of probable rapid eye movement sleep behavior disorder (RBD). Presence/absence of clinical features was based on the 2005 International Consensus Criteria for probable DLB (McKeith et al., 2005), to allow harmonized diagnosis across the four centers because many of the patients were assessed prior to 2017 International Consensus Criteria (McKeith et al., 2017). Polysomnogram confirmation was not required for RBD, and the International Classification of Sleep Disorders-II diagnostic criteria B was used for the diagnosis of probable RBD (AASM, 2005). The Mini-Mental State Examination (MMSE) was selected as a measure of global cognition.

An institutional ethics committee at each E-DLB center as well as the Mayo Clinic Institutional Review Board approved the study. Informed consent on participation was obtained from all of the patients or an appropriate surrogate according to the Declaration of Helsinki.

2.2. Magnetic resonance imaging

A high-resolution 3D T1-weighted magnetization prepared rapid gradient echo (MPRAGE) sequence and a FLAIR sequence were acquired in all four of the centers included in this study. Supplementary Table 1 shows the scanning parameters by center. 3T scanners were used in the Day Hospital of Geriatrics, Memory Resource and Research Centre (CMRR, Strasbourg, France), the Mayo Clinic (Rochester, US), and the VU University Medical Center (VUmc, Amsterdam, the Netherlands). A 1.5T scanner was used in the Motol University Hospital (Prague, Czech Republic).

2.3. Infarcts and WMHs

MRIs from the four centers contributing to this study were centralized at Mayo Clinic and graded by two neurologists (J.G.-R. and Z.N.), both for infarcts and WMHs, according to established standards (Graff-Radford et al., 2020). Infarcts were graded on FLAIR images that were co-registered with T1-weighted MPRAGE images as previously described.

Infarcts were initially identified by trained image analysts and subsequently confirmed by a vascular neurologist (J.G.-R.). The intra-rater reliability based on blinded reading of 50 possible infarcts on two separate occasions was excellent ($\kappa = 0.92$) (Graff-Radford et al., 2020). Cortical infarcts were defined as hyperintense lesions (gliosis) on the FLAIR sequence, which were located in the cortical gray matter and extending to the cortical edge with or without involvement of the adjacent white matter. A corresponding T1 hypointensity was required for confirmation. Subcortical infarcts were defined as hyperintense lesions with a dark center on FLAIR images, which were located in the white matter, infratentorial, and central gray-capsular regions. The dark center (tissue loss) was required to be greater than or equal to 3 mm in diameter as measured on the FLAIR or T1 sequences. As previously noted (Graff-Radford et al., 2020), the dark center may not be seen on FLAIR images in infarcts located in the thalamus and caudate, giving fully hyperintense lesions, while having CSF intensity on T1-weighted images. For this reason, infarcts in the thalamus and caudate did not need to meet the 3-mm diameter criteria, central hypointensity, or surrounding rim of hyperintensity thresholds. Further, a subset of cerebellar infarcts with CSF intensity on the FLAIR and T1 sequences may have no hyperintense

ring on FLAIR, but the infarcts still needed to meet the 3-mm criteria.

WMH volume was visually assessed by a neurologist (Z.N.), centrally at Mayo Clinic and under the same technical conditions (i.e., monitor, lighting, contrast adjustments, etc.). WMH volume was assessed using a semi-quantitative scale of six volume categories. WMHs were defined as signal abnormalities of variable size in the white matter that present as hyperintensities on FLAIR images and are not associated with infarcts identified on FLAIR images. WMH volume was estimated as in a previous study (Kantarci et al., 2008). Briefly, each subject's FLAIR image was compared with a bank of ten FLAIR image templates with increasing WMH volume in patients with probable DLB (from 1 to 100 cm^3), as determined by a semi-automated image segmentation algorithm (Raz et al., 2013). A continuous scale with a slider bar was used to estimate each subject's WMH volume by matching to the WMH templates (Wu et al., 2002). The WMH volume estimation algorithm was previously validated against quantification using an automated image segmentation of the WMH volume. The concordance correlation coefficient was 0.88 (95% confidence interval (CI) = 0.83, 0.94) (Kantarci et al., 2008). Intra-rater reliability for WMH assessments in the current study was excellent (weighted $\kappa = 0.96$, 95% CI = 0.92, 0.99). Fig. 1 shows representative cases with mild WMH, moderate WMH, and severe WMH burden (similar to Fazekas (Fazekas et al., 1987) scores of 1, 2, and 3, respectively), and their correspondence with the six volume categories of the WMH visual scale. In the current study, the measure used in most of the analyses was the six-level variable, representing WMH volume. When specified, the three WMH burden categories variable was used instead to facilitate clinical interpretability and comparability with similar WMH scales such as the Fazekas scale (Fazekas et al., 1987).

Assessment of both WMHs and infarcts was blinded to clinical information.

2.4. Cortical thickness and subcortical gray matter volume

Using ANTs (Avants et al., 2008), the Mayo Clinic Adult Lifespan Template (MCALT) (<https://www.nitrc.org/projects/mcalt/>) atlases were propagated to individuals' native MPRAGE space and regional estimations of thickness across the cortical mantle and volume across subcortical gray matter structures were calculated. Tissue probabilities were determined for each MPRAGE using the unified segmentation algorithm in SPM12 (Wellcome Trust Centre for Neuroimaging, London, UK), with MCALT tissue priors and settings (Schwarz et al., 2017), and cortical thickness was estimated from these probabilities using ANTs DiReCT (Das et al., 2009). Left and right regions of interest (ROIs) were combined, giving a total of 41 bilateral cortical ROIs and 6 subcortical ROIs. The total intracranial volume was calculated from the tissue probabilities and included in statistical models involving subcortical gray matter volumes, to account for between-subject variability in head size.

2.5. Statistical analysis

Demographic and clinical characteristics were reported using means and standard deviations for continuous variables, and counts and percentages for categorical variables. Distributions of infarcts and WMH were described using an exploded pie chart, histogram, and bar chart. Because automated quantification of cortical thickness and subcortical gray matter volumes is influenced by field strength (Guo et al., 2019), we restricted our statistical analyses on cortical thickness and subcortical gray matter volumes to the subsample including 3T scanners ($n = 136$). In contrast, visual

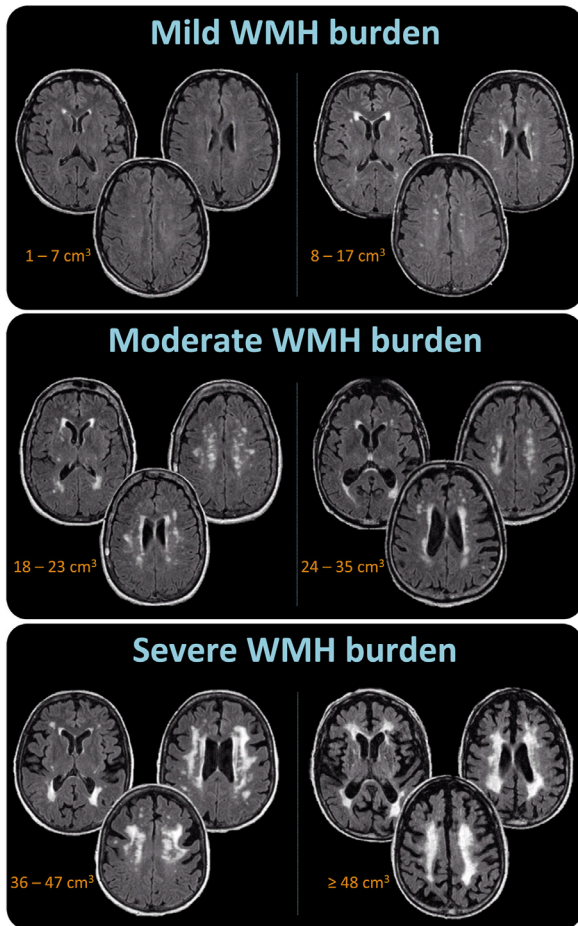


Fig. 1. Visual examples of mild, moderate, and severe WMH burden the mild WMH burden category includes the two lower volume categories corresponding to WMHs 1 to 7 cm³ large (first volume category), and WMHs 8 to 17 cm³ large (second volume category). The moderate WMH burden category includes the two intermediate volume categories corresponding to WMHs 18 to 23 cm³ large (third volume category), and WMHs 24 to 35 cm³ large (fourth volume category). The severe WMH burden category includes the two higher volume categories corresponding to WMHs 36 to 47 cm³ large (fifth volume category), and WMHs 48 cm³ or larger (sixth volume category). Abbreviations: WMH, white matter hyperintensities. (For interpretation of the references to color in this figure legend, the reader is referred to the Web version of this article.)

assessment of infarcts and WMHs are less influenced by the variability in scanners and MRI protocols across centers, and were assessed centrally by the same two raters (J.G.R. and Z.N.). Hence, we used the entire cohort ($n = 165$) when analyzing infarcts and WMHs. We ran linear mixed effects (continuous outcomes) or logistic mixed effects (binary outcomes) models that included the infarcts and WMHs as fixed effect variables and center as a random variable. All models were also adjusted for age and sex. When analyzing the subcortical gray matter volumes as the response variable there was an additional adjustment for total intracranial volume. Heterogeneity across centers was tested by comparing nested models: the above restricted model with MRI measures and centers, and a more general model with MRI measures within centers. The restricted model assumes a common association with the MRI measures across centers, and the more general model allows each center to have different associations with the MRI measures. A significant p -value would indicate heterogeneity in the associations with MRI measures by center, and that a common measure of association is not appropriate. Our results showed that the test for heterogeneity was not significant in any of the models. In addition,

we used linear mixed or logistic mixed models to compare women and men, and $APOE \epsilon 4$ non-carriers and carriers (at least one $\epsilon 4$ allele), as well as to test for age associations across demographic and clinical variables. A p value ≤ 0.05 (two-tailed) was deemed significant in all these analyses. The False Discovery Rate (FDR) (Genovese CR, Lazar NA, 2002) was applied to deal with multiple testing in the analyses involving the cortical thickness and subcortical gray matter volume ROIs.

3. Results

Table 1 shows the main demographic and clinical characteristics of the whole cohort ($n = 165$) and the subsample with available 3T MRI data ($n = 136$). The 3T MRI subsample involved 82% of the whole cohort and was largely comparable in terms of demographic and clinical characteristics.

3.1. Infarcts and WMHs

Fig. 2A shows that 81.2% of the patients had no infarcts while 18.8% of the patients had cortical or subcortical infarcts. The overall frequency of cortical infarcts was 5.5% and subcortical infarcts was 15.7%. In particular, only subcortical infarcts were present in 3.1% of the patients, while cortical and subcortical infarcts were jointly present in 2.4% of the patients. Fig. 2B shows that 49.1% of the patients had a mild WMH burden, 40.0% had a moderate WMH burden, and 10.9% had a high WMH burden. There was a significant association between having an infarct and WMH burden ($p = 0.015$). Fig. 3 shows that a higher number of subcortical infarcts was associated with greater WMH burden, while a higher number of cortical infarcts tended to associate with severe WMH burden. We also tested for associations with age, sex, and $APOE$ genotype. Older patients had more infarcts ($p = 0.006$) and a higher WMH volume ($p < 0.001$), while no significant associations were found for sex. Further, $APOE$ genotype was significantly associated with WMHs ($p = 0.044$) when entered in a model together with age ($p < 0.001$) and sex ($p = 0.77$), indicating a higher WMH volume in $APOE \epsilon 4$ non-carriers than in carriers. In contrast, there was no significant association between $APOE$ genotype and the infarcts.

3.2. Clinical features and cognitive performance

A higher WMH volume was significantly associated with the presence of visual hallucinations (odds ratio = 1.06; 95% confidence interval (CI) = 1.02, 1.09; $p = 0.002$) and with lower MMSE scores (estimate = -0.09; 95% CI = -0.16, -0.03; $p = 0.008$). We also observed a trend towards a significant association between a higher WMH volume and the absence of probable RBD (odds ratio = 0.96; 95% CI = 0.92, 1; $p = 0.051$). In addition, the presence of any infarct was significantly associated with the absence of parkinsonism (odds ratio = 0.21; 95% CI = 0.07, 0.64; $p = 0.006$) (Fig. 4).

3.3. Cortical thickness and subcortical volumes

For these analyses, we excluded estimations of cortical thickness for ROIs displaying cortical infarcts (exclusively for those patients and ROIs that displayed a cortical infarct).

Supplementary Figure 1 shows that after the FDR adjustment for multiple testing, a higher WMH volume was associated with a thinner cortex in three regions of the orbitofrontal cortex (gyrus rectus and superior and medial orbital regions), and a lower volume of the thalamus and pallidum. Furthermore, a higher WMH volume was associated with a higher volume of the caudate.

Table 1
Demographic and clinical characteristics

| | Whole sample (N = 165) | | 3T MRI subsample (n = 136) | |
|----------------------------------|---------------------------|--------------------------|-------------------------------|--------------------------|
| | N | Mean (SD) / count (%) | N | Mean (SD) / count (%) |
| Age, years | 165 | 69.1 (8.6) | 136 | 68.0 (8.3) |
| min - max | | 45 - 88 | | 45 - 88 |
| Sex, men | 165 | 119 (72%) | 136 | 105 (77%) |
| Education, years | 165 | 13.6 (3.9) | 136 | 13.3 (4.0) |
| APOE, ϵ 4 carriers | 159 | 69 (43%) | 131 | 59 (45%) |
| MMSE, total score | 164 | 22.9 (5.2) | 135 | 23.1 (5.4) |
| Visual hallucinations, presence | 162 | 89 (55%) | 133 | 75 (56%) |
| Cognitive fluctuations, presence | 157 | 131 (83%) | 128 | 112 (88%) |
| Parkinsonism, presence | 163 | 142 (87%) | 134 | 118 (88%) |
| Probable RBD, presence | 150 | 117 (78%) | 124 | 101 (81%) |
| Center | 165 | | 136 | |
| CMRR, n | | 34 (21%) | | 34 (25%) |
| Mayo Clinic, n | | 68 (41%) | | 68 (50%) |
| Motol University Hospital, n | | 29 (17%) | | - |
| VUmc, n | | 34 (21%) | | 34 (25%) |

Mean (standard deviation, SD) is listed for the continuous variables and count (%) for categorical variables.

Key: 3T MRI, 3 tesla magnetic resonance imaging; APOE, Apolipoprotein E; MMSE, mini-mental state examination; RBD, rapid eye movement sleep behavior disorder; CMRR, Day Hospital of Geriatrics, Memory Resource and Research Centre (Strasbourg, France); VUmc, VU University Medical Center (Amsterdam, the Netherlands).

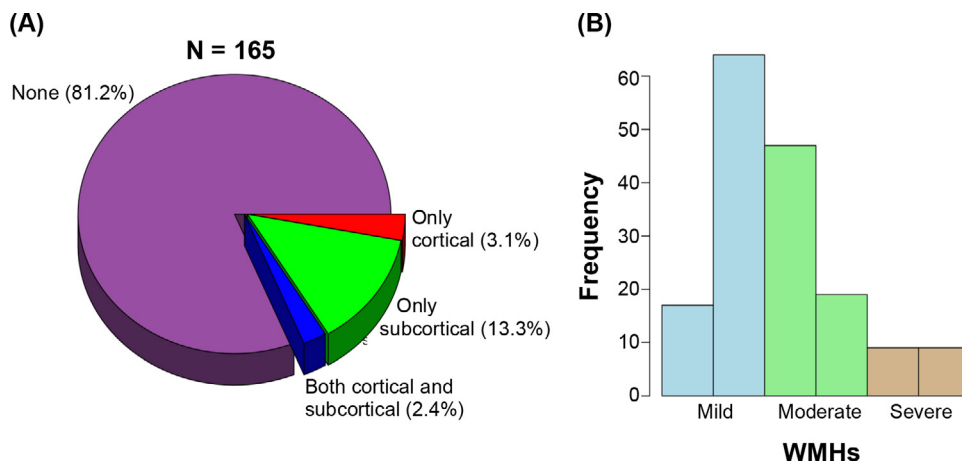


Fig. 2. Infarcts and WMHs (A) Pie chart displaying percentage of DLB patients with only cortical infarcts (in red), only subcortical infarcts (in green), or both cortical and subcortical infarcts (in blue). (B) Histogram displaying the distribution of the six WMH volume categories (bars) colored by WMH burden (mild, moderate, and severe), as follows: WMHs 1 to 7 cm³ large (first volume category), 8 to 17 cm³ large (second volume category), 18 to 23 cm³ large (third volume category), 24 to 35 cm³ large (fourth volume category), 36 to 47 cm³ large (fifth volume category), and 48 cm³ or larger (sixth volume category) (please see also Fig. 1). Abbreviations: WMHs, white matter hyperintensities. (For interpretation of the references to color in this figure legend, the reader is referred to the Web version of this article.)

Fig. 5 shows the cluster of cortical regions with the highest estimates (strongest association between higher WMH volume and lower cortical thickness, fully detailed in Supplementary Fig. 1). These regions included the middle and inferior orbitofrontal, retrosplenial, and anterior and posterior cingulate cortices, in addition to gyrus rectus and superior and medial orbital regions). No significant associations were observed between infarcts and cortical thickness or subcortical volumes.

4. Discussion

This multi-center study demonstrates that WMHs and infarcts are associated with each other in probable DLB. Moreover, we demonstrated that a higher WMH burden in DLB is associated with increased neurodegeneration, lower cognitive performance, the presence of visual hallucinations, and the absence of RBD. The presence of infarcts was associated with the absence of parkinsonism.

We found that subcortical infarcts were more common than cortical infarcts, in line with previous reports in patients with probable DLB (Kim et al., 2015; Sarro et al., 2017). We also found a positive association between infarcts and WMH burden. The frequency of subcortical infarcts increased with greater WMH burden, while cortical infarcts were observed almost exclusively in the presence of severe WMH burden. Only two MRI studies investigated infarcts and WMHs in DLB (Kim et al., 2015; Sarro et al., 2017). However, none of these previous studies investigated the association between infarcts and WMHs. Our current study may thus help to clarify the association between these two widely used MRI markers of cerebrovascular disease (Wardlaw et al., 2013). This significant association between infarcts and WMHs suggest common pathophysiological mechanisms underlying both infarcts and WMHs in probable DLB. Although the pathogenesis of these lesions is not well understood and could be multifactorial (Gouw et al., 2011), deep WMHs may be primarily related to ischemic damage

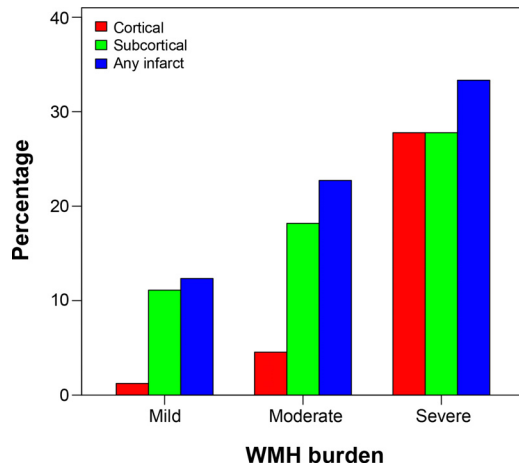


Fig. 3. Infarcts within mild, moderate, and severe WMH burden. The association between infarcts and WMH burden. Abbreviations: WMH, white matter hyperintensities.

(Ballard et al., 2000; Barber et al., 1999; Kenny et al., 2004), while cortical infarcts and periventricular WMHs especially in posterior brain areas may be related to neurodegeneration and cerebral amyloid angiopathy (Barber et al., 2000, 1999; De Reuck et al., 2014; Ghebremedhin et al., 2010). Previous research has mostly focused on the association of infarcts or WMHs with vascular factors in probable DLB (Ballard et al., 2000; Barber et al., 2000; Kenny et al., 2004; Sarro et al., 2017). In our current study we sought to fill in the important gap in the DLB literature regarding the association of infarcts and WMHs with markers of neurodegeneration. Although we can not confirm whether the association between WMHs and infarcts in our current study is specific to probable DLB, previous reports showed that the WMH burden is higher in probable DLB patients than in healthy controls (Barber et al., 1999; Joki et al., 2018; Kim et al., 2015; Koikkalainen et al., 2016; Sarro et al., 2017). However, it should be noted that volume of WMHs and frequency of infarcts tend to cluster together as the age increases in non-demented individuals (Graff-Radford et al., 2020). Hence, our cur-

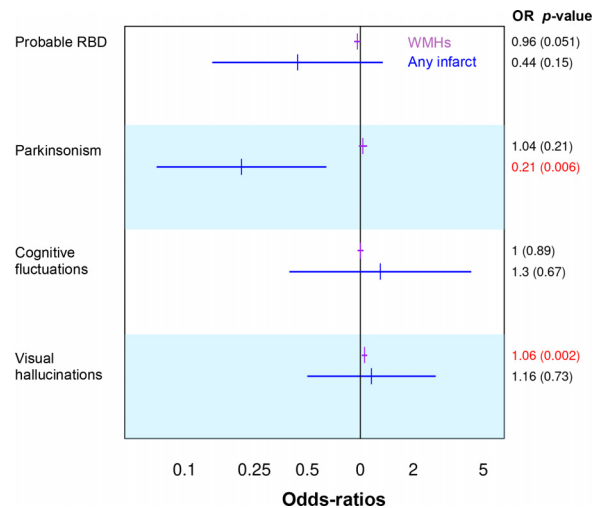


Fig. 4. The association of infarcts and WMHs with clinical features. Odds-Ratios and *p*-values for infarcts and WMHs from a linear mixed model with center as a blocking variable included as a random effect in the models, and age and sex adjustment. Significant *p*-values (≤ 0.05) are displayed in red. Abbreviations: RBD, rapid eye movement sleep behavior disorder; WMHs, white matter hyperintensities volume; OR, odds-ratios. (For interpretation of the references to color in this figure legend, the reader is referred to the Web version of this article.)

rent association between WMHs and infarcts may not be entirely exclusive of DLB.

The association between infarcts and neurodegeneration has not been investigated in DLB, and only two MRI studies reported data on the association between WMHs and neurodegeneration (Barber et al., 2000; Joki et al., 2018). Barber et al. (2000) showed that periventricular WMHs were associated with increased global brain atrophy, while no association was found for deep WMHs. Similarly, Joki et al. (2018) showed that periventricular WMHs were associated with increased atrophy in medial temporal lobes, while no association was found for deep WMHs. Our current study extends these previous reports by providing detailed data on the association of infarcts and WMHs with cortical thickness across the whole cortical mantle, as well as with the volume of key sub-

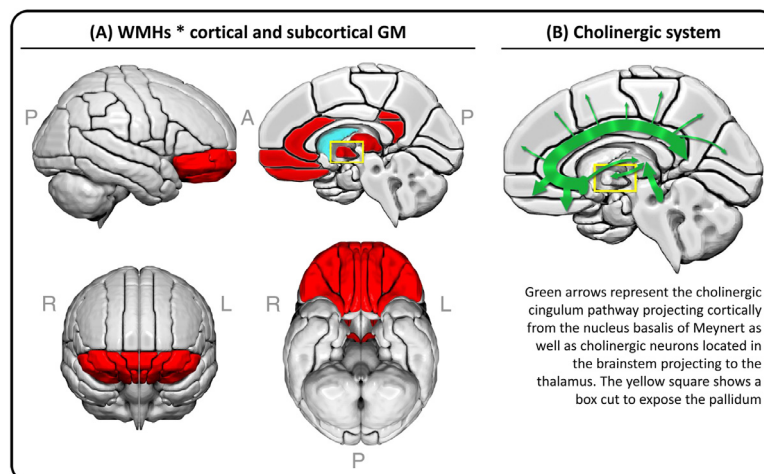


Fig. 5. The association of WMHs with cortical thickness and subcortical gray matter volumes (A) Red areas represent combined results from two models: the cluster of cortical regions with the highest estimates from a linear mixed effects model with WMHs as a fixed effect variable and center as a random variable, adjusted for age and sex; plus all the significant regions from a linear mixed effects model for subcortical volume ROIs with WMHs as a fixed effect variable and center as a random variable, adjusted for age, sex, and total intracranial volume (please see Supplementary Fig 1 for forest plot results including estimates, confidence intervals, and both uncorrected and FDR-adjusted *p*-values). (B) A schematic representation of the cholinergic system. Abbreviations: A, anterior; FDR, False Discovery Rate; GM, gray matter; L, left; P, posterior; R, right; WMHs, white matter hyperintensities. (For interpretation of the references to color in this figure legend, the reader is referred to the Web version of this article.)

cortical gray matter structures. We found that a higher WMH volume was associated with increased neurodegeneration in the orbitofrontal cortex, thalamus, and pallidum. We also found that the cluster with the highest estimates (i.e., strongest association between higher WMH volume and lower cortical thickness) included the orbitofrontal, retrosplenial, and posterior cingulate cortices.

The orbitofrontal, retrosplenial, and posterior cingulate cortices receive dense cholinergic input from the cholinergic cingulum pathway, which emerges from the anteromedial nucleus basalis of Meynert (Nemy et al., 2020; Selden et al., 1998). The thalamus also receives cholinergic input from cholinergic neurons located in the brainstem and possibly also from the nucleus basalis of Meynert (Mesulam, 2013). The pallidum is closely connected to the thalamus. Hence, our data suggest that these cortical and subcortical regions could be particularly vulnerable to cholinergic disruption due to cerebrovascular disease, an interpretation that is supported by the known interplay between cholinergic and vascular systems (Claassen and Jansen, 2006; Engelhardt et al., 2007; Liu et al., 2017). While it is not possible to determine a cause and effect relationship in this cross-sectional study, future prospective studies with longitudinal MRI may help determine the temporal relationships between cerebrovascular lesions and neurodegeneration.

In addition, we found that a higher WMH volume was associated with a larger volume (less neurodegeneration) of the caudate. The caudate is possibly the subcortical region that receives the least cholinergic input (Mesulam, 2013). Instead, the caudate receives prominent dopaminergic innervation and is heavily targeted by Lewy body pathology affecting the nigrostriatal dopaminergic system (Jellinger, 2018). Early atrophy of the caudate can be detected already in prodromal to moderate DLB patients and has been associated with impairment of attentional processing speed (Botzung et al., 2019). The lack of cholinergic input to the caudate could explain its larger volume in the context of high WMH burden. The dopaminergic system may be more spared in the context of a cholinergic system that is severely targeted by cerebrovascular disease, in mild to moderate DLB patients who are eligible for MRI studies like in our cohort. This interpretation is further supported by a dual finding in our study: (1) the presence of infarcts was associated with the absence of parkinsonism, a symptom that is closely related to dopaminergic deficits; (2) the trend towards a significant association ($p = 0.051$) between a higher WMH volume and the absence of probable RBD, a feature that is highly specific to Lewy body pathology (McKeith et al., 2017). Other studies also reported an inverse association between Lewy body pathology and cerebrovascular disease (Fukui et al., 2013; Ghebremedhin et al., 2010).

While brain atrophy is not prominent in DLB (Yousaf et al., 2019), a large multi-center study recently identified the signature pattern of atrophy in probable DLB, involving atrophy in the posterior cortex and preservation of the medial temporal lobes (Oppedal & Ferreira et al., 2018). This pattern also involves several subcortical gray matter structures, including the thalamus, caudate, putamen, and pallidum (Watson and Colloby, 2016). An important observation is that this pattern of atrophy overlaps spatially with the hypometabolic pattern characteristic of DLB (McKeith et al., 2017), as well as with the spatial pattern of white matter abnormalities in diffusion MRI (Nedelska et al., 2015b; Watson et al., 2012), the distribution of reduced blood perfusion (Nedelska et al., 2018), and the pattern of tau binding in positron emission tomography (PET) (Kantarci et al., 2017). In a recent study, we further demonstrated that atrophy in the posterior cortex is increased in probable DLB patients with positive amyloid and tau biomarkers (Abdelnour et al., 2020). Further, all the cortical regions reported in our current study spatially overlap with brain areas that show increased longitudinal atrophy in DLB patients with concomitant

Alzheimer's disease pathology (Nedelska et al., 2015a). Hence, our current results together with these previous reports suggest that there seems to be a spatial correspondence between two common pathologies in DLB (i.e., tau neurofibrillary tangles (NFT) and cerebrovascular disease), potentially contributing to the neurodegeneration and cognitive impairment in part through involvement of the cholinergic system. The potential synergistic interaction between Lewy body pathology, tau NFT, and cerebrovascular disease is a topic of utmost interest that cannot be investigated in-vivo at present due to the lack of reliable biomarkers for alpha-synuclein.

Very few studies have investigated the association of infarcts and WMHs with clinical features of DLB. We found that a higher WMH volume was significantly associated with the presence of visual hallucinations, and we already discussed above the trend towards a significant association between a higher WMH volume and the absence of probable RBD. Further, we found that the presence of infarcts was associated with the absence of parkinsonism. Our current study is in agreement with Sarro et al. (2017). Using a different method for WMHs, we also did not find an association between WMH volume and parkinsonism and cognitive fluctuations. However, in contrast to Sarro et al. (2017), we found that an increased WMH volume was associated with visual hallucinations in our larger and more heterogeneous cohort of DLB patients in the current study. Although 24% of the patients from the current study are shared with the sample used in Sarro et al. (2017), only 8% include MRI scans from the same time frame. The positive association between WMHs and visual hallucinations has also been reported by Fukui et al. (2013), but the opposite result was reported when combining DLB patients with other dementias in Barber et al. (1999), i.e., WMHs in occipital areas were associated with the absence of visual hallucinations (Barber et al., 1999). The authors suggested that perhaps an occipital lobe spared of pathology is necessary to develop visual hallucinations, and that the disruption of neural circuits involving visual association areas might prevent hallucinations (Barber et al., 1999). This hypothesis remains to be tested. Previous studies have reported a higher frequency of visual hallucinations in DLB patients with Alzheimer's disease co-pathology (Lemstra et al., 2017). Hence, visual hallucinations in DLB seem to be more frequent in the context of co-pathologies, whether cerebrovascular disease or Alzheimer's disease.

Previous studies including small samples did not find any association between WMHs and cognition (Barber et al., 1999; Burton et al., 2006; Fukui et al., 2013; Oppedal et al., 2012). Our relatively large multi-center cohort of probable DLB patients could thus have helped to capture the heterogeneity within probable DLB better and reveal the association between increased WMHs and lower cognitive performance. This interpretation is supported by two studies that further reduced part of that heterogeneity by stratifying DLB patients based on APOE genotype or focused on cholinergic white matter pathways (Mirza et al., 2019; Park et al., 2015). Mirza et al. (2019) reported an association exclusively in APOE $\epsilon 4$ carriers, and Park et al. (2015) showed that when WMHs are located in cholinergic white matter pathways they seem to have an impact on cognitive performance. We did not investigate the location of WMHs but, as discussed above, we observed that they were associated with neurodegeneration of gray matter areas that receive dense cholinergic input.

Both infarcts and WMHs increase with age in non-demented individuals (Graff-radford et al., 2020). Since we applied an age correction in our statistical models, our current findings cannot be explained by the effect of aging. Further, our current results do not spatially overlap with the effect of age on cortical thickness and subcortical gray matter volumes commonly seen in healthy individuals (Machado et al., 2018). This suggests that our current results go beyond the association of age with WMHs and neurode-

generation, and are likely specific to DLB. Nonetheless, whether WMHs are due to Lewy-induced cerebrovascular disease or are due to vascular risk factors cannot be answered at present in-vivo, due to the lack of reliable biomarkers for alpha-synuclein. In addition to age, our findings were independent of the effects of sex, *APOE* genotype, and center.

Two previous studies showed that WMHs and infarcts are associated with older age and female sex, but they do not seem to have an association with *APOE* genotype in probable DLB (Barber et al., 1999; Sarro et al., 2017). We found that older patients had more infarcts and WMHs, but we did not find any association with sex. Further, *APOE* genotype was not significantly associated with the infarcts, but it was associated with WMHs after adjusting for age, indicating a higher WMH volume in *APOE* $\epsilon 4$ non-carriers. This finding has also been reported in Alzheimer's disease, with *APOE* $\epsilon 4$ non-carriers (in particular, *APOE* $\epsilon 2$ carriers) having a higher WMH volume than *APOE* $\epsilon 4$ carriers (Groot et al., 2018). The suggested mechanism was the reduced integrity of amyloid-affected cerebral vasculature, increasing the risk of cerebral amyloid angiopathy, but amyloid-independent pathways might also be possible (Groot et al., 2018). Importantly, our statistical tests for heterogeneity did not show any significant results. This means that there was no evidence that our results differed across centers, highlighting the generalizability of the reported associations in probable DLB patients across four centers in Europe and the US. Our relatively large multi-center data may thus help to clarify some of the contradictory results from previous studies using smaller samples from a single center.

Our current study has some limitations. A semi-quantitative assessment of WMHs was the preferred method due to the multi-center nature of our study, which included some variability in MRI scanners and scanning parameters (Oppedal & Ferreira et al. 2019). Hence, we were unable to obtain separate estimations of periventricular and deep WMHs, which may differ in their underlying pathophysiology (Barber et al., 1999). Vascular risk factors have previously been associated with increased cerebrovascular disease in DLB (Sarro et al., 2017; Donaghy et al., 2020), so that they might partially explain some of our current findings. However, vascular risk factors were not consistently recorded across the four centers included in this study, which prevented us to consider them in our statistical analysis. Cerebrovascular disease may be one of the factors contributing to neurodegeneration in probable DLB. The spatial concordance between the pattern of tau PET binding and the neurodegeneration identified in our current study claims in favor of future studies investigating the association between tau PET, WMHs, and cortical thickness. Because the data was collected through a consortium on DLB, a matching control group was not available at each site. While this is a limitation of our cohort future studies that compare DLB patients to controls can determine the differences between DLB and normal aging. Finally, the diagnosis of probable DLB was based on clinical grounds, without autopsy confirmation, which has known limitations (Rizzo et al., 2018). However, it is reassuring from previous studies that most of the patients in the E-DLB cohort who had a dopamine transporter SPECT scan available were positive (Oppedal & Ferreira et al. 2019), and that the Mayo patients showed a high rate of Lewy body disease at autopsy (Sarro et al., 2017).

In conclusion, this multi-center study demonstrates an association between WMHs and the neurodegeneration of brain areas that receive dense cholinergic input, and that WMHs and infarcts have an impact on several clinical features and cognitive performance in probable DLB. This suggests a synergistic interaction between cerebrovascular disease and Lewy body pathology, which possibly extends to other highly concomitant pathologies in probable DLB, including amyloid-beta and tau NFT tangles (Ferreira et al., 2020).

Hence, prevention and therapy of cerebrovascular disease should be considered for the multifactorial treatment of probable DLB.

Disclosure statement

D Ferreira, SA Przybelski, TG Lesnick, AW Lemstra, Z Nedelska, CG Schwarz, H Botha, ML Senjem, JA Fields, DS Knopman, R Savica, NR Graff-Radford, RC Petersen, J Hort, K Oppedal, and E Westman report no disclosures relevant to the manuscript. J Graff-Radford receives research support from NIH. T Ferman receives funding from the Mangurian Foundation for Lewy body research and NIH. VJ Lowe serves as a consultant for AVID Radiopharmaceuticals, Bayer Schering Pharma, Eisai Inc, Philips Molecular Imaging, and Piramal Imaging and receives research support from GE Healthcare, Siemens Molecular Imaging, AVID Radiopharmaceuticals, the NIH (NIA, NCI), and the MN Partnership for Biotechnology and Medical Genomics. CR Jack has consulted for Lily, serves on an independent data monitoring board for Roche, and as a speaker for Eisai, but he receives no personal compensation from any commercial entity. He receives research support from NIH and the Alexander Family Alzheimer's Disease Research Professorship of the Mayo Clinic. F Blanc, has served as national coordinator and principal investigator for clinical trials sponsored by Biogen, Roche, Axovant and Eisai. BF Boeve has served as an investigator for clinical trials sponsored by Biogen and Alektor. He receives royalties from the publication of a book entitled Behavioral Neurology Of Dementia (Cambridge Medicine, 2017). He serves on the Scientific Advisory Board of the Tau Consortium. He receives research support from NIH, the Mayo Clinic Dorothy and Harry T. Mangurian Jr. Lewy Body Dementia Program and the Little Family Foundation. D Aarsland has received research support and/or honoraria from AstraZeneca, H. Lundbeck, Novartis Pharmaceuticals and GE Health, and served as paid consultant for H. Lundbeck, Eisai and Evonik. K Kantarci serves on the data safety monitoring board for Takeda Global Research and Development Center, Inc.; receives research support from Avid Radiopharmaceuticals and Eli Lilly, and receives funding from NIH and Alzheimer's Drug Discovery Foundation.

Acknowledgements

The authors particularly thank the patients and their family members for participating in this research. This work was supported by the National Institutes of Health (U01- NS100620, P50-AG016574, U01-AG006786, R37-AG011378, R01-AG041851, R01-AG040042, C06-RR018898 and R01-NS080820), Foundation Dr. Corinne Schuler, the Mangurian Foundation for Lewy Body Research, the Elsie and Marvin Dekelboum Family Foundation, the Little Family Foundation, the Robert H. and Clarice Smith and Abigail Van Buren Alzheimer's Disease Research Program, the Western Norway Regional Health Authority, the Swedish Foundation for Strategic Research (SSF), the Swedish Research Council (VR), Karolinska Institutet travel grants, Center for Innovative Medicine (CIMED), the Foundation for Geriatric Diseases at Karolinska Institutet, the NIHR biomedical research centre at UCLH, and the Projet Hospitalier de Recherche Clinique (PHRC, IDCRB 2012-A00992-41) and fondation Université de Strasbourg. The sponsors played no role in study design; in the collection, analysis, and interpretation of data; in the writing of the report; or in the decision to submit the article for publication.

Supplementary materials

Supplementary material associated with this article can be found, in the online version, at doi:10.1016/j.neurobiolaging.2021.04.029.

REFERENCES

- AASM, 2005. *International Classification of Sleep Disorders–2: Diagnostic and Coding Manual*. American Academy of Sleep Medicine, Chicago.
- Abdelnour, C., Ferreira, D., Oppedal, K., Cavallini, L., Bousiges, O., Olof, L., Hort, J., Nedelska, Z., Padovani, A., Pilotto, A., Bonanni, L., Kramberger, M.G., Boada, M., Westman, E., Pagonabarraga, J., Kulisevsky, J., Blanc, F., Aarsland, D., 2020. The combined effect of amyloid- β and tau biomarkers on brain atrophy in dementia with Lewy bodies. *Neuroimage Clin* 27, 102333. doi:10.1016/j.nicl.2020.102333.
- Avants, B.B., Epstein, C.L., Grossman, M., Gee, J.C., 2008. Symmetric diffeomorphic image registration with cross-correlation: Evaluating automated labeling of elderly and neurodegenerative brain. *Med Image Anal* 12, 26–41.
- Ballard, C., Brien, J.O., Barber, B.O.B., Scheltens, P., Shaw, F., McKeith, I.A.N., Anne, R., 2000. Neurocardiovascular Instability, Hypotensive Episodes, and MRI Lesions in Neurodegenerative Dementia. *Ann. N Y Acad Sci* 442–445. doi:10.1111/j.1749-6632.2000.tb06396.x.
- Barber, R., Gholkar, A., Scheltens, P., Ballard, C., McKeith, I.G., O'Brien, J.T., 2000. MRI volumetric correlates of white matter lesions in dementia with Lewy bodies and Alzheimer's disease. *Int J Geriatr Psychiatry* 15, 911–916. doi:10.1002/1099-1166(200010)15:10(911::AID-GPS217)3.0.CO;2-T.
- Barber, R., Scheltens, P., Gholkar, A., Ballard, C., McKeith, I., Ince, P., Perry, R., O'Brien, J., 1999. White matter lesions on magnetic resonance imaging in dementia with Lewy bodies, Alzheimer's disease, vascular dementia, and normal aging. *J Neurol Neurosurg Psychiatry* 67, 66–72. doi:10.1136/jnnp.67.1.66.
- Botzung, A., Philippi, N., Noblet, V., Sousa, P.L.De, Blanc, F., 2019. Pay attention to the basal ganglia: a volumetric study in early dementia with Lewy bodies. *Alzheimers Res Ther* 11, 108. doi:10.1186/s13195-019-0568-y.
- Burton, E.J., McKeith, I.G., Burn, D.J., Firbank, M.J., O'Brien, J.T., 2006. Progression of white matter hyperintensities in Alzheimer disease, dementia with Lewy bodies, and Parkinson disease dementia: a comparison with normal aging. *Am J Geriatr Psychiatry* 14, 842–849. doi:10.1097/01.JGP.0000236596.56982.1c.
- Chimowitz, M.I., Estes, M.L., Furlan, A.J., Awad, I.A., 1992. Further observations on the pathology of subcortical lesions identified on magnetic resonance imaging. *Arch Neurol* 49, 747–752.
- Claassen, J.A.H.R., Jansen, W.M.M., 2006. Cholinergically mediated augmentation of cerebral perfusion in alzheimer's disease and related cognitive disorders: the cholinergic – vascular hypothesis. *J Gerontol A Biol Sci Med Sci* 61, 267–271. doi:10.1093/gerona/61.3.267.
- Das, S.R., Avants, B.B., Grossman, M., Gee, J.C., 2009. Registration based cortical thickness measurement. *Neuroimage* 45, 867–879. doi:10.1016/j.neuroimage.2008.12.016.
- De Reuck, J., Auger, F., Durieux, N., Cordonnier, C., Deramecourt, V., Pasquier, F., Muraige, C.A., Leys, D., Bordet, R., 2016. Topographic distribution of white matter changes and lacunar infarcts in neurodegenerative and vascular dementia syndromes: a post-mortem 7.0-tesla magnetic resonance imaging study. *Eur Stroke J* 1, 122–129. doi:10.1177/2396987316650780.
- De Reuck, J., Deramecourt, V., Auger, F., Durieux, N., Cordonnier, C., Devos, D., Defebvre, L., Moreau, C., Caparros-Lefebvre, D., Bordet, R., Muraige, C.A., Pasquier, F., Leys, D., 2014. Post-mortem 7.0-tesla magnetic resonance study of cortical microinfarcts in neurodegenerative diseases and vascular dementia with neuropathological correlates. *J Neurol Sci* 346, 85–89. doi:10.1016/j.jns.2014.07.061.
- Donaghy, P.C., Firbank, M., Mitra, D., Petrides, G., Lloyd, J., Barnett, N., Olsen, K., Thomas, A.J., O'Brien, J.T., 2020. Microbleeds in dementia with Lewy bodies. *J Neurol* 267, 1491–1498. doi:10.1007/s00415-020-09736-0.
- Engelhardt, E., Moreira, D.M., Laks, J., 2007. Vascular dementia and the cholinergic pathways. *Dement Neuropsychol* 1, 2–9. doi:10.1590/S1980-57642008DN10100002.
- Fazekas, F., Chawluk, J.B., Alavi, A., Hurtig, H.I., Zimmerman, R.A.M.R., 1987. Signal abnormalities at 1.5 T in Alzheimer's Dementia and Normal Aging. *AJR Am J Roentgenol* 149, 351–356. doi:10.2214/ajr.149.2.351.
- Fazekas, F., Kapeller, P., Schmidt, R., Offenbacher, H., Payer, F., Fazekas, G., 1996. The relation of cerebral magnetic resonance signal hyperintensities to Alzheimer's disease. *J Neurol Sci* 142, 121–125.
- Ferman, T.J., Aoki, N., Crook, J.E., Murray, M.E., Graff-Radford, N.R., van Gerpen, J.A., Uitti, R.J., Wszolek, Z.K., Graff-Radford, J., Pedraza, O., Kantarci, K., Boeve, B.F., Dickson, D.W., 2018. The limbic and neocortical contribution of α -synuclein, tau, and amyloid β to disease duration in dementia with Lewy bodies. *Alzheimers Dement* 14, 330–339. doi:10.1016/j.jalz.2017.09.014.
- Ferreira, D., Przybelski, S.A., Lesnick, T.G., Lemstra, A.W., Londos, E., Blanc, F., Nedelska, Z., Schwarz, C.G., Graff-Radford, J., Senjem, M.L., Fields, J.A., Knopman, D.S., Savica, R., Ferman, T.J., Graff-Radford, N.R., Lowe, V.J., Jack, C.R., Petersen, R.C., Mollenhauer, B., Garcia-Portecak, S., Abdelnour, C., Hort, J., Bonanni, L., Oppedal, K., Kramberger, M.G., Boeve, B.F., Aarsland, D., Westman, E., Kantarci, K., 2020. Amyloid- β and tau biomarkers and clinical phenotype in dementia with Lewy bodies. *Neurology* 95 (24), e3257–e3268. doi:10.1212/WNL.0000000000010943.
- Fukui, T., Oowan, Y., Yamazaki, T., Kinno, R., 2013. Prevalence and clinical implication of microbleeds in dementia with lewy bodies in comparison with microbleeds in alzheimer's disease. *Dement Geriatr Cogn Dis Extra* 3, 148–160. doi:10.1159/000351423.
- Genovese, C.R., Lazar, N.A., 2002. N.T. Thresholding of statistical maps in functional neuroimaging using the false discovery rate. *Neuroimage* 15, 870–878.
- Ghebremedhin, E., Rosenberger, A., Rüb, U., Vuksic, M., Berhe, T., Bickeböller, H., De Vos, R.A.I., Thal, D.R., Deller, T., 2010. Inverse relationship between cerebrovascular lesions and severity of lewy body pathology in patients with lewy body diseases. *J Neuropathol Exp Neurol* 69, 442–448. doi:10.1097/NEN.0b013e3181d88e63.
- Gouw, A.A., Seewann, A., Flier, W.M., Van Der, Barkhof, F., Rozeumuller, A.M., Scheltens, P., Geurts, J.J.G., 2011. Heterogeneity of small vessel disease: a systematic review of MRI and histopathology correlations. *J Neurol Neurosurg Psychiatry* 82, 126–135. doi:10.1136/jnnp.2009.204685.
- Graff-Radford, J., Aakre, J.A., Knopman, D.S., Schwarz, C.G., Flemming, K.D., Rabinstein, A.A., Gunter, J.L., Ward, C.P., Zuk, S.M., Spychalla, A.J., Preboske, G.M., Petersen, R.C., Kantarci, K., Huston, J., 2020. Prevalence and heterogeneity of cerebrovascular disease imaging lesions. *Mayo Clin Proc* 95, 1195–1205. doi:10.1016/j.mayocp.2020.01.028.
- Groot, C., Sudre, C.H., Barkhof, F., Teunissen, C.E., van Berckel, B.N.M., Seo, S.W., Ourselin, S., Scheltens, P., Cardoso, M.J., van der Flier, W.M., Ossenkoppele, R., 2018. Clinical phenotype, atrophy, and small vessel disease in APOE ϵ 2 carriers with Alzheimer disease. *Neurology* 91, e1851–e1859. doi:10.1212/WNL.0000000000006503.
- Guo, C., Ferreira, D., Fink, K., Westman, E., Granberg, T. Repeatability, FreeSurfer, reproducibility of, 2019. FSL-SIENAX and SPM brain volumetric measurements and the effect of lesion filling in multiple sclerosis. *Eur Radiol* 29, 1355–1364. doi:10.1007/s00330-018-5710-x.
- Jellinger, K.A., 2018. Dementia with Lewy bodies and Parkinson's disease-dementia: current concepts and controversies. *J Neural Transm (Vienna)* 125, 615–650. doi:10.1007/s00702-017-1821-9.
- Joki, H., Higashiyama, Y., Nakae, Y., Kugimoto, C., Doi, H., Kimura, K., Kishida, H., Ueda, N., Nakano, T., Takahashi, T., Koyano, S., Takeuchi, H., Tanaka, F., 2018. White matter hyperintensities on MRI in dementia with Lewy bodies, Parkinson's disease with dementia, and Alzheimer's disease. *J Neurol Sci* 385, 99–104. doi:10.1016/j.jns.2017.12.018.
- Kantarci, K., Lowe, V.J., Boeve, B.F., Senjem, M.L., Tosakulwong, N., Lesnick, T.G., Spychalla, A.J., Gunter, J.L., Fields, J.A., Graff-Radford, J., Ferman, T.J., Jones, D.T., Murray, M.E., Knopman, D.S., Jack, C.R., Petersen, R.C., 2017. AV-1451 tau and β -amyloid positron emission tomography imaging in dementia with Lewy bodies. *Ann Neurol* 81, 58–67. doi:10.1002/ana.24825.
- Kantarci, K., Petersen, R.C., Przybelski, S.A., Weigand, S.D., Shiung, M.M., Whitwell, J.L., Negash, S., Ivnik, R.J., Boeve, B.F., Knopman, D.S., Smith, G.E., Jack, C.R.J., 2008. Hippocampal volumes, proton magnetic resonance spectroscopy metabolites, and cerebrovascular disease in mild cognitive impairment subtypes. *Arch Neurol* 65, 1621–1628. doi:10.1017/CBO9781107415324.004.
- Kenny, R.A., Shaw, F.E., O'Brien, J.T., Scheltens, P.H., Kalara, R., Ballard, C., 2004. Cortical sinus syndrome is common in dementia with Lewy bodies and correlates with deep white matter lesions. *J Neurol Neurosurg Psychiatry* 75, 966–971. doi:10.1136/jnnp.2003.023812.
- Kim, S.W., Chung, S.J., Oh, Y.S., Yoon, J.H., Sunwoo, M.K., Hong, J.Y., Kim, J.S., Lee, P.H., 2015. Cerebral microbleeds in patients with dementia with lewy bodies and Parkinson disease dementia. *Am J Neuroradiol* 36, 1642–1647. doi:10.3174/ajnr.A4337.
- Koikkalainen, J., Rhodius-Meester, H., Tolonen, A., Barkhof, F., Tijms, B., Lemstra, A.W., Tong, T., Guerrero, R., Schuh, A., Ledig, C., Rueckert, D., Soininen, H., Remes, A.M., Waldemar, G., Hasselbalch, S., Mecocci, P., Van Der Flier, W.M., Lötjönen, J., 2016. Differential diagnosis of neurodegenerative diseases using structural MRI data. *Neuroimage Clin* 11, 435–449. doi:10.1016/j.nicl.2016.02.019.
- Kramberger, M.G., Auestad, B., Garcia-Portecak, S., Abdelnour, C., Olmo, J.G., Walker, Z., Lemstra, A.W., Londos, E., Blanc, F., Bonanni, L., McKeith, I., Winblad, B., de Jong, F.J., Nobili, F., Stefanova, E., Petrova, M., Falup-Pecurariu, C., Rektorova, I., Bostantjopoulou, S., Biundo, R., Weintraub, D., Aarsland, D., 2017. Long-term cognitive decline in dementia with lewy bodies in a large multicenter, international cohort. *J Alzheimers Dis* 57, 787–795. doi:10.3233/JAD-161109.
- Lemstra, A.W., Beer, M.H., De, Teunissen, S.C.E., Schreuder, C., Scheltens, P., Flier, W.M., Van Der, Sikkes, S.A.M., 2017. Concomitant AD pathology affects clinical manifestation and survival in dementia with Lewy bodies. *J Neurol Neurosurg Psychiatry* 88, 113–118. doi:10.1136/jnnp-2016-313775.
- Liu, Q., Zhu, Z., Teipel, S.J., Yang, J., Xing, Y., Tang, Y., Jia, J., 2017. White matter damage in the cholinergic system contributes to cognitive impairment in subcortical vascular cognitive impairment, no dementia. *Front Aging Neurosci* 9, 47. doi:10.3389/fnagi.2017.00047.
- Machado, A., Barroso, J., Molina, Y., Nieto, A., Díaz-Flores, L., Westman, E., Ferreira, D., 2018. Proposal for a hierarchical, multidimensional, and multivariate approach to investigate cognitive aging. *Neurobiol Aging* 71, 179–188. doi:10.1016/j.neurobiolaging.2018.07.017.
- McKeith, I., Boeve, B.F., Dickson, D.W., Halliday, G., Taylor, J.P., Weintraub, D., Aarsland, D., Galvin, J., Attems, J., Ballard, C.G., Bayston, A., Beach, T.G., Blanc, F., Bohnen, N., Bonanni, L., Bras, J., Brundin, P., Burn, D., Chen-Plotkin, A., Duda, J.E., El-Agnaf, O., Feldman, H., Ferman, T.J., Ffytche, D., Fujishiro, H., Galasko, D., Goldman, J.G., Gomperts, S.N., Graff-Radford, N.R., Honig, L.S., Iranzo, A., Kantarci, K., Kaufer, D., Kukull, W., Lee, V.M.Y., Leverenz, J.B., Lewis, S., Lippa, C., Lunde, A., Masellis, M., Masliah, E., McLean, P., Mollenhauer, B., Montine, T.J., Moreno, E., Mori, E., Murray, M., O'Brien, J.T., Orimo, S., Postuma, R.B., Ramaswamy, S., Ross, O.A., Salmon, D.P., Singleton, A., Taylor, A., Thomas, A., Tiraboschi, P., Toledo, J.B., Trojanowski, J.Q., Tsuang, D., Walker, Z., Yamada, M., Kosaka, K., 2017. Diagnosis and management of dementia with Lewy bodies: Fourth report of the DLB Consortium. *Neurology* 89, 88–100. doi:10.1212/WNL.0000000000004058.
- McKeith, I.G., Dickson, D.W., Lowe, J., Emre, M., O'Brien, J.T., Feldman, H., Cummings, J., Duda, J.E., Lippa, C., Perry, E.K., Aarsland, D., Arai, H., Ballard, C.G., Boeve, B., Burn, D.J., Costa, D., Del Ser, T., Dubois, B., Galasko, D., Gauthier, S., Goetz, C.G., Gomez-Tortosa, E., Halliday, G., Hansen, L.A., Hardy, J., Iwatsubo, T., Kalara, R.N.,

- Kaufer, D., Kenny, R.A., Korczyn, A., Kosaka, K., Lee, V.M., Lees, A., Litvan, I., Londo, E., Lopez, O.L., Minoshima, S., Mizuno, Y., Molina, J.A., Mukaetova-Ladinska, E.B., Pasquier, F., Perry, R.H., Schulz, J.B., Trojanowski, J.Q., Yamada, M., 2005. Diagnosis and management of dementia with Lewy bodies: Third report of the DLB Diagnosis and management of dementia with Lewy bodies Third report of the DLB consortium. *Neurology* 65, 1863–1972. doi:[10.1212/01.wnl.0000187889.17253.b1](https://doi.org/10.1212/01.wnl.0000187889.17253.b1).
- Mesulam, M., 2013. Cholinergic Circuitry of the Human Nucleus Basalis and Its Fate in Alzheimer's Disease. *J Comp Neurol* 521, 4124–4144. doi:[10.1002/cne.23415](https://doi.org/10.1002/cne.23415).
- Mirza, S.S., Saeed, U., Knight, J., Ramirez, J., Stuss, D.T., Keith, J., Nestor, S.M., Yu, D., Swardfager, W., Rogava, E., St George Hyslop, P., Black, S.E., Masellis, M., 2019. APOE ϵ 4, white matter hyperintensities, and cognition in Alzheimer and Lewy body dementia. *Neurology* 93, e1807–e1e19. doi:[10.1212/WNL.00000000000008377](https://doi.org/10.1212/WNL.00000000000008377).
- Nedelska, Z., Ferman, T.J., Boeve, B.F., Przybelski, S.A., Lesnick, T.G., Murray, M.E., Gunter, J.L., Senjem, M.L., Vemuri, P., Smith, G.E., Geda, Y.E., Graff-radford, J., Knopman, D.S., Petersen, R.C., Parisi, J.E., Dickson, D.W., Jack, C.R., Kantarci, K., 2015a. Pattern of brain atrophy rates in autopsy-confirmed dementia with Lewy bodies. *Neurobiol Aging* 36, 452–461. doi:[10.1016/j.neurobiolaging.2014.07.005](https://doi.org/10.1016/j.neurobiolaging.2014.07.005).
- Nedelska, Z., Schwarz, C.G., Boeve, B.F., Lowe, V.J., Reid, R.I., Przybelski, S.A., Lesnick, T.G., Gunter, J.L., Senjem, M.L., Ferman, T.J., Smith, G.E., Geda, Y.E., Knopman, D.S., Petersen, R.C., Jack, C.R., Kantarci, K., 2015b. White matter integrity in dementia with Lewy bodies: A voxel-based analysis of diffusion tensor imaging. *Neurobiol Aging* 36, 2010–2017. doi:[10.1016/j.neurobiolaging.2015.03.007](https://doi.org/10.1016/j.neurobiolaging.2015.03.007).
- Nedelska, Z., Senjem, M.L., Przybelski, S.A., Lesnick, T.G., Lowe, V.J., Boeve, B.F., Arani, A., Vemuri, P., Gra, J., Ferman, T.J., Jones, D.T., Savica, R., Knopman, D.S., Petersen, R.C., Jack, R., Kantarci, K., 2018. Regional cortical perfusion on arterial spin labeling MRI in dementia with Lewy bodies: Associations with clinical severity, glucose metabolism and tau. *Neuroimage Clin* 19, 939–947. doi:[10.1016/j.nicl.2018.06.020](https://doi.org/10.1016/j.nicl.2018.06.020).
- Nemy, M., Cedres, N., Grothe, M.J., Muehlboeck, J.-S., Lindberg, O., Nedelska, Z., Stepankova, O., Vyslouzilova, L., Eriksdotter, M., Barroso, J., Teipel, S., Westman, E., Ferreira, D., 2020. Cholinergic white matter pathways make a stronger contribution to attention and memory in normal aging than cerebrovascular health and nucleus basalis of Meynert. *Neuroimage* 211, 116607. doi:[10.1016/j.neuroimage.2020.116607](https://doi.org/10.1016/j.neuroimage.2020.116607).
- Oppedal, K., Aarsland, D., Firbank, M.J., Sonnesyn, H., Tysnes, O.B., O'Brien, J.T., Beyer, M.K., 2012. White Matter Hyperintensities in Mild Lewy Body Dementia. *Dement Geriatr Cogn Dis Extra* 2, 481–495. doi:[10.1159/000343480](https://doi.org/10.1159/000343480).
- Oppedal, K., Borda, M.G., Ferreira, D., Westman, E., Aarsland, D., 2019. European DLB consortium: diagnostic and prognostic biomarkers in dementia with Lewy bodies, a multicenter international initiative. *Neurodegener Dis Manag* 9, 247–250. doi:[10.2217/nmt-2019-0016](https://doi.org/10.2217/nmt-2019-0016).
- Oppedal, K., Ferreira, D., Cavallin, L., Lemstra, A., ten Kate, M., Padovani, A., Rektorova, I., Bonanni, L., Wahlund, L.-O., Engedal, K., Nobili, F., Kramberger, M., Taylor, J.-P., Hort, J., Snædal, J., Blanc, F., Walker, Z., Antonini, A., Westman, E., Aarsland, D., 2019. A signature pattern of cortical atrophy in dementia with Lewy bodies: a study on 333 patients from the European DLB Consortium. *Alzheimers Dement* 15, 400–409. doi:[10.1016/j.jalz.2018.09.011](https://doi.org/10.1016/j.jalz.2018.09.011).
- Park, H.E., Park, I.S., Oh, Y.S., Yang, D.W., Lee, K.S., Choi, H.S., Ahn, K.J., Kim, J.S., 2015. Subcortical white matter hyperintensities within the cholinergic pathways of patients with dementia and parkinsonism. *J Neurol Sci* 353, 44–48. doi:[10.1016/j.jns.2015.03.046](https://doi.org/10.1016/j.jns.2015.03.046).
- Raz, L., Jayachandran, M., Tosakulwong, N., Lesnick, T.G., Wille, S.M., Murphy, M.C., Senjem, M.L., Gunter, J.L., Vemuri, P., Jack, C.R., Miller, V.M., Kantarci, K., 2013. Thrombogenic microvesicles and white matter hyperintensities in postmenopausal women. *Neurology* 80, 911–918. doi:[10.1212/WNL.0b013e3182840c9f](https://doi.org/10.1212/WNL.0b013e3182840c9f).
- Rizzo, G., Arcuti, S., Copetti, M., Alessandria, M., Savica, R., Fontana, A., Liguori, R., Logroscino, G., 2018. Accuracy of clinical diagnosis of dementia with Lewy bodies: a systematic review and meta-analysis. *J Neurol Neurosurg Psychiatry* 89, 358–366. doi:[10.1136/jnnp-2017-316844](https://doi.org/10.1136/jnnp-2017-316844).
- Sarro, L., Tosakulwong, N., Schwarz, C.G., Graff-Radford, J., Przybelski, S.A., Lesnick, T.G., Zuk, S.M., Reid, R.I., Raman, M.R., Boeve, B.F., Ferman, T.J., Knopman, D.S., Comi, G., Filippi, M., Murray, M.E., Parisi, J.E., Dickson, D.W., Petersen, R.C., Jack, C.R., Kantarci, K., 2017. An investigation of cerebrovascular lesions in dementia with Lewy bodies compared to Alzheimer's disease. *Alzheimers Dement* 13, 257–266. doi:[10.1016/j.jalz.2016.07.003](https://doi.org/10.1016/j.jalz.2016.07.003).
- Schwarz, C., Gunter, J., Ward, C., Vemuri, P., Senjem, M.L., Wiste, H., 2017. The mayo clinic adult life span template: better quantification across the life span. *Alzheimers Dement* 13, P93–PP4.
- Selden, N.R., Gitelman, D.R., Salamon-murayama, N., Parrish, T.B., Mesulam, M., 1998. Trajectories of cholinergic pathways within the cerebral hemispheres of the human brain. *Brain* 121, 2249–2257. doi:[10.1093/brain/121.12.2249](https://doi.org/10.1093/brain/121.12.2249).
- Wardlaw, J., Smith, E.E., Biessels, G.J., Cordonnier, C., Fazekas, F., Frayne, R., Lindley, R.I., O'Brien, J.T., Barkhof, F., Benavente, O.R., Black, S.E., Brayne, C., Breteler, M., Chabriat, H., Decarli, C., de Leeuw, F.E., Doubal, F., Duering, M., Fox, N.C., Greenberg, S., Hachinski, V., Kilimann, I., Mok, V., Rv, Oostenbrugge, Pantoni, L., Speck, O., Stephan, B.C., Teipel, S., Viswanathan, A., Werring, D., Chen, C., Smith, C., van Buchem, M., Norrving, B., Gorelick, P.B., Dichgans, M., 2013. Neuroimaging standards for research into small vessel disease and its contribution to ageing and neurodegeneration. *Lancet Neurol* 12, 822–838. doi:[10.1016/S1474-4422\(13\)70124-8](https://doi.org/10.1016/S1474-4422(13)70124-8).
- Watson, R., Blamire, A.M., Colloby, S.J., Wood, J.S., Barber, R., Brien, J.T.O., 2012. Characterizing dementia with Lewy bodies by means of diffusion tensor imaging. *Neurology* 79, 906–914. doi:[10.1212/WNL.0b013e318266fc51](https://doi.org/10.1212/WNL.0b013e318266fc51).
- Watson, R., Colloby, S.J., 2016. Imaging in Dementia with Lewy Bodies: An Overview. *J Geriatr Psychiatry Neurol* 29, 254–260. doi:[10.1177/0891988716654984](https://doi.org/10.1177/0891988716654984).
- Wu, C., Mungas, D., Petkov, C.I., Eberling, J.L., Zrelak, P.A., Buonocore, M.H., Brunberg, J.A., Haan, M.N., Jagust, W.J., 2002. Brain structure and cognition in a community sample of elderly Latinos. *Neurology* 59, 383–391. doi:[10.1212/wnl.59.3.383](https://doi.org/10.1212/wnl.59.3.383).
- Yousaf, T., Dervenoulas, G., Valkimadi, P.E., Politis, M., 2019. Neuroimaging in Lewy body dementia. *J Neurol* 266, 1–26. doi:[10.1007/s00415-018-8892-x](https://doi.org/10.1007/s00415-018-8892-x).